Towards Gene Therapy for Primary Ciliary Dyskinesia

Mustafa Mohamed Munye

Institute of Child Health

University College London

A thesis submitted for the degree of Doctor of Philosophy

July 2014

DECLARATION

I, Mustafa Mohamed Munye confirm that the work presented in this thesis is my own. Where information has been derived from other sources, I confirm that this has been indicated in the thesis.

ABSTRACT

Primary ciliary dyskinesia is a genetic disorder where patients develop lung disease as they are unable to clear airway infections effectively. There is currently no treatment for the underlying genetic defect. This thesis describes advances towards the development of a gene therapy targeting the airway disease in PCD patients with *DNAH5* mutations, the most common cause of PCD. Little work has been done in the field so many challenges remain. *DNAH5* is a large gene and the cDNA has not been cloned. In addition PCD models are currently inadequate. Finally, non-viral vectors for airway gene delivery produce sub-optimal levels of transgene expression and more efficient viral vectors cannot package the large DNAH5 cDNA. To address these issues functional DNAH5 cDNA was cloned from healthy airway cells and the cDNA validated by sequencing and expression studies. Lentiviral shRNA transduction of healthy cells was used to knock down *DNAH5* in airway cells semi-immortalised with BMI-1, a proto-oncogene that allows extended growth capacity of cells whilst retaining their mucociliary differentiation potential. The novel cell lines lacked cilia motility as is seen in patient cells. Minicircle DNA, in the context of airway gene delivery, was found to enhance gene expression *in vitro* and *in vivo*. A non-viral vector was optimised, characterised and used to deliver DNAH5 coding minicircle DNA to PCD models but poor transfection efficiency of DNAH5 prevented functional correction. Transfection of smaller genes was efficient so the vector in its current form could be useful for gene therapy treatment of the majority of PCD causing genes. Studies are needed to determine and overcome the bottlenecks in the efficient transfection of large transgenes to help advance PCD gene therapy.

PUBLICATIONS ARISING

Onoufriadis, A., Shoemark, A., **Munye, M. M.** et al., (2014) Combined exome and whole-genome sequencing identifies mutations in ARMC4 as a cause of primary ciliary dyskinesia with defects in the outer dynein arm. *J Med Genet.* **51**: 61-67.

Tagalakis, A. D., Kenny, G. D., Bienemann, A. S., McCarthy, D., **Munye, M. M.** et al., (2014) PEGylation improves the receptor-mediated transfection efficiency of peptide-targeted, self-assembling, anionic nanocomplexes. *J Control Release.* **174**: 177-187.

Tagalakis, A. D., Lee do, H. D., Bienemann, A. S., Zhou, H., **Munye, M. M.** et al., (2014) Multifunctional, self-assembling anionic peptide-lipid nanocomplexes for targeted siRNA delivery. *Biomaterials.* **35**: 8406-8415.

Munye, M. M. et al., Minicircle plasmids result in enhanced and prolonged transgene expression of airway epithelial cells both in vitro and in vivo. *Manuscript in preparation.*

Munye, M. M. et al., Novel human bronchial epithelial cell lines for the study of airway diseases. *Manuscript in preparation.*

Munye, M. M. et al., The Interactions of lipid and peptide components with DNA and with each other in the synergistic enhancement of transfection in a lipopolyplex vector. *Manuscript in preparation.*

Published Abstracts

Munye, M. M. et al., (2012). Towards gene therapy for primary ciliary dyskinesia. *Hum Gene Ther.* **23**: A11.

Munye, M. M. et al., (2013). Novel human bronchial epithelial cell lines for the study of gene therapy approaches to treat primary ciliary dyskinesia*. Mol Ther.* **21**: S168.

Munye, M. M. et al., (2013). Minicircle plasmids result in enhanced and prolonged transgene expression of airway epithelial cells both in vitro and in vivo. *Mol Ther.* **21**: S167.

ACKNOWLEDGMENTS

I am eternally grateful to Professor Stephen Hart and Dr Steven Howe for their encouragement, supervision and seemingly limitless consumables money without which this project would not have been completed. I am also grateful to Professor Stephen Hart and Dr Steven Howe for their intellectual discussions and the freedom to explore my own ideas whilst keeping me on track.

I must extend a special thanks to Aris Tagalakis and Maria Manunta for their help, friendship, support and tutelage throughout. I am also grateful to past and present members of the Molecular Immunology Unit for their kindness, generosity and willingness to support which has made this a special place to work.

I must also thank the many collaborators without whom this work would not have been possible. This includes the PCD diagnostic services team at the Leicester Royal Infirmary NHS Trust and the Royal Brompton Hospital NHS Trust. Particular thanks goes to Rob Hirst for teaching me all he knows about ALI cultures and Amelia Shoemark for being forever optimistic and never turning my cultures away no matter how poor they were. I would also like to thank Robin McAnulty and Jo Barnes at the UCL Respiratory Centre for Inflammation and Tissue Repair for their help and expertise with the mice work described in this thesis and Dr Tristan McKay for his help and expertise on stem cells and BMI-1.

Finally I would like to thank my parents for their encouragement, support, life itself and instilling in me a sense that anything is achievable. To my wife Amena; thank you for keeping me sane when the lab got too much and all your support.

CONTENTS PAGE

LIST OF FIGURES

LIST OF TABLES

ABBREVIATIONS

$2^{-\Delta\Delta Ct}$	Delta-delta Ct
AAV	Adeno-associated virus
ADA	Adenosine deaminase
ALI	Air-liquid interface
ANOVA	Analysis of variance
BALF	Bronchoalveolar lavage fluid
BEBM	Bronchial epithelial basal media
BEGM	Bronchial epithelial growth media
BSA	Bovine serum albumin
CAR	Coxsackievirus and adenovirus receptor
CBF	Cilia beat frequency
CBP	Cilia beat pattern
cDNA	Complementary DNA
CF	Cystic fibrosis
CMV	Cytomegalovirus
CRC	Conditionally reprogrammed cells
CRISPR	Clustered regularly interspaced short palindromic repeats
D	DNA
DAPI	4',6-diamidino-2-phenylindole
dATP	Deoxyadenosine triphosphate
Dc-Chol	3β-[N- (N',N'-Dimethylaminoethane)carbamoyl]cholesterol
dCTP	Deoxycytidine triphosphate
dGTP	Deoxyguanosine triphosphate
DHDTMA	1-Propanaminium, N,N,N-trimethyl-2,3-bis (11Z-hexadecenyloxy)-iodide
DLS	Dynamic light scattering
DMEM	Dulbecco's Modified Eagle Medium
DMSO	Dimethyl sulfoxide
DNA	Deoxyribonucleic acid
dNTP	Deoxyribonucleotide triphosphate
DOPC	1,2-Dioleoyl-sn -glycero-3-phosphocholine
DOPE	1,2-Dioleoyl-sn-Glycero-3-Phosphoethanolamine
DOTAP	1,2-Dioleoyl-3-trimethylammonium-propane
DOTMA	N-[1- (2,3-dioleyloxy)propyl]-N,N,N-trimethlylammonium chloride
dsRNA	Double-stranded RNA
dTTP	Deoxythymidine triphosphate
dUTP	Deoxyuridine Triphosphate
E. coli	*Escherichia coli*
EDTA	Ethylenediaminetetraacetic acid
EF1α	Elongation factor 1 alpha
eGFP	Enhanced green fluorescent protein
EGTA	Ethyleneglycoltetraacetic acid

EIAV	Equine infectious anaemia virus
F	Fusion
F-actin	Filamentous actin
FBS	Foetal bovine serum
FIV	Feline immunodeficiency virus
GFP	Green fluorescent protein
GL67A	Genzyme lipid 67A
GM-CSF	Granulocyte-macrophage colony-stimulating factor
HBE	Human bronchial epithelial
HDR	Homology directed repair
HGPRT	Hypoxanthine-guanine phosphoribosyl transferase
HIV	Human immunodeficiency virus
HIV-1	HIV type 1
HN	Hemagglutinin-neuraminidase
HRP	Horseradish peroxidase
IDA	Inner dynein arm
IFN	Interferon
IFT	Intraflagellar transport
IL	Interleukin
iPSC	Induced pluripotent stem cells
IRES	Internal ribosome entry site
$K_{16}E$	K_{16}GACSERMNFCG
L	Liposome
L2K	Lipofectamine 2000
LB	Lysogeny broth
L_C	DHDTMA:DOPC liposome
L_E	DHDTMA:DOPE liposome
LPC	Lysophosphatidylcholine
LTR	Long terminal repeat
MCS	Multiple cloning site
MEM	Minimum Essential Media
MFI	Mean fluorescence intensity
miRNA	Micro RNA
MOI	Multiplicity of infection
MuLV	Murine leukemia virus
NA	Neuraminidase
NHBE	Normal human bronchial epithelial
NHEJ	Non-homologous end joining
NS	Not significant
ODA	Outer dynein arm
ORF	Open reading frame
ORPK	Oak Ridge polycystic kidney
P	Peptide
PBS	Phosphate buffered saline
PBST	PBS with 0.05% (v/v) Tween-20
PCD	Primary ciliary dyskinesia
PCR	Polymerase chain reaction

PEI	Polyethylenimine
PVDF	Polyvinylidene fluoride
qRT-PCR	Quantitative reverse transcription-PCR
rAAV	Recombinant AAV
RFU	Relative fluorescence units
RLU	Relative luminescence units
RNA	Ribonucleic acid
RNAi	RNA interference
RSV	Respiratory syncytial virus
RT-PCR	Reverse transcription PCR
SEM	Standard error of the mean
SeV	Sendai Virus
SFFV	Spleen focus-forming virus
shRNA	Short-hairpin RNA
siRNA	Small-interfering RNA
SIV	Simian immunodeficiency virus
SLIC	Sequence- and ligation-independent cloning
SNP	Single nucleotide polymorphism
SOB	Super optimal broth
SOC	Super optimal broth with catabolite repression
SV40	Simian virus 40
$t^1/_2$	Half-life
TAE	Tris-acetate-EDTA
TALEN	Transcription activator-like effector nuclease
Tat	Transactivator of transcription
TB	Terrific broth
TE	Tris-EDTA
TEM	Transmission electron microscopy
T_m	Melting temperature
TNF	Tumor necrosis factor
TU/mL	Transducing units per millilitre
UbC	Polyubiquitin C
UCOE	Ubiquitous chromatin opening element
UV	Ultraviolet
VSV	Vesicular stomatitis virus
VSV-G	VSV G glycoprotein
X-SCID	X-linked severe combined immunodeficiency
ZFN	Zinc-finger nuclease

CHAPTER ONE

INTRODUCTION

1. INTRODUCTION

1.1. PRIMARY CILIARY DYSKINESIA

Primary ciliary dyskinesia (PCD) refers to a family of genetic disorders affecting cilia motility and has an incidence of approximately 1 in 10,000 births (1). PCD, having ciliary dysfunction as its root cause, falls within a broader class of disorders called ciliopathies.

1.1.1. HISTORY OF PCD

In 1904 Siewert (2) was the first to describe what we now call PCD after reporting a patient displaying the unusual symptoms of bronchiectasis and *situs inversus* (a condition where the positions of the major structures of the thorax and abdomen are reversed). In 1933 Kartagener (3) described the same symptoms in four of his patients but also noted sinusitis. Presentation with this triad of bronchiectasis, *situs inversus* and sinusitis has since been referred to as Kartagener's syndrome.

The cause of Kartagener's syndrome remained elusive until seminal discoveries in the mid-1970s. In 1975 Afzelius et al., (4) and Pedersen and Rebbe (5) described immotile spermatozoa in male patients with *situs inversus*. In the case of Pedersen and Rebbe (5) the single male patient described had *situs inversus* but was otherwise healthy. Afzelius et al., (4) described two brothers both of whom were suffering with chronic sinusitis and bronchitis, with only one of the brothers also displaying *situs inversus* (i.e. Kartagener's syndrome). All the patients described had immotile spermatozoa. In both publications the authors found immotile

spermatozoa to be due to a lack of dynein arms – the structures responsible for powering cilia and flagella movement - in the sperm tails.

The link between immotile cilia and Kartagener's syndrome was further supported by Camner et al., (6) who showed impaired mucociliary clearance in male patients with Kartagener's syndrome. The following year Afzelius (7) reported that both the sperm tail and respiratory cilia from four patients with immotile spermatozoa lacked dynein arms. Impaired mucociliary clearance was also evident. Three of the patients reported chronic sinusitis and bronchitis. *Situs inversus* was also described in three patients although it is not made clear whether those who had *situs inversus* were the same patients who reported chronic sinusitis and bronchitis. In a number of patients described by Afzelius (7) and Eliasson et al., (8) Kartagener's syndrome was associated with impaired mucociliary clearance, immotile spermatozoa in males and ultra-structural abnormalities of cilia. However in these studies impaired mucociliary clearance, immotile spermatozoa in males and ultra-structural abnormalities of cilia were also found in patients without *situs inversus*. The authors correctly hypothesised that *situs inversus* was likely due to an importance of cilia motility in determining body situs and that the absence of cilia motility would lead to randomisation of body situs. Eliasson et al., (8) thus coined the "immotile-cilia syndrome" to describe a congenital disorder of cilia that causes male sterility and chronic respiratory infections where half of the patients would also have *situs inversus*. Immotile-cilia syndrome thus encompassed Kartagener's syndrome.

However, it quickly became clear that there was heterogeneity in the cilia of patients with immotile-cilia syndrome both with regards to cilia ultra-structure (9)

and motility (10, 11). Pederson and Mygind (11) and Rossman et al., (10) described a number of patients with Kartagener's syndrome who had asynchronous and dyskinetic cilia rather than immotile cilia. Rossman et al., (10) proposed renaming the immotile-cilia syndrome to the “dyskinetic cilia syndrome”. However, neither the immotile-cilia syndrome nor the dyskinetic cilia syndrome names distinguished between congenital (i.e. primary) and acquired (i.e. secondary) ciliary dyskinesia. In a letter to the editor of *The Lancet*, Sleigh (12) together with a number of other signatories proposed the name “primary ciliary dyskinesia”, in place of immotile-cilia syndrome, to describe a congenital disorder in patients with or without *situs inversus* that is characterised by chronic sinusitis, chronic bronchitis which often develops into bronchiectasis and impaired mucociliary clearance. This name has since been adopted and so will be used hereafter.

1.1.2. Cilia in Health and Disease

Cilia have important sensory, signalling and motility functions so it is not surprising that cilia dysfunction produces disorders with a myriad of symptoms affecting a variety of tissues and organs. Genetic diseases resulting from cilia dysfunction are classed as ciliopathies.

Motile cilia were probably first described in 1677 by Leewenhoeck (13) in a letter to the Royal Society of London describing microorganisms found in water with a round upper body and “thin feet, which moved very nimbly”- most likely describing ciliate protozoa. In contrast primary cilia were not described until at least 200 years later.

Zimmerman is widely credited for being one of the first to describe primary cilia in 1898 using the name “central flagellum” and proposed a sensory function (14).

However, many later scientists dismissed primary cilium as a vestigial or rudimentary organelle. This idea was overturned only relatively recently- the beginning of the 21st century- with the demonstration of sensory roles for primary cilia of kidney tubule cells (15), the localisation of transient receptor potential ion channels (16) and membrane receptors involved in cellular signalling pathways (17, 18) to the ciliary membrane and the realisation that primary cilia are involved in left-right patterning (19, 20) which followed the discovery that polycystic kidney disease mice with *situs inversus* had primary cilia defects (20, 21). The *inv (22)* and Oak Ridge polycystic kidney disease (ORPK) (23) mice were two such mice that were generated by chance in insertional mutagenesis screens.

The *INVS* gene was found to be mutated in the *inv* mouse *(22)* whilst hypomorphic mutation of the gene Tg737, whose product was called Polaris and now called IFT88, produced the phenotypes seen in the ORPK mouse which resembled aspects of human polycystic kidney disease. IFT88 is a protein involved in intraflagellar transport (IFT) and shown to be vital for cilia formation and maintenance in *Chlamydomonas* (21). Pazour et al., (21) demonstrated that Tg737 was the mouse homolog of IFT88 and that the ORPK mouse had a ciliary defect. The authors correctly predicted that defects in IFT were likely to play a role in human disease and recently mutation of IFT88 was shown to play a role in human pathology (24). In addition, mutation of *INVS* was shown to cause nephronophthisis type 2– a human ciliopathy (25). A number of human ciliopathies have since been attributed to defects in primary cilia (26, 27).

Pathology resulting from dysfunction of motile cilia was described almost a century before primary cilia defects were shown to cause human disease. As described above, defects in cilia motility cause PCD in humans.

1.1.3. PCD Symptoms and Pathophysiology

Patients with PCD exhibit symptoms involving a variety of organ systems, testament to the fact that motile cilia are found on numerous cell types in the body. Motile cilia that line the upper and lower airways, around 200 per ciliated cell, move in a co-ordinated waveform fashion, the metachronal wave, to sweep the periciliary fluid and mucus, on the apical surface of the cells, to the larynx where it is swallowed or expectorated; this is known as mucociliary clearance. This clearance is an important defence mechanism of the airways and the disruption caused by dysmotile cilia results in chronic respiratory infections and inflammation of the airways (28). The recurrent infections cause bronchiectasis and can potentially lead to chronic lung failure with the need for lung transplantation (29, 30). In the majority of PCD cases respiratory distress in the neonatal period is evident as well as unexplained tachypnea and neonatal pneumonia (28).

Reduced fertility or infertility is another symptom seen in PCD patients which is more pronounced in male patients than female patients (31). Dysmotility of sperm flagella is the cause of reduced fertility in males (32) and ciliary dysmotility in the fallopian tubes and uterine lining contributes in females (33).

In the brain, ependymal cells lining the brain ventricles also have motile cilia and it is thought that the ependymal cilia play a role in transport of cerebrospinal fluid. Impeded cerebrospinal fluid flow can potentially lead to hydrocephalus. Despite

hydrocephalus being common in animal models of PCD (34, 35) its rarity in patients suggests that ciliary beating is not responsible for bulk transport of cerebrospinal fluid in humans (36, 37). Indeed in families where hydrocephalus is seen with PCD not every family member with PCD develops it (38).

Situs inversus is another symptom of PCD affecting around half of all patients. Around 25% of people with *situs inversus* are thought to have PCD (39). Patients with PCD tend to also have a higher incidence of congenital cardiovascular defects associated with heterotaxia syndromes (situs ambiguus) (40, 41). That PCD patients develop laterality defects suggests cilia motility has a role to play in determination of body situs. During gastrulation motile nodal cilia can be found at the ventral node of 7.5dpc mouse embryos. The nodal cilia beat in a helical manner moving extracellular fluid leftwards -i.e. generating a leftward nodal flow. In PCD this leftward nodal flow is not generated with the result being randomization of body situs (42). Supporting this idea, Nonaka et al., (42) showed that if nodal flow was disrupted in mice (which was due to a lack of nodal cilia in their Kif3B$^{-/-}$ knockout mice) randomisation of body situs was observed. Later work by Nonaka et al., (43) showed that use of an artificial leftward flow in *iv/iv* embryos, a PCD mouse model with immotile cilia, was able to rescue the *situs inversus* typically seen in half of *iv/iv* homozygotes. In addition, artificial rightward flow was able to induce *situs inversus* in wild-type and *iv/iv* embyros (43). In light of this evidence the importance of nodal flow in situs determination was widely accepted. How the rotary movement of nodal cilia generates a biased leftward flow as opposed to a vortical flow was less clear. *In silico* fluid dynamic simulations by Cartwright et al., (44) and

Browkaw (45) suggested that a linear flow could be generated by the rotatory nodal cilia if the axis of rotation had a posterior tilt. Experimental data by Okada et al., (46) and Nonaka et al., (47) confirmed these predictions.

With high-speed video microscopy Okada et al., (46) and Nonaka et al., (47) showed that the rotational axis of nodal cilia was posteriorly tilted. In addition both groups found that the nodal cilia protruded from the posterior side of the nodal pit and that the basal bodies of the nodal cilia were also located in the posterior half of nodal cells. Finally, Nonaka et al., (47) developed a mechanical model where rotating wires with conical paths were used to represent the nodal cilium and viscous silicone fluid to represent the nodal fluid. With this model the rotating wires were able to generate a unidirectional leftward flow but only if titled. How leftward flow is translated to left-right asymmetry remains a topic of debate and two hypotheses have been put forward. The morphogen hypothesis states that leftward flow results in the accumulation of a morphogen to the left which then cements left-right asymmetry. The two-cilia hypothesis in contrast suggests that leftward nodal flow generated by motile nodal cilia is sensed by nodal primary cilia subsequently cementing left-right asymmetry.

1.1.4. CILIA STRUCTURE

Given the importance of cilia in a number of disorders including PCD, it is worth pausing to explore the organelle in more detail. Cilia are complex, evolutionarily-conserved, microtubule-based hair-like appendages that are found protruding from most eukaryotic cells. The majority of cells assemble a single cilium but some cells have multiple cilia- notable examples include respiratory and ependymal cells. Cilia

are structurally related to the eukaryotic flagellum and as a result the names are often used interchangeably. In humans the tail of the spermatozoa is classed as a flagellum and is longer than cilia, such as those found on the ciliated airway epithelial cells. Cilia can be divided into sub-compartments that differ structurally and functionally. The sub-compartments are the basal body, transition zone, axoneme and ciliary tip (Figure 1.1).

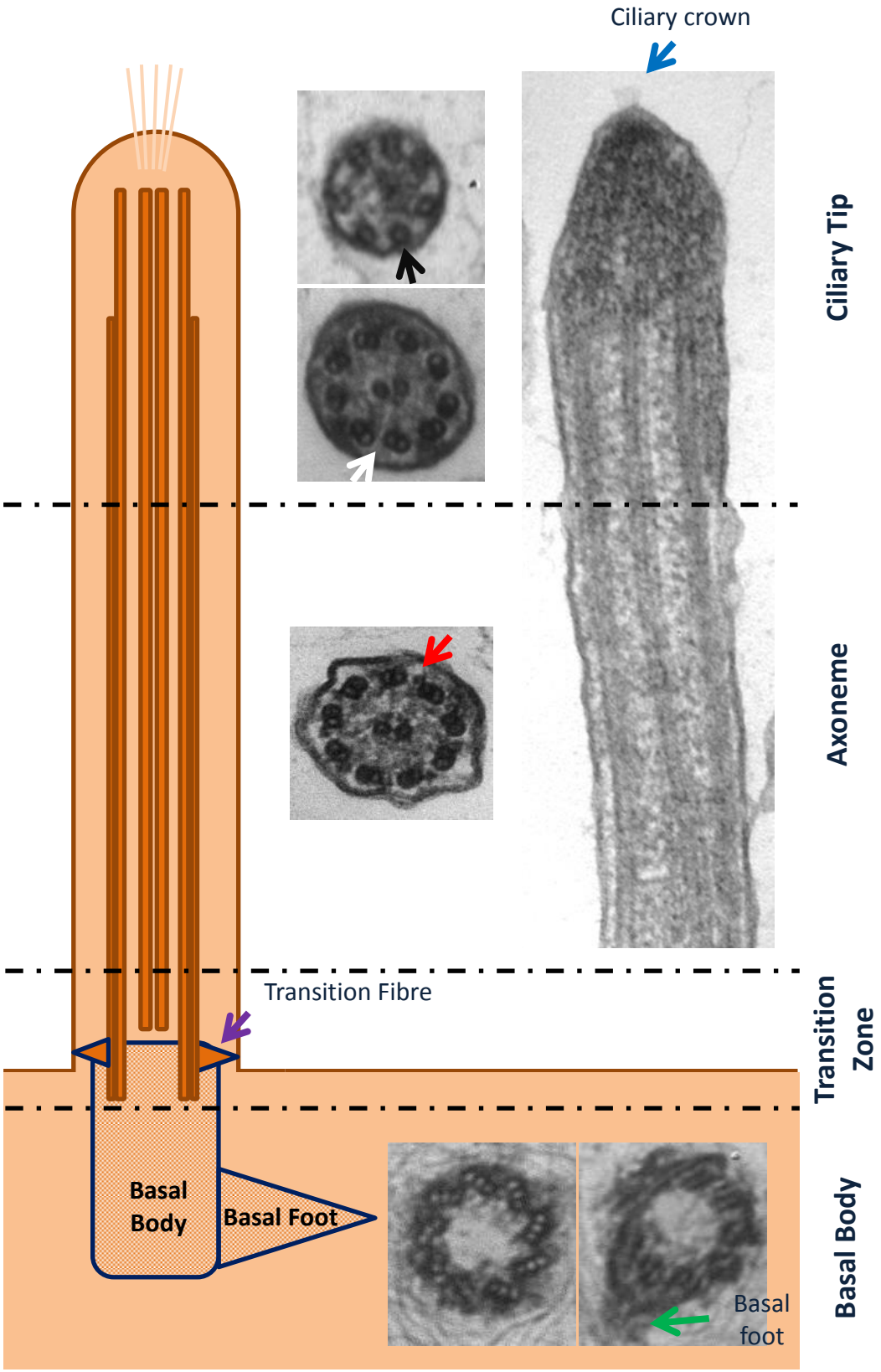

Figure 1.1. Sub-compartments of a cilium.

Four main sub-compartments of a cilium are shown highlighting the change in cilia ultrastructure where dynin arms are present in the axoneme (red arrow) but lost at the ciliary tip (white arrow) as are the B tubules (black arrow).

All cilia are derived from a basal body which is a cylindrical microtubule containing structure that is derived from the mother centriole of the centrosome- an organelle that acts as a microtubule organising centre and directs spindle formation during mitosis. The basal body is located at the base of cilia and the cilium emerges from the distal end of the basal body which nucleates microtubule assembly and growth (48). Each basal body acts as the site of nucleation for a single cilium thus in multiciliated cells centriolar replication is necessary to provide sufficient quantities of basal bodies (49).

Given the need for the mother centriole in both cell division (as part of the centrosome) and cilia formation (to form the basal body) it is widely accepted that disassembly of primary cilia is a prerequisite for cell division in most cells (50, 51). That the basal body is derived from the centrosome was first hypothesised in 1898 by Henneguy (52) and Lenhossek (53) (the Henneguy-Lenhossek hypothesis). Whilst the need for cilia disassembly prior to cell division is now accepted the question of whether the primary cilium actively regulates cell cycle entry remains a source of controversy.

Microtubules are the scaffold of the cilium and are formed from polymers of alpha and beta tublin protein heterodimers known as protofilaments. Typically thirteen protofilaments associate to form a hollow tube- the microtubule. The basal body consists of 9 sets of interconnected triplet microtubules termed the A, B and C tubules (54). The A tubule in cilia is a complete microtubule and consists of thirteen protofilaments whilst the B tubule consists of ten protofilaments of its own and

shares three protofilaments with the A tubule (55). The C tubule also consists of ten protofilaments and shares a further three with the B tubule (55).

The transition zone lies between the basal body and the ciliary axoneme and marks the end of the triplet microtubule structure of the basal body in favour of the doublet structure of the axoneme. Amongst its functions the transition zone establishes a diffusion barrier between the cilium and the cytoplasm thus compartmentalising the cilia from the cell body. There is no protein synthesis machinery in the cilium so materials required for cilia assembly and function must be transported from the cytoplasm. IFT is the system utilised to transport proteins into and out of the cilium and the transition zone acts as the gate for IFT. IFT complexes carry cargo into and out of the cilium with IFT-A and IFT-B complexes being responsible for directing retrograde (out of the cilium) and anterograde (into the cilium) transport respectively (56).

The transition zone is characterised by distinct structures such as the transition fibres, Y-links and the terminal and basal plates. The transition fibres, also known as alar sheets, radiate from the B tubule of the basal body triplet microtubules and anchor the basal body to the cell membrane (57). Immunolocalisation studies revealed that transition fibres also act as docking sites for particles involved in IFT (58). As the IFT system is the sole means by which proteins localise to the cilium the transition fibres are thus important in regulating this traffic.

The Y-links are distal to the transition fibres and connect the outer doublet microtubules of the transition zone to the cilia membrane. Loss of the Y-links, as in CEP290 mutants, led to an abnormal protein composition of *Chlamydomonas*

reinhardtii flagella and the production of flagella of varied lengths (59), both results being indicative of problems with IFT. As such, the Y-links, in conjunction with the transition fibres, are likely to be important in the regulation of protein traffic into and out of cilia.

The axoneme is distal to the transition zone and contains nine peripheral outer microtubule doublets with each outer doublet composed of an A and B tubule. As in the basal body, the A tubule of the axoneme is a complete microtubule whilst the B tubule appears fused with the A tubule and consists of 10 protofilaments of its own and shares three protofilaments with the A tubule (60, 61). Additionally the axoneme may contain a central pair of complete microtubules, the C1 and C2 tubules, which form the central pair apparatus. Each central pair tubule is associated with unique accessory proteins that distinguish the two tubules from each other (62). Cilia can be classified by the arrangement of microtubules within their axonemes which contain either nine outer doublets only (termed 9+0 cilia) or a central pair of single microtubules surrounded by nine outer microtubule doublets (termed 9+2 cilia). Classically 9+0 cilia are classified as primary, sensory or non-motile cilia with the 9+2 cilia being known as motile (Figure 1.2). It is now evident that this view is naïve, for example the motile nodal cilia of the developing embryo has a 9+0 arrangement (63) (Figure 1.2) whilst the non-motile cilia of the vertebrate inner ear, termed kinocilia, has a 9+2 axoneme (64). In addition, sensory roles for motile cilia have also been reported (65-67). Perhaps what best differentiates motile from non-motile cilia are structures associated with the outer doublets.

In motile cilia the A microtubule is studded with dynein arm complexes, both inner and outer dynein arms (IDA and ODA respectively). The dynein arms are perhaps what best differentiates motile from non-motile cilia (Figure 1.2). These large protein complexes are comprised of heavy, intermediate and light chains and display ATPase activity (68, 69). The dynein arms attach, retract and release the neighbouring microtubule doublet upon ATP hydrolysis and moves toward the minus end of the microtubule (towards the cell) causing the doublets to slide with respect to one another (70).

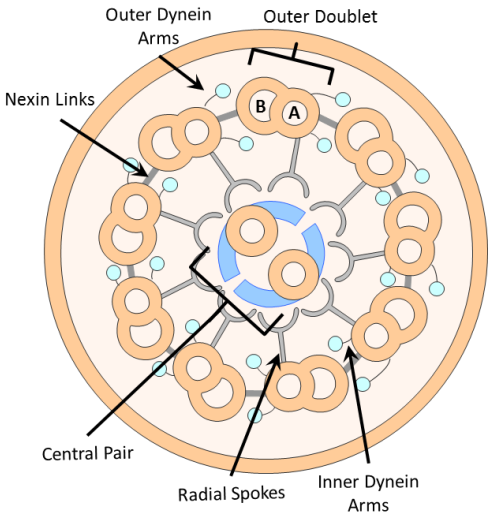

9+2 Motile Cilia

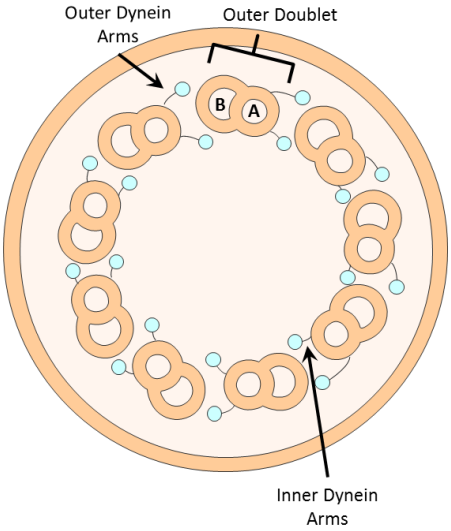

9+0 Motile Cilia

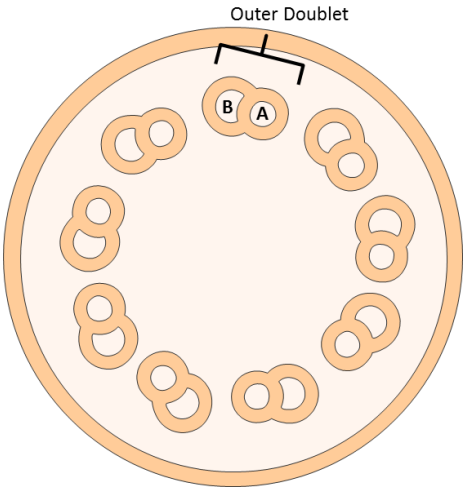

9+0 Immotile Cilia

Figure 1.2. Ultrastructure of 9+2 and 9+0 motile and 9+0 immotile cilia

Accessory structures such as the nexin links, radial spokes and the central pair apparatus (Figure 1.2) act to transition this sliding motion to the bending waveform commonly associated with respiratory cilia or *Chlamydomonas* flagella (71). Supporting this, the 9+0 motile nodal cilia of the developing embryo lack central pair microtubules and radial spokes and so rotates helically (46) and loss of the central pair produces respiratory cilia that rotate helically (72). The dynein arms are thus important for force generation and thus control beat frequency whilst the radial spokes, nexin links and the central pair apparatus regulate beat pattern. Axonemal structures such as the dynein arms and radial spokes are formed from a number of different polypeptides and have been shown to be pre-assembled, at least partially, in the cytoplasm before being chaperoned into the ciliary axoneme via IFT (73, 74).

Distal to the axoneme is the ciliary tip, the zone in which growth and resorption of the cilium takes place (48). Structurally the ciliary tip is the region where the B-tubule, along with the associated dynein arms in motile cilia, are no longer present leaving singlet A-tubules and, in 9+2 motile cilia, the central pair. The loss of B-tubules has been shown to happen simultaneously for all doublets in rat ependymal (75) and frog olfactory (76) cilia whereas the loss of B-tubules in protozoan (54, 77) and mouse renal cilia (78) is staggered. Microtubules of the ciliary axoneme are capped at the tip helping to regulate microtubule growth and resorption (79). The ciliary crown, a cluster of bristles that protrude from the cilia membrane at tip (80), is attached to this capping structure and forms the distal most structure of the ciliary tip (81). Although the molecular composition of the

crown is unknown it is known to bind cationic compounds demonstrating the presence and enrichment of anionic groups at this site (81-83). In the trachea the crown is in physical contact with the overlying mucus (84) and in the oviduct the ciliary crown is important in the cilium mediated transport of the ovum (85, 86). As such, it has been speculated that the ciliary crown facilitates mucus transport (87).

1.1.5 PCD GENETICS

The ciliary axoneme is complex and contains many proteins so it is unsurprising that PCD is a genetically heterogeneous disorder. A number of genes that give rise to PCD have been described accounting for 59-88% of patients (Table 1.1). The majority of PCD cases result from mutations in genes coding for ODA proteins which typically result in the absence of ODA from the ciliary axoneme (88, 89). The ODA gene *DNAH11* curiously deviates from this trend in that the ODA remains present in the ciliary axoneme and so the cilia ultrastructure appears normal (90-94).

Cases of PCD associated with other genetic disorders have also been described. Mutations in the retinitis pigmentosa guanosine triphosphatase regulator (RPGR) gene cause retinitis pigmentosa, a group of inherited disorders which lead to progressive loss of vision. RPGR has been shown to be expressed in bronchial and sinus epithelial cells and patients have been described where retinitis pigmentosa and PCD resulted from X-linked transmission of mutations in the RPGR gene (95-97).

Gene	ORF (bp)	Patients affected (%)	Protein localization	Ultra-structural defect	References
AK7	2,172	Not assessed	Cytoplasm	Varied dynein arm defects	(98, 99)
ARMC4	3,135	Not assessed	Axoneme	ODA defects	(100, 101)
C21orf59	873	1	Cytoplasm	IDA and ODA defects	(102)
CCDC103	729	Not assessed	Cytoplasm and axoneme	Varied dynein arm defects	(103)
CCDC114	1,392	3-4	Axoneme	ODA defects	(104-106)
CCDC164	2,223	Not assessed	Axoneme	Nexin link defects	(107)
CCDC39	2,826	11	Axoneme	IDA, nexin link and radial spoke defects	(108, 109)
CCDC40	3,428	4	Cytoplasm and axoneme	Central pair defects	(109, 110)
CCDC65	1,455	1	Cytoplasm and axoneme	IDA and nexin link defects	(102)
DNAAF1	2,178	4-5	Cytoplasm	IDA and ODA defects	(111)
DNAAF2	2,514	Not assessed	Cytoplasm	IDA and ODA defects	(112)
DNAAF3	1,767	Not assessed	Cytoplasm	IDA and ODA defects	(113)
DNAH11	13,572	6-7	Axoneme	None	(90-94, 114)
DNAH5	13,875	15-28	Axoneme	ODA defects	(115-118)
DNAI1	2,100	2-10	Axoneme	ODA defects	(119-122)
DNAI2	1,818	Not assessed	Axoneme	ODA defects	(123)
DNAL1	843	Not assessed	Axoneme	ODA defects	(124)
HEATR2	2,568	Not assessed	Cytoplasm	ODA defects	(125)
HYDIN	15,363	Not assessed	Axoneme	Rare central pair defects	(126, 127)
LRRC6	1,401	3-4	Cytoplasm	IDA and ODA defects	(128, 129)
OFD1	3,039	Not assessed	Cytoplasm	Not assessed	(130)
RPGR	3,459	Not assessed	Cytoplasm	Varied defects	(96, 97)
RSPH1	930	4	Axoneme	Central pair defects	(131-133)
RSPH4A	2,151	2	Axoneme	Central pair defects	(134-136)
RSPH9	831	Negligible	Axoneme	Central pair defects	(134, 135, 137)
TXNDC3	1,767	Not assessed	Axoneme	ODA defects	(138)
ZMYND10	1,323	3-7	Cytoplasm	IDA and ODA defects	(139, 140)

Table 1.1 PCD causing genes

Abbreviations – ORF, open reading frame; bp, base pairs; ODA, outer dynein arm; IDA, Inner dynein arm.

Mutations in the dynein arm genes *DNAH5* and *DNAI1* are the most common causes of PCD with mutations seen in 15-28% and 2-10% of all patients with PCD respectively (117-119). These figures rise to 49% for *DNAH5* mutations and 14% for *DNAI1* mutations when only patients with ODA defects are taken into account (118, 119).

DNAH5 encodes for a large axonemal dynein heavy chain protein that forms part of the ODA complex. *DNAH5* is an orthologue to the γ-heavy chain in *Chlamydomonas* and was first described as a candidate PCD causing gene by using homozygosity mapping in one large consanguineous family (115). Further studies employing sequence analysis and more families identified *DNAH5* as a PCD causing gene mutations in which lead to ODA defects, randomisation of left-right asymmetry and male infertility (116, 118). A genotype-phenotype correlation study found that mutations introducing a premature stop codon results in total absence of ODAs whilst splice site mutations which predict a loss of exon 75 resulted in short stubby ODA (141).

1.1.6 PCD TREATMENTS

Despite affecting many organ systems the primary aim of current therapy for PCD is the prevention of progressive lung damage. This approach is somewhat similar to the treatment for cystic fibrosis (CF) where, like PCD, lack of mucociliary clearance is the driver of lung pathology. Unsurprisingly then PCD treatment is informed by CF therapy. Ellerman and Bisgaard (142) used a disease management regimen not dissimilar to that used for CF on PCD patients and concluded that this approach was key to preventing lung deterioration and progressive lung damage. The regimen

included regular physiotherapy for airway clearance, monthly sputum collection with subsequent bacterial culture and appropriate antibiotic therapy based on antibiotic sensitivity cultures. Monitoring patients lung function routinely also helped slow disease progression (142). If a patient does reach end-stage lung disease then lung transplantation is also an option shown to be successful in PCD patients (30).

The establishment of a PCD management service in the UK that will review patients and provide "individualised management plans" should improve patient prognosis and provide valuable data on what treatments are best for managing PCD (143). As it is, with current treatment regimens, almost all patients develop bronchiectasis by adulthood. A gene therapy treatment option that corrects the primary defect in PCD, administered before extensive lung damage is present, would improve the quality of life for patients and reduce morbidity. This goal would be aided by improvements in diagnosis of PCD as currently, despite symptoms in the neonatal period, median age at diagnosis is around 5.3 years which falls to 3.5 years when *situs inversus* is present (144).

1.2 GENE THERAPY

Gene therapy is the introduction of genetic material into cells to provide a therapeutic benefit and has classically been thought of as the introduction of deoxyribonucleic acid (DNA) encoding a functional gene to replace a mutated one. Given that PCD results from genetic mutations it is reasonable to suspect that introduction of the wild-type gene into ciliated cells could rescue normal ciliary beating and so correct the disease phenotype.

1.2.1 HISTORY

In 1928 Frederick Griffith (145) showed that non-pathogenic R form of Type I pneumococcus became pathogenic upon mixing with heat-inactivated S form of Type II pneumococcus and that this mixture was capable of inducing lethal pneumonia infections in mice. In addition, Griffith was able to isolate the S form of Type II pneumococcus in these mice. As the original S form of Type II pneumococcus had been heat-inactivated Griffith concluded that the R form must have been transformed into the S form and that the pneumococcal type must also have been transformed from Type I to Type II. These experiments were the first to show that the phenotype of an organism can be changed by the introduction of foreign material.

James Alloway (146) later found that filtered cell free extracts from S form of pneumococcus was also able to transform R form pneumococcus. Alloway therefore concluded that something in the cell free extract was responsible for transforming the pneumococcus and named this the “transforming principle”. Avery et al., (147) subsequently identified this transforming principle as DNA. In

support of the notion that DNA is heritable and sufficient for transformation Hershey and Chase (148) showed that only the DNA of bacteriophage was taken up by infected bacteria. In these experiments radiolabelled phage DNA was found to be transmitted to the new progeny whilst the sulphur-containing protein was not. As the infected bacteria produced bacteriophage progeny DNA must have contained all the information required to produce bacteriophage.

The identification of DNA as the heritable material was quickly followed by studies showing the incorporation of foreign genetic material into mammalian cells for the first time (149) and the demonstration that foreign DNA could be used to impart onto mammalian cells a new biochemical trait (150). The latter of these studies was described by Szybalska and Szybalski (150) and was based on the need for cells to synthesise nucleic acids in order to replicate and survive in culture. Typically dihydrofolate reductase is utilised for *de novo* synthesis of nucleic acids but Szybalska and Szybalski added the chemotherapeutic agent aminopetrin to inhibit this enzyme thus forcing the cells to utilise an alternative pathway involving hypoxanthine-guanine phosphoribosyl transferase (HGPRT). Cells with this enzyme ($HPGRT^{+}$) would be able to continue proliferating but those without the enzyme ($HPGRT^{-}$) would not. Szybalska and Szybalski found that introducing DNA isolated from $HPGRT^{+}$ cells into $HPGRT^{-}$ cells allowed the $HPGRT^{-}$ cells to proliferate despite aminopetrin treatment. If the transformed DNA was isolated from $HPGRT^{-}$ cells or pre-treated with DNase the proliferation phenotype was not observed thus providing the first evidence that gene transfer in mammalian cells could be used to

correct genetic defects in mammalian cells. However, this study involved the introduction of all the DNA content from donor cells and so was not gene specific.

Viruses deliver genetic information into cells but it would be necessary to remove pathogenic genes and replace them with therapeutic genes if viruses were to be useful for gene therapy. However, in 1975 and with the belief that Shope papilloma virus encodes an arginase that could be useful in the treatment of arginase deficiency in man (151), Terheggen et al., (152) conducted the first direct human gene therapy trial using wild-type Shope papilloma virus to treat arginase deficiency. Unfortunately the trial was unsuccessful and sequencing later revealed the Shope papilloma virus does not encode an arginase.

In order to achieve gene specific gene transfer it was vital to produce recombinant DNA molecules carrying the specific gene of interest and elements required for the efficient transcription and translation of the introduced DNA. This was made possible by discoveries in the 1960's that advanced our ability of manipulate DNA giving rise to the field of genetic engineering. The first major breakthrough came when Gellert first described that DNA ends could be joined together using *Escherichia coli* (*E. coli*) extracts (153). The same lab then purified the enzyme responsible (154)- now known as DNA ligase. The second major breakthrough in genetic engineering came with the discovery of restriction enzymes. This discovery was preceded by work from Luria and Human (155) and Bertani and Weigle (156) who showed that bacteriophage infection was restricted in certain bacterial strains but not others. Arber and Dussoix (157, 158) showed that this restriction was due to degradation of bacteriophage DNA by the host cell. Linn and Arber (159) found

this degradation was initiated by restriction enzymes- so called because they restricted bacteriophage infection. Restriction enzymes cleave DNA at specific sequence motifs called restriction sites. The discoveries of DNA ligases and restriction enzymes allowed the cutting and pasting of different DNA sequences to produce recombinant DNA molecules and this technology was used by Cohen et al., (160) to produce the first biologically functional plasmid that afforded transformed *E. coli* antibiotic resistance.

Maniatis et al., (161) used the discoveries of restriction enzymes and DNA ligase to isolate and clone the β-globin gene from rabbit genomic DNA libraries. Genomic DNA libraries contain untranslated intron sequences as well as protein-coding exon sequences. Wilson et al., (162, 163) later used reverse transcriptase- an RNA-dependent DNA polymerase- to produce complementary DNA (cDNA) of mature human globin mRNAs (therefore lacking intron sequences) and inserted these into plasmids for sequencing and characterisation studies of the human globin genes (162, 163). Green et al., (164) showed β-globin expression after transfecting Wilsons β-globin plasmid into HeLa cells with cis- or trans-acting transcriptional regulatory factors from adenovirus and herepesvirus.

The potential for gene therapy *in vivo* was demonstrated by Cline et al., (165) who showed that *ex vivo* gene transfer of mouse bone marrow resulted in stable gene expression after the modified bone marrow was transplanted into irradiated mice. In these studies the gene transferred conferred resistance to methotrexate, an anti-cancer drug that inhibits dihydrofolate reductase preventing *de novo* synthesis of thymidine so affecting DNA synthesis and preventing cell growth and proliferation.

In the presence of methotrexate the genetically modified resistant cells had a selective advantage and were the majority population in the reconstituted bone marrow. Cline applied to the UCLA Human Subjects committee for permission to test the same approach of *ex vivo* gene transfer of bone marrow cells followed by bone marrow transplants of the cells in patients with β-thalassemia (a genetic disorder caused by mutations in the β-globin gene) with no adverse events or clinical benefit seen in the two patients enrolled. Despite applying to the UCLA Human Subjects committee for permission Cline commenced the trial without the board's approval (who had concerns about the potential efficacy of the trial) and attracted widespread criticism for this failing and for enrolling the two patients from Italy and Israel, countries with no specific regulations for gene therapy trials at the time (166). Cline used the calcium phosphate transfection method for gene transfer and the lack of efficacy in the infamous clinical trial highlighted the need for improved gene delivery technologies particularly when corrected cells have no selective advantage. Both viral and non-viral vectors have been developed for gene therapy and the main properties of commonly used vectors have been summarised in Table 1.2.

	Gammaretrovirus	Lentivirus	Adenovirus	AAV	Non-viral
Nucleic acid	RNA	RNA	DNA	DNA	RNA and DNA
Packaging capacity	~9kb	~10kb	~30kb	4.6kb	Unlimited
Integration into host genome	Yes	Yes	No	Rarely	Rarely
Duration of transgene expression	Long	Long	Transient	Long in post-mitotic tissues	Transient
Transduction of post-mitotic cells	-	+	+++	++	++
Pre-existing host immunity	No	No	Yes	Yes	No
Immunogenicity	++	++	+++	+	-
Safety concerns	Insertional mutagenesis	Insertional mutagenesis	Inflammatory response	Low risk of insertional mutagenesis	-
Germ-line transmission	-/+	+	-	-/+	-

Table 1.2. Properties of commonly used gene therapy vectors.

Adapted from Nathwani et al., (167). AAV, adeno-associated virus; -, zero; -/+, equivocal; +, low; ++, moderate; +++, high.

Viruses, as naturally occurring gene delivery vehicles, presented as obvious candidates for development. Goff and Berg (168) produced recombinant simian virus 40 (SV40) viruses containing λ phage sequences in place of 2kb of DNA from the late region of SV40 genome and this recombinant SV40 transduced cultured monkey cells. Mulligan et al., (169) later showed that replacing the VP1 capsid gene in wild-type SV40 with the rabbit β-globin cDNA produced recombinant SV40 virions that induced β-globin expression in cultured monkey kidney cells. Further publications showed that non-viral genes could also be expressed from recombinant retrovirus (170), adenovirus (171) and AAV (172) vectors- now the three major classes of viral vectors. Advances have been made to improve the safety profile of viral vectors including the removal of pathogenic genes and splitting viral genomes to produce replication defective virions (173, 174). Additionally, using foreign envelopes to coat viruses has allowed re-targeting of virions to non-natural target tissues increasing their utility for gene therapy (175, 176).

A number of non-viral methods and vectors for gene delivery were also developed. These are simple containing only a few components and are generally less immunogenic than viral vectors. Non-viral gene delivery methods can be physical or chemical. Physical methods include the use of ultrasound (177) or electrical currents (178) to temporarily increase the permeability of target cells (sonoporation and electroporation respectively), direct injection of DNA into single cells (179), ballistic propulsion of DNA-coated particles whose momentum allows penetration of cells (180) and hydrodynamic gene delivery involving the rapid injection (~5-7

seconds) of a large volume of DNA solution (8-10% of body weight) (181-183). However the physical methods are typically inefficient *in vivo* and difficult to translate to man. Chemical gene delivery vectors are therefore the most widely studied and developed non-viral method usually employing a cationic species to complex with anionic nucleic acid forming complexes for gene delivery. One of the earliest and still widely used involve calcium phosphate co-precipitation of DNA (184) which was more efficient than complexes of the polycation diethylaminoethyl-dextran with plasmid DNA (185) which preceded the calcium phosphate method. Of the polycations polyethylenimine (PEI) is the most utilised *in vitro* and *in vivo* showing relatively high transfection efficiency (186) thought to be in part due to the proton-sponge effect (187) where PEI's ability to buffer at low pH results in ion and water influx when inside the endosomal compartment causing osmotic swelling and endosomal rupture releasing the entrapped nucleic acid into the cytoplasm.

Cationic lipid species formulated into liposomes have also been extensively studied and are now among one of the most widely used non-viral vectors. Liposomes for gene delivery was first described in 1980 by Fraley et al., (188) and Wong et al., (189) who showed efficient transfection comparable to the co-precipitation method whilst Schaefer-Ridder et al., (190) showed stable integration of the selectable thymidine kinase gene in deficient mouse cells using liposomes. Felgner et al., (191) later showed that cationic liposomes formulated using only DOTMA lipid (N-[1- (2,3-dioleyloxy)propyl]-N,N,N-trimethlylammonium chloride) resulted in efficient transfection superior to calcium phosphate and diethylaminoethyl-dextran

methods in at least COS-7 and CV1 cell lines. A number of lipids have since been assessed for their ability to mediate efficient transgene expression. Later, the addition of cationic polymers was shown to enhance liposome-mediated gene delivery (192). Further attempts at improving non-viral formulations have been made with the addition of components to improve bioavailability *in vivo* through shielding of complexes using polyethyleneglycols (193), to enhance cell-specific targeting using targeting moieties (194, 195), to aid endosomal escape using fusogenic lipids (196, 197) or pH sensitive polymers that utilise the proton-sponge effect (187) and to improve nuclear entry using nuclear targeting sequences (198, 199) or nuclear localisation signal containing peptides (200-202).

The improvements to both viral and non-viral vectors led to a flurry of clinical trials being initiated in the 1990s- a so called boom period for gene therapy research. The first FDA approved gene therapy clinical trial was a study in which two patients with adenosine deaminase (ADA) deficiency were treated by *ex vivo* gene transfer of their T-cells with a gamma-retroviral vector encoding the ADA gene (203). The first patient to be treated was Ashanti DeSilva who showed temporary improvement in her condition no longer necessitating relative isolation and able to attend school without developing more infections than her classmates or siblings. Improvements in the second patient were also temporary and also more modest. It is important to note that both patients remained on enzyme replacement therapy during the trial leading to some debate to the efficacy of the gene therapy given. By the end of the decade none of the clinical trials showed clear long-lasting efficacy of a gene therapy protocol and the decade ended with the tragic death of Jesse Gelsinger in

1999 during a clinical trial for the treatment of ornithine transcarbamylase deficiency at the University of Pennsylvania (204). Jesse's death resulted from multi-organ failure due to the high dose of adenovirus administered inciting a substantial immune response. His death was the first to be attributed directly to a gene therapy product.

More recently gene therapy research has experienced a revival with reports of long-term clinical benefit in the treatment of a number of diseases including X-linked severe combined immunodeficiency (X-SCID) (205, 206), ADA deficiency (207, 208), haemophilia B (209), Leber congenital amaurosis (210), metachromatic leukodystrophy (211), Wiskott-Aldrich syndrome (212) and choroideremia (213). Gene therapy for lipoprotein lipase deficiency using an AAV vector has also been shown to be efficacious (214) and recently approved for clinical use by the European Medicines Agency (215) making it the first gene therapy medicine to be approved in Europe.

1.2.2 AIRWAY GENE THERAPY

The primary target for PCD gene therapy is to correct the airway disease which is the main cause of morbidity from PCD. A gene therapy approach for lung disorders has been a goal since the gene involved in CF was described and cloned (216), particularly given the accessibility of the airways for vector delivery. Proof-of-principle studies *in vitro* and in CF mice using viral and non-viral vectors soon followed (217-220) as well as a number of human clinical trials (221-227) but clinically viable gene therapy treatments for lung disorders have yet to materialise. This lack of clinical efficacy has been in large part due to the barriers the respiratory

system has evolved to clear foreign particles- not surprising given the systems exposure to the environment.

Mucus secreted by goblet cells and the mucous cells of submucosal glands act as one of the main barriers to respiratory infection. The mucus has a complex composition including cytokines, antioxidant proteins, lysozymes, defensins and importantly mucins which are large, highly charged and heavily glycosylated glycoproteins that form and re-form cross-links to give mucus it's highly tangled and dynamic structure (228). Airway mucus traps pathogens and inhaled particles thus hindering their ability to reach the apical surface of airway epithelial cells, a pre-requisite for gene transfer and infection. Mucociliary clearance, disrupted in PCD, then results in the removal of these particulates from the airway.

The innate immune system is another important barrier to respiratory cell infection. Resident airway macrophages internalize and degrade any pathogens trapped by the mucus (229). In addition, airway epithelial cells can recognize pathogens through toll-like receptors which then initiate the immune responses of the respiratory epithelium (230). Adaptive immune responses can also prevent repeated delivery of vectors which is necessary in the context of PCD as life-long treatment will be necessary given that a stem cell population that can be efficiently targeted has not been described.

In order to realise the promise of gene therapy for respiratory disease vectors capable of efficiently overcoming the extra- and intra-cellular barriers to gene transfer of the airway epithelium are required. In the case of PCD the vectors must also target ciliated cells and show low immunogenicity to avoid exacerbating the

characteristic inflammatory lung disease seen in PCD. The ability for repeated dosing without diminishing transfection/transduction efficiency is also required given that lifelong treatment would be necessary. These requirements are identical to those reported for CF gene therapy vectors and so a lot can be learnt from this field.

Viral vectors

Both viral and non-viral vectors have been investigated for CF gene therapy with viral vectors typically being more efficient, not surprising given that they have evolved to efficiently overcome the extra- and intra-cellular barriers to gene transfer. Viruses that naturally target the airway epithelium such as adenovirus, adeno-associated virus (AAV), parainfluenza virus and respiratory syncytial virus (RSV) have been assessed for airway gene transfer as well as lentiviral vectors which have been re-targeted through the use of envelope proteins from airway targeting viruses such as filoviruses, influenza virus, baculovirus and Sendai virus (SeV). Of these vectors adenovirus and AAV vectors have made it to clinical trials.

Despite showing early promise in pre-clinical models and being well tolerated at low and medium doses in humans, adenovirus vectors have, in clinical trials, shown transient expression, variable gene transfer efficiencies and diminished expression following repeated delivery with neutralising antibodies against the vector and adenovirus-specific T-cells being reported (231-239).

Adenoviruses are non-enveloped, double-stranded DNA viruses with numerous serotypes of which 2 and 5 have been assessed for respiratory gene transfer.

Adenovirus vectors do not integrate into the genome of the host thus negating the risk of insertional mutagenesis, the implications of which are unknown in the context of airway gene delivery given the terminally differentiated nature of the target cells versus the rapidly dividing nature of bone marrow cells in which insertional mutagenesis has been shown to lead to leukaemia (240).

Uptake of adenovirus vectors is by endocytosis following binding of viral particles to the coxsackievirus and adenovirus receptor (CAR) (241, 242) which are mainly expressed on the basolateral surface of polarised airway epithelial cells (243) making them inaccessible to vectors delivered by inhalation, the favoured route for respiratory gene therapy, as tight junctions between adjacent cells prevents access to the basolateral surface. This helps explain the inefficient gene transfer observed in clinical trials and transduction efficiency with adenovirus vectors can be improved through opening of tight junctions by the use of pharmacological agents such as sodium caprate (244), perfluorochemicals (245) and lysophosphatidylcholine (LPC) (246). Whether the use of such agents in patients with bacterial colonisation (as is the case in CF and PCD) is wise given the potential risk of systemic infection remains controversial.

AAV vectors have been the only other viral vector used in clinical trials for airway gene therapy. These are single-stranded DNA viruses and have not been associated with any human pathology. The wild-type virus integrates into human chromosome 19 but recombinant AAV (rAAV) vectors used for gene therapy are thought to integrate only rarely and instead remain episomal in the nucleus upon cellular uptake (247). A variety of serotypes of AAV have been described for transduction of

airway epithelia although species-specific differences have been observed (248, 249). In clinical trials rAAV derived from AAV2 has been commonly used and generally well tolerated in safety studies (224, 227). However, when utilised for CF gene therapy no significant improvement in lung function was observed in a well powered efficacy trial (226). Furthermore, virus shedding, production of neutralising antibodies against the vector and diminished transgene expression have been observed following repeated administration (226, 227). To date all CF clinical trials utilising AAV employed rAAV2 with an AAV2 capsid and were led by Targeted Genetics, Corp. using the TgAAV-CFTR vector in which CFTR expression is driven by a weak promoter found in the AAV long terminal repeat (LTR). The weak promoter activity combined with data showing that AAV2 only poorly transduces human airway cells could explain the lack of clinical efficacy. In the case of CF gene therapy the use of the weak AAV LTR promoter is necessary because AAV has a packaging capacity of around 4.6kb and so can carry the CFTR ORF (4.4kb) only in the absence of a strong exogenous promoter. The majority of PCD causing gene ORFs are significantly smaller than the CFTR ORF and so could be incorporated into rAAV vectors with a strong exogenous promoter.

Attempts have been made to address the poor transduction of human airway epithelial cells by rAAV2 vectors containing AAV2 capsid proteins by pseudotyping rAAV2-based vectors with capsids from AAV serotypes 1 and 6 (248-250). In addition to using naturally occurring capsids a directed evolution approach using random mutagenesis of the capsid encoding *cap* gene (251) has been used to generate novel capsids and rAAV vectors with enhanced transduction of the human

airway epithelium *in vitro (252)*. Whilst these advances are promising, they remain untested in clinical trials and do not address issues with diminished transgene expression following repeated administration.

Whilst other viral vectors have not been tested in clinical airway gene delivery studies, pre-clinical studies testing influenza (253) and parainfluenza (254) viruses have shown efficient apical transduction of human airway epithelial cells with these viruses. More promising still, in the context of PCD gene therapy, RSV has been shown to specifically target ciliated cells (255, 256). However, only SeV and lentiviral vectors have been tested *in vivo*.

SeV, otherwise known as murine parainfluenza virus type 1, is a respiratory pathogen that is endemic in rodents and belongs to the *Paramyxoviridae* family of viruses that includes human parainfluenza virus types 1 and 3. SeV is a single stranded ribonucleic acid (RNA) virus whose genome consists of a single stranded negative-sense RNA of around 15-16kb giving it a potentially large packaging capacity (257). The development of a SeV where the fusion (F) protein is provided *in trans* rather than being part of the viral genome results in viral particles capable of efficiently infecting airway epithelial cells but give rise to progeny that are incapable of further infection due to the need for the F protein in fusion of the virus to the cell membrane (258). This transmission defective virus was capable of efficiently transducing mouse airway epithelial cells *in vivo (259)* and importantly a non-natural host- the sheep airway epithelium *in vivo (260)*. Human airway epithelial cells were also efficiently transduced using the SeV vector (259). However, gene expression was found to be transient and repeated delivery of the

vector *in vivo* resulted in diminished transgene expression thus limiting the suitability of SeV for PCD gene therapy (260).

Lentiviruses are single-stranded, positive-sense RNA viruses with a genome of around 9.7kb, belong to the *Retroviridae* family and are capable of transducing non-dividing cells making them suitable for terminally differentiated airway epithelial cells. Reverse transcriptase and integrase proteins expressed by lentiviruses result in integration of the lentiviral genome into host chromosomes thus providing stable and sustained transgene expression.

Lentiviruses assessed for gene therapy include human immunodeficiency virus (HIV), feline immunodeficiency virus (FIV) simian immunodeficiency virus (SIV) and equine infectious anaemia virus (EIAV). These viruses naturally infect blood cells but have been re-targeted through the use of envelope proteins from other viruses- a process known as pseudotyping. The vesicular stomatitis virus (VSV) G glycoprotein (VSV-G) has been used for pseudotyping due to its broad tropism. HIV type 1 (HIV-1) pseudotyped with VSV-G has been used successfully in clinical settings for the treatment of metachromatic leukodystrophy (211) and Wiskott-Aldrich syndrome (212) by *ex vivo* correction of haematopoietic stem cells followed by re-infusion of the corrected cells into patients.

VSV-G pseudotyped HIV-1 and FIV vectors have been assessed for airway gene delivery but efficient gene transfer necessitated the disruption of tight junctions between airway epithelial cells thus allowing virus access to the basolateral cell surface and also underlying basal progenitor cells (261, 262). The poor efficiency following delivery to the apical surface of the airway epithelium is unsurprising

given the VSV infects the basolateral surface of polarised cells (263)- not accessible in the absence of tight junction disruption. Disruption of tight junction by pre-treatment with agents such as LPC (264) or ethyleneglycoltetraacetic acid (EGTA) (262) followed by VSV-G pseudotyped lentiviral gene transfer resulted in stable and persistent transgene expression in mice with evidence that progenitor populations had been transduced. In addition, a single dose was found sufficient to induce transgene expression that persisted for the life-time of the mice, although the proportion of cells expressing the introduced transgene did decline over time (264). Encouragingly, VSV-G pseudotyped HIV-1 introduced following pre-treatment with LPC has been shown to efficiently transduce lungs of the marmoset (265)- a non-human primate- the lungs of whom are far closer related to that of humans.

Despite the encouraging results with VSV-G pseudotyped lentiviral vectors, whether disruption of tight junctions is wise in the lungs of patients in whom bacterial colonisation is commonplace remains controversial given the potential risk for systemic disease. As such, efforts have been made to pseudotype lentiviral vectors with glycoproteins from organisms that naturally infect the apical surface of airway epithelial cells. To this end FIV has been pseudotyped with GP64, an envelope glycoprotein from *Autographa californica* that shares sequence identity with the influenza D GP75 glycoprotein and this novel vector has been shown, in human cell cultures and mice, to efficiently transduce the apical surface of airway epithelial cells. Transgene expression was shown to persist for over 11 months (266) and repeated administration did not diminish transgene expression (267). Buckley et

al., (268) further showed that intra-amniotic administration of GP64 pseudotpyed HIV resulted in efficient transduction of airway epithelia with evidence that progenitor/stem-cell populations had been transduced.

Lentivirus pseudotyped with i) the glycoprotein envelope of Ebola Zaire virus (269), ii) hemagglutinin-neuraminidase (HN) and F proteins from SeV (270-272) and iii) HA from fowl plague virus (H7) together with the fowl plague virus M2 proton channel protein and influenza H1N1 neuraminidase (NA) (273, 274) were all shown to efficiently transduce mice airway epithelia with stable and persistent transgene expression, as seen with other lentiviral vectors described above, again indicating that some progenitor population had been transduced.

Lentiviral based vectors thus fulfil most of the requirements for the ideal PCD gene therapy vector in that ciliated cells are transduced efficiently and repeated delivery is feasible without inducing a significant immune response. However, the limited packaging capacity of lentiviral vectors prevents *DNAH5*, *DNAH11* and *HYDIN* ORFs (13.9kb, 13.6kb and 15.4kb respectively) from being packaged and delivered with lentiviral vectors. This is a particular concern considering that *DNAH5* is the most common cause of PCD, accounting for around 1 in 4 patients and the three large genes together account for 21-35% of all PCD patients (Table 1.1). Alternative non-viral vectors have been developed for airway gene transfer and have an unlimited packaging capacity, are well tolerated following repeated delivery and can be easily produced in large quantities.

Non-viral vectors

Typical non-viral formulations contain a cationic component, usually a liposome or polymer, complexed to anionic plasmid DNA containing the transgene and necessary regulatory elements. The cationic and anionic components interact due to their opposing charges resulting in condensation of the plasmid DNA component and the formation of nanocomplexes with a cationic zeta potential. The nanocomplex interacts with the anionic cell surface and is taken up typically by endocytosis. The plasmid DNA cargo must then undergo endosomal escape to evade degradation in lysosomes and then be taken up into the nucleus where the transgene can be transcribed and then translated in the cytoplasm. Non-viral vectors are generally less efficient than viral vectors as they typically lack specific components to help with cell entry, endosomal escape (not a problem for viruses that undergo fusion), trafficking through the cytoplasm and nuclear uptake (Figure 1.3). Viruses in contrast have developed specific strategies and proteins to overcome these barriers to gene transfer. Nevertheless, the advantages of low immunogenicity and an unlimited packaging capacity have resulted in a flurry of studies assessing non-viral vectors for CF airway gene delivery.

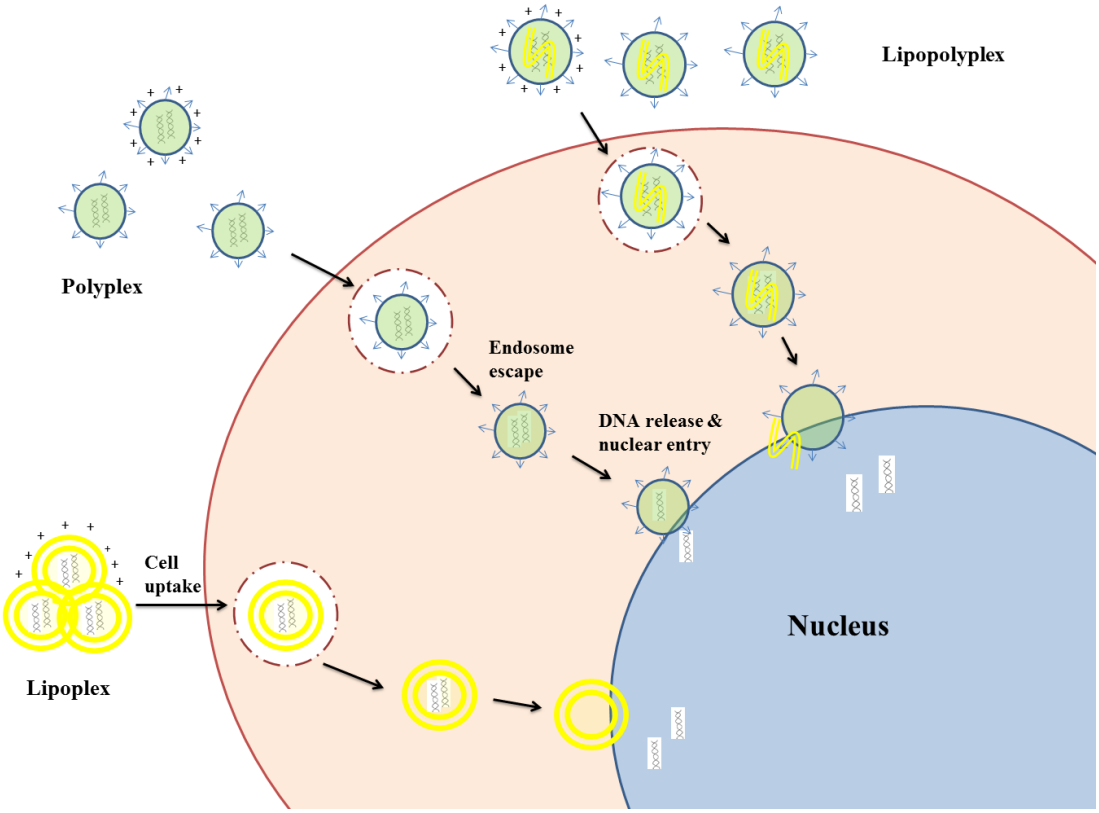

Figure 1.3. Schematic of non-viral gene transfer

A number of non-viral vector formulations have been assessed in clinical trials. The earliest airway gene delivery clinical trials involved the use of GL67A/DOPE (Genzyme lipid 67A/1,2-Dioleoyl-sn-Glycero-3-Phosphoethanolamine) (275), DC-Chol/DOPE (3β-[N- (N',N'-Dimethylaminoethane)carbamoyl]cholesterol/DOPE) (276, 277) or DOTAP (1,2-Dioleoyl-3-trimethylammonium-propane) (223) liposomes complexed with plasmid containing CFTR cDNA. These early clinical trials were single-dose safety and efficacy studies with the formulations administered to patient nostrils as a surrogate to the lungs and in all cases the non-viral vectors were well tolerated. In addition, partial but transient correction of the electrophysiological defects seen in CF was observed so paving the way for further clinical studies (223, 275-277).

Alton et al., (222) reported mild influenza-like symptoms that returned to normal 30 hours following pulmonary administration of GL67A/DOPE/plasmid DNA formulation. In addition the inflammatory markers C-reactive protein and IL-6 were elevated relative to placebo following pulmonary administration of GL67A/DOPE/plasmid DNA vector. This elevation was transient returning to baseline by the time of the next measurement at day 6 and was not observed following nasal administration of vector. As such, the vector was considered to be well tolerated. With regards to efficacy vector-specific DNA was found in all active-group patients at day 2 however no vector-specific mRNA could be detected despite chloride channel function being restored to around 25% of normal values in lungs of patients in the active group. In addition patients receiving the active drug showed a significant reduction in bacterial adherence *ex vivo* although no change in

mucociliary clearance was observed *in vivo*. This study thus showed good tolerance of the non-viral vector following a single administration to the lungs but efficiency of transfection was not sufficient to produce a clinical benefit to patients.

Repeated administration could hypothetically produce cumulative levels of transgene to be expressed and so potentially result in clinical efficacy. Prior to commencing clinical studies the UK CF Gene Therapy Consortium assessed repeated delivery of GL67A/DOPE/plasmid DNA complexes in pre-clinical animal models. Encouragingly, repeated administration did not produce increased toxicity relative to a single administration in mice (278) and sheep (279). In mice, repeated administration (one dose per fortnight – 12 doses total) did not result in accumulation of vector specific DNA or mRNA but diminished expression following repeated delivery was reassuringly not an issue (278). These findings also held true following repeated administration in sheep (one dose every four weeks – 9 doses total) (279). Similarly, in a small human clinical trial (12 patients total - 10 in active group, 2 in placebo group), Hyde et al., (280) found no accumulation of vector specific DNA or mRNA or increase in toxicity following repeated administration of DC-Chol/DOPE/plasmid DNA complexes to the nostrils of CF patients (one dose every four weeks – 3 doses total). In this study partial Cl^- ion transport correction was seen in some patients and importantly repeated administration did not result in diminished transgene expression.

Despite the lack of accumulated vector specific DNA or mRNA following repeated delivery, the lack of increased toxicity and partial Cl^- ion transport correction has led the UK CF Gene Therapy Consortium to commence a double-blind, placebo

controlled clinical trial sufficiently powered to detect clinical improvements to assess the safety and efficacy of repeated administration of GL67A/DOPE/plasmid DNA complexes for the respiratory treatment of CF (281). Whether this approach yields clinical improvements remains to be seen but it is clear that there is significant room for improvement of non-viral gene delivery formulations for airway gene transfer particularly for PCD gene therapy where the transfection efficiency required to correct the mucociliary clearance defect is higher than that for CF (25-40% of cells corrected for CF (282) vs 80-100% of cells corrected for PCD (283)). As such, improvements to non-viral vector technologies are clearly necessary for airway gene transfer to provide clinical benefit particularly when correcting defects caused by mutations in large genes.

In order to improve targeting and cell uptake of non-viral gene transfer agents techniques such as magnetofection (where plasmid DNA is coupled to magnetic particles making the DNA responsive to magnetic fields) and sonoporation (where ultrasound is used temporarily increase the permeability of target issues) have been assessed for the enhancement of transgene delivery using non-viral vectors but both techniques fared poorly *in vivo* (284, 285).

Alternatively, targeting ligands have also been used to target non-viral gene transfer agents to airway epithelial cells. Ziady et al., (286) used plasmid DNA complexed with a covalent conjugate containing cationic poly-L-lysine and a 17 amino acid peptide ligand to the serpin-enzyme complex receptor (expressed on the apical surface of airway epithelial cells) and found that the novel

nanocomplexes were capable of correcting the electrophysiological defect seen in CF mice.

In a similar approach, Tagalakis et al., (287) developed targeted nanocomplexes through the use of a 7 amino acid peptide sequence identified in phage display studies aimed at finding sequences targeting the apical surface airway epithelial cells (288). The final sequence SERSMNF was found to have close homology to parts of receptor targeting proteins from the respiratory pathogens rhinovirus (SDRSMN) and *Listeria monocytogenes* (ERSMNF) which target ICAM-1 and E-cadherin receptors respectively. A short peptide sequence (P) containing the targeting sequence conjugated to a K_{16} DNA binding domain was complexed together with a cationic liposome (L) and anionic plasmid DNA (D) to produce small cationic nanocomplexes that can be nebulised (289) and efficiently transfects airway epithelial cells with low toxicity in mice (287) and importantly pigs (290) whose lung physiology is closer to that of humans. As well as containing the receptor-targeting sequence, which aids in cell uptake, the DOPE lipid contained within the liposome component of the LPD complex is known to aid in endosomal escape and plasmid DNA release (291).

The polymer PEI has also been complexed with DNA and shown to aid endosomal escape and plasmid DNA release through a proposed “proton-sponge” effect (187) where unprotonated amines from PEI become protonated in the acidic environment of lysosomes resulting in an influx of Cl^- ions and water. This influx results in osmotic swelling and eventual rupture of the lysosomal membrane and the release of its contents. PEI based complexes have been assessed for airway

gene delivery in studies by the UK Cystic Fibrosis Gene Therapy Consortium comparing a variety of non-viral gene delivery agents (292) including branched PEI (25kDa) and GL67A/DOPE liposome with GL67A/DOPE found to be most efficient and so moved forward to clinical trials.

In addition to optimising the cationic lipid and polymer components of non-viral vectors for airway gene transfer the nucleic acid component has also been improved upon. Choice of promoter element is known to have an effect on both the levels and persistence of transgene expression in a tissue specific manner (293-295). Comparing the constitutive viral promoters from cytomegalovirus (CMV), Rous sarcoma virus and SV40 to human polyubiquitin C (UbC) and elongation factor 1 alpha (EF1α) gene promoters in the context of airway transgene expression Gill et al., (296) found the UbC and EF1α promoters provided greater persistence of transgene expression whilst the viral promoters provided higher initial levels of transgene expression. Addition of human CMV enhancer sequences to the UbC and EF1α promoters was shown to increase the initial levels of transgene expression whilst complete removal of CpG motifs resulted in further enhancement to transgene expression and persistence (297). CpG motifs induce an immune response in vertebrates (298-301) via toll-like receptor 9 (302) and so in addition to enhancing transgene expression and persistence their removal reduced the neutrophil count and levels of the inflammatory cytokines interleukin-12 (IL-12), tumor necrosis factor α (TNFα) and interferon γ (IFNγ) in bronchoalveolar lavage fluid (BALF) of transfected mice (297).

The use of CpG-free sequences reduces the inflammatory response to airway gene delivery by non-viral vectors (297, 303), an important advance given that airway inflammation is a characteristic of PCD that should not be exacerbated by gene delivery formulations. A number of studies have also implicated CpG motifs in transgene silencing (297, 304-306) but this remains controversial (307). Assessing an alternative hypothesis Lu et al., (308) found that the plasmid backbone sequence, typically rich in CpG motifs, when placed within the 3' untranslated region of a eukaryotic expression cassette yielded persistent transgene expression as did vectors devoid of a bacterial backbone (minicircle DNA). The group went on to show that the size of the backbone and not its sequence was responsible for producing a potent negative effect on transgene persistence (308). In the context of gene therapy, minicircles have been shown to exhibit sustained transgene expression to plasmids in a variety of organ systems *in vivo* including the liver (309, 310), heart (311, 312) and skeletal muscle (312) but minicircles have not been assessed in the context of airway gene delivery.

1.2.3 PCD GENE THERAPY

Research into gene therapy for CF has advanced airway gene delivery. Ciliated cells of the airway epithelium are the target cells for PCD gene therapy and also thought to be the target for CF gene therapy, although this remains controversial (313). As such, many of the advances in CF gene therapy are applicable to PCD but the latter has additional challenges associated. Genetic heterogeneity dictates that no single gene therapy product is likely to treat all forms of PCD. Chhin et al., (314) established proof-of-principle that gene therapy could be used to correct the cilia

motility and cilia ultrastructural defect in airway epithelial cells of a PCD patient with *DNAI1* mutations. Cells were corrected *ex vivo* using a lentiviral vector to transduce de-differentiated human airway epithelial cells which were then re-differentiated to ciliated cells using Jorissen's culture method (315). This method produces spheres of ciliated cells rather than the mucociliary pseudostratified airway epithelium seen *in vivo* so measurement of mucociliary clearance was not possible.

Using de-differentiated airway tissue followed by lentiviral gene transfer and re-differentiation of airway cells with an air-liquid interface (ALI) culture system that generates a pseudostratified mucociliary airway epithelium Ostrowski et al., (283) showed recovery of cilia motility in cells from their *Dnaic1* conditional knock-out mouse (316). PCD pathology (mucus accumulation, infection and inflammation) was evident in the nasal cavity but not the trachea of *Dnaic1* conditional knock-out mice (316). Gene transfer was shown to be less efficient in the nasal cavity of PCD mice than in control animals whilst no significant difference in transduction efficiency was seen in the trachea where PCD pathology was not evident (283) highlighting a need for administration of a gene therapy treatment before significant disease pathology develops. To this end, intra-amniotic or neonatal administration of vector may offer the dual benefits of transducing an undamaged lung as well as enhanced transduction relative to adult lung gene transfer (268).

Until recently the levels of correction required to restore mucociliary clearance in PCD was unknown. Using the conditional *Dnaic1* mouse model Ostrowski et al., (283) used varying doses of tamoxifen to titrate *Dnaic1* expression and found

around 20% of normal *Dnaic1* expression restored mucociliary transport to 33-66% of the wild-type clearance rate. Whether this will be sufficient to prevent PCD pathology or reduce its severity remains to be seen but the group also showed that around 40% of normal *Dnaic1* expression completely restored normal rates of mucociliary transport (283). Whether this finding holds true for PCD caused by *DNAH5* mutations has not been assessed but given both *DNAI1* and *DNAH5* mutations produce the same ultra-structural defect (absence of ODA) it is likely that the levels of correction required for both are similar.

For PCD gene therapy targeting patients with *DNAH5* gene mutations non-viral vectors are required due to the size of the transgene and the need for repeated administration. The ideal vector needs to also transfect the apical surface of the airway epithelium and likely needs to transfect at least 40% of ciliated cells if not more. These conditions rule out the use of established viral vectors such as lentiviruses which are unable to package the DNAH5 transgene or adenoviruses which are highly immunogenic and so do not allow repeat administration.

In order to assess PCD gene therapy targeting patients with *DNAH5* gene mutations suitable models are required and discussed below.

1.3 PCD Disease Models

To better understand disease mechanisms and assess potential therapies it is important to have appropriate models of disease on which to experiment. Models can be broadly categorised as being *in vitro, ex vivo* or *in vivo* with examples including cell lines, tissues obtained from patients or animal models and experiments performed on patients or animal models respectively. With regards to genetic disease human patients and their tissues are natural models. Several breeds of dog have also been identified suffering from PCD (108, 317-320) and are also natural models. Experimenting on human participants and large animal models presents significant ethical and economical barriers particularly with regards to their use at the early stages of drug development. The alternative is to use tissue samples obtained from human and animal models but the rarity of PCD and a lack of genotyping of human patients limit the ability of researchers to obtain suitable *ex vivo* samples. These limitations necessitate the use of gene technologies to produce suitable models of disease.

1.3.1 Technologies for Disease Modelling

Gene technologies used for production of disease models employ either post-transcriptional modification of gene expression (e.g. RNAi; antisense silencing) or alteration of chromosomal DNA (e.g. homology recombination; ZFN; TALENs; CRISPR/Cas).

Antisense Silencing

Antisense compounds are single-stranded molecules that function by complimentary base pairing with mRNA to modulate gene expression by i) blocking

assembly of the translational machinery, ii) promoting RNase H degradation of the RNA or iii) blocking splice acceptor sequences thereby inducing exon skipping. The use of antisense oligonucleotides to inhibit gene expression was first shown to be effective by Zamecnik and Stephenson (321, 322) who found that a 13-mer oligonucleotide sequence complimentary to 13 nucleotides of the 3'- and 5'-terminal repeat sequences of Rous sarcoma virus inhibited virus replication and transformation by inhibiting viral RNA translation. These studies utilised unmodified DNA oligonucleotides and since then a number of more potent single-stranded antisense molecules have been developed (323).

RNA Interference

RNA interference (RNAi) describes a physiological mechanism by which RNA is able to specifically and potently inhibit gene expression post-transcriptionally. That the introduction of exogenous sense-strand RNA could inhibit endogenous transgene expression was first described in 1990 by Napoli et al., (324) and van der Krol et al., (325) in two back-to-back papers in the journal *Plant Cell*. Both groups attempted to over-express chalcone synthase, a pigmentation enzyme, in petunia by introducing a cloned chalcone synthase gene and unexpectedly observed a reduction in endogenous chalcone synthase expression. This phenomenon was termed co-suppression (324) . Further study showed that introduction of a truncated gene sequence also induced co-suppression in tomato plants (326) and von Blokland et al., (327) showed that the mechanism occurred post-transcriptionally and resulted in an increased turnover of mRNA. Co-suppression was also described in non-plant species including the fungus *Neurospora*

crassa (328) (termed quelling by Romano and Macino), the fruit fly *Drosophila Melanogaster (329)* and the nematode worm *Caenorhabditis elegans (330)*.

Guo and Kemphues *(330)* showed that in *Caenorhabditis elegans* sense RNA was able to inhibit *par-1* expression, as did antisense RNA, but silencing mediated by sense RNA relied on homology to the coding region of *par-1* and so involved a different mechanism of gene silencing to antisense RNA. The mechanism by which sense RNA could inhibit gene expression which was termed "RNA-mediated interference" by Mello's group in 1997 (331). A year later the mechanism for RNAi was described by Fire et al., (332) with Andrew Fire and Craig Mello receiving the 2006 Nobel Prize in Physiology and Medicine for their discovery. Fire et al., (332) injected either sense, antisense or both sense and antisense RNA into *Caenorhabditis elegans* in order to inhibit expression of the *unc-22* gene which when reduced was known to produce twitching movements in the worm. Introduction of either sense and/or antisense RNA did not result in twitching but introduction of even a small amount of double-stranded RNA (dsRNA) produced a potent and specific inhibition in *unc-22* and resulted in twitching.

RNAi is an evolutionary conserved pathway and has been found to restrict viral infection in plants (333-335), invertebrates (336-339) and more recently mammals (340, 341). The mechanism of RNAi (Figure 1.4) involves first the cleavage of double stranded RNA into small 21-23 nucleotide double stranded small-interfering RNA (siRNA) molecules that have 2-nucleotide 3' overhangs. This cleavage is performed by Dicer (342), a protein within the RNase III family of nucleases. The antisense strand of the siRNA is then loaded into a multi-protein

complex, the RNA-induced silencing complex (RISC) (343) and guides the specific degradation of target mRNA via complimentary base-pairing. The antisense strand is therefore also known as the guide strand.

Introduction of siRNA into cells and organisms has been a valuable way of inducing specific gene silencing without triggering an IFN response in mammalian cells (344). As such, RNAi has been a useful tool for investigating the function of individual genes. However, the transient nature of siRNA makes its use for the generation of stable disease models unfeasible.

In addition to siRNA, RNAi can be induced by short-hairpin RNAs (shRNAs) (345). shRNAs are based on endogenous small non-coding micro RNA (miRNA) sequences that also make use of the RNAi machinery to effect gene regulation (Figure 1.4). miRNAs are initially long primary transcripts called pri-miRNA that undergo nuclear processing by the RNase III family Drosha enzyme (346) into short ~70-nucleotide stem-loop precursors called pre-miRNA. The pre-miRNAs are then exported from the nucleus into the cytoplasm where they are processed into ~22 nucleotide products by Dicer, incorporated into RISC and go on to mediate targeted gene silencing either through translational repression or mRNA degradation (347). In contrast to siRNA, miRNAs typically contain mismatches to their target sequences. Paddison et al., (345) aimed to re-target miRNA and found that introducing sequences that have perfect homology to the target mRNA sequence into miRNA stems i.e. shRNAs resulted in potent inhibition of transgene expression.

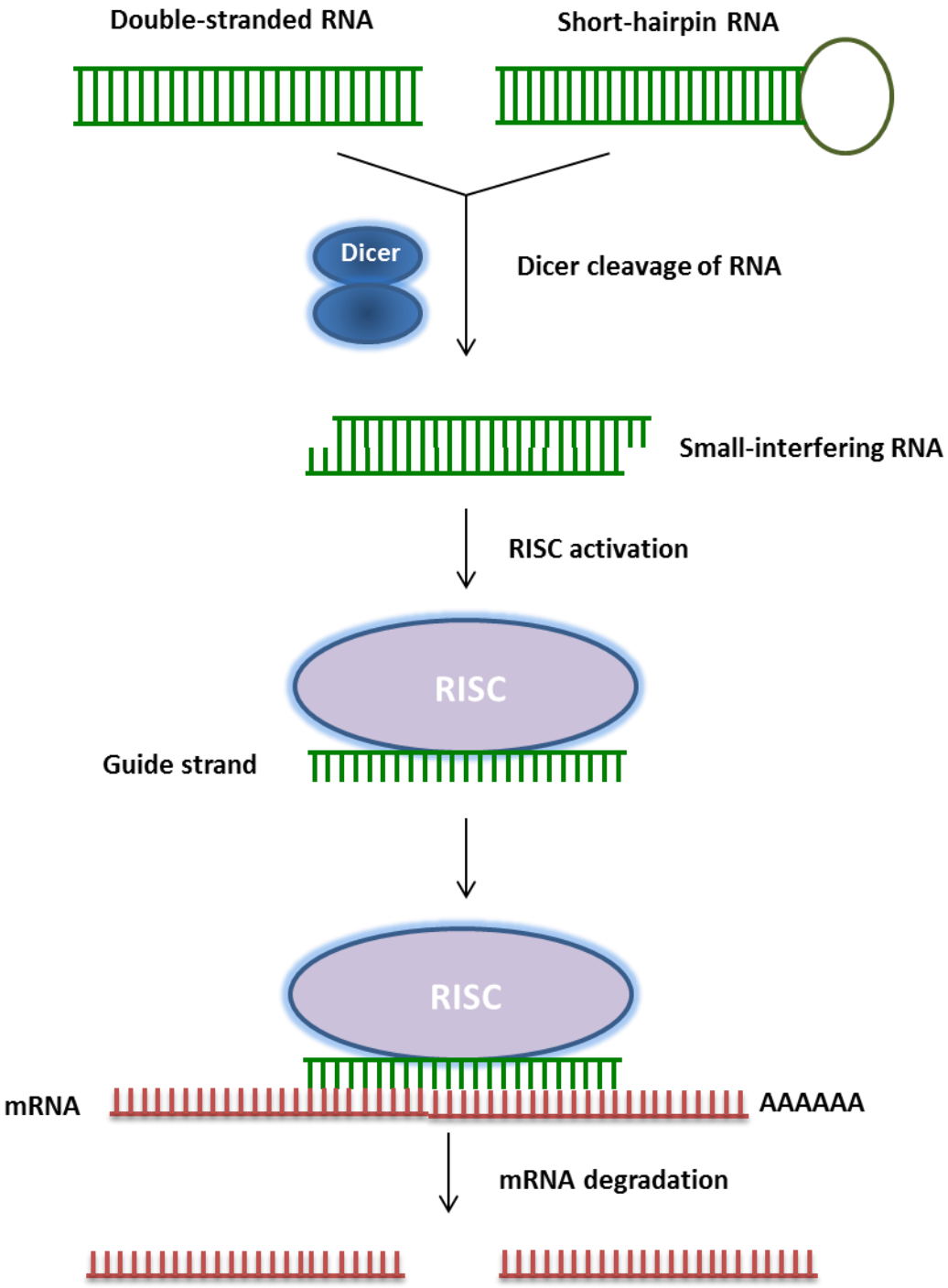

Figure 1.4. RNAi Mechanism

Expression of shRNA in cells can be achieved through the use of plasmid or viral vectors the latter of which can result in integration of the shRNA producing sequence into the host genome. Following transcription of the introduced shRNA producing sequence, the single stranded transcribed RNA is able to form hairpin structures mimicking endogenous pri-miRNA. These products are cleaved into pre-shRNA by Drosha and exported into the cytoplasm where Dicer processes the pre-shRNA into functional siRNA that is incorporated into RISC and produces potent and specific RNAi. The ability to integrate shRNA-encoding DNA sequences into cells has allowed the generation of animal models of disease in which shRNA expression is controlled by an inducible promoter thus allowing temporal control of gene silencing (348). In addition, shRNA-encoding lentiviral vectors have been used to produce stable shRNA expressing cell lines (349, 350) opening the door to the production of *in vitro* cell models of disease.

Chromosomal DNA alterations

The most common method of mutating chromosomal DNA to produce disease models is the use of a chemical mutagen such as ethylmethanesulfonate. This approach introduces random mutations and thus is most applicable to forward genetic screens where a specific phenotype is sought. If mutation of a specific gene is desired approaches utilising homology directed repair (HDR) or non-homologous end joining (NHEJ) are most suitable.

HDR and NHEJ are DNA repair mechanism with the former utilising a donor template (typically the sister chromatid) to repair double-stranded breaks whilst the latter simply joins non-homologous ends together following a double-stranded

break (351). NHEJ produces frame-shift mutations (insertions or deletions) which can lead to loss of protein or the production of a truncated protein. HDR is more accurate at restoring the wild-type sequence and can be used to introduce specific mutations. zinc-finger nucleases (ZFN) (352, 353), transcription activator-like effector nucleases (TALENs) (354-356) and clustered regularly interspaced short palindromic repeats/Cas9 (CRISPR/Cas9) (357-360) systems have been developed to induce double-stranded breaks at specific DNA locations to utilise NHEJ and HDR mechanisms for genetic engineering. Of these methods CRISPR/Cas9 has been shown to be the most efficient as well as being the easiest to manipulate (360).

1.3.2 PCD Disease Models

In Vitro Models

The only cell models for PCD currently described are tissues or cells derived directly from patients and animal models. Ciliated cells obtained through brushings or biopsies of the airway or brain epithelium can be directly manipulated for experimentation e.g. to look at cilia beat frequency (CBF), cilia beat pattern (CBP) and cilia ultrastructure. Alternatively, cells can be expanded in culture and subsequently differentiated to produce ciliated cells and/or a ciliated epithelium (361-363). For recapitulating the airway epithelium culturing on an ALI is best as the resulting epithelium displays the variety of cell types found *in vivo* (i.e. basal cells, mucus-producing goblet cells, non-ciliated columnar cells and ciliated columnar cells) and so would also display the barriers to gene transfer likely to be encountered *in vivo*. However, a major drawback of using primary cells to model PCD is their limited growth and differentiation capacity. Also, given that PCD is rare

and the specific gene defects rarer still, obtaining suitable samples for the purposes of developing gene therapy treatments is fraught with difficulty.

In Vivo Models

A variety of organisms have been used as model systems to study PCD including *Chlamydomonas*, zebrafish and mice. *Chlamydomonas* are single cell algae that have been used as a model organism for the study of flagella formation and function for some time due to its speedy life cycle, ease of growth and maintenance, existence of well-established protocols for the production and isolation of flagella mutants (364) and the sequencing of the *Chlamydomonas* genome (365). Proteomic studies suggest that over 650 proteins make up the ciliary axoneme of *Chlamydomonas reinhardtii* (the most widely used species) with 52% of the proteins conserved in humans (366) making findings in *Chlamydomonas* informative on the formation and function of human motile cilia and flagella. Indeed mutations in the IC78 dynein intermediate chain gene of *Chlamydomonas* was known to cause a PCD phenotype of immotile flagella with missing ODA (367) and this finding led to the identification of the human ortholog of IC78 (*DNAI1*) as a PCD causing gene in humans (120).

Most genetic studies with *Chlamydomonas* invoke forward genetic screening typically through the use of ultraviolet (UV) radiation to generate random mutations followed by selecting for immotile clones when flagella formation and function is being assessed (364). Although possible, knockdown of specific genes and so reverse genetic studies, is somewhat inefficient and unreliable in *Chlamydomonas* (368, 369). In contrast zebrafish are highly amenable to gene

knockdown through the use of anti-sense morpholinos injected into the yolks of 1-8 cell stage embryos. Given the ease at which zebrafish can be maintained and manipulated in large numbers Austin-Tse et al., (102) used a morpholino screen to identify *C21orf59* and *CCDC65* as candidate PCD causing genes which they then verified in humans. In zebrafish motile cilia can be found in the olfactory placode, pronephric duct and Kupffer's vesicles with ciliary dyskinesia, kidney cysts, body axis curvature, left-right asymmetry defects and hydrocephalus phenotypes used to identify ciliopathy mutants. Morpholino use in zebrafish for reverse genetics studies have been useful for validating human genetic studies when identifying PCD causing genes (103, 113, 370). In addition to gene-targeted morpholinos, random chemical mutagenesis has also been used to produce zebrafish PCD models (371).

Whilst *Chlamydomonas* and zebrafish offer inexpensive and easy to manipulate *in vivo* systems both are non-mammalian and have no lungs –the organ of most interest with regards to human PCD pathology and treatment. To this end, mammalian mouse models have been used to complement *Chlamydomonas* and zebrafish models for the study of PCD. The majority of PCD mouse models to date have been derived through chemical mutagenesis screens. These screens are phenotype driven and those looking for situs abnormalities resulted in the isolation of the *iv/iv* mouse (372), one of the earliest PCD mouse models. The *iv*/*iv* mouse resulted from a E2271K missense mutation in the *lrd* gene (now known as *Dnahc11)* (373) with confirmation that *Dnahc11* was involved coming in later studies where targeted mutations in the gene resulted in *iv*/*iv* phenotypes (374).

Dnahc11 is the mouse homolog of human *DNAH11*- a known PCD causing gene (90-94, 114).

Further PCD mouse models have been unexpectedly produced following chemical mutagenesis and screening for congenital heart disease with a notable one, with respect to this thesis, being the *Dnahc5* mouse model –the mouse ortholog of human *DNAH5* (375). This model recapitulated the phenotype observed in patients with *DNAH5* mutations such as missing ODA, randomised organ situs and hydrocephalus. Another *Dnahc5* mouse model was produced by Ibañez-Tallon et al., (35) whilst utilising an insertional mutagenesis approach attempting to target an unrelated gene. The resultant transgenic mice again displayed immotile cilia with missing ODA, randomised organ situs and hydrocephalus. However, with the exception of the *Dnahc11* mouse model (93), PCD mouse models produced by targeted deletions or random chemical mutagenesis of ciliary genes usually result in severe developmental defects including cardiac abnormalities and severe hydrocephalus that causes high levels of neonatal death with most mice surviving no more than 2-4 weeks in the case of the *Dnahc5* mouse model (375). This severity raises animal welfare concerns and makes such models difficult to work with when assessing efficacy of airway gene delivery approaches given that mortality results from hydrocephalus and cardiac abnormalities. A conditional knockout mouse in which *Dnaic1* (the mouse homolog of human DNAI1) can be removed following administration of tamoxifen is able to ameliorate the lethality observed with non-conditional PCD knockouts/mutants with conditional knockout mice surviving >11 months following knockout of *Dnaic1* (316). In the case of the *Dnaic1* mouse model

exons 17 and 18 of *Dnaic1* were flanked with loxP sites and homozygous progeny were mated with CreER expressing mice -those expressing a tamoxifen-inducible Cre recombinase. Administration of tamoxifen to 8-12 week old *Dnaic1*$^{flox/flox}$*/CreER*$^{+/-}$ resulted in absent ODA, impaired mucociliary clearance and chronic rhinosinusitis. Although the phenotypes took at least 2-3 months to manifest the lack hydrocephalus development and a more pronounced respiratory pathology makes these mice a better model of human PCD and of greater interest for studying respiratory gene therapy approaches for PCD. However it is important to note that pulmonary infections were not observed in these mice despite a lack of mucociliary clearance and the fact that mice were not housed in pathogen-free conditions. This contrasts with human PCD where chronic respiratory infections are a major feature. Nevertheless, conditional knockout alleles present the best way of producing mouse models of PCD to date and should be applicable to producing viable *Dnahc5* mouse models without hydrocephalus and severe cardiac abnormalities.

1.4 SUMMARY AND AIMS

PCD is a ciliopathy affecting cilia motility. In the airways PCD patients suffer significant lung damage resulting from chronic airway infections due to a lack of mucociliary clearance. Current treatment options do not address the primary defect although proof-of-principle studies have shown that correcting the genetic defect restores ciliary function in cases where PCD results from mutations in *DNAI1*. However, the most common cause of PCD is mutation of *DNAH5*, a gene with a 14kb ORF and so not amenable to delivery by the viral vectors used to correct *DNAI1*-null cells. Non-viral vectors have been optimised for airway gene delivery and are capable of delivering large DNA constructs but suitable and easily accessible models for assessing the efficacy of PCD are lacking.

Moving towards gene therapy for PCD the aims of this thesis are;

1. To clone wild-type DNAH5 cDNA into mammalian expression systems and assess transgene expression.
2. To assess the potential advantages of minicircle DNA in the context of airway gene delivery
3. To produce an *in vitro* model of PCD caused by loss of DNAH5.
4. To attempt gene therapy correction of PCD caused by loss of DNAH5.

CHAPTER TWO

MATERIALS AND METHODS

2. MATERIALS AND METHODS

2.1. MATERIALS

Unless stated otherwise tissue culture reagents were supplied by Gibco, Life Technologies; general chemicals were supplied by Sigma-Aldrich; restriction enzymes were FastDigest brand of restriction enzymes and supplied by Thermo Scientific; western blot reagents were supplied by Novex, Life Technologies.

2.1.1 EQUIPMENT

Name	Supplier
ABI PRISM 7000 Sequence Detection	Applied Biosystems, Life Technologies
Bio-Plex 100	Bio-Rad
FLUOstar Optima	BMG Labtech
Hitachi H7000 TEM	Hitachi
MotionPro X4 High-speed Motion Camera	DEL Imaging Systems
NanoDrop ND-1000 Spectrophotometer	Thermo Scientific
NanoZoomer Digital Pathology System	Hamamatsu Photonics
Nikon Digital Sight DS-QiMc	Nikon
Nikon Eclipse Ti-U Inverted Microscope	Nikon
Philips CM120 BioTwin TEM	Philips
Zetasizer Nano ZS	Malvern

2.1.2 KITS AND REAGENTS

Name	Supplier
10X PCR Buffer	Applied Biosystems, Life Technologies
5X Protein Assay Dye Reagent	Bio-Rad
5X Reporter Lysis Buffer	Promega
6x DNA Loading Dye	Thermo Scientific
BEBM Basal Medium	Lonza
Buffer TE	Qiagen
CellTiter 96 AQueous One Solution Assay	Promega
Cytokine Mouse 10-Plex Panel	Novex, Life Technologies

Dimethyl sulfoxide (DMSO)	Sigma-Aldrich
dNTP's	Promega
Eagle's Minimal Essential Medium (MEM)	Sigma-Aldrich
EndoFree Plasmid Giga Kit	Qiagen
EndoFree Plasmid Maxi Kit	Qiagen
Foetal Bovine Serum (FBS)	Sigma-Aldrich
GENECLEAN SPIN KIT	MP Biomedicals
Glycerol	Sigma-Aldrich
HiFi HotStart DNA Polymerase with dNTPs	Kapa Biosystems
Lysogeny broth (LB) Agar	Sigma-Aldrich
LB Broth	Sigma-Aldrich
Luciferase Assay System	Promega
Magnesium Chloride ($MgCl_2$; 25mM)	Applied Biosystems, Life Technologies
MuLV Reverse Transcriptase	Applied Biosystems, Life Technologies
PicoGreen	Invitrogen, Life Technologies
Pierce ECL Western Blotting Substrate	Thermo Scientific
Plasmid Maxi Kit	Qiagen
Platinum qPCR SuperMix-UDG with ROX	Invitrogen, Life Technologies
PureCol, bovine collagen	Nutacon
QIAprep Spin Miniprep Kit	Qiagen
QIAquick Gel Extraction Kit	Qiagen
QIAquick PCR Purification Kit	Qiagen
Random Primers	Applied Biosystems, Life Technologies
RNase Inhibitor	Applied Biosystems, Life Technologies
SingleQuot Kit Suppl. & Growth Factors	Lonza
SOC Media	Invitrogen, Life Technologies
T4 DNA Ligase and Buffer	Promega
T4 DNA Polymerase	Promega
Taq ReadyMix	Kapa Biosystems
TOPO XL PCR Cloning Kit	Invitrogen, Life Technologies
TURBO DNA-*free* Kit	Ambion, Life Technologies
ULS DNA labelling Kit (Cy5)	Kreatech

2.1.3 *E.COLI* CELLS

Strain	Supplier	Genotype
Stbl3	Invitrogen, Life Technologies	F^- mcrB mrr hsdS20 (rB^-, mB^-) recA13 supE44 ara-14 galK2 lacY1 proA2 rpsL20 (Str^R) xyl-5 λ^- leu mtl-1
TOP10	Invitrogen, Life Technologies	F^- mcrA Δ (mrr-hsdRMS-mcrBC) Φ80lacZΔM15 ΔlacX74 recA1 araD139 Δ (ara leu) 7697 galU galK rpsL (Str^R) endA1 nupG
ZYCY10P3S2T	System Biosciences	Cp8.araE ΔendA bla.lacY A177C 3BAD.I-SceI 2BAD.ΦC31 4BAD.Φ31 4BAD.Φ31

2.1.4 EUKARYOTIC CELLS

Name	Growth Media	Supplier/Reference
16HBE14o-	MEM with 10% FBS and 2mM L-glutamine	Prof. Dieter Gruenert (376)
HEK293T	DMEM with 10% FBS	ATCC
NHBE	BEGM or ALI media	Lonza

2.1.5 PLASMIDS

Name	Promoter	Transgene	Supplier/Reference
pCI	CMV	None, contains MCS	Promega
pCI-Luc	CMV	Firefly luciferase	(377)
pCMV-dR8.74	CMV	Gag, pol, rev and tat	Prof. Didier Trono
pCpGfree-LacZ	hEF1α, CMV enhancer	LacZ	Invivogen
pEGFP-N1	CMV	EGFP	Clontech
pGIPZ	CMV	GFP, PAC and shRNA	Open Biosystems
pGL4.10	None	Firefly luciferase	Promega
pHRsincpptSEClaI	SFFV	GFP	Dr. Joao Matelo
pMC.BESPX.MCS2	None	None, contains MCS	System Biosciences
pMD.G2	CMV	VSV-G	Prof. Didier Trono
pNL1.3	None	Secreted NanoLuc	Promega

2.1.6 LIPOSOMES AND PEPTIDES

Name	Composition	Supplier
DHDTMA:DOPE	50% DHDTMA and 50% DOPE (molar amounts)	Avanti Polar Lipids
$K_{16}E$	K_{16}GACSERSMNFCG	ChinaPeptides Co.
K_8E	K_8GACSERSMNFCG	ChinaPeptides Co.
$R_{16}E$	R_{16}GACSERSMNFCG	ChinaPeptides Co.

2.1.7 PRIMARY ANTIBODIES

Name	Supplier	Catalogue #
Anit-MUC5AC	Invitrogen, Life Technologies	18-2261
Anti-Acetylated α-tubulin	Sigma-Aldrich	T6793
Anti-BMI-1	Invitrogen, Life Technologies	37-5400
Anti-DNAH5	Sigma-Aldrich	HPA037470
Anti-GAPDH	Ambion, Life Technologies	AM4300
Anti-HSP90β	Invitrogen, Life Technologies	37-9400
Anti-MUC5B	Dallas Swallow, UCL	(378)
Anti-Occludin	Invitrogen, Life Technologies	71-1500
Anti-$p16^{INK4}$	Pharmingen, BD Biosciences	551153
Anti-p63	Invitrogen, Life Technologies	37-9500

Secondary antibodies for immunofluorescence were anti-IgG antibodies conjugated with AlexaFluor dyes (Invitrogen, Life Technoloies). Secondary antibodies for Western blots were horseradish peroxidase conjugated (HRP-conjugated) anti-IgG antibodies (Dako, Agilent Technologies). AlexaFluor dye conjugated Phalloidin toxin (Invitrogen, Life Technoloies) was used to stain filamentous actin (F-actin).

2.1.8 RECIPES

Solution	Composition
2.5% Glutaraldehyde	50mM sodium cacodylate,4mM HCl, 0.02% (w/v) $CaCl_2$ and 2.5% (v/v) glutaraldehyde
6X Crystal Violet Loading Dye	30% (v/v) glycerol, 20mM ethylenediaminetetraacetic acid (EDTA), 100 μg/mL crystal violet
ALI media	500 mL contains 50% (v/v) BEBM, 50% (v/v) DMEM, 1x SingleQuot Kit Suppl. & Growth Factors. 100 U/mL penicillin, 100 mg/mL streptomycin and 1nM retinoic acid (added at each feed)
Innoue Transformation Buffer	10mM PIPES, 15mM $CaCl_2.2H_2O$ and 55mM $MnCl_2.4H_2O$; adjusted to pH6.7
Minicircle Induction Media	LB broth with 0.02% (w/v) L-arabinose and 40mM NaOH
Super optimal broth (SOB)	2% (w/v) tryptone, 0.5% (w/v) yeast extract, 10mM NaCl, 2.5mM KCl and 10mM $MgCl_2$
Terrific Broth (TB)	12 g/L tryptone, 34 g/L yeast extract, 0.4% (v/v) glycerol, 2.31 g/L KH_2PO_4 and 12.54 g/L K_2HPO_4
Tris-acetate-EDTA buffer (TAE)	4.84 g/L Tris base, 0.114% (v/v) glacial acetic acid and 0.2% (v/v) 0.5M EDTA at pH8.0

2.2. METHODS

2.2.1. GROWTH AND MAINTENANCE OF *E. COLI*

E. coli were streaked or spread on solid LB agar plates and incubated at 37^{o}C overnight (15-17 hours). Alternatively, LB broth was inoculated with *E. coli* and incubated overnight at 37^{o}C with shaking at 250rpm in a vessel capable of holding at least five times the volume of inoculated LB broth used. LB broth or solid LB agar containing 100µg/mL or 50µg/mL of ampicillin or kanamycin respectively was used for antibiotic selection where appropriate.

2.2.2. LONG TERM STORAGE OF *E. COLI*

A single colony of *E. coli*, grown overnight at 37^{o}C on solid LB agar plates, was inoculated into 5mL of LB broth and grown overnight at 37^{o}C with shaking at 250rpm. 650µL of this culture was added to a cryovial with 150µL of sterile 80% (v/v) glycerol, mixed well and stored at -80^{o}C.

2.2.3. PRODUCTION OF CHEMICALLY COMPETENT *E. COLI*

The Inoue method (379) was used to produce chemically competent *E. coli*. A single colony of Stbl3, TOP10 or ZYCY10P3S2T strains of *E. coli* was used to inoculate 25mL of SOB media and incubated for 8 hours at 37^{o}C with shaking at 250rpm. This culture was then used to inoculate 250mL of SOB and incubated at room temperature with shaking at 200rpm to an OD_{600} of 0.5-0.6. The culture was then chilled in an ice-water bath for 10 minutes and centrifuged at 2500 x *g* for 10 minutes at 4^{o}C. The cells were gently re-suspended in 80mL of ice-cold Inoue transformation buffer and then centrifuged at 2500 x *g* for 10 minutes at 4^{o}C. The cells were gently re-suspended in 20mL of ice-cold Inoue transformation buffer,

1.5mL of dimethyl sulfoxide (DMSO) was added and gently mixed by swirling and cells kept in an ice-water bath whilst 50µL aliquots, suitable for single use, were dispensed into 1.5mL microfuge tubes, snap frozen in liquid nitrogen and stored at -80^{o}C.

2.2.4. Transformation of Chemically Competent *E. coli*

50µL aliquots of chemically competent *E. coli* were thawed on ice for 5 minutes. 1-100ng of DNA in a maximum volume of 5µL was added to competent *E.coli* and incubated on ice for 30 minutes. The cells were then heat shocked by incubation at 42^{o}C for 45 seconds and then immediately placed on ice for 2 minutes. 250µL of super optimal broth with catabolite repression (SOC) media was added to the cells and incubated for 1 hour at 37^{o}C with shaking at 250rpm. The culture was then spread on a solid LB agar plate with an appropriate antibiotic and incubated overnight at 37^{o}C.

2.2.5. Plasmid DNA Extraction

Transformed *E. coli* were grown on solid LB agar plates with an appropriate antibiotic and incubated overnight at 37^{o}C. A single colony was inoculated into 5mL of LB broth with an appropriate antibiotic and incubated overnight at 37^{o}C with shaking at 250rpm. Plasmid DNA was extracted by an alkaline lysis method and purified using the QIAPrep Spin Miniprep kit (≤20µg plasmid DNA). This uses a chaotropic salt solution to reversibly bind DNA to a silica-gel membrane and DNA is then eluted in low-salt conditions. If larger quantities of plasmid DNA were required the 5mL LB broth culture was used to inoculate larger volumes of LB broth and plasmid DNA extracted using Plasmid Maxi kit (≤500µg plasmid DNA). For

preparation of endotoxin-free plasmid DNA EndoFree Plasmid Maxi kit (≤500µg plasmid DNA) or EndoFree Plasmid Giga kit (≤10mg plasmid DNA) was used. These utilise an anion-exchange system using a silica-based resin with a high density of diethylaminoethyl groups which reversibly binds DNA over a wide range of salt concentrations allowing efficient removal of impurities. DNA is then eluted with a high-salt buffer and alcohol precipitation then performed to purify and concentrate the DNA. Plasmid DNA concentration was quantified by measuring the OD_{260} using a NanoDrop ND-1000 spectrophotometer and the 260/280 ratio was used to assess purity of the extracted DNA with a ratio of 1.8-2.0 considered sufficiently pure for use in further experiments.

2.2.6. MINICIRCLE DNA EXTRACTION

Transformed ZYCY10P3S2T *E. coli* strain containing a minicircle producer plasmid was grown on solid LB agar plates with 50µg/mL kanamycin and incubated overnight at 37^{o}C. A single colony was inoculated into 5mL of LB broth with 50µg/mL kanamycin and incubated for 8 hours at 37^{o}C with shaking at 250rpm. 100µL of this starter culture was used to inoculate 400mL of TB broth and incubated with 50µg/mL kanamycin at 37^{o}C with shaking at 250rpm to an OD_{600} of 4-6. 400mL of minicircle induction media was added to the culture and incubated at 30^{o}C with shaking at 250rpm for 6h. Minicircle DNA extraction and purification from *E.coli* was then performed as for plasmid DNA. Minicircle DNA concentration was quantified by measuring the OD_{260} using a NanoDrop ND-1000 spectrophotometer with the same criteria of purity used for plasmid DNA (method 2.2.5).

2.2.7. TOTAL RNA EXTRACTION

Harvested cells were pelleted at 378 x *g* for 5 minutes and total RNA was extracted using RNeasy Minit Kit. This uses a chaotropic guanidine-thiocyanate containing buffer together with ethanol to bind RNA to reversibly bind RNA to a silica-based membrane and RNA is then eluted in low-salt conditions with RNase-free water. RNA concentration was quantified by measuring the OD_{260} using a NanoDrop ND-1000 spectrophotometer and the 260/280 ratio was used to assess purity of the extracted DNA with a ratio of 1.9-2.1 considered sufficiently pure for use in further experiments. Potential DNA contaminants were removed by DNase digestion using TURBO DNase.

2.2.8. REVERSE TRANSCRIPTION

Up to 2µg of DNase digested purified total RNA was added to 0.8µL of a deoxyribonucleotide triphosphate (dNTP) mix containing 25mM of each dNTP, 2µL of 50µM random hexamers and topped up to 12µL with DNase/RNase-free water. This mix was incubated at 70^{o}C for 10 minutes and placed on ice. A reverse transcription enzyme mix consisting of 2µL GeneAmp PCR Gold Buffer, 4µL 25mM $MgCl_2$, 1µL 50U/µL murine leukemia virus (MuLV) reverse transcriptase and 1µL 20U/µL RNase Inhibitor was added and the mix incubated for 1 hour at 42^{o}C followed by 85^{o}C for 5 minutes. For no RT controls MuLV reverse transcriptase was replaced with DNase/RNase-free water.

2.2.9. Restriction Enzyme Digest

DNA was digested with appropriate restriction endonucleases using the appropriate reaction buffer and at the appropriate reaction temperature as per the manufacturer's instructions.

2.2.10. Filling of 5' Single Stranded DNA Overhangs

5' overhangs following restriction enzyme digest of 1-4µg of plasmid DNA were filled using the large Klenow fragment of DNA Polymerase I (1U/µg of DNA) in 1x DNA Polymerase I buffer (supplied by the manufacturer) and 40µM each of deoxyadenosine triphosphate (dATP), deoxycytidine triphosphate (dCTP), deoxyguanosine triphosphate (dGTP) and deoxythymidine triphosphate (dTTP). This reaction mixture was incubated at room temperature for 10 minutes and the reaction stopped by incubation for a further 10 minutes at 75^{o}C.

2.2.11. Removal of 3' Single Stranded DNA Overhangs

3' overhangs following restriction enzyme digest of 1-4µg of plasmid DNA were removed using the large Klenow fragment of DNA Polymerase I (1U/µg of DNA) in 1x DNA Polymerase I buffer (supplied by the manufacturer) with no dNTPs. This reaction mixture was incubated at room temperature for 10 minutes and the reaction stopped by incubation for a further 10 minutes at 75^{o}C.

2.2.12. Polymerase Chain Reaction (PCR)

PCR was performed in a total volume of 25µL using 1-100ng of template DNA, 0.4µM each of forward and reverse primers and 12.5µL of 2X Taq ReadyMix with dye (a pre-prepared mixture which at 1X contains 1U *Taq* polymerase, Tris-HCl, KCl, 0.2mM each dNTP, 1.5mM $MgCl_2$ and two inert tracking dyes enabling direct

loading of PCR products onto agarose gels). The PCR cycling conditions were 95^{o}C for 3 minutes followed by 30-35 cycles of 95^{o}C for 30 seconds, primer T_m -5^{o}C for 30 seconds and 72^{o}C for 1 minute/kb which was followed by a final extension step of 72^{o}C for 1 minute/kb.

2.2.13. HIGH FIDELITY PCR

PCR was performed in a total volume of 50µL using 100ng template DNA, 0.3µM each of forward and reverse primers, 0.3mM dNTP mix, 10µL of 5X PCR Buffer containing 2mM $MgCl_2$ (HiFi Fidelity Buffer) and 1U of a proofreading DNA polymerase (HiFi HotStart DNA Polymerase). The PCR cycling conditions were 95^{o}C for 3 minutes followed by 20 cycles of 98^{o}C for 20 seconds, 65^{o}C for 15 seconds and 72^{o}C for 1 minute/kb which was followed by a final extension step of 72^{o}C for 1 minute/kb.

2.2.14. QUANTITATIVE REVERSE TRANSCRIPTION PCR (qRT-PCR)

10-100ng of cDNA was mixed in a 25µL reaction with 12.5µL of Platinum Quantitative PCR SuperMix-UDG w/ROX (a 2X master-mix which at 1X contains hot-start *Taq* DNA polymerase, Tris-HCl, KCl, 3mM $MgCl_2$, 200µM each of dGTP, dATP and dCTP, 400µM deoxyuridine Triphosphate (dUTP), uracil DNA glycosylase and 1µM ROX reference dye) and 1.25µL TaqMan Gene Expression Assay primer/probe set and real-time quantitative PCR performed using an ABI PRISM 7000 Sequence Detection System. The PCR reaction cycles used were 50^{o}C for 2 minutes, 95^{o}C for 10 minutes, 40 cycles of 95^{o}C for 15 seconds and 60^{O}C for 1 minute. Fluorescence data was collected at the end of each 60^{o}C reaction and relative expression levels calculated using the delta-delta Ct ($2^{-\Delta\Delta Ct}$) method (380).

2.2.15. Ethidium Bromide Agarose Gel Electrophoresis

0.5-2% (w/v) of agarose was dissolved in TAE buffer by heating, allowed to cool to around 50^{o}C and 1µg/mL ethidium bromide added. The solution was then poured into an appropriately sized casting tray and allowed to set at room temperature. 6X DNA loading dye was added to DNA samples to a final concentration of 1X and the DNA fragments separated by electrophoresis in TAE at 80-120V for 60-90 minutes. DNA bands were visualised by exposure of the gel to UV light using the UVIdoc system.

2.2.16. Crystal Violet Agarose Gel Electrophoresis

0.5-2% (w/v) of agarose was dissolved in TAE buffer by heating, allowed to cool to around 50^{o}C and 1.6µg/mL crystal violet added. The solution was then poured into an appropriately sized casting tray and allowed to set at room temperature. 6X crystal violet loading dye was added to DNA samples to a final concentration of 1X and the DNA fragments separated by electrophoresis in TAE at 80-120V for 60-90 minutes. DNA bands could be seen under visible light.

2.2.17. Purification of DNA Fragments (<10kb)

DNA fragments following PCR, restriction enzyme digestion, 5’ overhang filling and 3’ overhang removal reactions that were not subsequently separated by gel electrophoresis were purified with using the QIAquick PCR Purification kit. DNA fragments separated by gel electrophoresis were excised using a scalpel and purified using the QIAquick Gel Extraction kit. Both kits use a chaotropic salt solution to reversibly bind DNA to a silica-gel membrane and DNA is then eluted in low-salt conditions.

2.2.18. Purification of DNA Fragments (≥10kb)

DNA fragments following PCR, restriction enzyme digestion, 5' overhang filling and 3' overhang removal reactions and fragments excised following crystal violet gel electrophoresis were purified using the GENECLEAN SPIN kit. This uses a chaotropic salt solution to reversibly bind DNA to silica beads and DNA is then eluted in low-salt conditions.

2.2.19. Ligation of DNA Fragments

25-100ng of plasmid backbone was ligated with an insert using T4 DNA ligase and T4 DNA ligase buffer in a final volume of 20µL. Ligation reactions were performed at 16^{o}C for 18 hours. Ligations where the fragments were flanked with compatible overhangs (sticky ends) were performed at a backbone: insert ratio of 1:4. Ligations where the fragments were flanked with no overhangs (blunt ends), or one sticky and one blunt end, were performed at a backbone: insert ratio of 1:6. Subsequently, 5µL of ligation product was transformed into competent *E. coli*.

2.2.20. TOPO Cloning

Single 3' A overhangs were added to gel purified PCR products, from high fidelity PCR, by incubation of PCR products at 72^{o}C for 30 minutes with 1U Taq DNA Polymerase, Standard Taq Buffer (10mM Tris-HCL, 50mM KCl and 1.5mM $MgCl_2$) and 0.2mM dATP. PCR products were then purified from the reaction solution and cloned into a pCR2.1-TOPO TA vector (fragments <3kb) or pCR-XL-TOPO vector (fragments ≥3kb) by incubation for 5-30 minutes at 22^{o}C of 4µL purified DNA product, 1µL salt solution (1.2M NaCl and 0.06M $MgCl_2$) and 1µL TOPO vector. 2-5µL of the reaction solution was the used to transform chemically competent *E.coli*

and plasmid extracted from the resultant colonies was sequenced by the UCL DNA Sequencing Service to verify the fidelity of the PCR reaction.

2.2.21. Site-Directed Mutagenesis

For single base pair mutagenesis mutagenic primers were designed using the QuickChange Primer Design Program (http://www.genomics.agilent.com/primerDesignProgram.jsp) and mutagenesis performed using QuickChange II XL Site-Directed Mutagenesis kit.

For multiple base-pair mutagenesis mutagenic primers were designed using the QuickChange Primer Design Program and the mutagenic primers were used in a high fidelity PCR reaction with 10ng of plasmid DNA as template. A 10µL aliquot of the PCR product was electrophoresed on an ethidium bromide agarose gel to verify the success of the PCR reaction. The remaining PCR product was purified and used in a sequence and ligation-independent cloning reaction (381) to obtain a circularised and mutated plasmid that was transformed into chemically competent *E. coli*. DNA sequencing was performed by the UCL DNA Sequencing Service to verify the success of site-directed mutagenesis.

2.2.22. Sequence- and Ligation-Independent Cloning (SLIC)

PCR products flanked with a 15-20bp sequence homologous to the ends of the PCR product (for multi base pair site-directed mutagenesis) or the ends of a restriction enzyme linearized plasmid backbone were purified and single-strand 5' overhangs were generated using the 3'-5' exonuclease activity of T4 DNA Polymerase in 20µL "chew-back" reactions containing 1µg of linearized backbone or PCR product, 0.5U T4 DNA Polymerase and 2µL of 10X T4 DNA Ligase Buffer (300mM Tris-HCl (pH 7.8

at 25°C), 100mM MgCl2, 100mM DTT and 10mM ATP) and incubated for 30 minutes at room temperature after which 2µL of 10mM dCTP was added to halt the exonuclease activity of T4 DNA Polymerase and the mixture placed on ice. An assembly reaction consisting of 100ng of chewed-back linearized backbone added to an equimolar amount of chewed-back PCR product insert and topped up to 15µL with 1X T4 DNA Ligase Buffer was incubated at 37^{o}C for 30 minutes and then placed on ice. For multi base pair site-directed mutagenesis the assembly reaction consisted of 100ng of chewed-back PCR amplified plasmid in 1X T4 DNA Ligase Buffer to a final volume of 15µL. 5µL of the assembly reaction was transformed into chemically competent *E. coli* and plasmid extracted from the resultant colonies was sequenced by the UCL DNA Sequencing Service to verify the fidelity of the PCR reaction.

2.2.23. Collagen Coating

Tissue culture plates, flasks and transwells were coated for at least 1 hour at room temperature with 1% (v/v) of a 3mg/mL bovine collagen solution (PureCol; 95% Type I and ~5% Type III collagen) in phosphate buffered saline (PBS), then washed once with 0.22µM filter sterilized distilled water and either seeded with cells immediately or allowed to air-dry overnight in a sterile hood and stored at room temperature until use.

2.2.24. Submerged Cell Culture

16HBE14o- cells are an SV40 Large T-Antigen transformed human bronchial epithelial cell line derived by Dr Dieter Gruenert (376). 16HBE14o- cells were cultured in Minimum Essential Media (MEM) based growth media. HEK293T cells

were cultured in Dulbecco's Modified Eagle Medium (DMEM) based growth media. Primary normal human bronchial epithelial (NHBE) and nasal epithelial cells and BMI-1 transduced NHBE cells were grown on collagen-coated plastic in bronchial epithelial growth media (BEGM). All cells were grown at 37^{o}C and 5% CO_2. Transduction was completed by adding concentrated BMI-1 coding VSV-G pseudotyped lentivirus to NHBE cells in submerged culture. Concentrated BMI-1 coding lentivirus was provided by Dr Tristan McKay.

2.2.25. ALI CULTURE

NHBE cells in BEGM were seeded onto collagen-coated Transwell Permeable Supports (0.4µm pore size, polyester membrane) at a seeding density of 900,000 cells/cm^2 and BEGM was added to the basolateral compartment and the cells incubated at 37^{o}C and 5% CO_2 for 48 hours. The apical and basolateral fluid was then removed and ALI media added to the basolateral compartment. The cells were then incubated at 37^{o}C and 5% CO_2 with apical fluid being removed and the ALI media from the basolateral compartment replaced every 2-3 days.

2.2.26. LONG TERM STORAGE OF EUKARYOTIC CELLS

1-4 x10^6 cells were pelleted by centrifugation at 378 x *g* for 5 minutes and re-suspended in 1mL freezing medium (90% FBS and 10% DMSO) and incubated overnight at -80^{o}C in a Mr Frosty Freezing container filled with isopropanol to allow slow freezing. Cells were then transferred to liquid nitrogen.

Frozen cells were revived by quick thawing in a 37^{o}C water-bath and the cells transferred to 10mL of pre-warmed complete growth media. The cells were pelleted at 378 x *g* for 5 minutes to remove the DMSO and re-suspended in 15mL

complete growth media, placed into a 75cm^2 tissue culture flask and incubated at 37^{o}C and 5% CO_2.

2.2.27. Preparation of Nanocomplexes

All complexes were prepared in water, OptiMEM or Buffer TE (10mM Tris.Cl pH 8.0 and 1mM EDTA). LPD complexes were prepared at a 0.75:4:1 weight ratio of liposome:pepide:DNA with the liposome and peptide components being mixed together first then the DNA component being added and mixed well. PD complexes were prepared at a 4:1 weight ratio of peptide:DNA, LD (0.75:1) complexes were prepared at a 0.75:1 weight ratio of liposome:DNA and LD (4:1) complexes were prepared at a 4:1 weight ratio of liposome:DNA. Following addition of the different components all formulations were incubated at room temperature for 30 minutes to allow self-assembly of nanocomplexes. Complexes were typically prepared to a DNA concentration of 10ng/µL or 333.3ng/µL for *in vitro* and *in vivo* applications respectively. An example of a LPD formulation for *in vitro* and *in vivo* use is given in Appendix A.

2.2.28. Transfection of Submerged Cultures

Cells were seeded so as to reach 70-80% confluency following 24 hours at 37^{o}C and 5% CO_2. For experiments where luciferase activity would be assessed cells were seeded in black plates with clear bottoms. The following day complexes were prepared in OptiMEM and the desired amount of DNA formed in complexes was added to cells in complete growth media. Cells were then incubated at 37^{o}C and 5% CO_2 for varying amounts of time depending on the assay to be performed.

2.2.29. TRANSFECTION OF ALI CULTURES

Once well ciliated (>4 weeks at ALI) the apical surface of cells were washed twice with bronchial epithelial basal media (BEBM). Varying amounts of DNA formulated into LPD complexes in OptiMEM were added to the apical, basolateral or both compartments and incubated at 37^{o}C and 5% CO_2 for 2 hours. Complexes were then aspirated from the cells and ALI media added to the basolateral compartment. Cells were then incubated at 37^{o}C and 5% CO_2 for varying amounts of time depending on the assay to be performed.

2.2.30. TRANSFECTION OF CELLS IN SUSPENSION (REVERSE TRANSFECTION)

LPD complexes were prepared in OptiMEM at varying concentrations of DNA and cells then detached from flasks using Trypsin-EDTA which was subsequently diluted in PBS to significantly slow Trypsin activity. Cells were then centrifuged at 378 x *g* for 5 minutes and the solution aspirated. After 30 minutes of incubation to allow self-assembly complexes were added to cells and incubated at room temperature for 30 minutes after which the cells were again centrifuged at 378 x *g*, complexes aspirated, cells re-suspended in complete media, seeded onto plates and/or transwells and incubated at 37^{o}C and 5% CO_2.

2.2.31. *IN VIVO* TRANSFECTIONS

Complexes were prepared in water and 50µL of complexes delivered via the oropharyngeal route to CD1 mice. Mice were anaesthetised with gaseous isoflurane and nostrils pinched closed using tweezers so as to ensure that breathing takes place through the mouth. Whilst the nostrils were held closed 50µL of complex solution was pipetted to the rear of the oral cavity and gripping of the nostrils

maintained until all the solution had been inhaled. This oropharyngeal route of delivery is less invasive than intratracheal instillation that provides direct application of vector to the lung. Oropharyngeal delivery is also preferred to nebulisation as it uses less material and allows more control over dosage.

2.2.32. Luciferase Assay For *In Vitro* Transfections

Cells were washed with 1x PBS 24 hours following transfection and lysed with 20 µL 1X Reporter Lysis Buffer for 20 minutes at 4^{o}C then -80^{o}C for at least 30 minutes followed by thawing at room temperature. Luciferase activity was assessed using the Luciferase Assay System and luminescence detected with a FLUOstar Optima plate reader. The results were standardised for protein content using the Bradford protein assay and expressed as relative luminescence units per milligram of protein (RLU/mg of protein).

2.2.33. Luciferase Assay For *In Vivo* Transfections

At least 24 hours following transfection mice were euthanized with 100µL of pentobarbital sodium (Euthatal) administered intraperitoneally. The chest cavity was exposed post-mortem and the heart perfused with 5mL of PBS after-which the lungs were dissected and stored at -80^{o}C for a minimum of 24 hours. Lungs were weighed, placed in 2mL tubes containing 1.4mm ceramic beads and 4µL of Reporter Gene Assay Lysis Buffer added per milligram of tissue. The mixture was then frozen at -80^{o}C for 20 minutes, left to thaw at room temperature for 10 minutes and then placed on ice for a further 10 minutes. Tissue homogenisation was then performed using a Percellys 24 tissue homogeniser at a 3D motion speed of 5700rpm for 30 seconds which was performed twice with a 30 second delay between the two steps.

Samples were then centrifuged at 14,196 x *g* for 10 minutes at 4^{o}C to pellet the ceramic beads and tissue debris. The supernatant was transferred into autoclaved microfuge tubes and assayed for luciferase activity using the Luciferase Assay System and luminescence detected with a FLUOstar Optima plate reader. The results were standardised for protein content using the Bradford protein assay and expressed as RLU/mg of protein.

2.2.34. Bradford Protein Assay

Following luciferase assay 20µL of cell lysate-luciferase assay system solution was added to 180µL Bio-Rad Protein Assay Reagent in new clear 96-well plates and incubated at room temperature for 10 minutes. Absorbance at 590nm was then read using a FLUOstar Optima plate reader and the protein content of the cell lysate was calculated using a standard curve generated with known concentrations of bovine serum albumin (BSA).

For *in vivo* samples supernatant obtained following tissue homogenisation was diluted 100X in water and 20µL mixed with 180µL Bio-Rad Protein Assay Reagent with later steps performed as for *in vitro* samples.

2.2.35. BALF Collection and Luminex Assay

24 hours following transfection mice were euthanized with 100µL of pentobarbital sodium (Euthatal) administered intraperitoneally. The chest cavity was exposed post-mortem, the trachea cannulated and the lungs lavaged ten times with 500µL of ice-cold PBS (total of 5mL PBS). Each aliquot of PBS was instilled slowly over 15 seconds and incubated in situ for 30 seconds prior to gentle removal over 15 seconds. The lavage fluid was kept on ice throughout and, upon completion,

centrifuged at 300 x g for 5 minutes at 4°C. The presence of inflammatory cytokines in BALF was assessed and quantified using the Cytokine Mouse 10-Plex Panel (Invitrogen) following the manufacturer's instructions. This is a multiplexed fluorescence based assay where specific antibodies are conjugated to dyed beads with differing intensities so allowing the detection of a number of different analytes from a single sample. Plates were read using a Bio-Plex 100 reader (Bio-Rad) and results analysed with Bio-Plex Manager software (v 4.1.1; Bio-Rad)

2.2.36. HISTOLOGY

24 hours following transfection mice were euthanized with 100µL of pentobarbital sodium (Euthatal) administered intraperitoneally. The chest cavity was exposed post-mortem and inflation-fixed by intratracheal instillation of 4% (w/v) paraformaldehyde in PBS at a pressure of 20 cm 4% paraformaldehyde. The lungs were then dissected and immersed in fixative overnight at 4^{o}C and then immersed in a 15% (w/v) sucrose solution in PBS overnight at 4^{o}C. The tissue was then dehydrated in alcohol and embedded in paraffin wax. 5µm thick sections were cut and dried onto microscope slides. Samples were then de-waxed, rehydrated, stained with haematoxylin, counter-stained with eosin, dehydrated and cleared using a Tissue-Tek DRS 2000 multiple slide stainer (Sakura). Briefly, de-waxing was performed by immersing the slides in xylene twice for 3 minutes. Samples were then rehydrated in graded alcohol by immersing twice for 2 minutes in 100% ethanol followed by &0% ethanol for 2 minutes, 30% ethanol for two minutes and dH_2O for 1 minute. Tissues were haematoxylin stained for 5 minutes before being rinsed with tap water for 20 seconds, decoloured in acid alcohol (2% HCl in alcohol)

for 6 seconds, rinsed again with tap water for 2.5 minutes, counterstained with eosin for 4 minutes and rinsed a final time with tap water for 15 seconds. Stained samples were then dehydrated in graded alcohol by immersing in 70% ethanol for 30 seconds followed by 100% ethanol once for 45 seconds and again for 30 seconds. The tissue was cleared by immersing in xylene twice for 2 minutes and mounted. Images were then taken using a NanoZoomer Digital Pathology System (Hamamatsu Photonics) and processed with NDP.scan software (v2.3; Hamamatsu Photonics).

2.2.37. Flow Cytometry

Cells grown on 96-well plates were detached using 50 µL Trypsin-EDTA and re-suspended with 150 µL PBS. Cells were then acquired with a BD FACSArray flow cytometer and analysis was performed with FlowJo software v. 8.8.3. Cells grown in larger plates or flasks were detached using an appropriate volume of trypsin and re-suspended in PBS. Cells were transferred to 5mL FACS tubes and cells acquired using CyAn ADP Analyser and analysis was performed with FlowJo software v. 8.8.3.

2.2.38. Cell Viability Assay

24 hours following transfection in 96-well plate's cell viability was assessed using the CellTiter 96 Aqueous One Solution Assay. Following transfection complete media was aspirated and replaced with 100µL of fresh complete media and 20µL CellTiter 96 Aqueous One Solution. The cells were then incubated at 37^{o}C and 5% CO_2 for 2 hours and absorbance at 490nm was then read using a FLUOstar Optima plate reader. Absorbance values of background corrected treated cells were normalised to values for untreated cells -set as 100% viable cells.

2.2.39. TRANSMISSION ELECTRON MICROSCOPY (TEM) FOR COMPLEXES

Complexes were prepared in water at a DNA concentration of 333ng/µL and a 5 µL aliquot was applied onto a 300-mesh copper grid coated with a Formvar carbon support film (Agar Scientific) then, after a few seconds, dried by blotting with filter paper. The sample was then negatively stained with 1% (w/v) uranyl acetate for a few seconds, before blotting with filter paper and air dried. Imaging was carried out with a Philips CM120 BioTwin Transmission Electron Microscope and operated at an accelerating voltage of 120 kV.

Processing of complexes for TEM was performed by Dr. Aristides Tagalakis and imaging by Mr. David McCarthy.

2.2.40. TEM FOR CILIA ULTRASTRUCTURE

Ciliated cells cultured at an ALI were scraped and cells washed off with 200µL warmed BEBM. Cells were fixed by addition of 2mL of 2.5% glutaraldehyde and stored at 4^{o}C for at least 24 hours prior to further processing by the PCD diagnostic service team at the Royal Brompton & Harefield NHS Foundation Trust, UK. Glutaraldehyde Fixed samples were centrifuged at 378 x *g* for 5 minutes, post-fixed in 1% (w/v) osmium tetroxide and incubated for 1 hour at room temperature. After incubation the samples were centrifuged at 378 x *g* for 5 minutes, washed with distilled water, centrifuged at 378 x *g* for another 5 minutes and embedded in 2% (w/v) agar. Next the sample was dehydrated by incubating 2x 20 minutes in 70%, 90% and 100% methanol at room temperature. The sample was then infiltrated with Araldite to provide blocks suitable for ultra-thin section cutting. This infiltration was done by first incubating, at room temperature, the dehydrated

samples for 2 x 30 minutes in propylene oxide, 20 minutes in a 1:1 mixture of propylene oxide and Araldite, 30 minutes in a 1:4 mixture of propylene oxide and Araldite and then 2x 3 hours in Araldite at 30^{o}C. Samples were then hardened by baking for 72 hours at 60^{o}C. Once cooled survey sections of around 1µm thickness were stained with 1% (w/v) toluidine blue for a few seconds and examined by light microscopy to select the area with the most cilia cut transversely. Ultra-thin sections of this area (~80–100nm thick) were stained with 2% (w/v) uranyl acetate in methanol for 5 minutes followed by lead citrate for 2 minutes. Cilia were then viewed with a Hitachi H7000 transmission electron microscope. Assessment of cilia ultrastructure was undertaken blinded by Dr Amelia Shoemark who is part of the PCD diagnostic service team at the Royal Brompton & Harefield NHS Foundation Trust, UK.

2.2.41. Hydrodynamic Size and Zeta Potential Measurements

Complexes were prepared in water and diluted in 1mL dH2O to a final concentration of 5µg/mL DNA and then analysed for hydrodynamic size and zeta potential using a Malvern Nano ZS. Liposome alone and a liposome-peptide mixture (LP; liposome: peptide ratio of 1:5.3) were also diluted in 1mL dH2O to a final concentration of 5µg/mL of liposome before being analysed as above. The data was collected and processed by the manufacturer's software, DTS version 5.03.

2.2.42. Gel Retardation Assay

Complexes were prepared in water and either left untreated or treated with 20U/mL heparan sulphate for 1 hour at room temperature. 250ng of plasmid DNA complexed into particles (or plasmid DNA alone as a control) were loaded onto a

1% agarose gel, made in TAE buffer and stained with 1µg/mL ethidium bromide and electrophoresed at a voltage of 100 V for 1 hour with TAE as the running buffer.

2.2.43. PicoGreen Fluorescence Assay

Plasmid DNA was mixed with 0.67% (v/v) PicoGreen reagent in TE buffer and incubated for 5 minutes at room temperature. The stained plasmid DNA was formulated into complexes at a DNA concentration of 10ng/µL in TE buffer. Varying concentrations of heparan sulphate (0-10 U/mL) diluted in TE buffer were mixed with the complexes and incubated for 1 hour at room temperature and fluorescence analysed at excitation and emission wavelengths of 485nm and 520nm respectively using the FLUOstar Optima plate reader. Values were collected as relative fluorescence units (RFU) and these were normalised to naked plasmid DNA stained with PicoGreen and treated with the varying concentrations of heparan sulphate.

2.2.44. Lentivirus Production

1.5 x10^7 HEK293T cells were seeded in 175cm^2 flasks so as to reach 70-80% confluency following 24 hours at 37^oC and 5% CO_2. For each flask 40µL of vector plasmid (containing the gene/shRNA to be integrated into target cells), 30µL of pCMV-dR8.74 plasmid (containing gag, pol, rev and tat elements from HIV-1) and 10µL of pMD.G2 plasmid (containing VSV-G) were added to 5mL OptiMEM and filtered through a 0.22µm filter. Separately 1µL of 10mM PEI was added to 5mL OptiMEM and filtered through a 0.22µm filter and the two solutions thoroughly mixed and incubated for 20 minutes at room temperature to allow complex formation. Cells were then washed with OptiMEM and incubated with the

complexes for 4 hours at 37^{o}C and 5% CO_2. The complexes were then removed and replaced with pre-warmed complete media. Lentivirus was harvested at 48 and 72 hours following transfection. The virus containing supernatant was centrifuged at 2,688 x *g* for 10 minutes, filtered through a 0.22µm filter and centrifuged at 98,000 x *g* for 2 hours to pellet lentiviral particles. Viral pellets were re-suspended in PBS, incubated on ice for 1 hour, centrifuged at 1,344 x *g* and aliquots stored at -80^{o}C.

2.2.45. LENTIVIRUS TITRATION (FLOW CYTOMETRY METHOD)

All lentivirus titrations were performed with HEK293T cells. 50,000 cells were seeded per well of a 12 well plate and incubated overnight to allow cell adherence. The following morning 30µL of lentivirus preparation was diluted 1:50 into 1,470µL of complete media. A 10-fold dilution series was prepared to a final dilution of 1:5,000,000. Complete media was then aspirated from HEK293T cells, replaced with diluted virus, the cells incubated for 72 hours at 37^{o}C and 5% CO_2 and green fluorescent protein (GFP) expression assayed by flow cytometry. The dilution at which 5-30% of cells were GFP positive was used to calculate virus titre. Above this range the probability that each GFP positive cell was transduced twice significantly increases thereby risking an underestimation of the true virus titre (382). The formula used to calculate virus titre, expressed in Transducing units per millilitre (TU/mL), was;

$$\mathrm{TU/mL} = \frac{\%\ \text{of GFP positive cells} \times \text{dilution factor} \times \text{number of cells seeded}}{100}$$

2.2.46. WESTERN BLOTTING

Pelleted cells were lysed with Cell Extraction Buffer Protein content of cell lysate was assessed using the Pierce BCA Protein Assay Kit 20-50µg of cell lysate was then mixed with an appropriate volume of NuPage LDS Sample Buffer and boiled at 90^{o}C for 15 minutes. Samples were then loaded onto NuPage Novex 4-12% Bis-Tris Gels (protein of interest <160kDa) or NuPage Novex 3-8% Tris-Acetate Gels (protein of interest >160kDa) with an appropriate protein ladder used (SeeBluePlus2 Pre-Stained Standard for 4-12% gels and HiMark Pre-Stained Protein Standard for 3-8% gels). Samples were electrophoresed through the gel at 175V for 1-2 hours with 1X NuPage MES SDS Running Buffer for Bis-Tris gels and 1X NuPage Tris-Acetate SDS Running Buffer for Tris-Acetate gels. Protein was transferred onto an Immobilon-P polyvinylidene fluoride (PVDF) membrane using an X-Cell II Blot Module at 25V for 2-4 hours and a solution of 1x NuPage Transfer Buffer and 20% methanol was used as the transfer buffer. The membrane was then blocked with 4% (w/v) BSA in PBST (PBS with 0.05% (v/v) Tween-20) for 1 hour at room temperature. The membrane was then washed with PBST thrice for 5 minutes at room temperature and primary antibody, diluted in 1% (w/v) BSA in PBST, added and incubated with the membrane at 4^{o}C overnight. The membrane was then washed with PBST thrice for 5 minutes at room temperature and HRP-conjugated secondary antibody, diluted in 1% (w/v) BSA in PBST, added and incubated with the membrane for 1 hour at room temperature. The membrane was then washed with PBST thrice for 5 minutes at room temperature and bands visualised by using the Pierce ECL Western Blotting Substrate and UVIchemi chemiluminescence imaging system.

2.2.47. Immunofluorescence Staining and Confocal Microscopy

Cells were fixed with 4% PFA for 10 minutes at room temperature and washed thrice with PBS. Cells were permeabilised by incubating with PBS-Triton (PBS 0.1% (v/v) Triton-X100) for 10 minutes at room temperature and then washed thrice for 5 minutes with PBS. Cells were then blocked with 4% (w/v) BSA in PBS-Triton for 1 hour at room temperature and washed thrice for 5 minutes with PBS before incubation at room temperature for 2 hours with primary antibody diluted in 1% (w/v) BSA in PBS-Triton and where stated with 4',6-diamidino-2-phenylindole (DAPI; 0.5µg/mL) and/or Alex Fluor conjugated Phalloidin (4U/mL) also included. Cells were then washed thrice for 5 minutes with PBS and incubated for 1 hour at room temperature with Alexa Fluor conjugated secondary antibodies diluted in 1% (w/v) BSA in PBS-Triton. Cells were then washed thrice for 5 minutes with PBS and rinsed once with dH_2O then mounted onto microscope slides with VECTASHIELD Mounting Medium and No. 0 coverslips. Images were then obtained using an Inverted Zeiss LSM 710 Confocal microscope with the appropriate excitation lasers selected for the dyes used.

2.2.48. High-Speed Video Microscopy

High-speed video was recorded using a MotionPro X4 high-speed motion camera attached to a Nikon Eclipse Ti-U inverted microscope built with an environmental chamber. Videos were recorded at a frame rate of 500fps using Motion Studio software (IDT Vision, v2.11) with cells maintained at $37^{o}C$. Cilia beat-frequency was assessed using CiliaFA software (383).

Whilst on transwells cells grown at an ALI were washed twice apically with 100µL BEBM and incubated at 37^{o}C and 5% CO_2 for 30 minutes to allow the cells to equilibrate before video recording was started.

Cells were also scraped off transwells using a metal spatula and suspended in 300µL of BEBM by washing the scraped transwells twice with 150µL BEBM. 100µL of this suspension was dropped onto a microscope slide, a cover-slip placed on top of the cells and high-speed videos recorded.

2.2.49. Fluorescence Microscopy

Bright-field and fluorescence images were captured with a Nikon Digital Sight DS-QiMC video camera attached to a Nikon Eclipse Ti-U inverted microscope. Videos and images were processed using NIS Elements AR software (Nikon, v4.00.12).

2.2.50. Statistics

Parametric tests; Student's t-test was used when comparing two groups whilst one-way analysis of variance analysis (ANOVA) followed by Bonferroni post-test analysis was used when comparing three or more groups. Where ANOVA showed that significant differences existed between the study groups but Bonferroni post-test analysis was unable to identify which means significantly differed then Tukey's post-test analyses was used. Non-parametric tests were used when normal distribution could not be assumed (animal studies). Kruskal-Wallis test followed by Dunn's post-test analysis was used when comparing three or more groups. Fisher's exact test was used when analysing contingency tables. Differences were considered significant when $p<0.05$. Where means or medians are displayed n values were three or more.

CHAPTER THREE

RESULTS

LPD OPTIMISATION AND CHARACTERISATION

3. LPD OPTIMISATION AND CHARACTERISATION

3.1. INTRODUCTION

Gene therapy targeted to the airway epithelium has been an objective for CF researchers for over two decades and a number of vectors have been developed in order to achieve efficient gene transfer. The ideal vector needs to be efficient *in vivo*, non-immunogenic given the potential need for repeated delivery, capable of withstanding nebulisation, simple to manufacture in large quantities and, to be suitable for PCD gene therapy, particularly when focussing on correcting *DNAH5* mutations, a large packaging capacity is required.

The Hart laboratory has developed a variety of synthetic receptor-targeted lipopolyplex vectors for gene delivery. These vectors contain lipid and peptide components that self-assemble into nanocomplexes upon mixing with DNA. An LED-1 vector (287) (hereafter referred to as LPD) was shown to give efficient *in vivo* transfection targeted to the airway epithelium, retained transfection activity following nebulisation and repeated delivery, targeted the tracheal and bronchial epithelium as opposed to the lower airways and transfected ciliated cells (287, 289, 290) making the vector a good candidate for use in PCD gene therapy. The LPD vector is formulated with a liposome (L), made up of DHDTMA (1-Propanaminium, N,N,N-trimethyl-2,3-bis (11Z-hexadecenyloxy)-iodide) and DOPE lipids, a dual functioning DNA-condensing and receptor-targeted peptide (P), with the sequence K_{16}GACSERSMNFCG (K_{16}E) and DNA (D) formulated at an L:P:D weight ratio of 0.75:4:1.

Lipopolyplexes that combine both liposomes and polymers have gained popularity due in large part to the higher transfection efficiencies observed when compared to their respective liposome-DNA or polymer-DNA (lipoplexes and polyplexes respectively) counterparts (384-388) though whether this holds true for the LPD nanocomplex described above has not been investigated nor have the biophysical properties for this nanocomplex been assessed in detail.

3.2. AIMS

In this chapter the peptide component of the LPD vector was optimised and its ability to transfect primary airway epithelial cells was assessed as well as its ability to transfect the DNAH5 transgene in mammalian cells. The biophysical properties of the LPD vector was also investigated and related to the transfection capabilities of the LPD lipopolyplex.

3.3. RESULTS

3.3.1. VECTOR OPTIMISATION

Tagalakis et al., (287) had previously optimised the liposome component of the LPD vector whilst the optimal targeting sequence for airway epithelial cells was found to be SERSMNF following phage display studies (288). This peptide sequence showed close homology to parts of the receptor targeting proteins of rhinovirus- a respiratory pathogen (288). However the effect on transfection efficiency of altering the lysine-based DNA binding domain of the targeting peptide had not previously been assessed.

Gene delivery vectors must balance the need for efficient DNA condensation, which help protect the DNA, with intracellular release of DNA so that it escapes degradation in lysosomes and is available to the transcription machinery. Both arginine and lysine-containing peptides have been used in vector complexes and these amino acids are also utilised in natural systems for DNA condensing. Protamines, proteins that condense DNA in sperm heads, are rich in arginine whilst histones, proteins that condense DNA in somatic cells, use both lysine and arginine for DNA condensation. Both amino acids have been shown to condense DNA differently with lysine-based peptides less able to densely pack DNA than arginine-based peptides (389, 390). Although efficient DNA condensation is important in the formation of small nanoparticles for gene delivery, very strong packaging of DNA can lead to inefficient intracellular release of DNA and so inefficient gene expression downstream. Poor transfection efficiencies were achieved as a result with long poly-L-lysine polymers (180 residues) over shorter ones (19-36 residues) because the former had a lower tendency to dissociate from bound DNA (391).

In comparing polyplexes formulated using either lysine or arginine peptides of varying lengths (K_9, R_9, K_{12}, R_{12}, K_{16}, R_{16}) Mann et al., (390) showed that condensation of plasmid DNA was different for lysine and arginine-based polyplexes and the types of particles formed, including linear rods or spheres, was dependent on both length and chemical composition of the peptides. Polyplexes formed from arginine-based peptides were superior with regards to transfection efficiency to those formed from lysine-based peptides and 16-mer peptides showed higher levels of transgene expression than 12- and 9-mer peptides. The superiority of

polyplexes formed from arginine-based peptides was down to greater intracellular release of plasmid DNA whilst poor cellular uptake and plasmid DNA release hampered the transfection efficiency of polyplexes based on short 9-mer and 12-mer peptides (390).

3.3.1.1. Optimising peptide component of LPD vector

Given the superiority of arginine homopeptides in polyplexes the effect of altering the DNA binding domain of the $K_{16}E$ peptide (K_{16}) on transfection efficiency of LPD lipopolyplexes was determined. Whilst retaining the targeting sequence, the DNA binding domain was altered to assess if shorter strings of lysine residues (K_8E) or the use of arginine ($R_{16}E$) in place of lysine could enhance the transfection efficiency of LPD vectors. Use of 8 lysine residues instead of 16 in the DNA binding domain resulted in a significant drop in luciferase expression with activity falling from $2.32\pm0.14x10^8$ RLU/mg of protein with $K_{16}E$ to $4.50\pm0.16x10^7$ RLU/mg of protein with K_8E (Figure 3.1; $p<0.001$; one-way ANOVA with Bonferroni post-test analysis). There was a smaller fall in transfection efficiency when $R_{16}E$ was used instead of $K_{16}E$ with luciferase activity falling to $1.36\pm0.14x10^8$ (Figure 3.1; $p<0.001$; one-way ANOVA with Bonferroni post-test analysis). Given the data the $K_{16}E$ peptide was considered optimal and therefore used in further experiments.

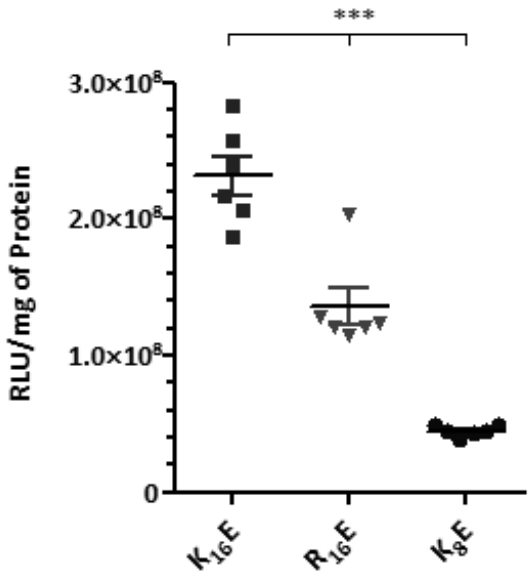

Figure 3.1. Optimising peptide component of LPD vector

Luciferase transfections of 16HBE14o- cells using LPD complexes formulated with $K_{16}E$, $R_{16}E$ and K_8E targeting peptides. ****P*<0.001; one-way ANOVA with Bonferroni post-test analysis used to assess significance. Values are background subtracted and displayed as mean ±SEM.

3.3.1.2. Synergy in transfection with LPD lipopolyplex

The LPD lipopolyplex contains three components making it more complex than binary peptide-DNA or liposome-DNA complexes. Being simpler to formulate the binary complexes are potentially more attractive if they displayed similar or greater levels of transgene expression than the LPD complex. However, lipopolyplexes have previously displayed a synergistic increase in transfection efficiency compared to their lipoplex and polyplex counterparts (384-388) and whether this finding held true with the LPD lipopolyplex was assessed. Transfected luciferase activity using the LPD complex was 3.5-fold higher than that achieved with the LD (4:1) complex - an optimised-for-transfection lipoplex (Figure 3.2; $p<0.001$; one-way ANOVA with Bonferroni post-test analysis), 15.9-fold greater than the LD (0.75:1) complex (Figure 3.2; $p<0.001$; one-way ANOVA with Bonferroni post-test analysis) and 1030.5-fold higher than with the PD complex (Figure 3.2; $p<0.001$; one-way ANOVA with Bonferroni post-test analysis). Moreover, LD (4:1) complexes, but not LD (0.75:1) complexes, gave significantly higher levels of luciferase activity than PD complexes (Figure 3.2; $p<0.001$; one-way ANOVA with Bonferroni post-test analysis). Therefore, the ternary combination of liposome, peptide and DNA in LPD complexes gave greater transgene expression compared to binary PD and LD complexes (Figure 3.2). Moreover having the liposome and peptide together provided a synergistic and not simply and additive increase in transgene expression as observed in other studies (384-388).

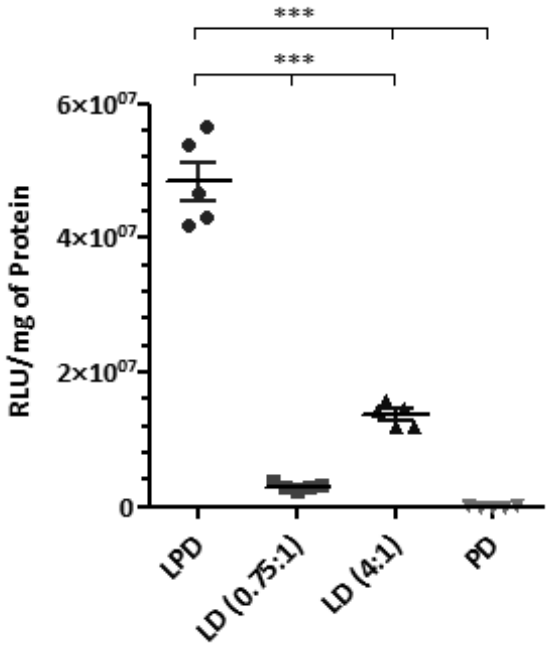

Figure 3.2. Synergy in transfection efficiency of LPD vector

Luciferase transfections of 16HBE14o- cells comparing transfection efficiency of ternary LPD complexes with binary LD and PD formulations. ***P<0.001; one-way ANOVA with Bonferroni post-test analysis used to assess significance. Values are background subtracted and displayed as mean ±SEM.

3.3.1.3. LPD vs L2K

To place the transfection capabilities of the LPD vector into perspective it was compared to the commercial reagent Lipofectamine 2000 (L2K). 16HBE14o- cells were transfected with either pEGFP-N1, to assess the percentage of cells each reagent would transfect, or pCILuc, to assess the level of transgene activity. L2K, at all the ratios tested, transfected a higher percentage of cells (Figure 3.3a; $p<0.001$; one-way ANOVA with Bonferroni post-test analysis) although luciferase activity was highest in the cells transfected with LPD (Figure 3.3b; $p<0.05$; one-way ANOVA with Bonferroni post-test analysis). Also, cells transfected with L2K showed a lower percentage of viable cells and so greater cell toxicity than the LPD particles (Figure 3.3c; $p<0.001$; one-way ANOVA with Bonferroni post-test analysis). This toxicity was also apparent under light microscopy (Figure 3.3d). Cells transfected with the LPD particles showed no observable difference to the OptiMEM control with both showing cells in a compact cobblestone appearance. In contrast, cells transfected using L2K were predominantly spherical at all the three different ratios used.

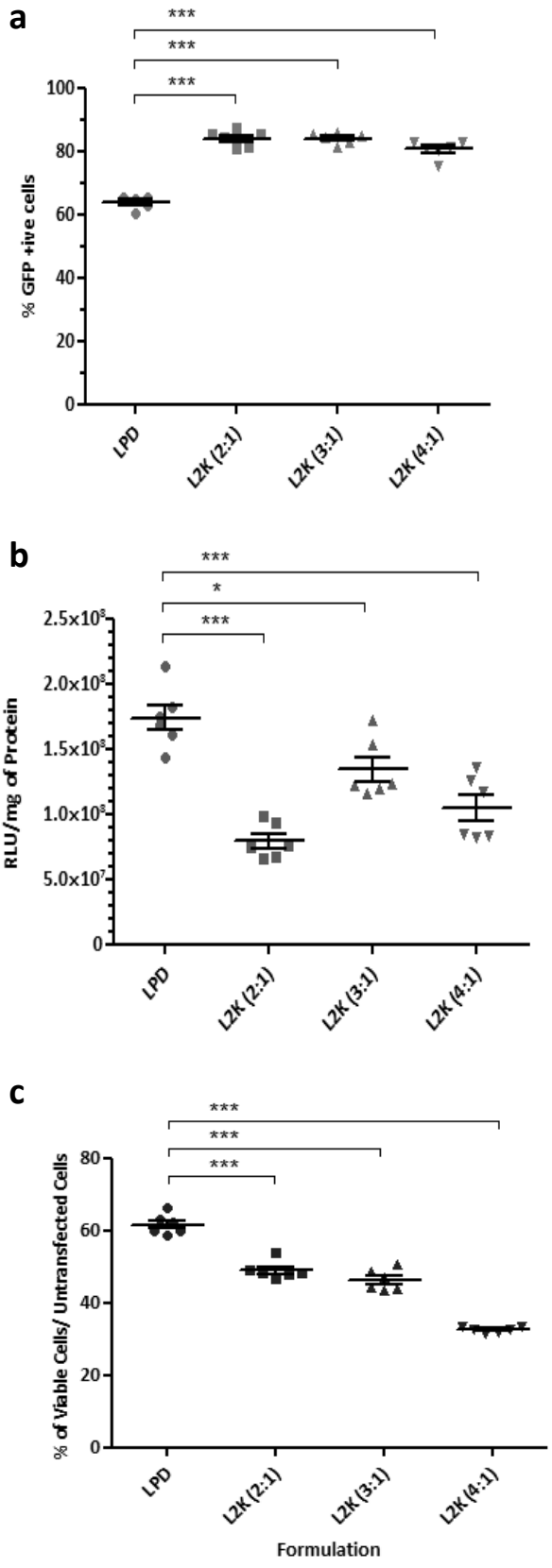
a
***
***
***
100
80
60
40
20
0
% GFP +ive cells
LPD
L2K (2:1)
L2K (3:1)
L2K (4:1)
b
***
*
***
2.5x10⁸
2.0x10⁸
1.5x10⁸
1.0x10⁸
5.0x10⁷
0
RLU/mg of Protein
LPD
L2K (2:1)
L2K (3:1)
L2K (4:1)
c
***
***
***
80
60
40
20
0
% of Viable Cells/ Untransfected Cells
LPD
L2K (2:1)
L2K (3:1)
L2K (4:1)
Formulation

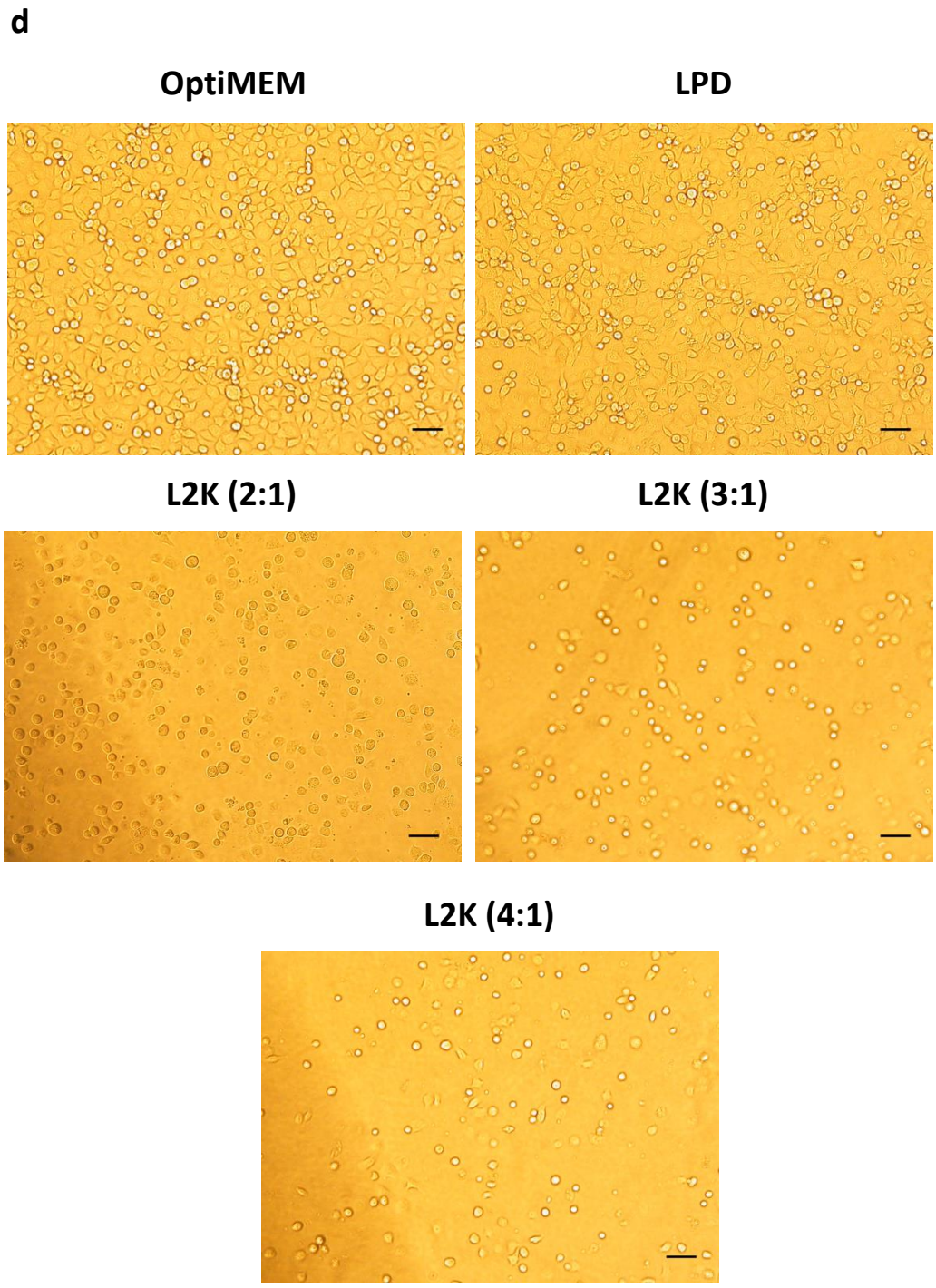

Figure 3.3. Transfections of 16HBE14o- cells using LPD and L2K

Following transfections with either LPD or L2K formulations cells were assayed for (a) the percentage of cells transfected, (b) luciferase transgene activity and (c and d) cell viability. *P<0.05; ***P<0.001; one-way ANOVA with Bonferroni post-test analysis used to assess significance. Scale bars are 100µm. Values are background subtracted and displayed as mean ±SEM.

Cell lines are generally easier to transfect than primary cells (392) most likely due to differences in endocytosis, cell metabolism, cell division and the numbers and types of receptors present on the cell surface. The ability of the LPD nanocomplex to transfect primary human airway epithelial cells, the target for PCD gene therapy, has not been previously assessed and was investigated here in transfection experiments with basal cells obtained from nasal brushings of healthy volunteers (V1-V4). Transfection efficiency of the LPD nanocomplex was again compared to L2K (4:1) which was found to be optimal for transfection of human nasal airway epithelial cells. The mean percentage of cells transfected varied between the volunteers and ranged from 21-23% with the LPD particles and from 13-21% when using L2K (Figure 3.4a). The percentage of transfected cells was significantly higher when using the LPD particles on cells from volunteers 2 and 3 (V2 and V3 respectively; $p<0.01$; Student's t-test). In all instances luciferase activity was significantly higher when using the LPD particles (Figure 3.4b; $p<0.01$; Student's t-test), even in volunteers 1 and 4 (V1 and V4 respectively) where there was no significant difference in the percentage of cells transfected. However, the LPD particles were more toxic to the primary cells than L2K (Figure 3.4c; $p<0.001$; Student's t-test).

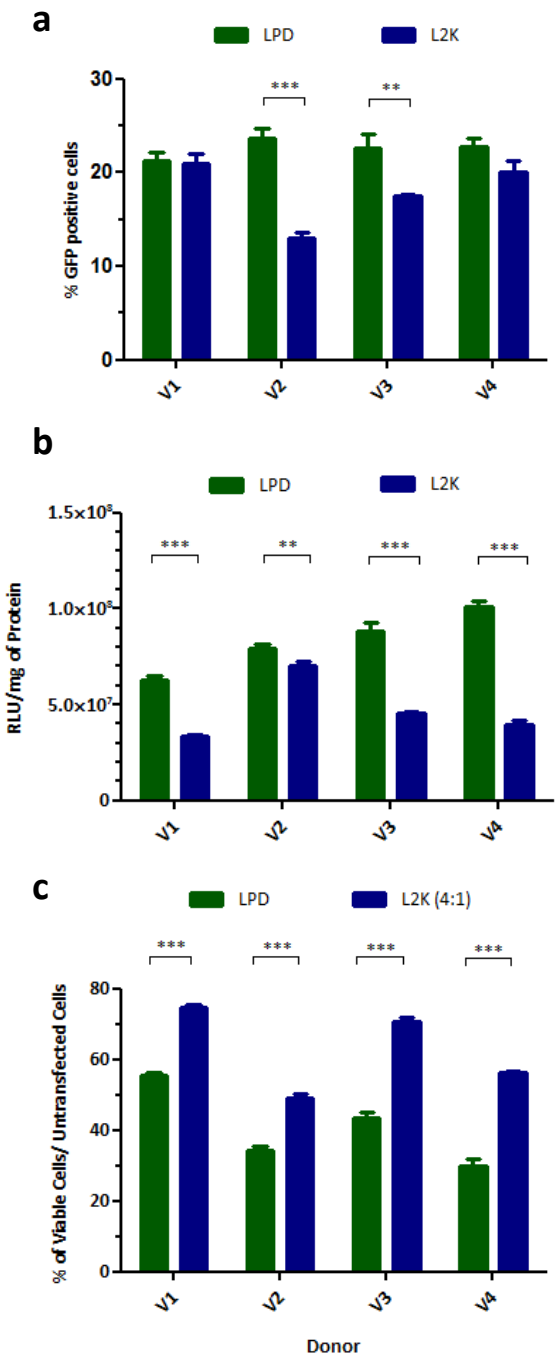

Figure 3.4. Transfection of nasal epithelial cells using LPD and L2K

Following transfection of nasal epithelial cells with either LPD or L2K formulations cells were assayed for (a) the percentage of cells transfected, (b) luciferase transgene activity and (c) cell viability. **P<0.15; ***P<0.001; Student's t-test used to assess significance. Values are background subtracted and displayed as mean ±SEM.

3.3.2. VECTOR CHARACTERISATION

Whilst it was shown that the LPD vector provides efficient gene delivery to airway epithelial cells, the functional significance of the three different components in the formation and function of the LPD vector has not been previously assessed. Detailed structural and functional studies were performed to answer these questions in an attempt to better understand why the LPD lipopolyplex displayed a synergistic enhancement in transfection when compared to binary LD and PD complexes (Figure 3.2). It was anticipated that this information will help in the rational design of more efficient vector systems.

3.3.2.1. Cellular uptake of Cy5-labelled plasmid DNA

One of the first steps in the process of transfection and an important barrier to transfection is vector binding and uptake. Differences in uptake could explain the differences in transgene expression seen when comparing LPD, PD and LD complexes (Figure 3.2). To address this, 16HBE14o- cells were transfected for 6 hours with Cy5-labelled pCI-Luc plasmid using LPD, PD and LD complexes. Cellular uptake of Cy5-labelled plasmid was then assessed using flow cytometry. With LD (0.75:1) complexes 2.5 ±0.1% of cells showed uptake of plasmid DNA compared to 25.2 ±0.9% with LD (4:1) complexes (Figure 3.5a; $p<0.001$; one-way ANOVA with Bonferroni post-test analysis). In both cases LD complexes showed significantly lower levels of plasmid uptake when compared to PD and LPD complexes that showed uptake of plasmid in 50.5 ±5.0% and 53.4 ±3.1% of cells respectively (Figure 3.5a; $p<0.001$; one-way ANOVA with Bonferroni post-test analysis). There were no

significant differences between PD and LPD complexes with regards to the percentage of cells that had taken up the Cy5 labelled plasmid.

Next, the mean fluorescence intensity (MFI) of Cy5 labelled plasmid was assessed to determine if there were any differences in the number of plasmid molecules taken up by transfected cells which may help explain the differences in transgene expression. There was no significant difference in MFI when comparing the two LD complexes (MFI of 56.7 ±4.8 and 126.8 ±3.1 for LD (0.75:1) and LD (4:1), respectively; Figure 3.5b). LD complexes showed a significantly lower MFI when compared to LPD and PD complexes which gave MFI levels of 1080 ±33.2 and 1472 ±54.2, respectively (Figure 3.5b; $p<0.001$; one-way ANOVA with Bonferroni post-test analysis). Whilst there was no significant difference between LPD and PD complexes in regards to percentage of transfected cells (Figure 3.5a), the latter did show significantly higher levels of Cy5 labelled plasmid within each transfected cell so suggesting greater plasmid uptake with PD complexes (Figure 3.5b; $p<0.001$; one-way ANOVA with Bonferroni post-test analysis).

Confocal microscopy images of transfected cells corroborated the flow cytometry findings and showed that uptake of Cy5 labelled plasmid was greatest when cells were transfected with PD and LPD complexes and lowest when using the LD (0.75:1) complex (Figure 3.5c). In order to explain the differences in vector and plasmid uptake the biophysical properties of the different vectors was assessed.

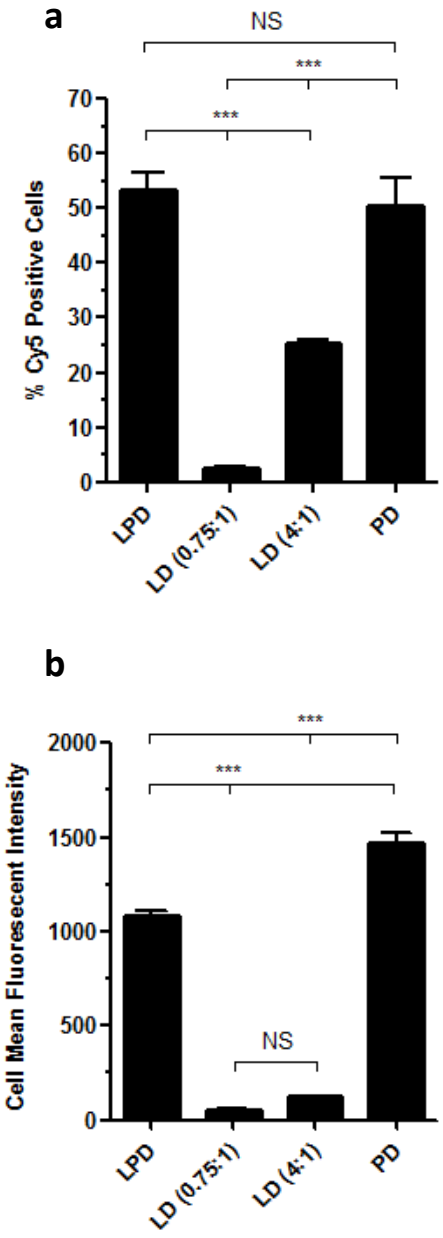
a
NS
***
***
70
60
50
40
30
20
10
0
% Cy5 Positive Cells
LPD
LD (0.75:1)
LD (4:1)
PD
b
***
***
2000
1500
1000
500
0
Cell Mean Fluoresecent Intensity
NS
LPD
LD (0.75:1)
LD (4:1)
PD

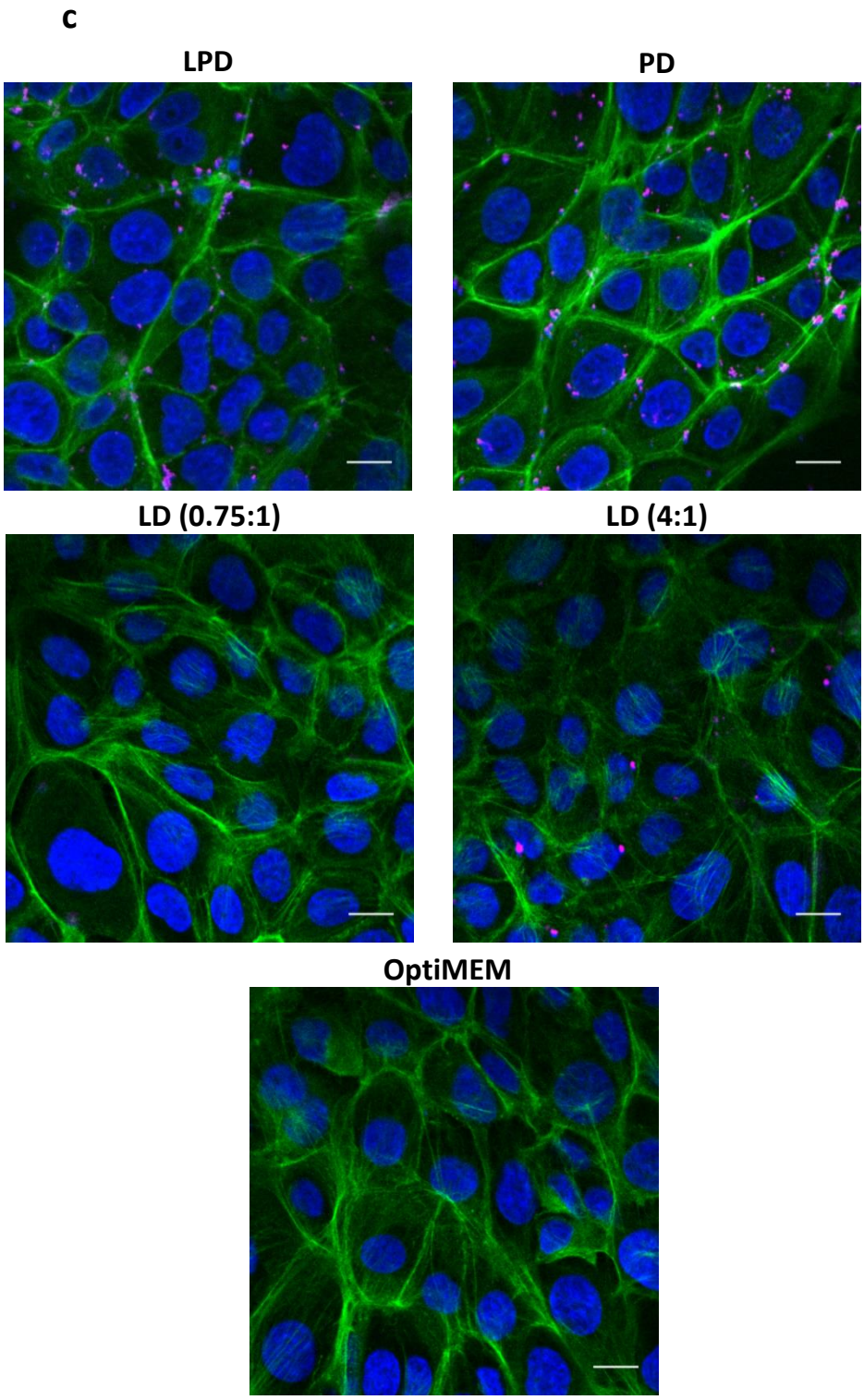

Figure 3.5. Cellular uptake of LPD, LD and PD complexes

16HBE14o- cells were transfected with Cy5-labelled pCI-Luc complexed into LPD, LD and PD complexes and flow cytometry used to assess the (a) percentage of Cy5 positive cells and (b) their MFI. (c) Laser scanning confocal microscopy was used to assess uptake of Cy5-labelled pCI-Luc (magenta). Nuclear (blue) and F-actin staining (green) was used to show cell boundaries. NS, not significant; ***P<0.001; one-way ANOVA with Bonferroni post-test analysis used to assess significance. Scale bars are 15µm. Values are background subtracted and displayed as mean ±SEM.

3.3.2.2. Morphology, size and charge characterisation

The morphology, size and zeta potential of gene delivery vectors influences cellular uptake of the vectors and potentially transfection efficiency. Given the differences observed in cellular uptake of plasmid DNA the morphology, size and zeta potential of LPD, PD and LD complexes was assessed to see if differences in these properties could explain the differences observed in the cellular uptake studies described above.

TEM revealed that the LPD complexes formed a heterogeneous population of roughly spherical particles with sizes around 100-200 nm in diameter (Figure 3.6a). PD complexes were also roughly spherical though particle sizes were smaller with the majority falling within 30-60 nm in diameter and a few particles with sizes of around 100 nm (Figure 3.6b). In contrast to LPD and PD complexes LD mixtures appeared as aggregated material (Figure 3.6c and d). At both the 0.75:1 and 4:1 liposome: DNA ratios multi-lamellar structures were observed (Figure 3.6c and d) while at the 4:1 weight ratio more rounded particles were apparent (Figure 3.6d).

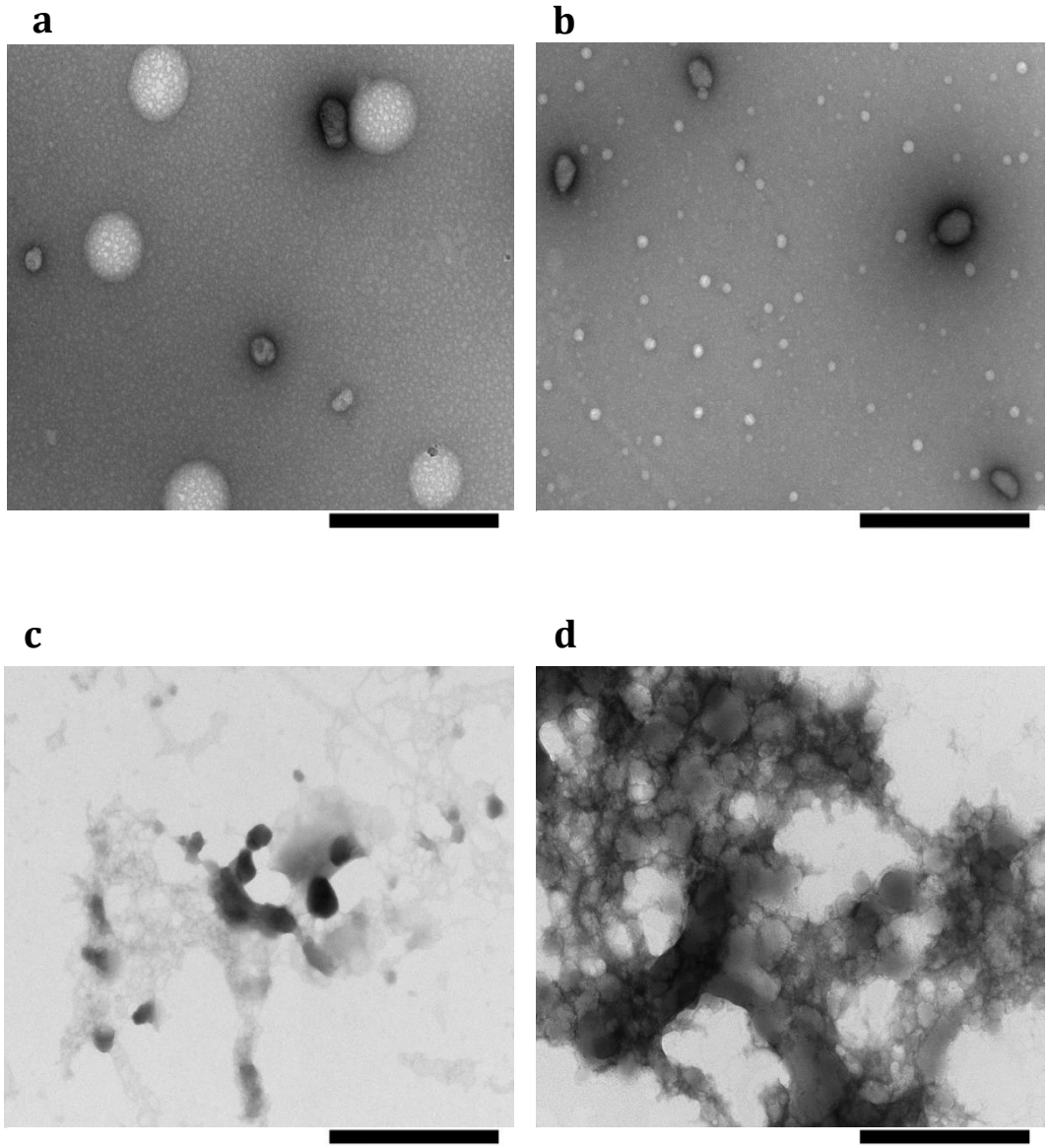

Figure 3.6. Morphology of LPD, LD and PD complexes

TEM micrographs of (a) LPD, (b) PD, (c) LD (0.75:1) and (d) LD (4:1) complexes. Scale bars are 500nm.

The average hydrodynamic size of particles, also known as the z-average size, was obtained using dynamic light scattering (DLS). DLS involves the use of a laser beam illuminating a sample and the intensity of the scattered light being detected and its decay measured over time. The decay in intensity of scattered light is related to the size of the particles which can be calculated using the Stokes-Einstein equation (393). It is important to note that the hydrodynamic diameter obtained using this method is the hydrodynamic diameter of a sphere that diffuses at the same speed as the particle being measured.

Zeta potential refers to the potential difference between the dispersion media and the fluid layer surrounding and electrically interacting with the dispersed particles. As such, the zeta potential describes the electrokinetic potential of a particle in a given solution and is related to the surface charge of the particle. To obtain the zeta potential an electric field is applied to particles in solution and their velocity measured to give the electrophoretic mobility of the particles (394). Zeta potential is then calculated from the electrophoretic mobility.

DLS (Table 3.1) of the four described complexes showed that the mean hydrodynamic size of the PD complexes was smallest at 44.6 ± 0.1 nm, followed by LPD at 58.0 ± 0.2 nm, LD (0.75:1) at 116.1 ± 1.1 nm and 280.3 ± 1.0 nm for LD at the 4:1 ratio. Zeta potential measurements (Table 3.1) for these particles were found to be +67.2 ± 2.1 mV, +32.5 ± 0.5 mV and +31.0 ± 0.6 mV for LPD, LD (4:1) and PD complexes, respectively. When formulated at the lower ratio of 0.75:1 LD complexes showed a negative zeta potential of -20.8 ± 0.2 mV suggesting that the DNA was not neutralized or condensed at all. The liposome used in this study had a

smaller hydrodynamic size, at 82.1 ± 1.1nm, than both LD complexes, as well as a higher zeta potential at +60.1 ± 0.9 mV. A mixture of liposome and peptide (LP) showed a similar hydrodynamic size to liposome alone (Table 3.1) suggesting no interaction between liposome and peptide. A higher zeta potential for the LP mixture compared to liposome alone was also observed (Table 3.1) and was likely due to the charge contribution from the cationic peptide. However, it was not possible to obtain a zeta potential value for the peptide alone so the charge contribution from the peptide could not be determined.

Table 3.1. Hydrodynamic size and zeta potential of LPD, LD and PD complexes

Nanocomplex	Hydrodynamic size (nm)	Zeta potential (mV)
LPD	58.0 ± 0.2	+67.2 ± 2.1mV
LD (0.75:1)	116.1 ± 1.1	-20.8 ± 0.2mV
LD (4:1)	280.3 ± 1.0	+32.5 ± 0.5mV
PD	44.6 ± 0.1	+31.0 ± 0.6mV
Liposome	82.1 ± 1.1	+60.1 ± 0.9mV
LP	86.6 ± 0.5	+74.9 ± 1.7 mV

3.3.2.3. DNA condensation and packaging properties of LPD, PD and LD complexes

Differences in the morphology, size and zeta potential of LPD, PD and LD complexes indicate differences in DNA condensation and packaging so the DNA packaging and release properties of the different complexes were assessed using the gel retardation assay and the fluorescence quenching assay which utilise ethidium bromide and PicoGreen respectively. Nanocomplexes are too large to travel through the pores of a 1% agarose gel so mobility of DNA, when condensed and packaged into nanocomplexes, is retarded and this can be observed by electrophoresing complexed DNA alongside naked DNA on an ethidium bromide stained agarose gel. Ethidium bromide and PicoGreen fluorescence can also be used to assess DNA condensation and packaging of DNA as these compounds upon intercalating with DNA have an intensified fluorescence profile that can be detected and measured. Well condensed and packaged DNA molecules become inaccessible to ethidium bromide and PicoGreen resulting in quenching of fluorescence. In addition to packaging, DNA release can be assessed by using a highly anionic species, such as heparan sulphate, that will compete with DNA to interact with cationic species within nanocomplexes thereby releasing the DNA.

The gel retardation assay was used to assess mobility and condensation of plasmid DNA complexed into LD, PD and LPD complexes (Figure 3.7a). There was no difference in DNA mobility between untreated and heparan sulphate treated naked plasmid DNA when run on an agarose gel showing that heparan sulphate itself does not retard plasmid mobility. At the liposome/DNA ratio used in the LPD complexes (0.75:1) some smearing of plasmid DNA was observed but a significant amount of

plasmid was not retarded indicating that at this low ratio there was little condensation of the plasmid. In contrast, LD complexes formulated at a 4:1 ratio completely retarded mobility of the plasmid DNA which was retained in the wells with strong ethidium bromide staining. It is important to note that complete dissociation of the LD (4:1) complexes could not be achieved even with 20 U/mL heparan sulphate with the majority of the DNA remaining within the wells. However, the intensity of the ethidium bromide staining of plasmid DNA increased suggesting that the heparan sulphate exposed the plasmid DNA, but was unable to effectively induce dissociation of the LD complex.

LPD and PD complexes also showed retarded plasmid mobility but with greater ethidium bromide exclusion than the LD (4:1) complexes as suggested by the faint staining in the wells compared to the LD (4:1) complexes. In contrast to the LD (4:1) complexes, heparan sulphate treatment liberated plasmid DNA from LPD and PD samples indicating that organisation and packaging of plasmid DNA is similar in LPD and PD complexes and dissimilar in LPD and LD (4:1) complexes. Taken together the data indicated that LPD and PD complexes condensed and packaged plasmid DNA more efficiently than LD complexes.

The observed differences in plasmid DNA condensation were further supported by quenching experiments using the PicoGreen assay (Figure 3.7b). When normalised to free plasmid, 30.5±1.2% of PicoGreen labelled plasmid was quenched in LD (4:1) complexes which contrasted with the 73.5±0.1% and 75.9±0.04% quenching of fluorescence seen when using LPD and PD complexes respectively. LD complexes

formulated at a 0.75:1 liposome: DNA ratio did not show noticeable quenching of PicoGreen labelled plasmid.

The addition of varying amounts of heparan sulphate to all four complexes revealed that LD (4:1) complexes were very sensitive to the lowest heparan sulphate concentration used in this study with the RFU values, expressed as a percentage relative to free DNA, having increased from 69.5±1.2% in the absence of heparan sulphate to 76.1±0.3% in the presence of 0.1 U/mL heparan sulphate. In contrast, LPD and PD complexes were more stable to heparan sulphate challenge and only showed a significant increase in fluorescence with the addition of 0.5 U/mL or more of heparan sulphate. At a heparan sulphate concentration of 5 U/mL the RFU values of the complexes followed the order of LD (0.75:1) >LD (4:1) > LPD > PD, with the values being 100.6 ±0.5%, 96.3 ±0.7%, 77.8 ±0.1% and 72.1 ±0.2% RFU, respectively. The difference in the amount of quenching of plasmid DNA with LPD and PD complexes was 2.4% in the absence of heparan sulphate (73.5% of fluorescence quenched for LPD and 75.9% for PD; Figure 3.7b; $p<0.001$; Student's t-test) which increased to 5.7% in the presence of 5 U/mL heparan sulphate (22.2% of fluorescence quenched for LPD and 27.9% for PD; Figure 3.7b; $p<0.001$; Student's t-test), with PD complexes showing greater quenching in both cases. Intracellular release of plasmid DNA may therefore be more efficient with the LPD complexes than with the PD complexes.

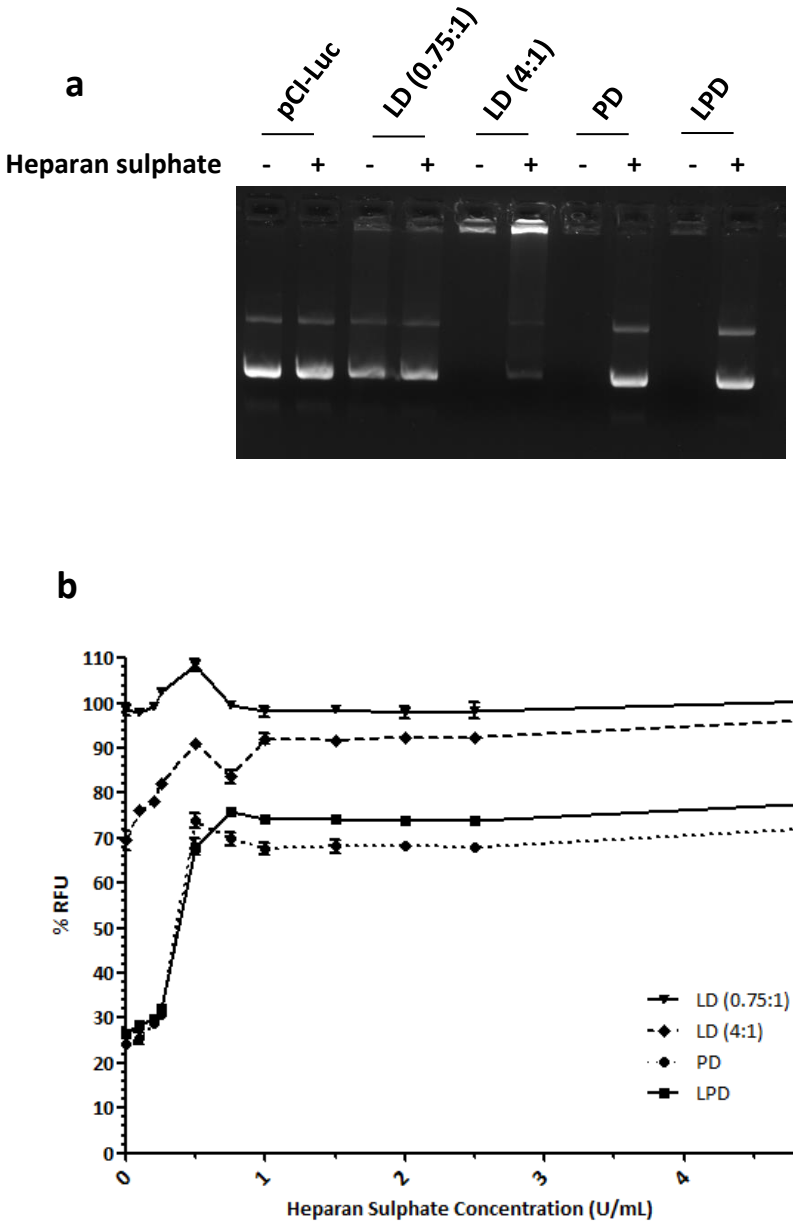

Figure 3.7. DNA packaging and release with LPD, LD and PD complexes

(a) Gel shift assay showing 250ng naked pCI-Luc, LD (0.75:1), LD (4:1), PD and LPD complexes incubated for 1 hour at room temperature in the presence or absence of 20U/mL heparan sulphate. (b) PicoGreen fluorescence quenching was used to assess the stability of the different complexes to heparan sulphate challenge as well as assess the quenching capabilities of the different complexes in the absence of heparan sulphate. The level of PicoGreen fluorescence was measured as RFU with naked PicoGreen labelled pCI-Luc plasmid set as 100% RFU. Values are mean ±SEM.

3.3.2.4. Endosomal escape

Differences in the biophyisical properties between LPD, PD and LD complexes could help explain the differences in vector uptake described above (Figure 3.5a-c) and the differences in uptake of plasmid DNA could also explain differences in transgene expression when comparing LPD and LD complexes. However, it was clear that LPD and PD complexes had similar biophysical properties and displayed similar uptake levels, yet the differences in transgene expression were substantial. As such, an explanation for this disparity must lie in the vectors abilities to overcome intracellular barriers to gene transfer.

For efficient transgene expression it is vital that complexes taken up into the cell are able to escape the endosome to avoid degradation later in lysosomes. The DOPE lipid used to produce the liposomes utilised in the LPD and LD complexes has been shown to aid in endosomal escape by fusing with the lipid bilayer of the endosome. Hypothesising that the major difference between the LPD and PD complexes was that the latter had no mechanism by which to avoid lysosomal degradation the DOPE lipid in DHDTMA:DOPE liposome (L_E) was replaced with the non-fusogenic DOPC lipid (1,2-Dioleoyl-sn -glycero-3-phosphocholine) to form DHDTMA:DOPC liposomes (L_c). These were then used to formulate LPD and LD complexes, along with PD complexes and transgene expression assessed following luciferase gene transfection.

When using L_E liposome the same trend in transfection efficiency seen previously (Figure 3.2) was observed again with transgene expression being greatest with L_EPD> L_ED (4:1)> L_ED (0.75:1)= PD (Figure 3.8). When the L_c liposome was used

transfection with L_cPD and L_cD complexes were not better than transfections with PD complexes so highlighting i) the importance of the DOPE lipid in the functionality of the LPD and LD complexes and ii) that endosomal escape is the main barrier to efficient transgene expression with PD complexes.

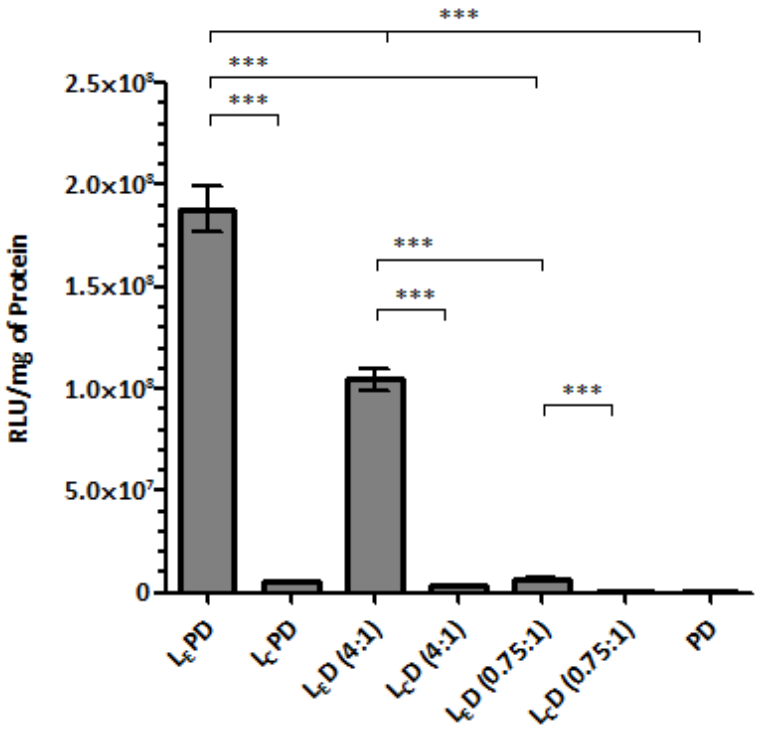

Figure 3.8. Function of DOPE lipid in LPD and LD complexes

16HBE14o- cells were transfected with pCI-Luc formulated into LPD, LD and PD complexes. Either the DHDTMA:DOPE (L_E) or DHDTMA:DOPC (L_C) liposomes were used in the formation of LPD and LD complexes. ***P<0.001; one-way ANOVA with Bonferroni post-test analysis used to assess significance. Values are background subtracted and displayed as mean ±SEM.

3.3.3. DNAH5 CLONING AND CHARACTERISATION

To assess gene therapy for PCD caused by *DNAH5* mutations the wild-type gene must first be cloned. The DNAH5 cDNA was cloned from ciliated NHBE cells grown at an ALI. The strategy used (Figure 3.9) involved cloning of the DNAH5 cDNA as three overlapping segments which were TOPO cloned into pCR-XL-TOPO plasmid. The primers used to clone the overlapping fragments were;

5' Fragment

Forward Primer; 5' – CTACA**GGTACC**ATGTTTAGGATTGGGAGGA– 3'

Reverse Primer; 5' – GCAGGGCATAAGATTCCTCAATAGGTCCTACTTG– 3'

Middle Fragment

Forward Primer; 5' – CCTGGATGGTTGTCATTGGACGCCACTG– 3'

Reverse Primer; 5' – CCTGAGGAGTACGAATGACACGAGAGATCTTGAC– 3'

3' Fragment

Forward Primer; 5' – GATCTTTCTCGGGTCTGGCAGGGAATGCTG– 3'

Reverse Primer; 5' – CCCAC**GTCGAC**TTACTTGACATCACACAGAAGG– 3'

DNAH5 cDNA was flanked with *KpnI* and *SalI* sites (bold; Figure 3.9; grey and yellow bars respectively) whilst naturally occurring *AfeI* and *SexAI* sites (Figure 3.9; green and orange bars respectively) were utilised to allow reconstruction of the full-length DNAH5 cDNA in later steps. Sequencing of three segments revealed several mutations which deviated from the expected DNAH5 cDNA sequence (NCBI

Reference Sequence: NM_001369.2). The majority of these were either silent mutations or known single nucleotide polymorphisms (SNP's) that do not cause disease. However, two missense mutations were also found which were of concern as their effects on the DNAH5 protein, if any, were unknown. These were corrected using site-directed mutagenesis and the three segments then reconstructed into the full-length DNAH5 cDNA in the pMK-Polylinker plasmid which was designed to contain a *KpnI-AfeI-SexAI-SalI* cloning cassette. The full-length DNAH5 cDNA was then cloned into the mammalian expression plasmid pCI using *KpnI* and *SalI* to produce the plasmid pCI.DNAH5.

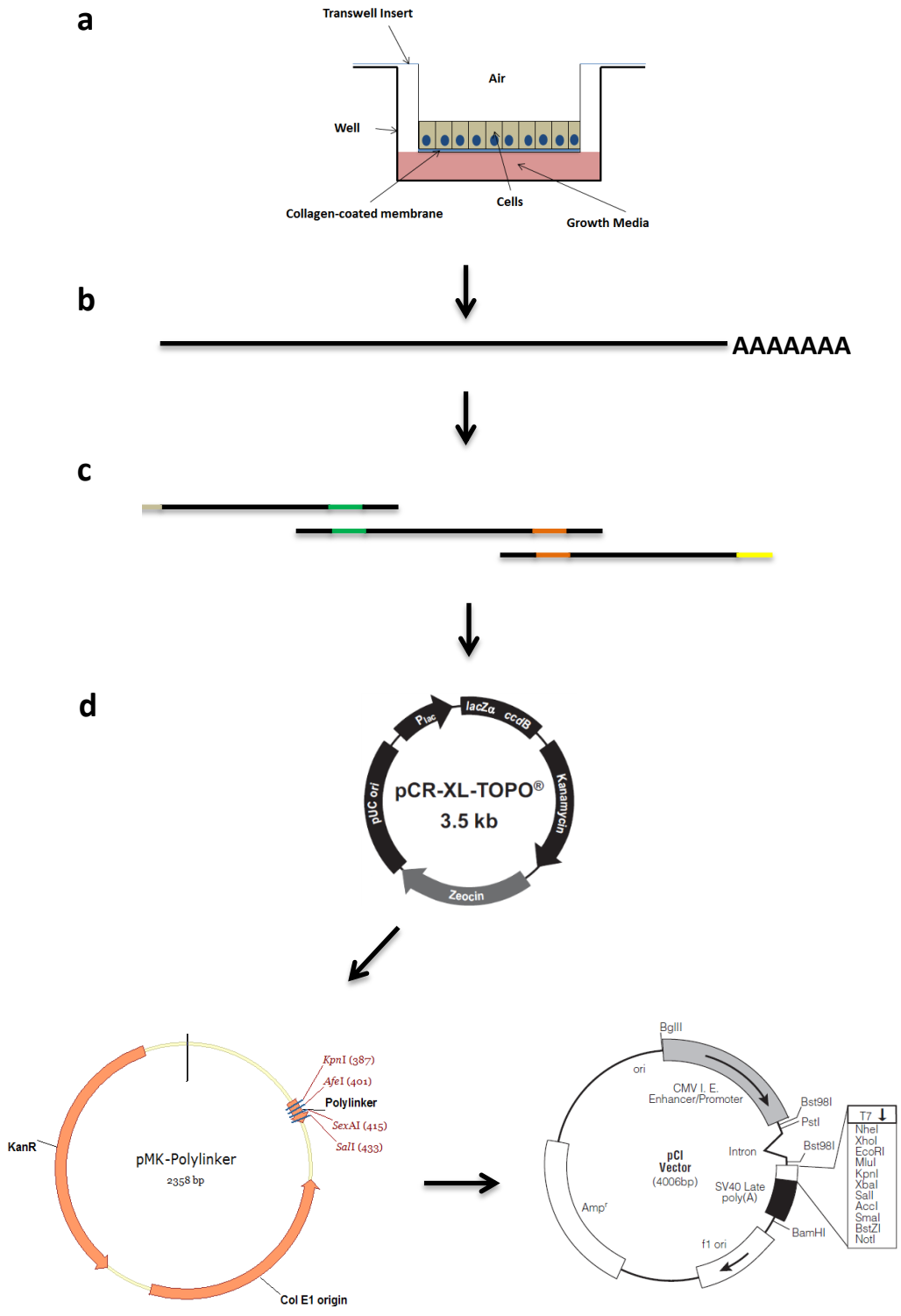

Figure 3.9. pCI.DNAH5 cloning strategy.

(a) NHBE cells were grown at an ALI to induce ciliogenesis and (b) DNAH5 mRNA isolated and (c) reverse transcribed and three overlapping sections amplified by PCR and (d) sub-cloned into the pCI expression plasmid after assembly in cloning plasmids.

To determine if the cloned DNAH5 cDNA provided expression of wild-type DNAH5 mRNA and protein the human embryonic kidney cell line HEK293T was transfected with pCI.DNAH5 using the LPD nanocomplex with DNAH5 mRNA and protein expression assessed using reverse transcription-PCR (RT-PCR), immunofluorescence and Western blot. DNAH5 mRNA was not detected in untransfected cells whilst a 637bp region of the DNAH5 mRNA was amplified using cDNA obtained by extracting total RNA from pCI.DNAH5 transfected cells (Figure 3.10a). A lack of potential plasmid or genomic DNA contamination was demonstrated in PCR reactions where no reverse transcriptase was added to the cDNA reaction. GAPDH was also amplified in the same reaction as an internal control using primers designed to produce a 447bp product so allowing separation of DNAH5 derived and GAPDH derived PCR products. At the protein level immunostaining with an anti-DNAH5 antibody was positive only in pCI.DNAH5 transfected cells (Figure 3.10b). The Western blot technique was used to assess if the protein expressed from the pCI.DNAH5 plasmid was of the correct size and so confirming its identity as DNAH5. To this end 250µg of total protein was run on a 3-8% tris-acetate gel and protein transferred to a PVDF membrane as described in material and methods. An anti-DNAH5 antibody was then used to blot for the DNAH5 protein and a protein greater than 460kDa in size (estimated weight for DNAH5 is 529kDa) was only detectable in transfected pCI.DNAH5 transfected cells. A number of other non-specific bands, most likely due to the amount of protein loaded, were seen in both untransfected and transfected cells. The data thus confirmed that the cloned DNAH5 cDNA in pCI.DNAH5 gave wild-type DNAH5 mRNA and protein expression.

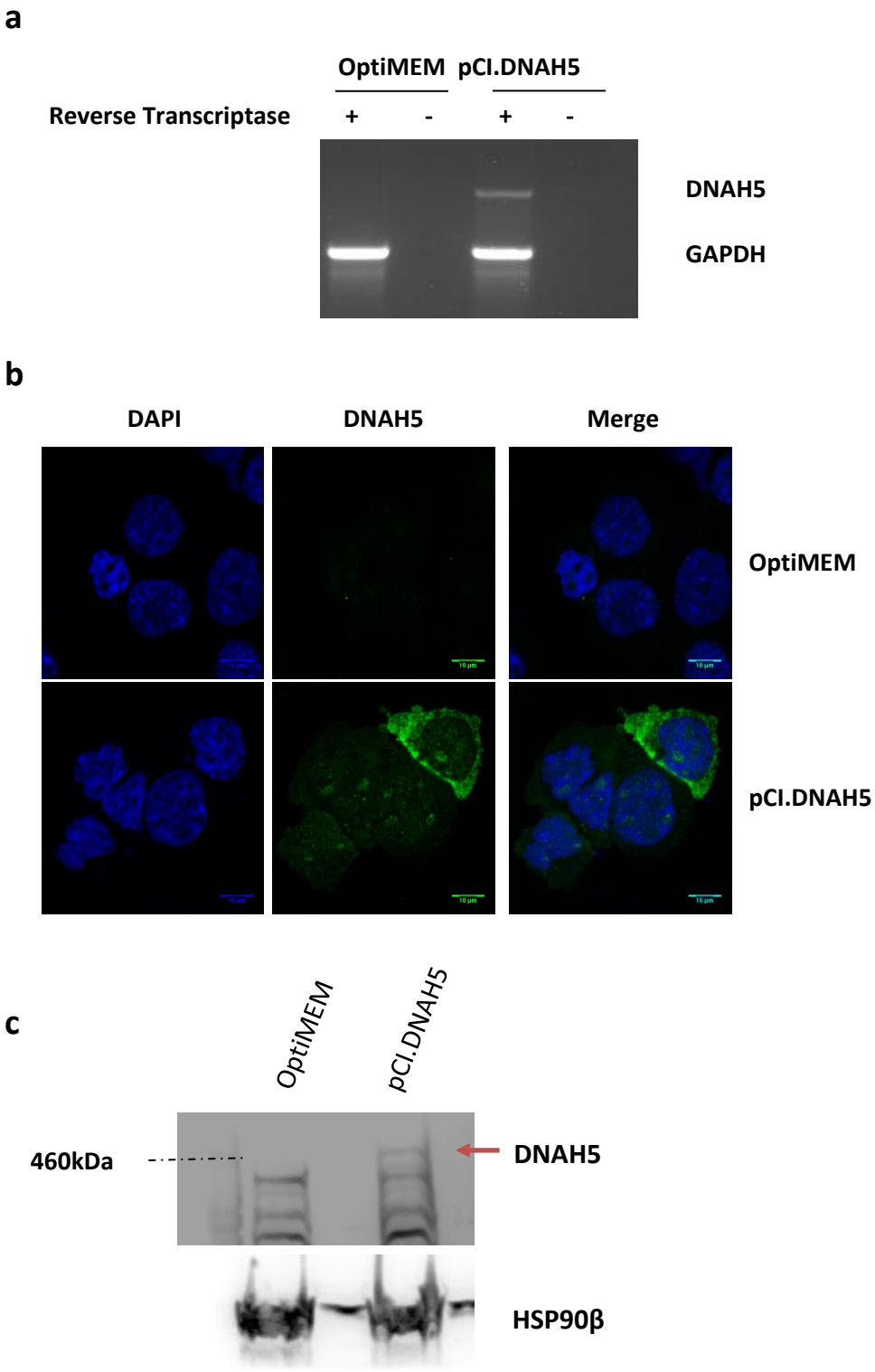

Figure 3.10. Transfection of large plasmid using LPD

Following transfection of HEK293T cells with pCI.DNAH5 (a) total RNA was extracted and RT-PCR performed to assess DNAH5 expression at the mRNA level. (b) Immunostaining and (c) a Western blot was performed to assess DNAH5 protein expression. Scale bars are 10µm.

Plasmid size has been shown to affect transfection efficiency (395) so to enable quantification of the percentage of cells transfected with the pCI.DNAH5 plasmid an enhanced green fluorescent protein (eGFP)-DNAH5 fusion construct was produced. The eGFP cDNA from pEGFP-N1 plasmid was amplified by PCR using the primers;

Forward Primer; 5' –GAGAATTCACGCGTGGTAC*CGCCACCATGGTGAGCAAG*– 3'

Reverse Primer; 5' –CTCCCAATCCTAAACAT**GTGATG***CTTGTACAGCTCGTCCATGCC*– 3'

The 5' ends of both primers contain over 15bp homology to the ends of *KpnI* digested pCI.DNAH5 (underlined) whilst the 3' ends of both primers were homologous to pEGFP-N1 plasmid (*italic*). The above primers amplified the GCCACCATGG Kozak sequence and eGFP cDNA sequence of pEGFP-N1 with the stop codon absent. In addition, the sequence CATCAC (2x His; **bold**) was introduced as a spacer following the eGFP cDNA sequence and preceding the DNAH5 cDNA sequence. The PCR product consisting of 5' and 3' ends that had 15bp homology to the 5' and 3' ends of KpnI digested pCI.DNAH5 was gel purified and cloned into KpnI digested pCI.DNAH5 using SLIC as described in Materials and Methods (Chapter 2.2.22; p93) to produce the plasmid pCI.eGFP.DNAH5. The eGFP transgene from pEGFP-N1 was also sub-cloned into the pCI vector using SalI-NotI restriction sites to both isolate eGFP and sub-clone it into pCI to give the plasmid pCI.eGFP. This was produced to provide a small eGFP expression plasmid contained within the same backbone as the larger eGFP-DNAH5 fusion transgene so allowing direct comparison of transfection efficiency when transfecting large and small transgenes.

16HBE14o- cells were transfected with the pCI.eGFP and pCI.eGFP.DNAH5 plasmids and expression of eGFP and the eGFP-DNAH5 fusion protein was assayed using flow cytometry. Transfection of the pEGFP-N1 plasmid was used as a positive control. When a total of 250ng/well of each plasmid was transfected (at a concentration of 1.25ng/µL) the large pCI.eGFP.DNAH5 plasmid transfected a lower proportion of cells compared to the smaller pCI.eGFP (0.75 ±0.11% for pCI.eGFP.DNAH5 and 8.82 ±0.40% for pCI.eGFP; Figure 3.11a; $p<0.001$; one-way ANOVA with Bonferroni post-test analysis). The size difference between the two plasmids (4.7kb for pCI.eGFP and 18.6kb for pCI.eGFP.DNAH5) means that when 250ng of each was transfected the number of plasmid molecules and so transgene cassettes, transfected was around four times lower when using pCI.eGFP.DNAH5 over pCI.eGFP. Taking this into account equimolar amounts of pCI.eGFP.DNAH5 was transfected (977.5ng/well; concentration of 4.89ng/µL) but this failed to significantly improve the proportion of cells expressing the eGFP-DNAH5 fusion protein (Figure 3.11a). It is also of note that the MFI and so the amount of transgene expressed, was ~12-fold higher when transfecting the small pCI.eGFP plasmid (Figure 3.11b; $p<0.001$; one-way ANOVA with Bonferroni post-test analysis). As such, both the percentage of cells transfected and the amount of transgene expressed is reduced when transfecting the large DNAH5 containing plasmid.

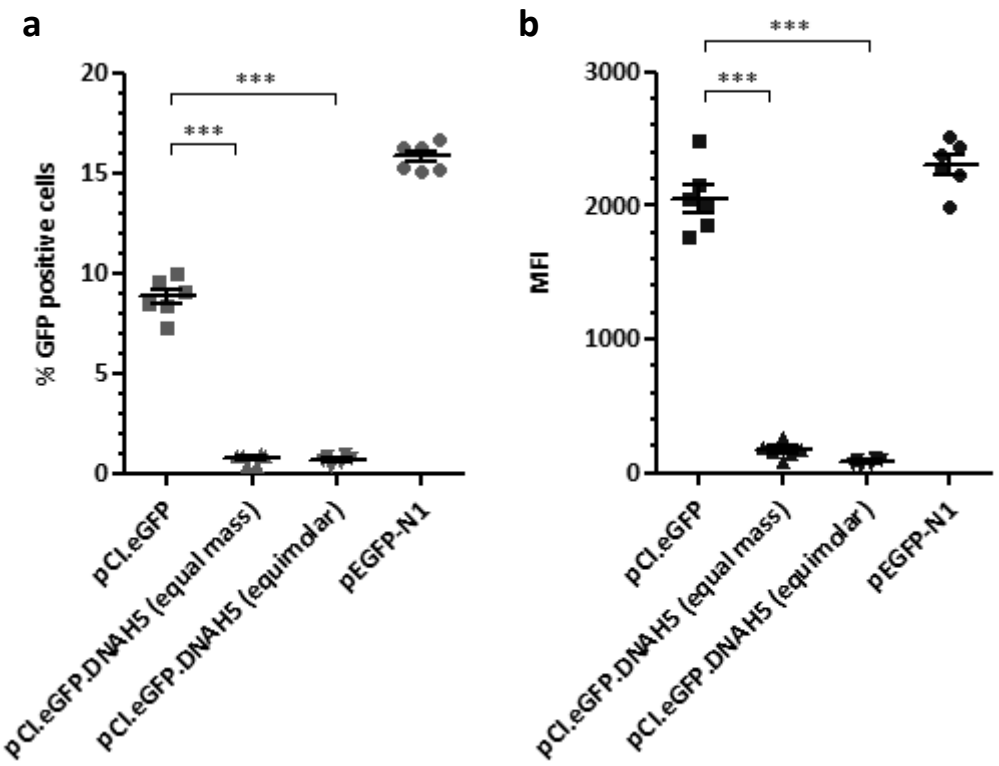

Figure 3.11. Transfection efficiency of large plasmids using LPD

16HBE14o- cells were transfected with the small pCI.eGFP plasmid and larger pCI.eGFP.DNAH5 and assayed by flow cytometry for (a) the percentage of cells transfected and (b) the MFI of transfected cells. ***P<0.001; one-way ANOVA with Bonferroni post-test analysis used to assess significance. Values are background subtracted and displayed as mean ±SEM.

To provide some insight into the causes of the low transfection efficiency when transfecting the large pCI.eGFP.DNAH5 plasmid the biophysical properties of LPD vectors containing the small pCI.eGFP and large pCI.eGFP.DNAH5 plasmid was assessed. No differences in LPD particle morphology could be seen with pCI.eGFP (Figure 3.12a) and pCI.eGFP.DNAH5 (Figure 3.12b) containing LPD complexes with both plasmids producing predominantly spherical nanocomplexes. LPD particles formed with pCI.eGFP.DNAH5 plasmid appeared larger than those formed with the pCI.eGFP plasmid by TEM (Figure 3.12a and b) and indeed quantification by DLS confirmed this observation. LPD nanocomplexes formed with the pCI.eGFP.DNAH5 plasmid were 136.0 ±1.9nm compared to 108.9 ±1.3nm for those formed with the pCI.eGFP plasmid (Figure 3.12c; $p<0.001$; Student's t-test). No significant differences in the zeta potential of the two nanocomplexes was observed. Whilst the difference in hydrodynamic sizes of the two complexes was significant, pCI.eGFP.DNAH5 containing complexes were not substantially larger. Being spherical and under 200nm both nanoparticles would have likely utilised the same uptake pathway (396) and so should have resulted in similar levels of vector and plasmid uptake, particularly when equimolar amounts of plasmid was transfected. It is unlikely then that differences in vector uptake could help explain the differences in transfection efficiency seen when comparing LPD complexes containing pCI.eGFP and pCI.eGFP.DNAH5 plasmids. However, further studies to test this hypothesis were not undertaken and should form the basis of future studies. This could be addressed with uptake studies utilising Cy5 labelled pCI.eGFP and pCI.eGFP.DNAH5.

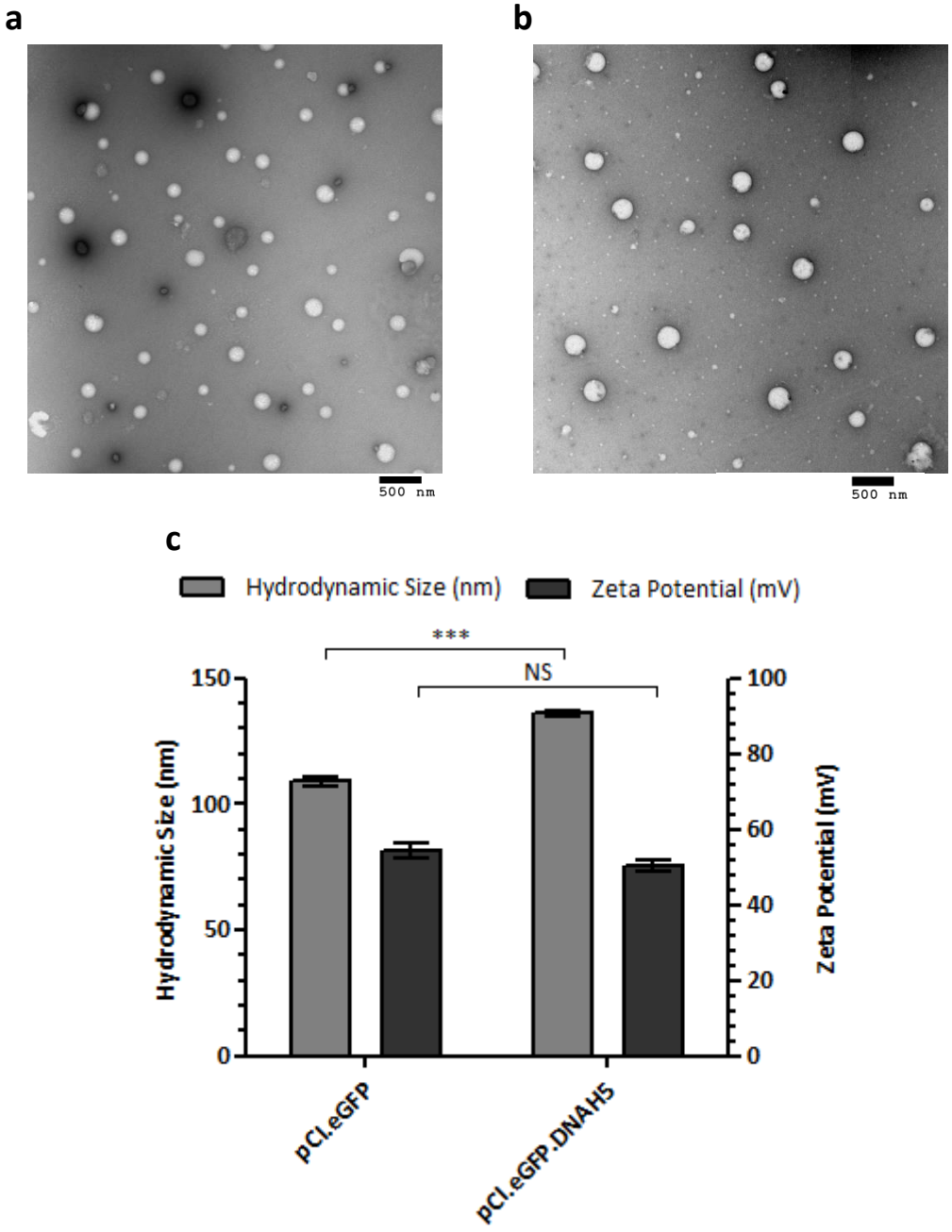

Figure 3.12. Biophyscial characterisation of pCI.eGFP and pCI.eGFP.DNAH5 containing LPD particles

The morphology, size and zeta potential of LPD nanocomplexes formulated with the small pCI.eGFP and large pCI.eGFP.DNAH5 plasmid was assessed by (a-b) TEM and (c) DLS technqiues. NS, not significant; ***p<0.001; Student's t-test used to assess significance. Values are mean ±SEM. Scale bars are 500nm.

3.4. DISCUSSION

In this chapter a non-viral vector system previously optimised for respiratory gene delivery (287) was investigated. This LPD complex contains a cationic liposome and cationic peptide which upon mixing with anionic DNA forms small cationic receptor-targeted nanocomplexes. The receptor-targeting properties of the LPD complex is afforded by the peptide component which consists of a K_{16} DNA binding domain and a receptor-targeting domain consisting the SERSMNF motif found by phage display to target airway epithelial cells (288). Previous studies have shown that use of arginine-based peptides rather than lysine-based peptides result in enhanced transfection with polyplexes (390). However, in the LPD lipopolyplex, exchanging the 16 lysine residues in the K_{16}E peptide for arginine residues produced an almost 50% fall in transfection efficiency. Reducing the number of lysine residues to 8 produced a larger drop in transgene expression which was likely due to inefficient DNA packaging resulting in unstable particles with poorer cellular uptake properties (390). The results therefore indicated that at least in the context of the LPD lipopolyplex, where the peptide is not a homopeptide, the use of arginine in place of lysine for DNA packaging dampens transgene expression. This difference was not further investigated but may be due to differences in DNA condensation and packaging, a key function of the cationic residues within the peptide, leading to differences in vector uptake and subsequently transgene expression.

For the first time the optimal LPD complex, previously shown capable of efficiently transfecting the mouse (287, 289) and pig airway *in vivo (290)*, was shown to efficiently transfect primary human airway epithelial cells obtained by nasal

brushing. The LPD vector consistently transfected around 20% of primary nasal cells irrespective of the donor from whom the cells were obtained. Gene delivery to around 20% of airway epithelial cells, at least in a mouse model of PCD, was sufficient to restore a low level of mucociliary clearance (283) which may offer some clinical benefit to PCD patients.

The LPD lipopolyplex showed transgene expression levels substantially higher than binary LD lipoplexes or PD polyplexes thus showing a co-operation between the liposome and peptide components in the enhancement of transfection. This has been observed by others utilising different lipids and polymers (384, 386, 397). In an attempt to explain the synergy in transfection detailed functional and biophysical analysis of LPD, LD and PD complexes were undertaken.

With respect to transfection, several key steps must take place to allow for efficient gene expression including, i) the formation of stable particles that can protect plasmid DNA from degradation, ii) attachment of vector to cells, iii) uptake of the vector into cells, iv) endosomal escape, v) nuclear entry and vi) release of plasmid DNA from the nanocomplex so that it is accessible to the transcription machinery.

LPD and PD nanocomplexes by TEM produced discrete and roughly spherical particles while the LD lipoplexes appeared as stacked lamellar aggregates. The formation of small discrete particles is thus primarily a consequence of peptide/DNA interactions suggesting they more efficiently condense DNA than cationic liposomes as found in other studies (398). PD and LPD nanocomplexes were both cationic and the zeta potential of the latter was twice that of the former which could lead to differences in cell binding and internalisation (197). However,

cellular uptake studies showed that PD and LPD nanocomplexes were bound and internalised to very similar degrees. This implied the differences between the nanocomplexes lay in their ability to overcome intracellular barriers to transfection.

Escape of nanocomplexes from the endosome compartment following cellular uptake is vital in evading lysosomal degradation of gene delivery nanocomplexes and therefore in the efficiency of transfection. The most common mechanisms by which vectors can undergo endosomal escape are i) destabilisation of the endosome bilayer through the use of fusogenic liposomes (399) or peptides (400) and ii) utilisation of the proton-sponge effect to burst the endosome (186). The presence of the fusogenic DOPE lipid within the LPD nanocomplex provides a mechanism of endosomal escape (401) for this nanocomplex. On the other hand, the PD complex has no obvious method of endosomal escape lacking both a fusogenic lipid/peptide component and, at physiological pH, free protonatable groups that would allow it to utilise the proton-sponge effect seen with PEI (186). Inefficient endosomal escape is thus most likely the major factor responsible for inefficient transgene expression following PD transfections. This is supported by the finding that removal of the DOPE lipid rendered LPD complexes no more efficient than PD complexes showing that the major difference between these two complexes is in their ability to escape lysosomal degradation.

Cellular uptake of the nanocomplexes was the primary barrier to gene transfer to the lipoplex whilst inefficient intracellular trafficking hampered transgene expression by the polyplex. Having both peptide and liposome components in the lipopolyplex produced a cationic nanocomplex small and stable enough to give

efficient cellular uptake, a function of the peptide component, as well as efficient endosomal escape and subsequent release of plasmid DNA for transcription in the anionic environment of the cell, a function of the liposome component. This increased functionality afforded by having both the liposome and peptide in lipopolyplexes can help explain the synergy observed in transgene expression when comparing lipoplexes, polyplexes and lipopolyplexes.

Moving towards PCD gene therapy, DNAH5 mRNA and protein expression was shown following transfection of a cloned DNAH5 cDNA construct. Importantly, it was shown that the large DNAH5 cDNA could be delivered to human bronchial epithelial (HBE) cells using the LPD vector. However, transfection of the large DNAH5 construct is likely to be less efficient than transfecting smaller transgenes as transfection of a GFP-DNAH5 fusion plasmid was found to give a significantly lower proportion of transgene positive cells than when a comparable eGFP only plasmid was transfected. The difference cannot be attributed simply to differences in the number of transgene constructs being delivered as even with equimolar amounts of both plasmids being transfected transgene expression from the large pCI.eGFP.DNAH5 (18.6kb) plasmid was lower than with the smaller pCI.eGFP plasmid (4.7kb). Whilst differences in the sizes of the two complexes were observed the values were not substantially different. That both complexes were under 200nm, spherical and cationic having similar zeta potentials suggests that both complexes would have utilised similar uptake pathways (396) thus suggesting the differences seen in biophysical properties could not explain the significant reduction in transgene expression when transfecting the pCI.eGFP.DNAH5 plasmid.

However, vector uptake studies will help address whether uptake was the rate limiting step for efficient transfection with the large DNAH5 plasmid or if processes downstream are limiting. These answers will aid in overcoming the inefficient transgene expression currently observed.

In summary, given that transfection of the large transgene was well below the target of 20% transfection efficiency required to recover some level of mucociliary clearance, at least in a *Dnaic1* PCD mouse model (283), it was clear that further improvements to enhance transfection efficiency, particularly of the DNAH5 transgene, were required.

The liposome and receptor targeting peptide moieties of the LPD component have been optimised previously (287, 288) but the DNA component, which is responsible for initiating and maintaining transgene expression, has not. In the next chapter the use of minicircle DNA in LPD complexes is explored in the context of airway gene delivery.

CHAPTER FOUR

RESULTS

MINICIRCLE DNA FOR AIRWAY GENE DELIVERY

4. MINICIRCLE DNA FOR AIRWAY GENE DELIVERY

4.1. INTRODUCTION

Plasmids have been engineered to carry the elements necessary for transgene expression in mammalian cells -namely a promoter element for the initiation of transcription, the transgene sequence and a polyadenylation signal to confer stability to the transcribed mRNA and enhance translation. Enhancer elements have also been included to improve transgene expression (304).

Plasmids also contain elements necessary for stable replication in *E. coli* including an origin of replication and an antibiotic resistance gene under the control of a prokaryotic promoter but these are surplus in the context of mammalian gene transfer. In addition, bacterial sequences are typically rich in CpG dinucleotides which remain unmethylated in the *E.coli* host and unmethylated CpG dinucleotides have been shown to induce an immune response in vertebrates (298-301) via toll-like receptor (TLR) - 9 (302).

Minicircle DNA, like plasmids, are circular DNA molecules and have been developed through the use of site-specific recombination (309, 402, 403). Minicircle DNA lacks the prokaryotic elements required for replication in *E. coli*. Two methods are commonly used to derive minicircle DNA both starting with producer plasmids where the transgene expression cassette is flanked with recombination sequences, for example attB and attP sequences. In both systems producer plasmids are propagated in *E. coli* genetically modified to express recombinase under an inducible promoter. Following induction of the recombinase, recombination of the

producer plasmid yields minicircle and miniplasmid DNA. Minicircle is then purified either by use of affinity chromatography binding a specific recognition sequence found in the minicircle but not the miniplasmid (404), or by *in vivo* digestion of the miniplasmid resulting in its degradation thus allowing extraction of relatively pure minicircle DNA (405). The latter system is more convenient as both recombination and miniplasmid removal take place in *E. coli* thus allowing utilisation of standard plasmid extraction protocols and kits for purifying minicircle DNA.

In the context of gene therapy, minicircles have been shown to exhibit sustained transgene expression to plasmids in a variety of organ systems *in vivo* including the liver (309, 310), heart (311, 312) and skeletal muscle (312). Whether the advantages of minicircle DNA are translatable to airway gene delivery have yet to be assessed.

4.2. AIMS

To assess if minicircle DNA would provide enhanced and prolonged transgene expression in the context of airway gene delivery *in vitro* and *in vivo* and to assess if minicircle DNA offers advantages over plasmid DNA when expressing large genes-namely *DNAH5*.

To address these aims reporter genes and the DNAH5 cDNA were sub-cloned into a minicircle producer plasmid, minicircle DNA and plasmid DNA were extracted and transgene expression and persistence assessed *in vitro* and *in vivo*. Toxicity following minicircle and plasmid DNA administration was also assessed *in vivo.*

4.3. RESULTS

4.3.1. PLASMID SUB-CLONING

Figure 4.1 shows a schematic of the sub-cloning steps involved in the production of minicircle producer plasmids containing reporter genes and the DNAH5 cDNA under the control of an EF1α core promoter. A minicricle producer plasmid with a multiple cloning site (MCS) flanked with attB and attP sequences was purchased (pMC.BESPX-MCS2; System Biosciences) and promoter/enhancer elements together with a polyadenylation signal were sub-cloned into this plasmid to produce a cloning vector into which reporter genes and the DNAH5 cDNA could be sub-cloned. An EF1α core promoter was chosen as previous studies have shown that this promoter provides high transgene persistence compared to CMV (296), the only other promoter available for use in the course of this thesis project. It was anticipated that this enhanced transgene persistence would beneficial when transfecting airway cells and then promoting mucociliary differentiation.

All plasmid maps can be found in Appendix B.

pMC.EF1α-MCS

The CpG-free chimeric promoter from pCpGfree-LacZ (Invivogen), containing a CMV enhancer, EF1α core promoter and a downstream synthetic intron, was placed into the pMC.BESPX-MCS2 minicircle producer plasmid by digestion with NcoI and BglII respectively and overhangs filled in using large Klenow fragment. Both plasmids were further digested with EcoR1 and the liberated chimeric promoter then ligated into pMC.BESPX-MCS2 to produce the plasmid pMC.EF1α-MCS.

pMC.EF1α.MCS.SV40pA

The CpG-free late SV40 polyadenylation signal from pCpGfree-LacZ (Invivogen) was PCR amplified and flanked with SalI and ApaI sites using the primers;

Forward Primer; 5' – CTGAGTCGACGCTAGCTGGCCAGACATGATA– 3'

Reverse Primer; 5' – GACTGGGCCCGAATTCCATACCACATTTGTA– 3'

The PCR product was digested with SalI and ApaI and ligated into SalI-ApaI digested pMC.EF1α-MCS plasmid.

pMC.eGFP

pMC.EF1α.MCS.SV40pA and pEGFP-N1 were digested with SalI and NotI respectively and overhangs filled in using large Klenow fragment. SalI digested pMC.EF1α.MCS.SV40pA was then digested with BamHI and the eGFP gene isolated from NotI digested pEGFP-N1 by digestion with BamHI. eGFP was then ligated into the SalI-BamHI digested pMC.EF1α.MCS.SV40pA to produce pMC.eGFP.

pMC.Luc2

Firefly luciferase gene (luc2) and the late SV40 polyadenylation signal were isolated from pGL4.10 using NheI and SalI digestion and ligated into pMC.EF1α-MCS, digested with the same enzymes, to produce pMC.Luc2.

pMC.NL1.3

A secreted form of NanoLuc luciferase, i.e. with an N-terminal secretion signal and the late SV40 polyadenylation signal were isolated from pNL1.3 using NheI and SalI

digestion and ligated into pMC.EF1α-MCS, digested with the same enzymes, to produce pMC.NL1.3.

pMC.DNAH5

pCI.DNAH5 was digested with Acc65I and SalI to isolate the DNAH5 cDNA which was ligated into BsrGI-SalI digested pMC.EF1α.MCS.SV40pA to produce pMC.DNAH5.

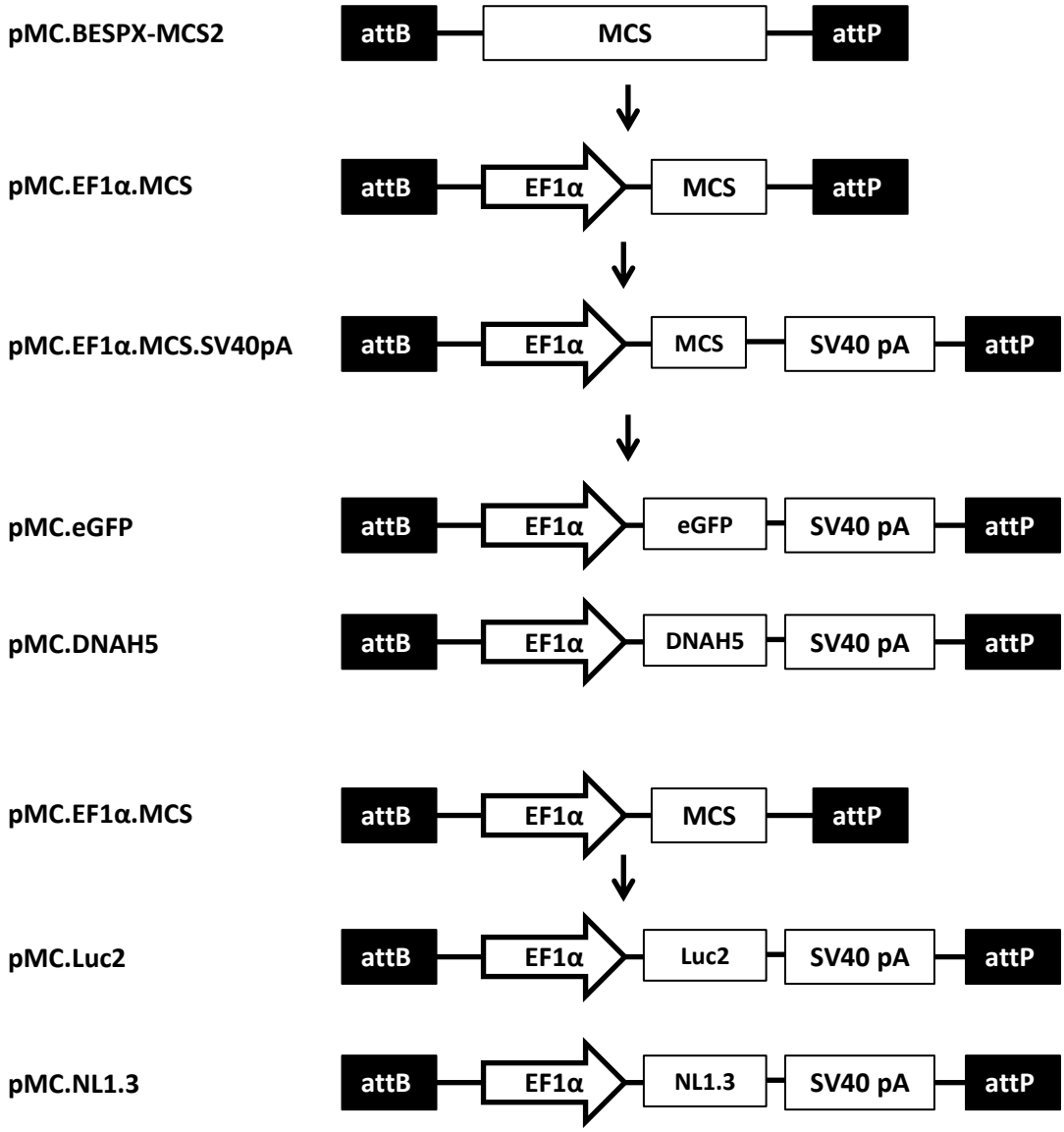

Figure 4.1. Schematic of the plasmids described in this chapter

4.3.2. Efficient Production of Minicircle DNA

Minicircle producer plasmids (pMC.xxxx) were transformed into the ZYCY10P3S2T *E. coli* bacterial strain and minicircle produced as described in Materials and Methods (Chapter 2.2.6; p87). ZYCY10P3S2T cells express ϕC31 integrase and the I-SceI endonuclease upon introduction of L-Arabinose to the bacterial culture. The ϕC31 integrase causes recombination of attB and attP sites, which separate the transgene expression cassette from the bacterial backbone, to produce the minicircle DNA (MC.xxxx) and the plasmid backbone (miniplasmid). The I-SceI endonuclease digests I-SceI recognition sequences in the bacterial backbone thus linearizing the backbone resulting in its degradation within the *E. coli* host (406). The ϕC31 integrase and the I-SceI endonuclease gene copy numbers in ZYCY10P3S2T strain *E. coli* were optimised by Kay et al., (405) to maximise minicircle DNA yield and purity. Minicircle DNA was then extracted and purified using conventional alkaline-lysis plasmid purification kits. Growth of *E.* coli for extraction and purification of the producer plasmid was no different to standard protocols for plasmid purification.

Purified plasmid and minicircle DNA were digested by a relevant single cutting restriction enzyme and 500ng of the digest product was run on an ethidium bromide stained agarose gel and visualised under UV light. There was no visible producer plasmid contamination within minicircle DNA preparations (Figure 4.2) thus the DNA was considered sufficiently pure to be used for further studies. For DNAH5 coding DNA (pMC.DNAH5 and MC.DNAH5) the differences in size when comparing plasmid and minicircle DNA, whilst visible, was minimal given the resolution limits of agarose gels.

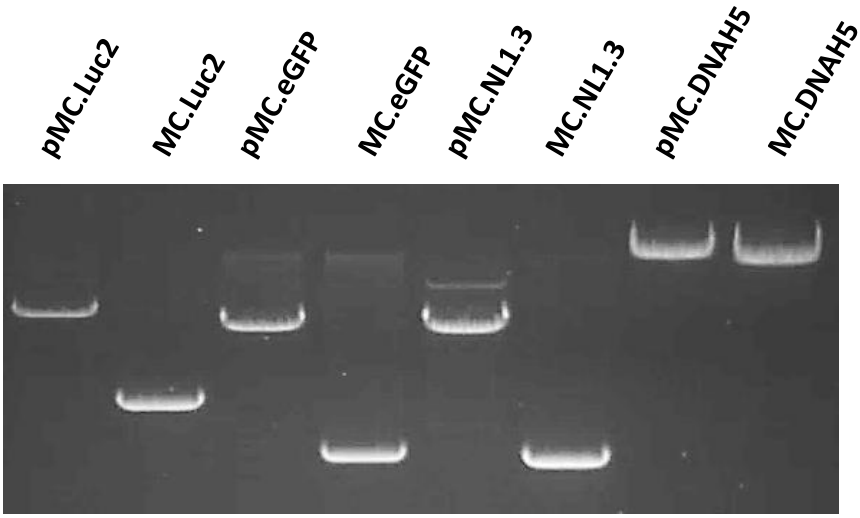

Figure 4.2. Purity of minicircle DNA produced in *E. coli* from plasmid constructs

500ng of plasmid (pMC.xxxx) and minicircle (MC.xxxx) DNA were digested with single cutting restriction enzymes thus linearising the DNA. Minicircle preparations were considered relatively pure if only one band was observed as a second band running down to the same length of the producer plasmid DNA would be visible if significant producer plasmid contamination was present.

4.3.3. TRANSGENE EXPRESSION *(IN VITRO)*

Varying amounts of minicircle DNA and plasmid DNA carrying either the firefly luciferase gene (MC.Luc2 and pMC.Luc2 respectively) or the eGFP gene (MC.eGFP and pMC.eGFP respectively) were transfected into 16HBE14o- cells using LPD nanocomplexes. Using firefly luciferase as the reporter gene, cells transfected with minicircle DNA showed 5-10-fold higher levels of luciferase activity than plasmid DNA transfected at equal mass (Figure 4.3a; minicircle vs plasmid $p<0.001$ at all mass quantities used; Student's t-test) and equimolar amounts of DNA (Figure 4.3b; minicircle vs plasmid $p<0.001$ at all molar quantities used; Student's t-test) indicating that minicircle DNA results in higher levels of transgene protein production.

Transfection of cells with DNA carrying the eGFP gene confirmed that minicircles resulted in higher levels of protein production. By fluorescence microscopy, cells transfected with minicircle DNA were brighter than those transfected with an equimolar amount of plasmid DNA (i.e. expressed higher levels of eGFP protein; Figure 4.3c) and cells expressing eGFP also appeared to be more numerous when minicircle DNA was used. Flow cytometry (Figure 4.3d-g) revealed that cells transfected with minicircle DNA typically showed a 4-fold higher percentage of cells expressing eGFP when compared to cells transfected with plasmid DNA at equal mass (Figure 4.3d; minicircle vs plasmid $p<0.001$ at all mass quantities used; Student's t-test) and equimolar amounts of DNA (Figure 4.3e; minicircle vs plasmid $p<0.001$ at all molar quantities used; Student's t-test). Supporting the microscopy images further, the mean fluorescent intensity of cells transfected with eGFP coding

minicircle DNA were 2.5-3-fold higher than cells transfected with plasmid DNA at equal mass (Figure 4.3f; minicircle vs plasmid $p<0.001$ at all mass quantities used; Student's t-test) and equimolar amounts of DNA (Figure 4.3g; minicircle vs plasmid $p<0.001$ at all molar quantities used; Student's t-test).

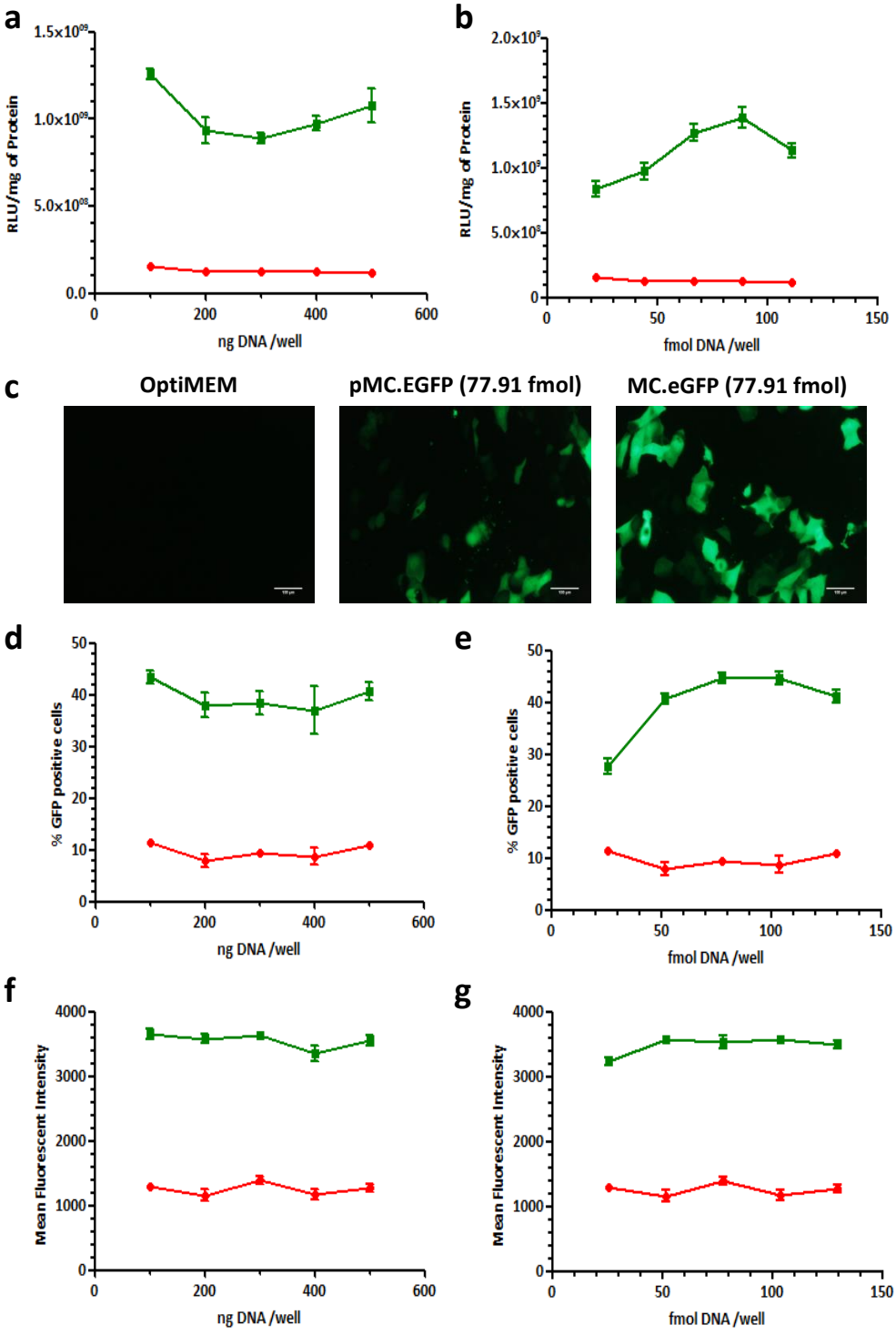

Figure 4.3 Transgene expression following *in vitro* minicircle and plasmid DNA transfections

16HBE14o- cells were transfected with minicircle DNA (green line) or plasmid DNA (red line) carrying the firefly luciferase gene (a-b) or the eGFP gene (c-g). Either equal mass amounts of DNA was used (a, d, f) or equimolar amounts (b, c, e, g). For eGFP transfections both the percentage of positive cells (d-e) and the MFI (f-g) were assessed. Scale bars are 100µm. Values are background subtracted and displayed as mean ±SEM.

4.3.4. LPD Biophysical Characterisation

pCI.eGFP.DNAH5, an 18.6kb plasmid, produced larger LPD complexes than complexes formed with pCI.eGFP, a 4.7kb plasmid (Chapter 3.3.3; p144). Plasmid size therefore affected the biophysical properties of LPD complexes, at least when the plasmid sizes are significantly different. Alteration of the biophysical properties could in turn impact on transgene expression and so the size and charge properties of LPD complexes formulated with 2µg of pMC.Luc2 were compared to complexes formulated with 2µg of MC.Luc2. pMC.Luc2 produced LPD complexes of 111.1 ±0.6nm which were slightly larger than MC.Luc2 containing LPD complexes of 103.2 ±1.1nm (Figure 4.4a; $p<0.001$; Student's t-test). There was also a significant difference in zeta potential with pMC.Luc2 containing complexes exhibiting a zeta potential of 35.0 ±1.6mV compared to 18.2 ±3.4mV for MC.Luc2 containing complexes (Figure 4.4a; $p<0.01$; Student's t-test). However, there were no significant differences in hydrodynamic size or zeta potential of LPD complexes formulated with pMC.eGFP and MC.eGFP (Figure 4.4b). As such, differences in the size and charge properties when comparing LPD complexes formulated with plasmid and minicircle plasmids were minimal and so unlikely to have affected transgene expression.

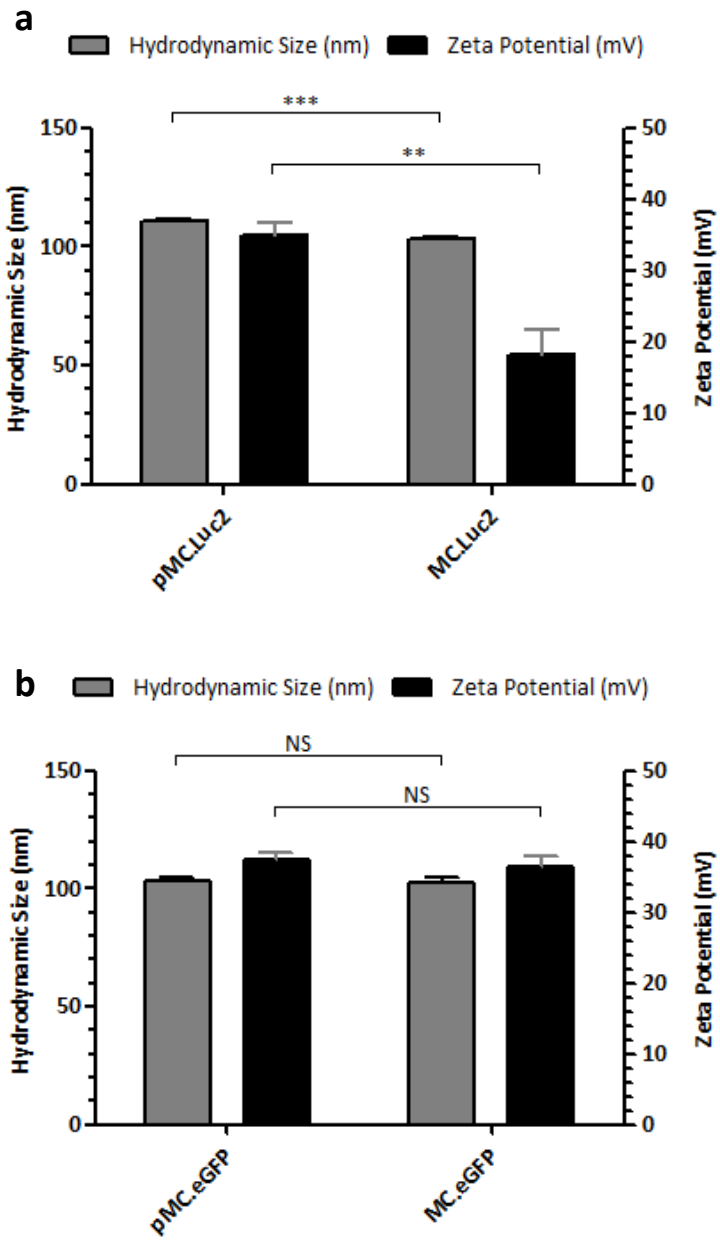

Figure 4.4. Biophysical characterisation of LPD complexes

The hydrodynamic sizes (nm) and zeta potential (mV) of LPD complexes formulated with 2µg of (a) pMC.Luc2 or MC.Luc2 DNA and (b) pMC.eGFP and MC.eGFP DNA were assessed. NS, not significant; **P<0.01; ***P<0.001; Student's t-test used to assess significance. Values are mean ±SEM.

4.3.5. Persistence of Transgene Expression *(In Vitro)*

Persistence of transgene expression is one of the main benefits of minicircle DNA over plasmid DNA (309, 312). To assess transgene persistence *in vitro* NHBE BMI-1 cells (described in Chapter 5; p183) were transfected at equimolar amounts with either plasmid DNA or minicircle DNA encoding a secreted luciferase gene (NanoLuc; Promega) derived from the deep sea shrimp *Oplophorus gracilirostris*. The cells were transfected 48 hours after seeding on permeable transwell supports with equal amounts of plasmid being added to both apical and basolateral sides for 4 hours before the basolateral surface was replaced with ALI media and the apical surface aspirated to maintain an ALI. The basolateral media was collected and replaced daily thus ensuring that only new luciferase expression was being measured as opposed to accumulated luciferase expression. As the NHBE cells were at an ALI, had formed tight junctions and were no longer dividing but rather differentiating issues of plasmid dilution due to cell division were minimal.

Consistent with earlier data using firefly luciferase and eGFP transfections, minicircle DNA resulted in significantly higher levels of NanoLuc expression (Figure 4.5a; $p<0.05$; Student's t-test). NanoLuc expression was followed for 10 days and the decay in new NanoLuc expression shown with day 1 luciferase activity displayed as 100% (Figure 4.5b). In doing this it was clear that the decay curve for minicircle DNA was shifted to the right of that for plasmid DNA indicating slower decay of NanoLuc expression (Figure 4.5b). Natural log transformed RLU values plotted against days post-transfection showed that the decay was exponential thus following first-order decay kinetics (Figure 4.5c; curves were transformed to a

straight line) and so half-life ($t^1/_2$) was measured for the 10-day period using equation (1) where *k* is the decay constant (slope of linear regression line).

(1) $$t^1/_2 = \frac{\ln 2}{k}$$

The levels of gene expression fell to half on average every 1.02±0.05 days (24.5 hours) for plasmid DNA transfections but 1.78±0.12 days (42.7 hours) for minicircle DNA transfections implying greater persistence of transgene expression from minicircle DNA in this *in vitro* ALI model (Figure 4.5d; $p<0.01$; Student's t-test).

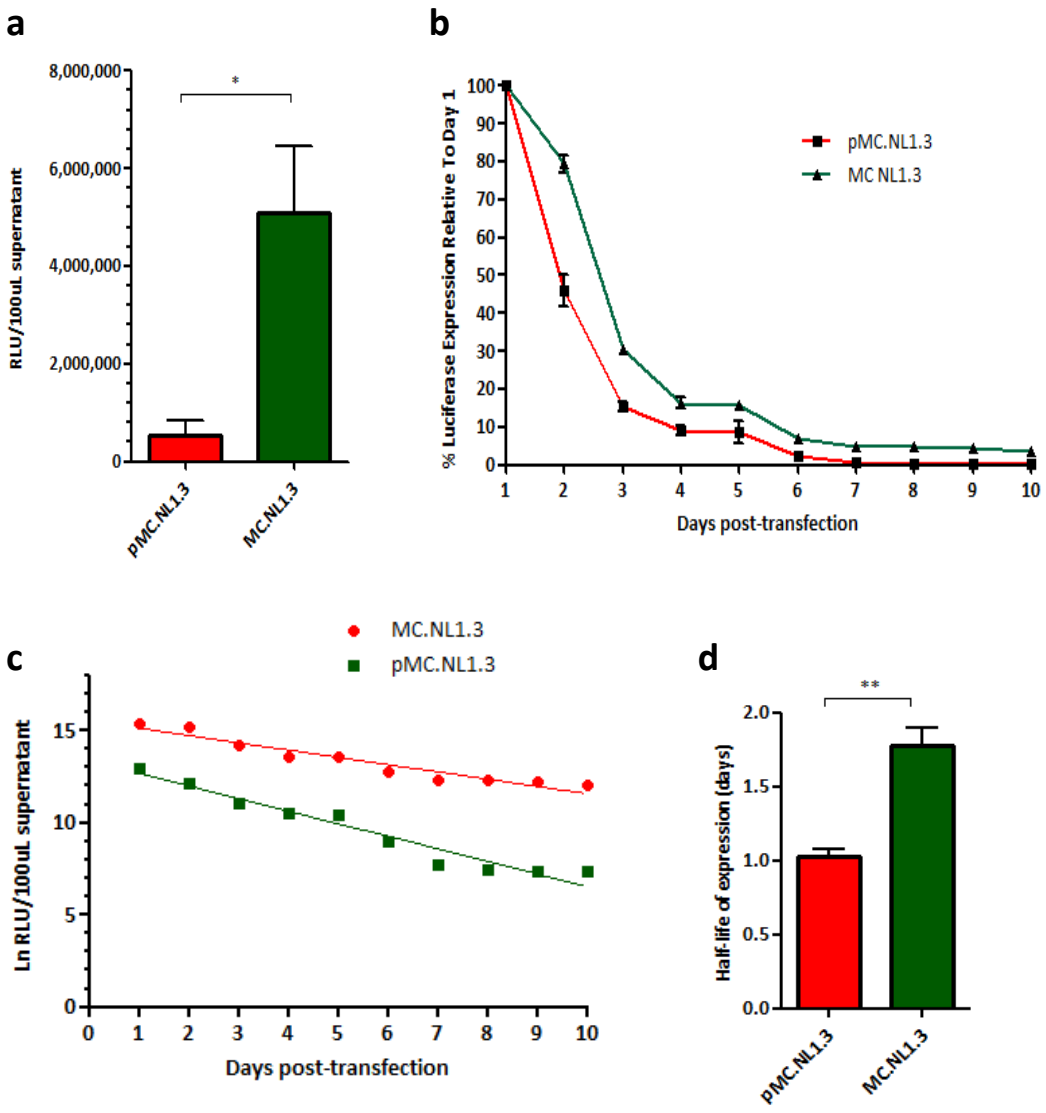

Figure 4.5. Persistence of transgene expression following *in vitro* minicircle and plasmid DNA transfections

NHBE BMI-1 cells were transfected with minicircle or plasmid DNA encoding a secreted luciferase (NanoLuc) and (a) luciferase activity 24 hours following transfection compared. (b) Transgene expression was followed for 10 days following transfection and luciferase activity displayed relative to day 1 levels. (c) Ln transformed luciferase activity values (RLU/100µL of supernatant) were used to determine the decay kinetics and (d) mean half-life of gene expression over the 10 day period calculated. *P<0.05; **P<0.01; Student's t-test used to assess significance. Values are background subtracted and displayed as mean ±SEM.

4.3.6. DNAH5 transfections *(In Vitro)*

Having assessed the advantages of minicircle DNA when transfecting airway epithelial cells with standard reporter genes it was important to validate whether minicircle DNA would result in enhanced expression of the large DNAH5 transgene by transfection of equimolar amounts of pMC.DNAH5 or MC.DNAH5 into 16HBE14o- cells. 48 hours following transfection RNA and DNA was extracted and DNAH5 expression and the amount of plasmid present quantified. As expected there was no significant difference in the levels of DNAH5 DNA in transfected cells (Figure 4.6a) but at the mRNA level cells transfected with minicircle DNA expressed 66% more DNAH5 mRNA than cells transfected with pMC.DNAH5 plasmid (Figure 4.6b; $p<0.01$; Student's t-test) thus highlighting the value of using minicircle DNA for DNAH5 transfections *in vitro*.

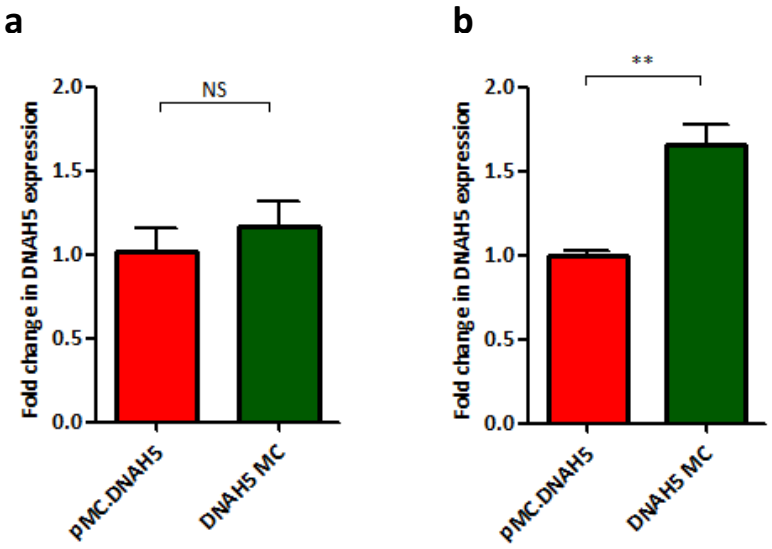

Figure 4.6. DNAH5 expression following *in vitro* minicircle and plasmid DNA transfections

16HBE14o- cells were transfected with pMC.DNAH5 or MC.DNAH5 complexed into LPD particles and the relative amounts of DNAH5 (a) DNA and (b) mRNA quantified using qPCR and the $2^{-\Delta\Delta Ct}$ method. NS, not significant; **P<0.01; Student's t-test used to assess significance. Values are mean ±SEM.

4.3.7. TRANSGENE EXPRESSION *(IN VIVO)*

Whether the superiority of minicircle DNA when transfecting airway epithelial cells *in vitro* was translatable *in vivo* was assessed by transfection of CD1 mice with LPD complexes formulated with plasmid DNA (pMC.Luc2) or minicircle DNA (MC.Luc2). Luciferase assay of lung extracts 24 hours following luciferase gene delivery showed that minicircle DNA gave a 6.5-fold higher median level of transgene expression compared to plasmid DNA when 16.7µg of DNA packaged into LPD complexes was administered via the oropharyngeal route (Figure 4.7; median value of 8115.9 RLU/mg of protein for 16.7µg of minicircle DNA and 1249 RLU/mg of protein for 16.7µg plasmid DNA; $p<0.01$; Kruskal-Wallis test followed by Dunn's post-test analysis). There was no significant difference in luciferase activity between plasmid DNA and minicircle DNA when equimolar amounts of DNA were transfected *in vivo*. Persistence of transgene expression was also assessed *in vivo* by assessing transgene expression 7 days following transfection. Luciferase activity was not detectable in mice transfected with plasmid DNA and in 3 out of 6 mice transfected with an equimolar amount of minicircle DNA (Figure 4.7). The median RLU value following an equimolar amount of minicircle DNA transfection fell over 190-fold from 1823 RLU/mg of protein on day 1 to 9.5 RLU/mg of protein on day 7 (Figure 4.7; $p<0.01$; Mann-Whitney U test). Following transfection of 16.7µg minicircle DNA (equal weight) luciferase activity fell 2.5-fold from 6565 RLU/mg of protein on day 1 to 2613.2 RLU/mg of protein on day 7 (Figure 4.7; $p<0.01$; Mann-Whitney U test).

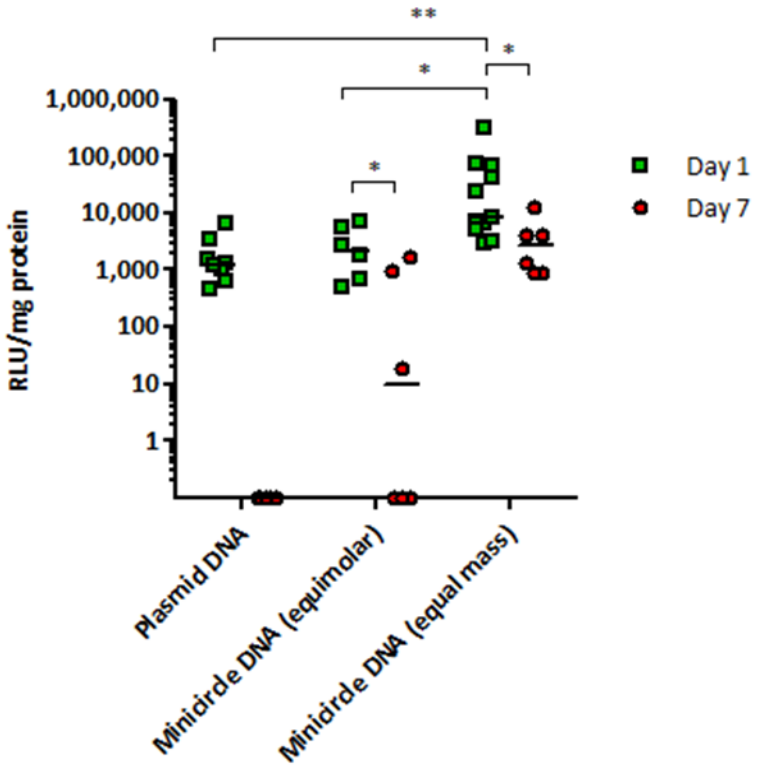

Figure 4.7. Transgene expression following *in vivo* minicircle and plasmid DNA transfections

Luciferase activity following oropharyngeal instillation of CD1 mice with LPD complexes containing pMC.Luc2 plasmid DNA or MC.Luc2 minicircle DNA at either equimolar or equal mass quantities. *P<0.05; **P<0.01; Kruskal-Wallis test followed by Dunn's post-test analysis to assess significance. Values are background subtracted and bar represents median RLU/mg of protein.

4.3.8. TOXICITY *(IN VIVO)*

In vivo equimolar amounts of minicircle DNA did not enhance transgene expression compared to plasmid DNA, instead providing similar transfection efficiencies. However, LPD nanocomplexes formulated with equimolar amounts of minicircle DNA contain less liposome, peptide and DNA which could potentially translate to reduced toxicity *in vivo*. Toxicity was therefore assessed *in vivo*.

24 hours after LPD transfections, with luciferase encoding pMC.Luc2 plasmid or MC.Luc2 minicircle DNA, lungs were fixed by perfusion with 4% PFA and processed for H&E staining as described in materials and methods. PEI complexed pMC.Luc2 was used as a positive control and MilliQ water as the vehicle control. Lungs of mice receiving the vehicle control showed no signs of inflammation or cellular infiltration by histology (Figure 4.8a). In contrast, the lungs of mice transfected with plasmid or minicircle DNA showed varied levels of alveolar, peribronchiolar and perivascular inflammation with predominantly monocyte and macrophage infiltration (Figure 4.8b-e). Mice transfected with pMC.Luc2 complexed with 25kDa PEI (Figure 4.8e) showed more extensive inflammation and cellular infiltration than mice treated with LPD complexes containing pMC.Luc2 (Figure 4.8b) or MC.Luc2 (Figure 4.8c and d). In all LPD treatment group's only foci of cellular infiltration and inflammation were observed rather than extensive inflammation but there were no clear differences when comparing pMC.Luc2 and MC.Luc2 transfections (Figure 4.8b-d). It is not possible to determine from this data whether the mild inflammation observed with LPD transfections was acute or represented chronic changes.

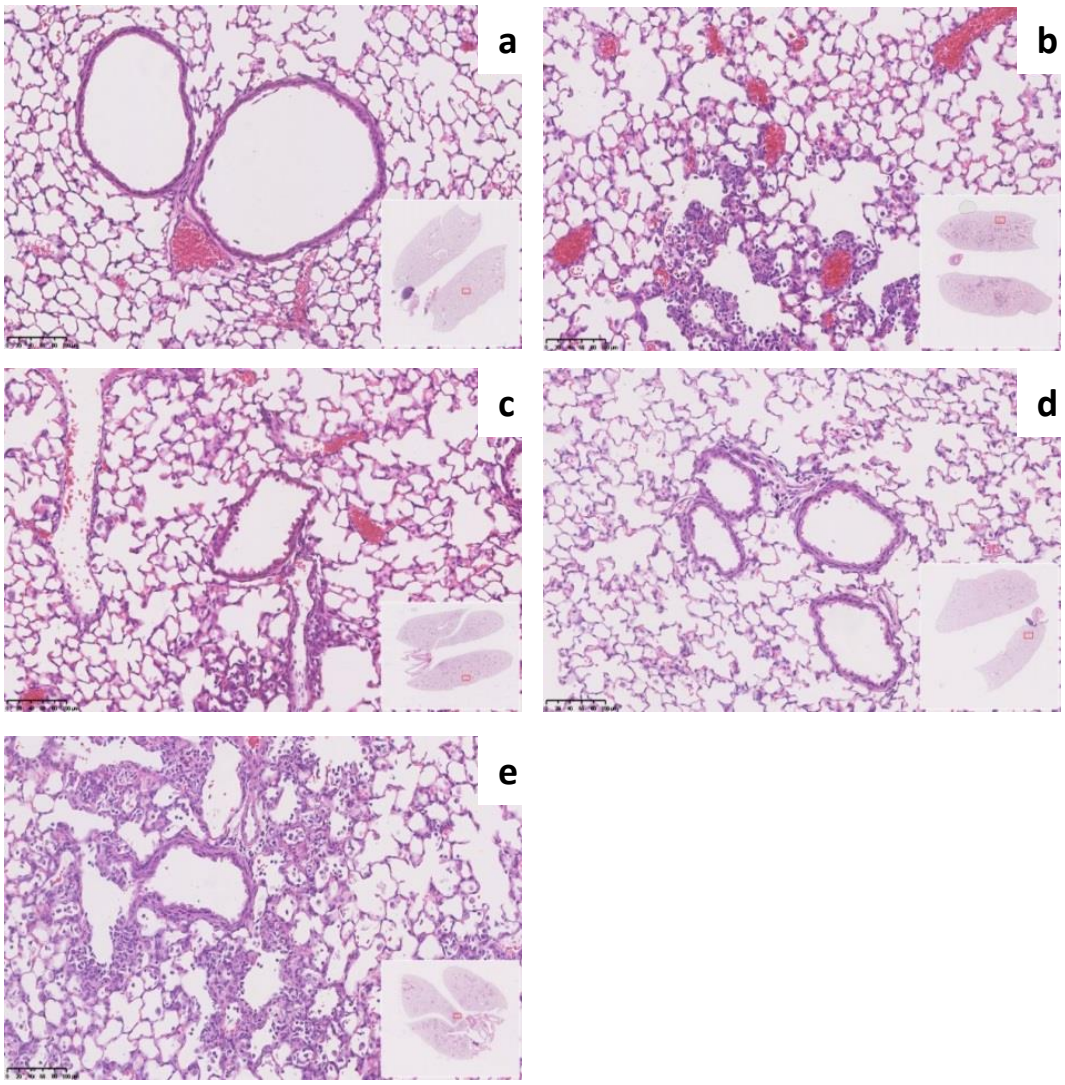

Figure 4.8. H&E staining of mouse lungs following *in vivo* minicircle and plasmid DNA transfections

H&E stained CD1 mice lung sections following oropharyngeal instillations of (a) water as a vehicle control, LPD vectors containing (b) pMC.Luc2, (c) MC.Luc2 at an equal mass to pMC.Luc2, (d) MC.Luc2 equimolar to pMC.Luc2 and (e) PEI complexed with pMC.Luc2.

Toxicity was further assessed by quantification of cytokine release. BALF was obtained 24 hours following transfections with pMC.Luc2 plasmid or MC.Luc2 minicircles. Cytokine concentrations within the BALF were then assessed using the Cytokine Mouse 10-plex panel. PEI complexed pMC.Luc2 was again used as a positive control and MilliQ water as the vehicle control.

Of the cytokines assessed (mouse granulocyte-macrophage colony-stimulating factor (GM-CSF), IFN-γ, IL-1β, IL-2, IL-4, IL-5, IL-6, IL-10, IL-12 and TNF-α) only IFN-γ, IL-12 and TNF-α were detectable. Levels of IL-12 in BALF were similar in mice receiving LPD vectors containing pMC.Luc2 and MC.Luc2 when the same mass of each DNA was transfected (Figure 4.9a). There was also no significant difference in the levels of IFN-γ when transfecting the same mass of pMC.Luc2 and MC.Luc2 complexed into LPD vectors (Figure 4.9b). pMC.Luc2 transfections using LPD nanocomplexes yielded no detectable TNF-α expression which contrasted with a median of 67.22pg/mL of TNF-α in BALF following an equal mass of MC.Luc2 transfections (Figure 4.9c; $p<0.05$; Kruskal-Wallis test followed by Dunn's post-test). Transfections of an equimolar amount of MC.Luc2 plasmid complexed in LPD complexes yielded no detectable GM-CSF, IFN-γ, IL-1β, IL-2, IL-4, IL-5, IL-6, IL-10, IL-12 and TNF-α cytokines in BALF (data not shown).

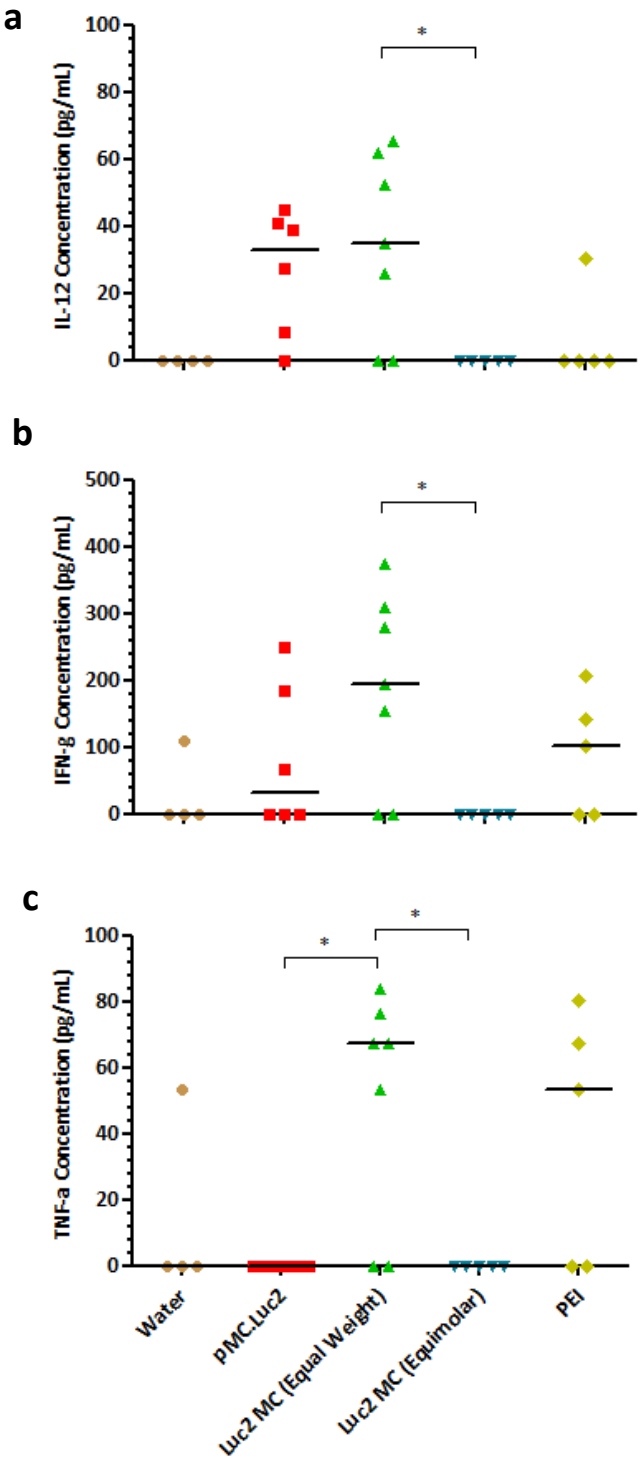

Figure 4.9. Cytokine response in BALF following *in vivo* minicircle and plasmid DNA transfections

Concentration of (a) IL-12, (b) IFN-γ and (c) TNF-α cytokines in BALF following instillation of LPD vectors containing luciferase encoding minicircle or plasmid DNA. Water was used as a vehicle control and PEI complexed with pMC.Luc2 used as a positive control. *P<0.05; Kruskal-Wallis test followed by Dunn's post-test used to assess significance. Bar represents median.

4.4. DISCUSSION

Efficient airway gene delivery has been a goal for CF researchers for over two decades. Non-viral vectors received significant attention in this field due to the need for repeated delivery and scalability of vector production. A major focus for the enhancement of gene delivery has been to find molecules capable of efficiently packaging and delivering plasmid DNA. More recently attention has been focussed on optimising the plasmid DNA itself in order to improve transgene expression and persistence and so maintain therapeutic levels of gene expression.

In this chapter it was shown that minicircle DNA enhanced transgene expression and persistence in airway cells *in vitro* regardless of whether an equimolar or equal mass amount of minicircle DNA was transfected relative to plasmid DNA. GFP expression studies showed that both the percentage of cells expressing eGFP and the amount of eGFP protein produced in each transfected cell was higher when using minicircle DNA. Importantly for PCD gene therapy enhanced transgene expression with minicircle DNA was also seen when transfecting DNAH5.

The mechanisms behind the enhanced gene expression with minicircle DNA was not fully investigated as the primary aim was to assess whether minicircle DNA could enhance transgene expression and persistence in the context of airway gene therapy. Nevertheless, it is highly likely that the enhancement in transgene expression when transfecting an equal mass of plasmid and minicircle DNA is at least in part due to the increased molar amounts of minicircle DNA delivered relative to plasmid DNA.

LPD complexes formulated with minicircle DNA were slightly smaller (~10nm smaller) than their counterparts formulated with plasmid DNA when luciferase coding DNA was used but no differences were seen when using eGFP coding DNA. Regardless of whether minicircle or plasmid DNA was used all LPD particles were around 100nm so the same uptake pathway would have been utilised, namely via clathrin-mediated endocytosis (396). As such, it would be expected that transfection of equimolar amounts of plasmid and minicircle DNA would result in equimolar amounts of DNA being found within transfected cells. This was not assessed for luciferase and eGFP coding DNA but held true following equimolar amounts of DNAH5 plasmid and minicircle DNA transfections. Despite equimolar amounts of DNAH5 plasmid and minicircle DNA being found in transfected cells greater mRNA expression resulted from minicircle DNA. This phenomenon has been observed in other studies where enhanced transgene expression with minicircle DNA has been associated with greater transcriptional silencing of plasmid DNA (309, 404, 407).

Along with enhanced initial transgene expression levels transgene persistence was also higher with minicircle DNA *in vitro* where an ALI culture system was used to minimise the effect of cell division on plasmid loss. In this system basolateral media was replaced daily so only new and not cumulative protein production was assessed. Given that equimolar amounts of DNA were transfected, that protein production declined faster with plasmid DNA supports the notion that transcriptional silencing occurred more rapidly with plasmid DNA in line with previous observations (309, 404, 407).

In contrast to *in vitro* studies, *in vivo* no significant differences in the initial levels of transgene expression were seen when comparing equimolar amounts of plasmid and minicircle DNA transfections. Nevertheless, when an equal mass of minicircle was transfected an ~8-fold increase in transfection efficiency was observed. Transgene expression following minicircle delivery persisted for at least 7 days but was not detectable at this time point after transfection of an equal mass of plasmid DNA. The MC.Luc2 minicircle used in this study was almost half (42.8%) the size of the pMC.Luc2 plasmid so an equal mass transfection of the two would result in 2.3-times more copies of minicircle DNA being transfected. The enhancement and persistence of transgene expression following an equal mass transfection of minicircle DNA, at least in part, thus likely resulted from more copies of transgene being transfected.

Whilst equimolar transfections of minicircle and plasmid DNA showed no differences in transgene expression, the former being smaller in size resulted in less liposome, peptide and DNA being delivered given that LPD complexes are formulated based on a mass ratio. Histological analysis of mice lungs following transfections showed mild inflammation in mice transfected with the LPD vector, as seen previously (287), with no obvious differences in severity when comparing minicircle and plasmid DNA transfections. However, analysis of BALF for a number of inflammatory mediators showed no detectable levels of a panel of common inflammatory cytokines and chemokines when minicircle was transfected at an equimolar amount relative to plasmid DNA. In contrast, IFN-γ and IL-12 levels were elevated in BALF following plasmid DNA transfections. The lower dose therefore

manifested as a reduced inflammatory response. There were no significant differences in IFN-γ and IL-12 expression following transfection of an equal mass of minicricle and plasmid DNA although TNF-α was found to be elevated following transfection of 16.6μg of minicircle DNA but not plasmid DNA. The levels of liposome and peptide delivered were the same when delivering an equal mass of minicircle and plasmid DNA so this would not have contributed to the elevated TNF-α levels. Unmethylated CpG-dinucleotides, typically rich in plasmid DNA backbones, have been shown to induce an immune response in vertebrates (298-301) via toll-like receptor 9 (302). However, the minicircle, containing CpG-free promoter/enhancer elements with no plasmid backbone, has fewer unmethylated CpG-motifs than the plasmid DNA used. Instead, it is more likely that the elevated cytokine release with minicircle DNA was due to the significantly increased amount of luciferase expressed. The development of an immune response to transgene products has been reported previously following airway gene delivery (408) and greater transgene expression would be expected to lead to a more robust immune response. This hypothesis requires further investigation.

Despite the minicircle being CpG reduced the role that unmethylated CpG-motifs may have had on transgene expression and persistence *in vivo* was not assessed here. The removal of CpG dinucleotides has been implicated in enhancing transgene expression and persistence as well as minimising inflammatory responses following airway gene delivery (297, 303-306). However, in these studies control CpG containing plasmids were not directly comparable to the CpG-free plasmids for a number of reasons.

In the studies from the Rudolph lab (303, 306) the CpG-free plasmid contained a CpG-free chimeric promoter with a CMV enhancer and EF1α core promoter whilst in the CpG containing plasmid transgene expression was driven by a CMV promoter. As such, this variable rather than removal of CpG motifs may have produced the results obtained particularly given that the use of different promoters is known to affect both the initial levels of transgene expression (293-295) as well as transgene persistence (295). In addition the backbones of the two plasmids contained different elements with the CpG-free plasmids containing scaffold/matrix attachment region sequences known to prolong transgene expression by promoting extra-chromosomal stability through attachment of the plasmid to components of the nuclear matrix (409-411).

In the studies from the Gill lab (297, 304, 305) the CpG-free plasmids had shorter backbone lengths compared to CpG containing or CpG-reduced plasmids, a variable recently shown to affect persistence of transgene expression (308). As such, in these studies it is difficult to isolate the specific effects of removing CpG motifs. Indeed Chen et al., (307) showed that transgene silencing in the mouse liver at least is independent of CpG methylation status and that removal of CpG motifs altogether did not abolish transgene silencing. Furthermore, Lu et al., (308) found that the plasmid backbone sequence, typically rich in CpG motifs, was not crucial in transgene silencing as when it was placed within the 3' untranslated region of the eukaryotic expression cassette persistent transgene expression resulted at levels similar to minicircle DNA completely devoid of a bacterial backbone. Lu et al., went on to show that the size and not the sequence of the backbone outside of the

transgene cassette is what produced a potent negative effect on transgene persistence.

In summary, the advantages of using minicircle DNA in the airways include enhanced transgene expression when using an equal mass of minicircle DNA with reduced toxicity using an equimolar amount of minicircle DNA without diminishing transfection efficiency. This enhanced gene expression is also seen when delivering the DNAH5 transgene having clear implications for PCD gene therapy. Minicircles were therefore to be used in further studies assessing efficacy of gene therapy for PCD. However, a suitable model for assessing PCD gene therapy was required and its development is described in the following chapter.

CHAPTER FIVE

RESULTS

IN VITRO MODEL OF PCD

5. *IN VITRO* MODEL OF PCD

5.1. INTRODUCTION

To assess the efficacy of gene therapy for PCD caused by *DNAH5* mutations a suitable disease model is required. *Dnahc5* mutant mouse models have been produced but these develop severe developmental defects including cardiac abnormalities and severe hydrocephalus causing high levels of neonatal death (35, 375). The models are therefore difficult to work with when assessing efficacy of respiratory gene therapy for PCD. Use of conditional knockout mouse models could potentially alleviate the severe developmental defects as was observed with the conditional *Dnaic1* conditional knockout mouse (316). However producing a conditional knockout *Dnahc5* mouse would be both time consuming and expensive so was not attempted here.

In vitro models of disease, such as tissue samples obtained from patients, offer a cheaper and convenient alternative however the rarity of PCD and a lack of genotyping in the UK makes obtaining suitable samples difficult. One way around this is to use shRNA technology to produce a PCD phenotype in airway cells capable of undergoing differentiation to a ciliated phenotype. Primary nasal and bronchial epithelial cells when placed on ALI are capable of undergoing mucociliary differentiation but have a very limited life-span and diminished differentiation capacity following 2-4 passages. Manipulating primary nasal and bronchial epithelial cells to produce a model of disease and attempt correction whilst not exceeding the cell doubling threshold for mucociliary differentiation is difficult to achieve. In addition high donor-to-donor variability combined with the expense of obtaining

commercial primary human airway epithelial cells restricts their use and has stimulated the production of immortalised cell lines.

Immortalised airway epithelial cell lines have been isolated from human lung cancers (412) and produced by using viral oncogenes with (413, 414) and without (376, 415, 416) hTERT to overcome the limited replication of primary cells thus enabling extensive manipulation. These cell lines have been shown to polarise and form tight junctions when placed on ALI but do not differentiate to a pseudo-stratified and well ciliated airway epithelium on ALI.

The viral oncogene products used for immortalisation act by inhibiting the pRB and p53 tumour suppressor genes so forcing cells through the G1/S checkpoint of the cell cycle and initiating cell division. Centrioles, which are essential for cell division, also function as basal bodies that nucleate cilia assembly in quiescent and differentiated cells (417) and cells also resorb their cilia during cell division (418). Controls for limiting the function of centrioles to either cell division or cilia assembly must therefore exist and work is taking place to elucidate the mechanisms involved (419). In the context of human airway epithelial cell lines cell division is promoted by inducing entry into the cell cycle. Cell division must therefore occur at the expense of ciliary differentiation- a possible explanation for why these cell lines have a limited differentiation capacity.

Whilst production of cell lines typically relies on promoting entry into the cell cycle, preventing senescence should enhance the number of replications a cell undergoes. BMI-1 is an anti-senescence protein that is known to function in the self-renewal and maintenance of the multipotency of stem cells (416, 420-422). By using mouse

BMI-1 in combination with hTERT Fulcher et al., (423) have been able to extend the growth capacity of primary HBE cells, although not as potently as viral oncogenes and show that unlike cells transformed with viral oncogenes these cell lines had no chromosomal abnormalities and recapitulated most of the structure and function of primary cells when placed on ALI. However, the BMI-1-hTERT transduced cells, whilst showing a pseudo-stratified epithelium, gave only sparse ciliogenesis. The limited differentiation capacity may be explained by reports that hTERT, following long-term growth in culture, up-regulates expression of the potent mitogen c-Myc, so promoting entry into the cell cycle and that c-Myc itself up-regulates hTERT in a positive feedback loop that eventually results in apoptosis (424). In addition, the combination of BMI-1 and hTERT in fibroblasts resulted in loss of both hTERT telomerase activity and BMI-1 inhibition of $p16^{Ink4a}$ thus negating the anti-senescent and stem cell maintenance effects of BMI-1 (425). Using BMI-1 alone may overcome the issues of c-Myc up-regulation and the inhibition of both hTERT and BMI-1 activities and so potentially provide a cell model capable of extensive passaging and mucociliary differentiation.

5.2. AIMS

To produce an *in vitro* model of PCD caused by *DNAH5* mutations.

To achieve this aim BMI-1 transduction of NHBE cells was used and the differentiation capacity of the cells lines assessed. shRNA knockdown of *DNAH5* was subsequently used to model PCD with cilia motility, DNAH5 protein localisation and cilia ultrastructure studies undertaken to determine whether this *in vitro* model recapitulated PCD phenotypes.

5.3. RESULTS

5.3.1. CHARACTERISATION OF BMI-1 TRANSDUCED CELLS IN SUBMERGED CULTURE

NHBE cells in submerged cultures showed a typical cobblestone appearance at a low passage (Figure 5.1a; passage 1) but further passaging resulted in a change in cell morphology where elongated cells were present (Figure 5.1b; passage 3; white arrow) and squamous differentiation was evident (Figure 5.1b; passage 3; black arrow). To produce BMI-1 expressing NHBE cells lentivirus containing the human BMI-1 cDNA was added to the culture media, incubated with passage 2 NHBE cells in submerged culture and incubated at 37^{o}C for 48 hours. In contrast to passage 3 untransduced NHBE cells, BMI-1 transduced NHBE cells (NHBE BMI-1) maintained a characteristic cobblestone appearance following extensive passaging (Figure 5.1c, passage 11; Figure 5.1d, passage 17) but began showing squamous differentiation following 25 passages (Figure 5.1e) after which the cells senesced (defined as 10 days with no observable cell division). Encouragingly, the cells maintained a normal diploid karyotype despite extensive passaging (Figure 5.1f, passage 23).

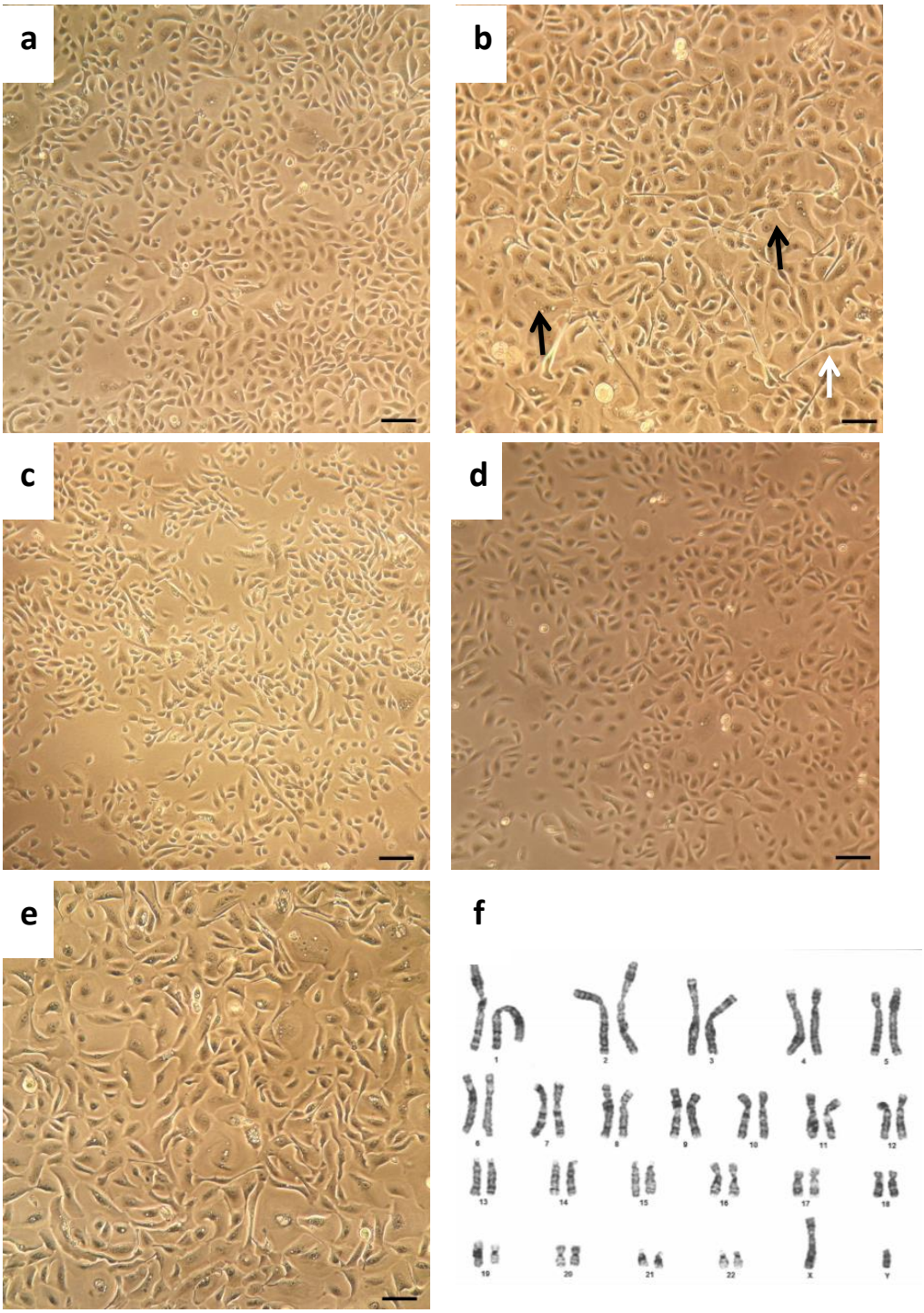

Figure 5.1. Morphology and Karyotype of NHBE BMI-1 cells

The morphology of (a) NHBE cells at passage 1 and (b) passage 3 was observed under light microscopy and compared to NHBE BMI-1 cells after passages (c) 11, (d) 17 and (e) 25. (f) Karyotype of NHBE BMI-1 cells at passage 23 was also assessed. Examples of squamous cells are indicated by the black arrows and white arrows highlight examples of elongated cells. Scale bars are 100µm.

Next, the doubling times of NHBE BMI-1 cells was assessed and compared to NHBE cells at passage 2 (Figure 5.2a). Untransduced cells at passage 2 had a doubling time of 1.18 days which was not too dissimilar to BMI-1 transduced cells at passages 12 and 15 (doubling times of 1.25 and 1.21 days respectively). Given that BMI-1 transduced cells had senesced following 25 passages it is not surprising that the doubling time increased to 1.49 days after 23 passages.

BMI-1 is known to function by down-regulating expression of the anti-senescent protein $p16^{Ink4A}$. NHBE cells transduced with BMI-1 had low levels of $p16^{Ink4A}$ protein and high levels of BMI-1 (Figure 5.2b). Levels of BMI-1 in untransduced NHBE cells declined with an increase in passaging whilst levels of $p16^{Ink4A}$ increased and were highest in senesced passage 6 untransduced NHBE cells. In senesced cells BMI-1 expression was not evident by western blot (Figure 5.2b).

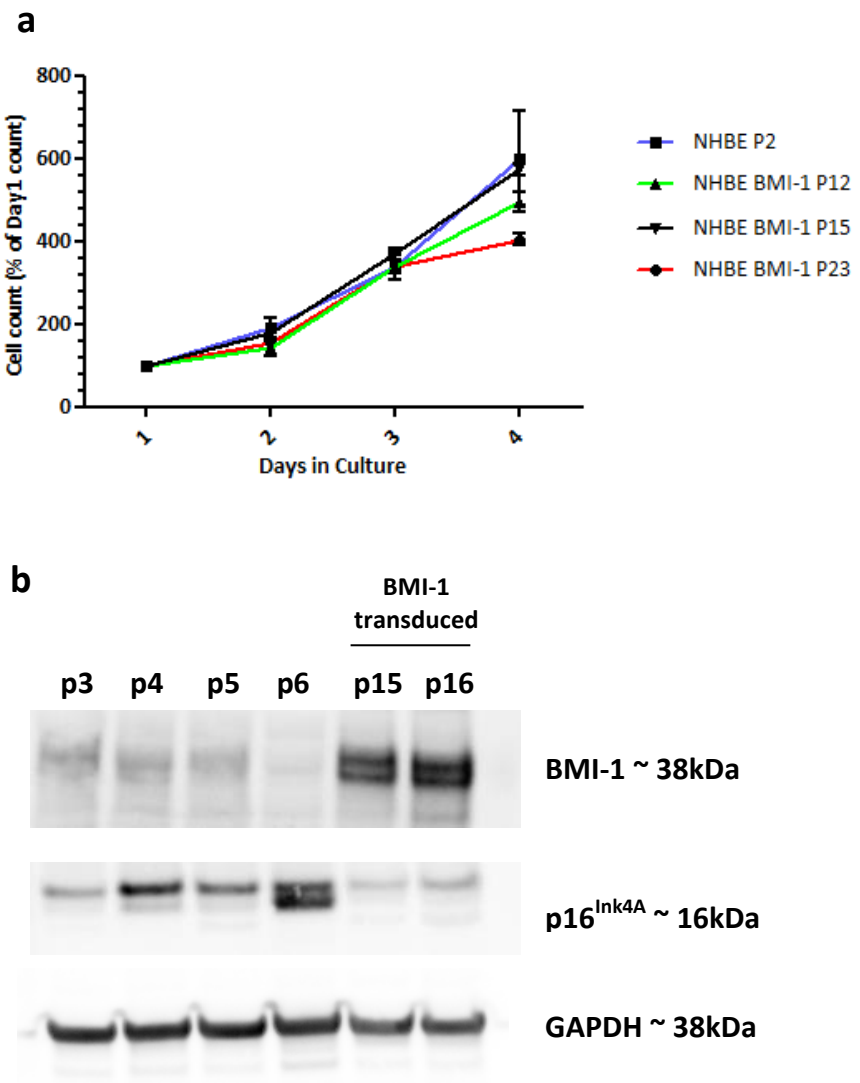

Figure 5.2. Growth Kinetics and BMI-1 expression of NHBE cells

Cell counting was used to determine the replication kinetics of NHBE and NHBE BMI-1 cells at varying passages and (b) a Western blot was used to assess the levels of BMI-1 and $p16^{Ink4A}$ in untransduced NHBE cells and NHBE BMI-1 cells. Values are mean ±SEM

5.3.2. Characterisation of BMI-1 Transduced Cells on ALI Culture

Having established that NHBE BMI-1 cells could be passaged more than untransduced NHBE cells in submerged culture, the differentiation potential of NHBE BMI-1 cells was investigated. Culture of NHBE BMI-1 cells at an ALI resulted in mucociliary differentiation with motile cilia evident (Video 1a and b). Immunostaining showed the presence of the tight junction marker occludin (Figure 5.3a), Muc5aC producing cells (Figure 5.3b), Muc5b producing cells (Figure 5.3c), p63+ basal cells (Figure 5.3d) and ciliated cells (cilia was stained for using anti-acetylated α-tubulin; Figure 5.3e). BMI-1 protein was also found to be localised in all nuclei (Figure 5.3f). TEM sowed that the cilia had a normal 9+2 ultrastructure with both inner and outer dynein arms present (Figure 5.3g). Video microscopy followed by CBF analysis with CiliaFA ImageJ plugin (383) showed a mean CBF of 15.28 ±0.19 Hz- within the normal range for respiratory cilia of 9-17Hz (383, 426).

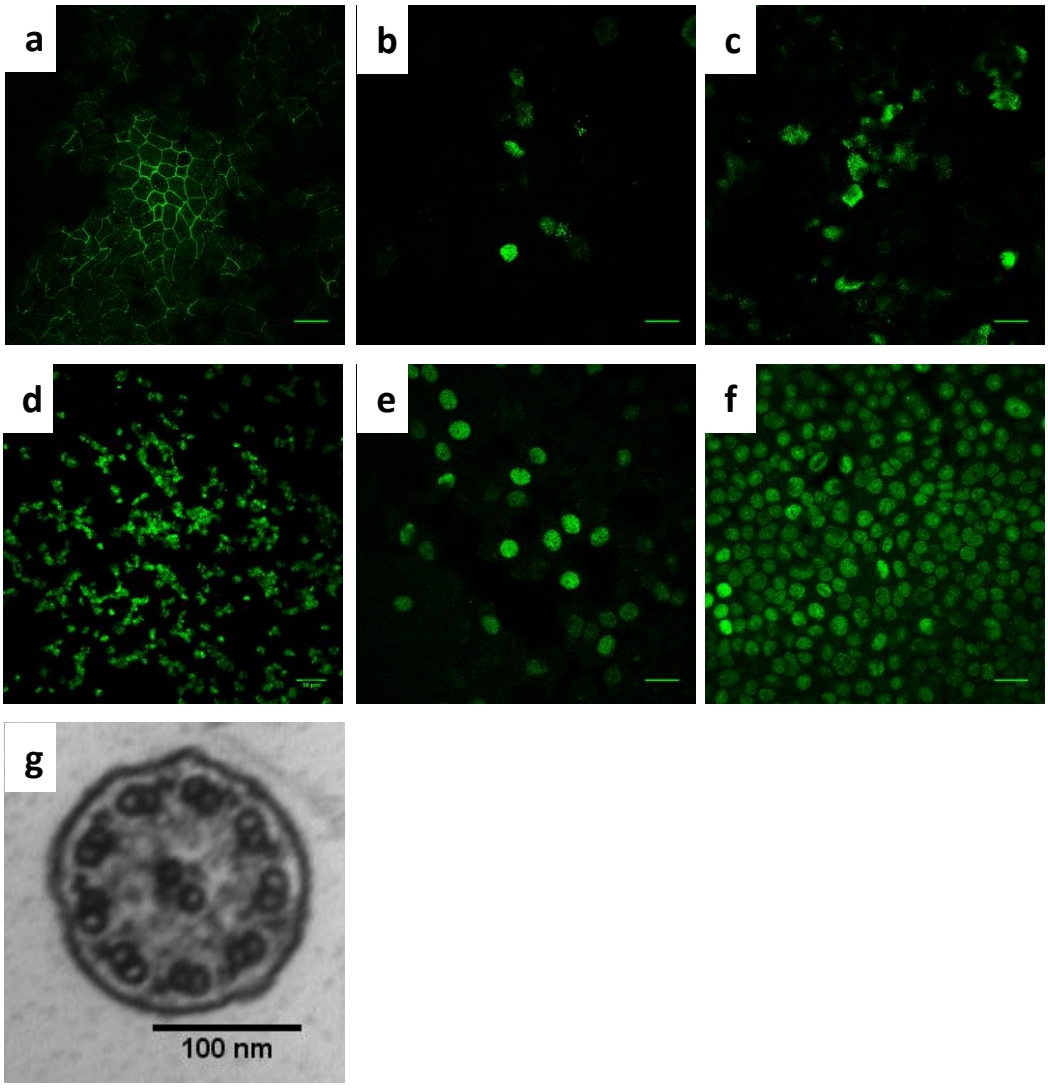

Figure 5.3. Mucociliary differentiation of NHBE BMI-1 cell line.

Once placed at an ALI the extensively passaged NHBE cells (passage 15) maintain their ability to differentiate into a pseudostratified columnar airway epithelium with immunostaining showing tight junction formation (occludin; a), mucus production (MUC5AC and MUC5B; b and c respectively), extensive ciliation (acetylated α-tubulin; d), the presence of basal cells ($p63^{+}$; e) and widespread BMI-1 expression (BMI-1; f). TEM also revealed a normal ciliary ultrastructure (g).

5.3.3. shRNA Knockdown of DNAH5

The development of NHBE cell lines capable of extended passaging yet still capable of differentiation to a mucociliary phenotype allows for further manipulation of these cells such as the production of PCD disease models through the use of gene modification technologies. Mutations in *DNAH5* are the most common cause of PCD resulting in loss of protein function. As such, reducing *DNAH5* expression sufficiently should have the same phenotypic effect on cells as mutations in the *DNAH5* gene that result in PCD. This reduction in *DNAH5* expression can be achieved through the use of shRNA. In order to provide a stable reduction of *DNAH5* expression an shRNA lentivirus construct was used to enable integration of shRNA into the host chromosome. Commercial shRNA library vectors exist and the pGIPZ library developed by Open Biosystems is a library of lentiviral vectors containing shRNA targeted against human genes. The pGIPZ library was utilised in this study because of low cost. Along with the shRNA to the gene of interest the pGIPZ vectors also contain a GFP and puromycin selection cassette (Appendix B; p298). These markers allow the user to identify which cells are expressing the shRNA.

An issue with the pGIPZ plasmids is their size. The pGIPZ plasmids are around 11.7kb thus relatively large in comparison to typical plasmids. The provirus derived from the plasmid is also larger than typical lentivirus vectors and provirus length is inversely proportional to viral titre (427). It is unsurprising then that pGIPZ plasmids gave viral titres of 1-5 $x10^7$ TU/mL making their use impractical for efficient transduction of NHBE cells. To improve viral titres a 3.5kb cassette consisting of

zeocin resistance gene-CMV promoter-turbo GFP- Internal ribosome entry site (IRES)-puromycin resistance gene was excised from the pGIPZ plasmids using *SanDI* and *XhoI* restriction sites and replaced with a 1.6kb cassette consisting of eGFP under the control of the spleen focus-forming virus (SFFV) promoter obtained from the pHRsincpptSEClaI plasmid also using *SanDI* and *XhoI* restriction sites. This reduced the pGIPZ plasmids from a size of 11.7kb to 9.8kb and increased viral titres to 5-10 $x10^8$ TU/mL.

To achieve efficient knockdown of *DNAH5* three different shRNA constructs targeting *DNAH5* were assessed (DNAH5 1, clone Id: V2LHS_263786; DNAH5 2, clone Id: V2LHS_225844; DNAH5 3, clone Id: V2LHS_113470). 16HBE14o- cells were transfected with *DNAH5* shRNA plasmids using the LPD vector system. 48 hours following transfection total RNA was extracted and qRT-PCR performed to assess the relative amounts of *DNAH5* mRNA remaining. The most efficient construct was DNAH5 3 which resulted in ~70% knockdown of *DNAH5* mRNA relative to cells transfected with a scrambled shRNA construct (Figure 5.4). Relative to OptiMEM treated cells the DNAH5 3 construct showed 87.7 ±0.6% knockdown of *DNAH5* expression (Figure 5.4; $p<0.01$; one-way ANOVA with Bonferroni post-test used to assess significance.). The scrambled shRNA construct gave a 50.8 ±8.2% knockdown of *DNAH5* relative to OptiMEM treated cells whilst DNAH5 1 and 2 constructs gave 57 ±14.3% and 43.8 ±18.0% knockdown respectively (Figure 5.4). Providing the most efficient knockdown of *DNAH5* the DNAH5 3 shRNA construct was therefore used for further studies.

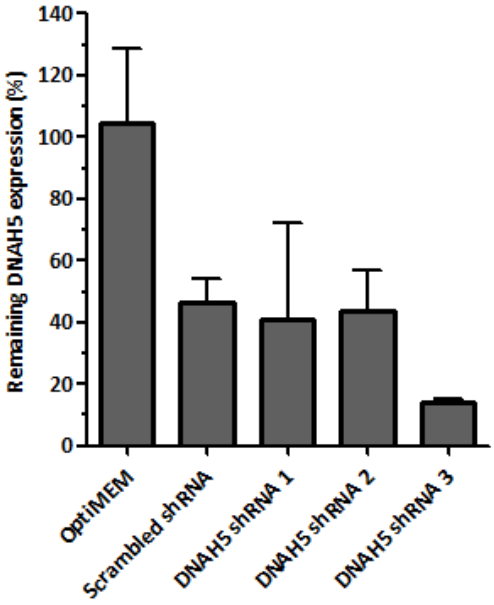

Figure 5.4. *DNAH5* knockdown in 16HBE14o- cells

16HBE14o- cells were transfected with difference shRNA constructs and *DNAH5* mRNA expression was quantified and presented relative to *DNAH5* expression in OptiMEM treated cells. NS, not significant;**P<0.01; one-way ANOVA with Bonferroni post-test used to assess significance. Values are mean ±SEM.

Lentivirus containing the DNAH5 3 shRNA construct was to be used to produce a *DNAH5* deficient PCD model. The multiplicity of infection (MOI) required to give efficient transduction of NHBE BMI-1 cells was determined by transduction of submerged cultures with varying MOIs of scrambled shRNA lentivirus titrated on HEK293T cells. An MOI of 75 was found to transduce almost 100% of cells and so used for further studies. It is of note that at all MOIs assessed there were two populations of GFP positive cells, GFP_{low} and GFP_{high} (Figure 5.5).

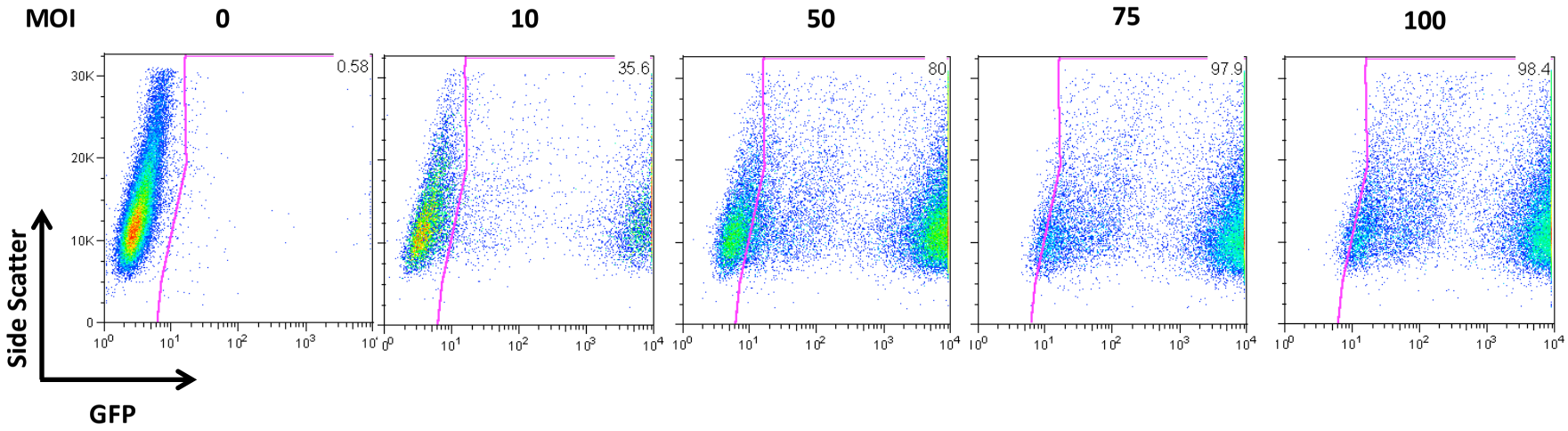

Figure 5.5. shRNA transduction of NHBE BMI-1 cells

NHBE BMI-1 cells were transfected with varying MOIs of lentivirus containing a scrambled shRNA construct together with the eGFP reporter gene. Transduction efficiency was determined with flow cytometry to assess the percentage of cells expressing eGFP.

Having optimised the MOI required for efficient transduction NHBE BMI-1 cells were transduced at an MOI of 75 using lentivirus containing the DNAH5 3 construct and *DNAH5* expression was assessed by qRT-PCR. In these *DNAH5* knockdown cells *DNAH5* expression was reduced by around 75% relative to untransduced cells (Figure 5.6; $p<0.01$; one-way ANOVA with Bonferroni post-test analysis). When cells were transduced with a scrambled shRNA no knockdown of *DNAH5* expression was observed relative to untransduced cells showing that *DNAH5* knockdown using DNAH5 3 construct was sequence specific in NHBE BMI-1 cells (Figure 5.6).

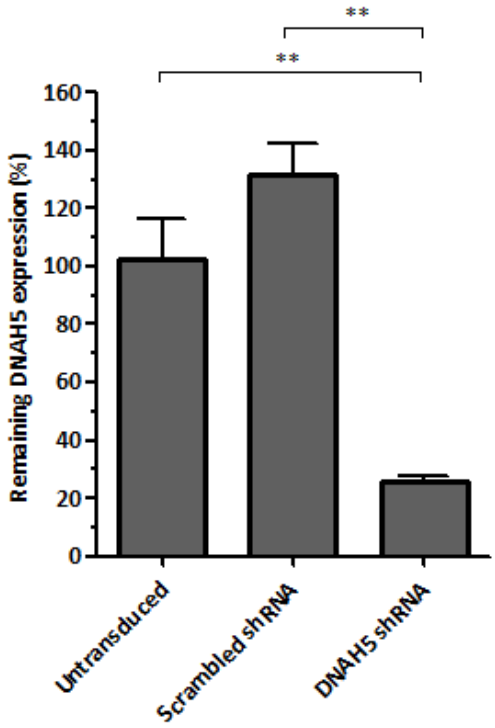

Figure 5.6. Knockdown of *DNAH5* in NHBE BMI-1 cells

DNAH5 mRNA expression was assessed following transduction of NHBE BMI-1 cells with scrambled or *DNAH5*-targeted shRNA. *DNAH5* expression is presented relative to untreated NHBE BMI-1 cells. **P<0.01; one-way ANOVA with Bonferroni post-test analysis used to assess significance. Values are mean ±SEM.

To assess if the levels of *DNAH5* knockdown achieved in NHBE BMI-1 cells was sufficient to produce a PCD phenotype DNAH5 3 and scrambled shRNA transduced NHBE BMI-1 cells were cultured on ALI to induce mucociliary differentiation and cilia function and ultrastructure assessed.

Following mucociliary differentiation NHBE BMI-1 cells transduced with the scrambled shRNA had motile cilia in ciliated cells where the shRNA was expressed (GFP positive; Video 2a and b). In contrast, *DNAH5* knockdown cells grown on ALI had immotile cilia when the ciliated cells were expressing the shRNA (GFP positive; Video 2a and b) but motile cilia was observed in cells not expressing the shRNA (GFP negative; Video 2c).

To quantify the numbers of motile and immotile cilia present high-speed videos of untransduced and transduced NHBE BMI-1 cells grown on ALI were taken and the percent active area, used as a surrogate for the proportion of beating cilia in a given area, together with the CBF were determined using CiliaFA ImageJ plugin (383). In untransduced and scrambled shRNA transduced NHBE BMI-1 cells percent active area was 20% and this value dropped to 11.6 ±2.0% in *DNAH5* knockdown cells (Figure 5.7a; $p<0.05$; one-way ANOVA with Tukey's post-test). CBF was 14.15 ±0.28Hz in *DNAH5* knockdown cells which was slightly higher than that seen for untransduced or scrambled shRNA transduced cells which had CBF values of 12.96 ±0.28Hz and 13.21 ±0.15Hz respectively (Figure 5.7b; $p<0.05$; one-way ANOVA with Tukey's post-test). Nevertheless the CBF were all within the normal range for respiratory cilia (9-17Hz) (383, 426).

The reduction in the percent active area seen when cells were transduced with the *DNAH5*-targeted shRNA (Figure 5.7a) could have resulted from either i) a greater proportion of immotile cilia being present or ii) a reduction in the levels of ciliogenesis. To assess whether ciliogenesis was disrupted following *DNAH5* knockdown, the same cells which were used to determine the percent active area and cilia CBF where fixed and immunostained for acetylated tubulin and DAPI. Next, confocal images of at least 25 fields of view were obtained at x40 magnification and the number of ciliated cells counted. There were no significant differences in the number of ciliated cells when comparing untreated NHBE BMI-1 cells with scrambled shRNA or *DNAH5*-targeted shRNA treated cells with the number of ciliated cells per field found to be 18.6 ± 1.0, 21.2 ±1.0 and 19.9 ±1.4 respectively (Figure 5.7c; one-way ANOVA). As such, the fall in percent active area in cells transduced with the *DNAH5*-targeted shRNA resulted from a greater proportion of immotile cilia being present.

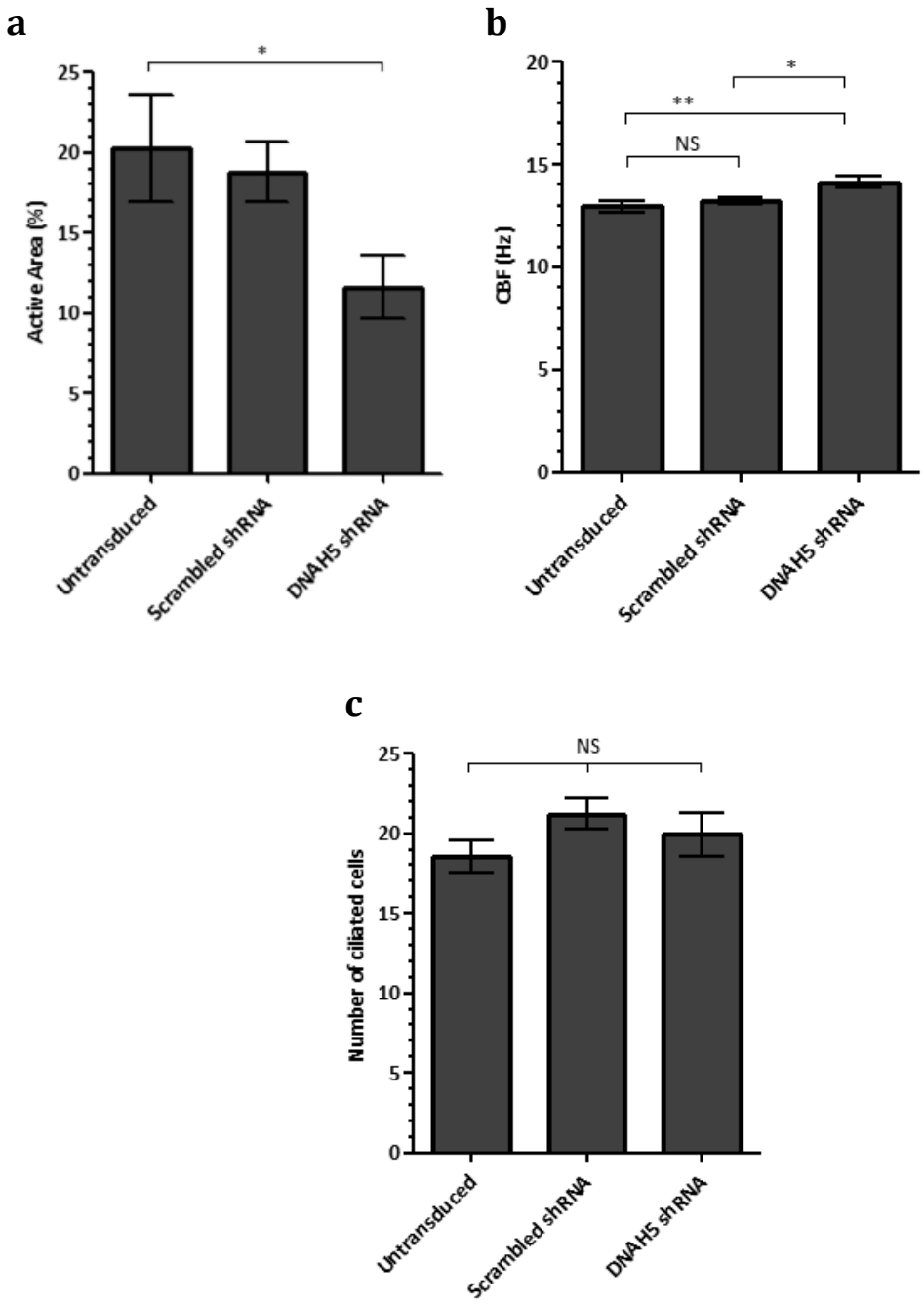

Figure 5.7. Cilia beating analysis

Videos of shRNA transduced and untreated NHBE BMI-1 cells grown at an ALI were taken and the proportion of the field of view containing actively beating cilia was determined (a) along with the CBF (b) using CiliaFA plugin. (c) The average number of cilia in at least 5 fields of view per well was counted to determine the level of ciliation obtained.*P<0.05; **P<0.01; one-way ANOVA with Bonferroni post-test used to assess significance. Values are mean ±SEM.

PCD patients with *DNAH5* mutations typically lack the DNAH5 protein in the ciliary axoneme and have missing ODAs (116). To assess this in the knockdown model produced, immunostaining followed by confocal microscopy was used to assess if the *DNAH5* knockdown model recapitulated the lack of DNAH5 protein within the axoneme of ciliated cells. In shRNA transduced cells only cells that were GFP positive and so expressing the shRNA, were counted. Untransduced NHBE BMI-1 cells and those transduced with the scrambled shRNA were found to have DNAH5 localising to the ciliary axoneme in all the ciliated cells assessed. In contrast, only 2.9% of ciliated cells had DNAH5 localised to the ciliary axoneme in *DNAH5* knockdown cells (Figure 5.8; $p<0.001$; Fisher's exact test).

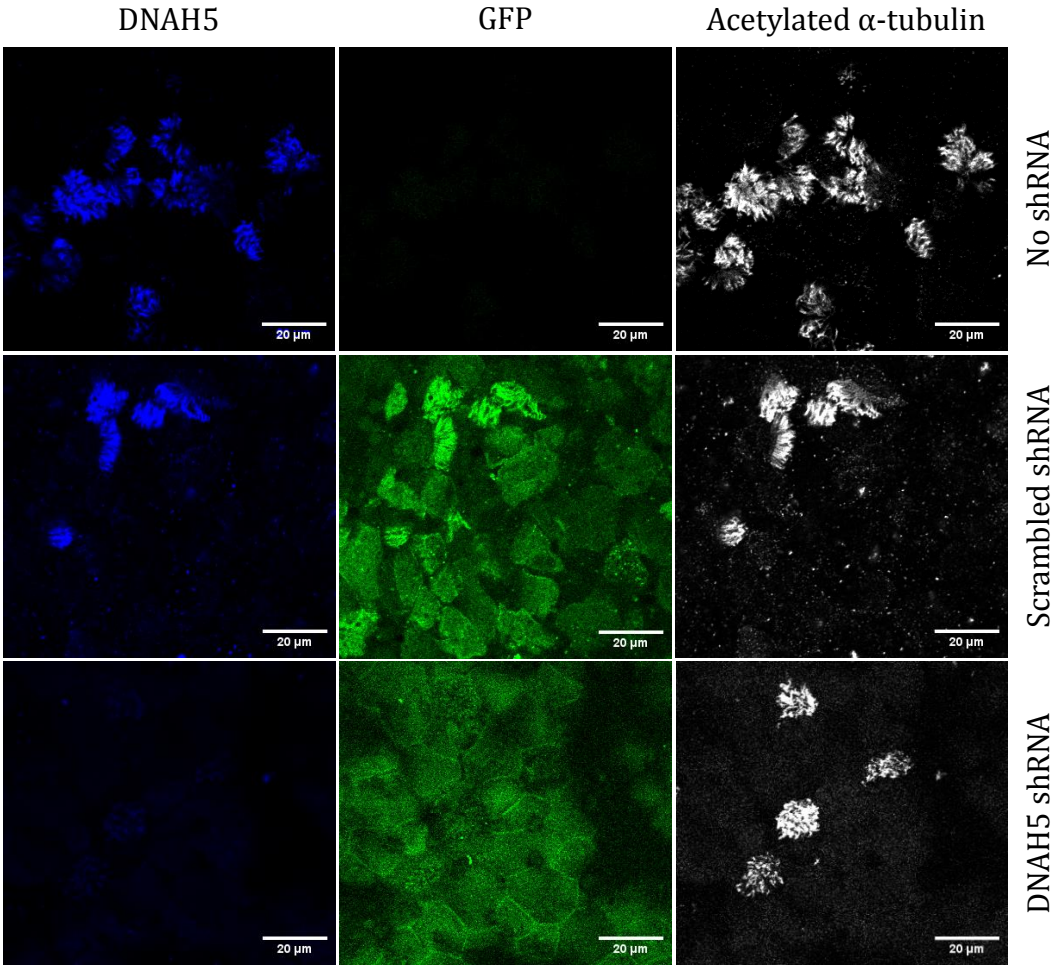

shRNA Target	Is DNAH5 located in ciliary axoneme? Yes	No
Untransduced	157	0
Scrambled	147	0
DNAH5	5	173

***
***

Figure 5.8. DNAH5 localisation

Immunostaining of shRNA transduced and untreated NHBE BMI-1 cells grown at an ALI was used to quantify the number of ciliated cells with DNAH5 in the ciliary axoneme. Only eGFP positive cells were counted in NHBE BMI-1 cells transduced with scrambled or *DNAH5*-targeted shRNA to ensure only shRNA expressing cells were counted. ***P<0.001; Fisher's exact test.

With DNAH5 not localising to the ciliary axoneme in *DNAH5* knockdown cells it was predicted that the ODA would also be absent, as it is in patients, so axoneme ultrastructure was assessed in these cells. However, utilising standard PCD diagnostic methodology and criteria TEM showed no abnormalities in cilia ultrastructure outside of normal ranges in cilia from untransduced, scrambled shRNA and *DNAH5*-targeted shRNA transduced NHBE BMI-1 cells grown on ALI (Figure 5.9). In these studies over 200 individual cilia per condition were assessed for ultrastructural defects. Loss of ODA was therefore not detected in these studies, however, it is important to note that in the TEM studies, in contrast to the DNAH5 localisation studies described above, there was no way to differentiate between cilia from cells expressing the shRNA and those not expressing the shRNA.

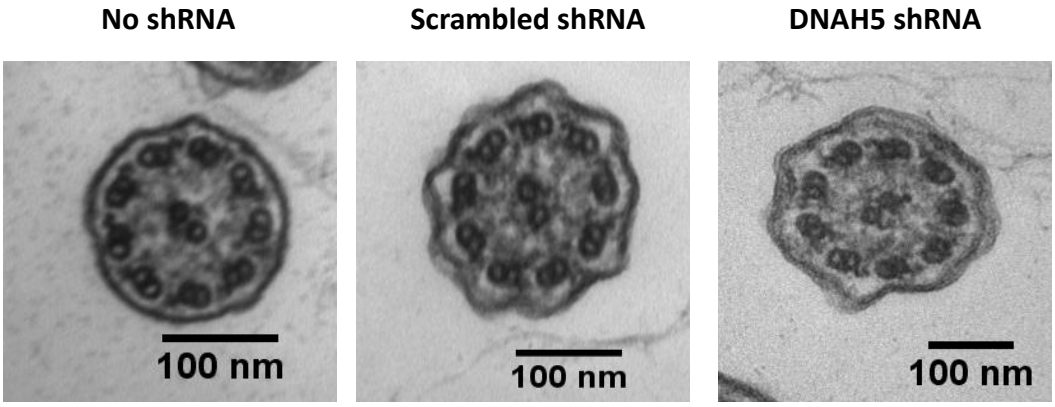

Microtubule Organisation	shRNA Construct: None	Scrambled shRNA	DNAH5 shRNA
Normal 9+2	92.05	95.45	90.33
Central Pair Defect	0.66	0.38	2.6
Dissaranged	3.31	3.03	5.58
Other Defect	3.97	1.14	1.49

Dynein Arms	shRNA Construct: None	Scrambled shRNA	DNAH5 shRNA
ODA and IDA Present	100.00	98.86	100.00
ODA Only	0.00	1.14	0.00
IDA Only	0.00	0.00	0.00
ODA and IDA Absent	0.00	0.00	0.00

Figure 5.9. Cilia ultrastructure

TEM was used to determine microtubule organisation and the presence of absence of dynein arms following mucociliary differentiation of shRNA transduced and untreated NHBE BMI-1 cells. Values are percent of total. Defects in microtubule organisation were assessed in at least 200 individual cilia cross-sections (n=202, 294 and 323 for untransduced, scrambled shRNA transduced and DNAH5 shRNA transduced cells respectively). The presence/absence of dynein arms was assessed in at least 70 individual cilia cross-sections (n=71, 94 and 104 individual cilia from untransduced, scrambled shRNA transduced and DNAH5 shRNA transduced cells respectively).

Despite cells pre-ALI showing an almost 100% transduction efficiency it has been observed that following differentiation of lentivirus transduced cells transgene silencing can occur (428). Given that PCD is a recessive disease a reduction in efficiency of *DNAH5* knockdown could help explain the lack of a missing ODA phenotype using typical diagnostic TEM methodology designed for detecting defects in samples were all cells display a complete lack of protein. To address if silencing of shRNA expression had occurred the level of *DNAH5* knockdown was assessed at the basal cell stage (pre-ALI) and following mucociliary differentiation (>4 weeks on ALI; post-ALI). *DNAH5* knockdown was 91.67 ±0.88% pre-ALI but only 62.00 ±6.66% post-ALI (Figure 5.10a; $p<0.01$; Students *t*-test). An over 600-fold up-regulation in *DNAH5* expression in cells post-ALI (Figure 5.10b; $p<0.01$; Students *t*-test) may have contributed to the reduction in the percentage knockdown observed post-ALI. DNAH5 is an axonemal protein with no known cytoplasmic function so it is unsurprising that extensive gene expression only occurs in multi-ciliated cells. Supporting this, *DNAI1* expression, a gene that codes for another axonemal protein, was also significantly up-regulated post-ALI (Figure 5.10b; $p<0.01$; Students *t*-test).

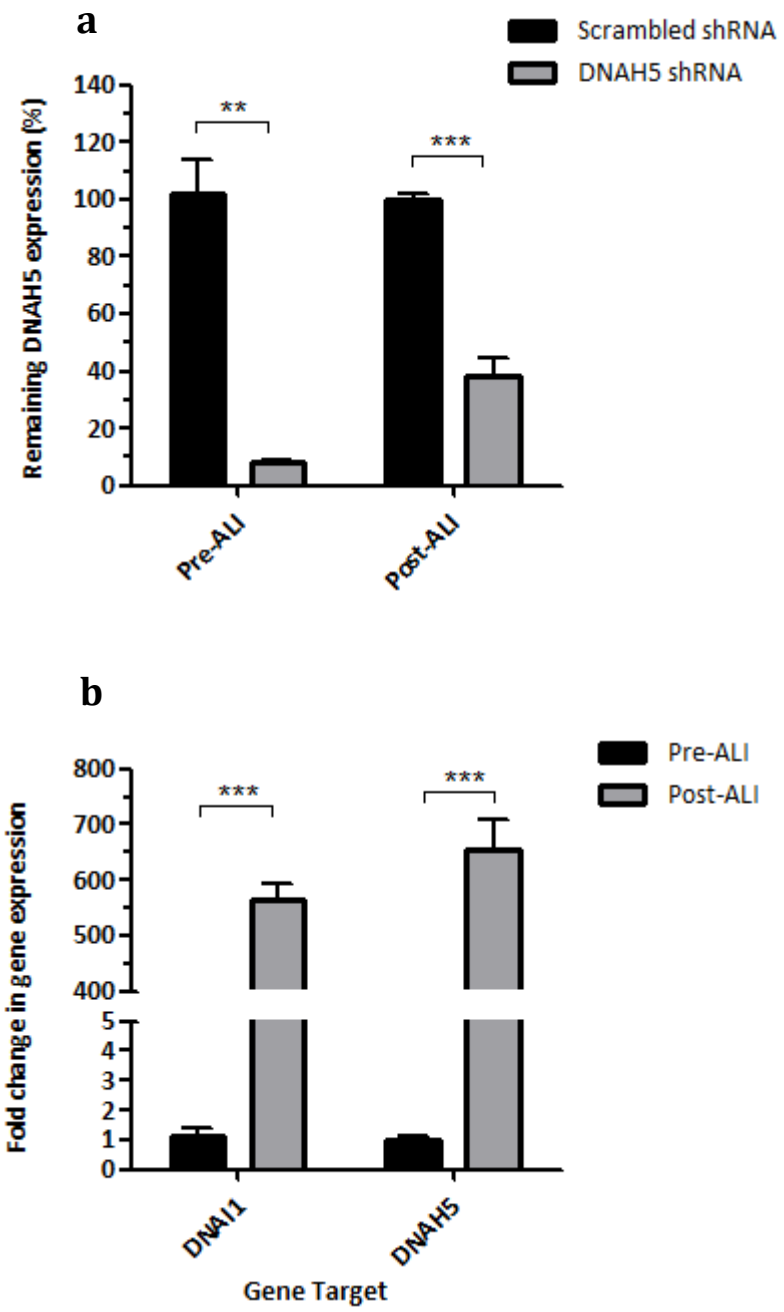

Figure 5.10. *DNAH5* expression pre- and post-ALI

DNAH5 expression was quantified using qRT-PCR and (a) *DNAH5* knockdown pre- and post-ALI in cells transduced with a *DNAH5*-targeted shRNA was determined relative to *DNAH5* expression in cells transduced with scrambled shRNA. (b) *DNAI1* and *DNAH5* expression in NHBE BMI-1 cells post-ALI was also quantified and expression shown relative to NHBE BMI-1 cells pre-ALI. **P<0.01; ***P<0.001; Students *t*-test. Values are mean ±SEM.

To further assess if transgene silencing was occurring whilst removing the confounding effect that up-regulation of *DNAH5* expression post-ALI could have the percentage of GFP positive cells (a reporter gene introduced together with the shRNA construct) was assessed pre-ALI and post-ALI. Manual counting showed that the percentage of GFP positive cells post-ALI was 71.2 ±1.24% (Figure 5.11a) whilst pre-ALI almost 100% of transduced cells were GFP positive (Figure 5.11b). This indicates that the transgene and so the shRNA, was being silenced after cells underwent mucociliary differentiation. Around 28.8% of cells were GFP negative post-ALI, as assessed by manual counting, which is similar to the proportion of cells found by FACS to express only low levels of GFP pre-ALI (32.7%; Figure 5.11b).

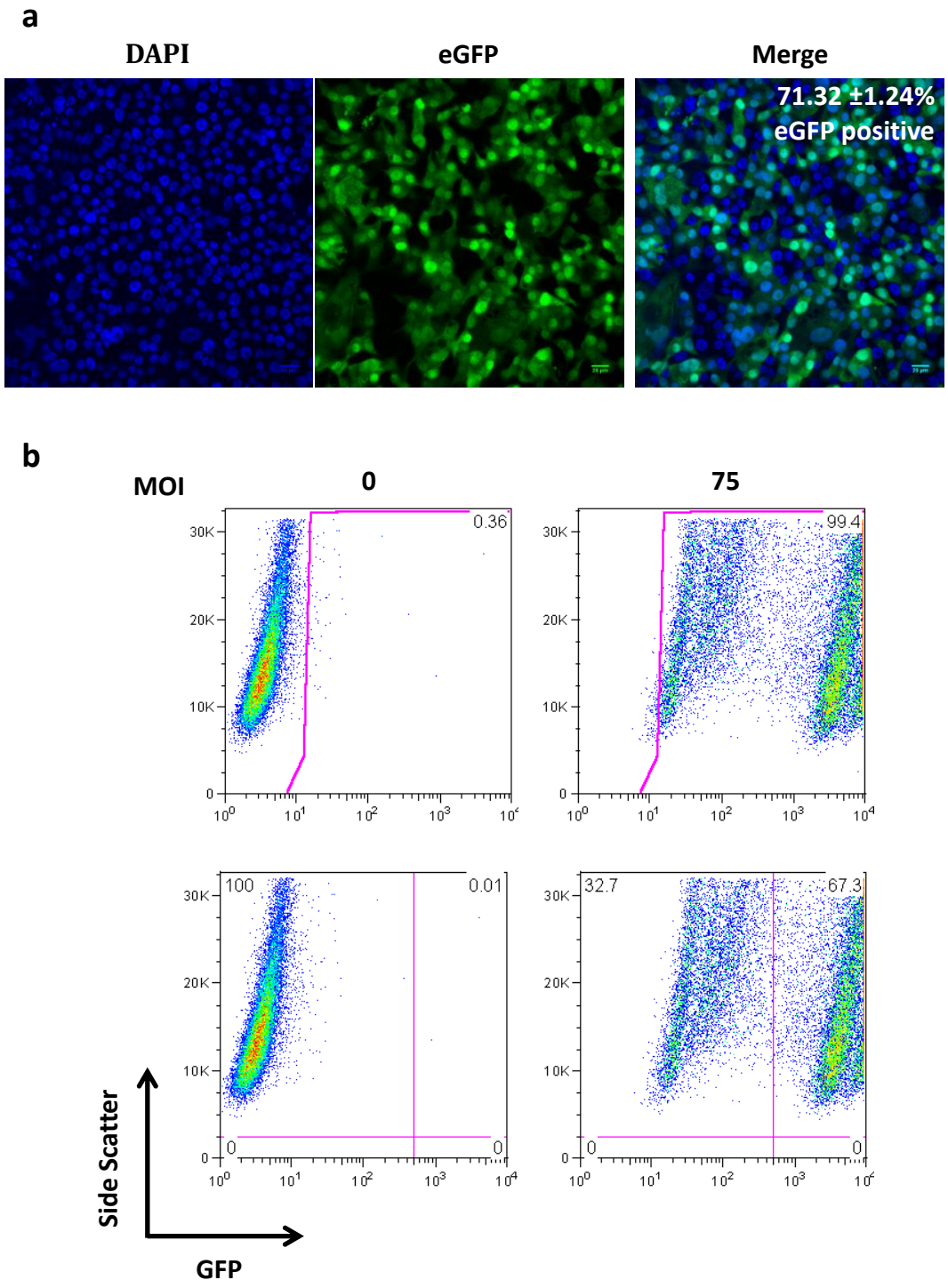

Figure 5.11. Transgene silencing post-ALI

DNAH5 knockdown NHBE BMI-1 cells were (a) stained with DAPI following mucociliary differentiation and the percentage of eGFP positive cells post-ALI was determined. (b) The percentage of eGFP positive cells pre-ALI was determined by flow cytometry with the top panel showing gating such that all eGFP positive and GFP negative populations are differentiated. The bottom panel shows gating such that high and low eGFP expressing cells are differentiated. Values are mean ±SEM.

5.4. DISCUSSION

Suitable models for studying gene therapy approaches for PCD are lacking. In this chapter studies aimed at the production of a suitable cell model from NHBE cells have been described. In the first instance it was vital to produce NHBE cells capable to long-term growth and differentiation to a mucociliary phenotype. Transduction of NHBE cells with BMI-1 resulted in significant extension of the growth potential of these cells without diminishing their differentiation capacity. Whilst greatly improving the number of population doublings NHBE cells could undergo, BMI-1 transduction did not immortalise the NHBE cells in contrast to viral antigens such as the SV40 large T-antigen used to produce the 16HBE14o- cell line (376). Nevertheless the combined properties of extended growth capacity and maintenance of mucociliary differentiation potential of HBE cells is something not previously described and of importance in the production of a PCD disease model.

Whilst Fulcher et al., (423) previously described the transformation of NHBE cells with BMI-1 alone no attempts at mucociliary differentiation of these cells has been described and the data in this chapter provides evidence that transformation of NHBE cells with BMI-1 alone allows for extensive ciliogenesis following ALI culture.

Transduction with BMI-1 of HBE cells from PCD patients could potentially provide semi-immortalised cell lines that could be used to model PCD *in vitro* however in the course of this thesis project no such samples could be obtained. shRNA knockdown of *DNAH5* in BMI-1 transduced NHBE cells was therefore used to attempt to model the PCD phenotype. Knockdown of *DNAH5* at the mRNA level was observed as was immotile cilia and loss of axonemal localisation of DNAH5 protein

all faithfully recapitulating a PCD phenotype. However, TEM analysis, in which it was impossible to determine whether the cilia being observed were protruding from cells expressing *DNAH5*-targeted shRNA, failed to show missing ODA -a phenotype seen in PCD patients. The methodology for analysing cilia ultrastructure was the same as that used clinically for the diagnosis of PCD. In brief this involved characterising at least 200 individual cilia, not ciliated cells. Given that each ciliated cell has a few hundred cilia the count could therefore be biased to a few cells in which the vast majority of cilia were well aligned to the plane being observed. This is not an issue in the clinical diagnosis of PCD as all cells from a single patient should display a PCD phenotype. However, in the context of a heterogeneous population of knockdown cells where it was found that some shRNA expression was silenced in cells expressing low levels of transgene and potentially dampened in cells expressing high levels of transgene, a phenomenon also seen in the course of differentiating induced pluripotent stem cells (iPSCs) (428-430), such a counting method may not be sensitive enough to detect a PCD phenotype and a larger sample size should be used with only a single cilium per cell being characterised.

The data in this chapter provide evidence that knockdown of *DNAH5* could be used to recapitulate at least some aspects of a PCD phenotype. However, a number of improvements could be made. Firstly, a homogenous population of shRNA expressing cells would be desirable to ensure that all cells within a given culture behaved similarly and had similar levels of *DNAH5* knockdown. Given the extended growth capacity of NHBE BMI-1 cells it is now plausible to establish and expand single cell clones expressing high levels of shRNA. However, even with a

homogenous population of cells transgene silencing following differentiation on ALI would remain an issue. Transgene silencing following lentivirus transduction typically involves DNA methylation or histone modification of the promoter element (428). The use of an alternative promoter more resistant to DNA methylation, such as a ubiquitous chromatin opening element (UCOE) (431), may offer a solution. Use of UCOE has been shown to prevent transgene silencing in iPSCs and importantly their differentiated progeny (432). Alternatively, cell specific promoters could prevent silencing in certain cell types. To this end the human FOXJ1 promoter, expressed in multi-ciliated cells (433), would help maintain shRNA expression in multi-ciliated cells. An alternative option to the use of shRNA knockdown of *DNAH5* is the use of gene modification technologies, such as CRISPR/Cas9 systems, to introduce frameshift mutations, or patient specific mutations, that prevent wild-type *DNAH5* expression.

In summary, this chapter describes the generation of an airway epithelial cell line capable of mucociliary differentiation and with an extended growth potential. This advance paves the way to modelling PCD *in vitro* by direct transformation of patient cells with BMI-1, or the use of gene modification technologies in healthy cells to mutate *DNAH5*. The shRNA studies described here provide proof-of-principle that knockdown of *DNAH5* faithfully reproduces the immotile cilia and lack of axonemal DNAH5 expression seen in PCD patients. As such, correcting these phenotypes would still provide proof-of-principle that gene therapy could restore cilia beating in PCD caused by *DNAH5* mutations. This model was therefore moved forward to experiments testing this hypothesis.

CHAPTER SIX

RESULTS

CORRECTION OF *IN VITRO* PCD MODELS

6. CORRECTION OF *IN VITRO* PCD MODELS

6.1. INTRODUCTION

Two proof-of-principle studies have demonstrated that cilia beating can be restored in PCD cells by introduction of a functional copy of the mutated gene. In these studies PCD resulted from mutations in *DNAI1 (283)* or its mouse homolog *Dnaic1* (314), the second most common cause of PCD. No study has yet determined whether cilia beating can be restored in PCD caused by mutations in *DNAH5*, the most common cause of PCD and so of highest potential benefit to PCD patients.

Previous chapters in this thesis have described the cloning of wild-type DNAH5 cDNA into a mammalian expression plasmid, enhancement of transgene expression using minicircle vectors and the production of a model in which to assess PCD gene therapy. This provided the tools required for assessing the hypothesis that gene therapy could be used to restore cilia beating in PCD caused by *DNAH5* mutations.

6.2. AIMS

To test the hypothesis that gene therapy would restore cilia beating in PCD caused by *DNAH5* mutations.

To achieve this aim, reporter genes were used to optimise transfection of well differentiated ALI cultures and a reverse transfection protocol, previously optimised for siRNA transfections, was assessed for DNA transfections. The latter approach relied on transfecting de-differentiated cells and so the persistence of transgene expression was also assessed. Finally, correction of the PCD model previously

described was attempted by transfection of DNAH5 cDNA using the method of transfection found to be optimal.

6.3. RESULTS

6.3.1. PCI-DNAH5 MUTAGENESIS

The DNAH5 cDNA cloned earlier (Chapter 3.3.3; p137) was of a wild-type sequence and so would be silenced by the shRNA used to produce the PCD model described earlier (Chapter 5; p183). To avoid this knockdown 6bp spaced along the 21bp shRNA recognition sequence were mutated. The recognition sequence of the *DNAH5*-targeted shRNA was;

5’ – GGACTGACTTTCTAATTCAAA – 3’

A codon optimised DNAH5 cDNA sequence was obtained from Blue Heron Bio (https://wwws.blueheronbio.com) and the wild-type shRNA recognition sequence was mutated to the codon optimised sequence (red denotes the mutated nucleotides);

5’ – GAACGGACTTCCTTATCCAGA – 3’

The overlapping primers used for this mutagenesis were;

Forward primer; 5'-
GGTGCCAAATGTTGACAATGTGAGAACGGACTTCCTTATCCAGACCATTGCTAAACAGGG
CAAGGCT-3'

Reverse primer; 5'-

AGCCTTGCCCTGTTTAGCAATGGTCTGGATAAGGAAGTCCGTTCTCACATTGTCAACATTTG

GCACC-3'

Site-directed mutagenesis using QuickChange II XL Site-Directed Mutagenesis kit was unsuccessful yielding no PCR product or colonies. The primers used had a high melting temperature (T_m) of 79.6^{o}C whose sequences had the potential for hairpin formation, self-annealing and primer dimerization. In addition, that the amplification temperature for the DNA polymerase used was 68^{o}C, below the recommended annealing temperature of primer T_m-5^{o}C, secondary annealing would have been a problem and all of this could have contributed to the lack of a PCR product and so lack of colonies.

To overcome these issues the mutagenic primers were used with a high-fidelity polymerase whose maximal activity was achieved at 72^{o}C. In addition both annealing and extension steps were performed at this temperature (Table 6.1) thus reducing the potential for hairpin formation, self-annealing, primer dimerization and secondary annealing. Following this PCR reaction the PCR product was purified and a SLIC reaction performed as described in materials and methods (Chapter 2.2.22; p93). The mutated portion of the DNAH5 cDNA was sub-cloned into pMC.DNAH5 using AfeI and SexAI restriction sites to yield the plasmid pMC.DNAH5 (shRNA). MC.DNAH5 (shRNA) minicircle DNA was produced from the pMC.DNAH5 (shRNA) producer plasmid.

Step	Temperature (°C)	Duration	Number of Cycles
Initial denaturation	95	3 minutes	1
Denaturation	98	20 seconds	17
Annealing	72	15 seconds	
Extension	72	1 minute/kb	
Final extension	72	1 minute/kb	1

Table 6.1. Cycling conditions for 6bp mutagenesis

To assess if the mutations introduced to the DNAH5 cDNA were sufficient to allow escape of the resultant transcripts from shRNA-mediated degradation HEK293T cell clones stably expressing either a scrambled shRNA (HEK293T Scrambled KD) or the *DNAH5*-targeted shRNA (HEK293T *DNAH5* KD) were produced by transducing HEK293T cells with lentivirus carrying either a scrambled shRNA or the *DNAH5*-targeted shRNA used to produce the PCD model described earlier (Chapter 5; p183). HEK293T Scrambled KD and HEK293T *DNAH5* KD cells were then transfected using L2K with either MC.DNAH5 or MC.DNAH5 (shRNA) minicircle DNA and DNAH5 expression was quantified by qRT-PCR. When wild-type DNAH5 was transfected DNAH5 expression was knocked down in HEK293T *DNAH5* KD cells by 44.0 ±2.3% relative to HEK293T Scrambled KD cells (Figure 6.1; $p<0.01$; Students t-test). No significant knockdown was seen in HEK293T *DNAH5* KD cells when MC.DNAH5 (shRNA) was transfected (Figure 6.1) indicating that mRNA transcribed from this DNA evaded knockdown by the *DNAH5*-targeted shRNA used to model PCD. Therefore MC.DNAH5 (shRNA) DNA was to be used in studies attempting to correct the PCD model described earlier.

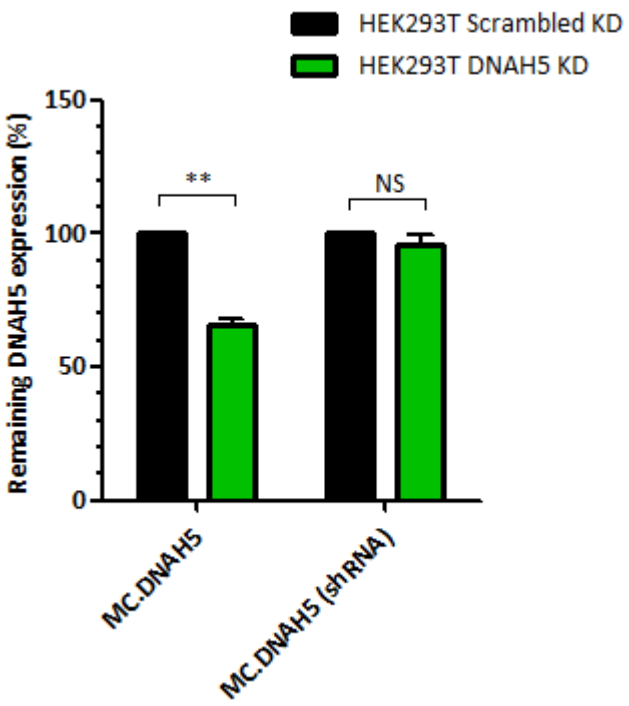

Figure 6.1. MC.DNAH5 mutagenesis

Wild-type (MC.DNAH5) and mutated (MC.DNAH5 (shRNA)) were transfected into HEK293T cells stably transduced with a scrambled or *DNAH5*-targeted shRNA and DNAH5 expression assessed by qRT-PCR. NS; not significant; **P<0.01; Student's t-test used to assess significance. Values are mean ±SEM.

6.3.2. TRANSFECTIONS OF CILIATED ALI CULTURES

To assess whether gene therapy could restore cilia beating in PCD caused by *DNAH5* mutations it was vital that the DNAH5 transgene could be efficiently transfected and expressed in ciliated cells. The human airway contains ciliated and mucus producing cells connected together by tight junctions and overlaid with a mucus barrier all of which act to restrict cell entry of external agents. The *in vivo* barriers are best recapitulated *in vitro* by mucociliary differentiation of human airway epithelial cells induced by use of an ALI culture system. The ALI culture system was therefore considered to be the most relevant system for assessing the potential efficacy of PCD gene therapy.

Prior to attempting correction of *in vitro* PCD models on ALI systems the transfection efficiency of this approach was optimised using reporter genes to assess the likelihood of successes when transfecting the DNAH5 cDNA. Transfection efficiency of ciliated ALI cultures using the LPD vector was assessed by transfecting DNA encoding a secreted luciferase gene (NanoLuc) to enable easy quantification.

First the site of application of nanocomplexes was assessed comparing apical, basolateral and apical+basolateral (both) applications. A total of 2µg of MC.NL1.3 DNA was transfected per well with 1µg apical application and 1µg basolateral application used when both sides were transfected simultaneously. To assess transgene expression 700µL of ALI media was added to the apical surface and incubated for 30 minutes at 37^{o}C and 5% CO_2 to allow the secreted luciferase protein to diffuse into the media. Luciferase activity within this media was assessed

along with luciferase activity in the 700µL basolateral media which the cells were cultured with.

Basolateral application of nanocomplexes was found to provide no detectable transgene expression above background levels (untransfected cells). There was no significant difference in transgene expression following application of nanocomplexes to the apical surface alone or both the apical and basolateral surface (Figure 6.2a) although both gave transgene expression above background levels. That transgene expression was only present following apical delivery of the LPD vector highlights that the LPD vector preferentially transfects the apical surface of ALI cultured cells.

Whilst there was no significant difference in transfection efficiency with apical or apical and basolateral application of nanocomplexes, the latter was chosen for future studies as it allowed efficient transfection via the apical surface and would allow basolateral surface transfection events if later treatments assessing the use of tight junction modulators permitted this route of gene delivery.

Having optimised the route of delivery the amount of DNA required for ALI transfections was optimised by transfecting well-ciliated ALI cultures with a total of 1, 2 or 4µg of DNA per well. No significant differences between the different treatment groups were detected likely due to the high variability in transfection efficiencies within groups combined with the low sample sizes per group (Figure 6.2b; n=3 for each group).

It was clear that to be successful for the assessment of gene therapy treatment the methodology used to transfect ALI cultures would need to be further optimised to enhance efficiency and the use of 4µg of DNA per well was used in these further studies as at this dose all treated wells produced RLU values above that of background levels (untreated wells) which contrasted with when 1 and 2µg of DNA were transfected where 1/3 and 2/3 of treated wells respectively did not display RLU values above background.

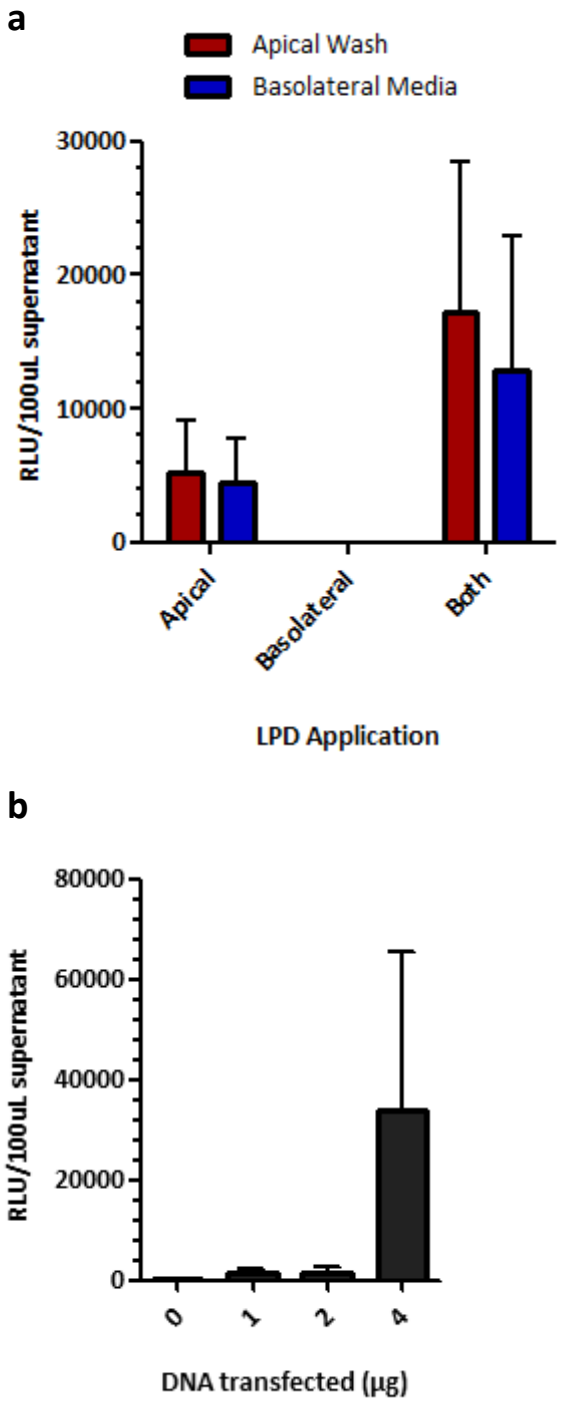

Figure 6.2. Transfections of differentiated ALI cultures

LPD transfections were optimised using a secreted luciferase and both the (a) route and (b) dose for efficient transfection determined. Values in (a) are background subtracted and displayed as mean ±SEM. Values in (b) are mean ±SEM.

ALI cultures are known to be difficult to transfect and transduce so a number of methods have been developed to enhance gene delivery with the most common being the use of LPC (261, 434), EGTA (435-437) and sodium decanoate (also known as sodium caprate) (244, 438). Treatment of ALI cultures with these compounds has the effect of reversibly disrupting the integrity of tight junctions. How this disruption translates to enhanced transgene expression for non-viral vectors is not clear. In contrast, access to receptors on the basolateral surface is thought to be the mechanism by which disruption of tight junctions enhances viral transduction (263, 439).

To enhance transfection of ALI cultures by LPD complexes EGTA, sodium decanoate and ethanol treatments were assessed. The latter has not previously been assessed for enhancement of airway gene delivery but was included due to evidence that ethanol increased the permeability of ALI cultures formed from NHBE cells (440). In brief, five different treatment conditions were tested i) 2 hour treatment with LPD alone, ii) 24 hour pre-treatment of ALI cultures with 0.6% (v/v) ethanol followed by 2 hour treatment with LPD, iii) 2 hour treatment with LPD together with 0.6% (v/v) ethanol, iv) 2 hour treatment with LPD together with 10mM EGTA and v) 3 minute pre-treatment of ALI cultures with 30mM sodium decanoate followed by 2 hour treatment with LPD. All incubations were performed at 37^{o}C and 5% CO_2 and apical washes and basolateral media were collected for luciferase assays 48 hours following transfection. These treatment conditions and concentrations were used as they were previously shown to be optimal for enhancing transgene expression

with viral and non-viral vectors (244, 435-438) or enhancing the permeability of ALI cultures in the case of ethanol pre-treatment (440).

Treatment of ALI cultures with LPD together with EGTA produced a 145-fold enhancement in transgene expression compared to treatment with LPD alone as assessed by luciferase activity from basolateral media (Figure 6.3a; $p<0.01$; one-way ANOVA with Tukey's post-test analysis). Pre-treatment of ALI cultures with sodium decanoate similarly enhanced transfection with a 115-fold increase in luciferase activity (Figure 6.3a; $p<0.01$; one-way ANOVA with Tukey's post-test analysis) whilst ethanol did not significantly enhance transgene expression. Assessing luciferase activity in the apical washes of the same cells 48 hours following transfections there were no significant differences between the different treatment groups (Figure 6.3b).

Whilst toxicity was not quantified in this study it was of note that sodium decanoate pre-treatment of ALI cultures resulted in significant toxicity with cell monolayer integrity being compromised most likely due to significant cell death given that a confluent monolayer was no longer present (Figure 6.3c). Whether this toxicity resulted from the sodium decanoate treatment alone, or the combination of sodium decanoate treatment followed by LPD application was not assessed but given that the toxicity has not been reported in previous studies employing the same conditions used here (438) it is likely that the latter produced the toxicity observed.

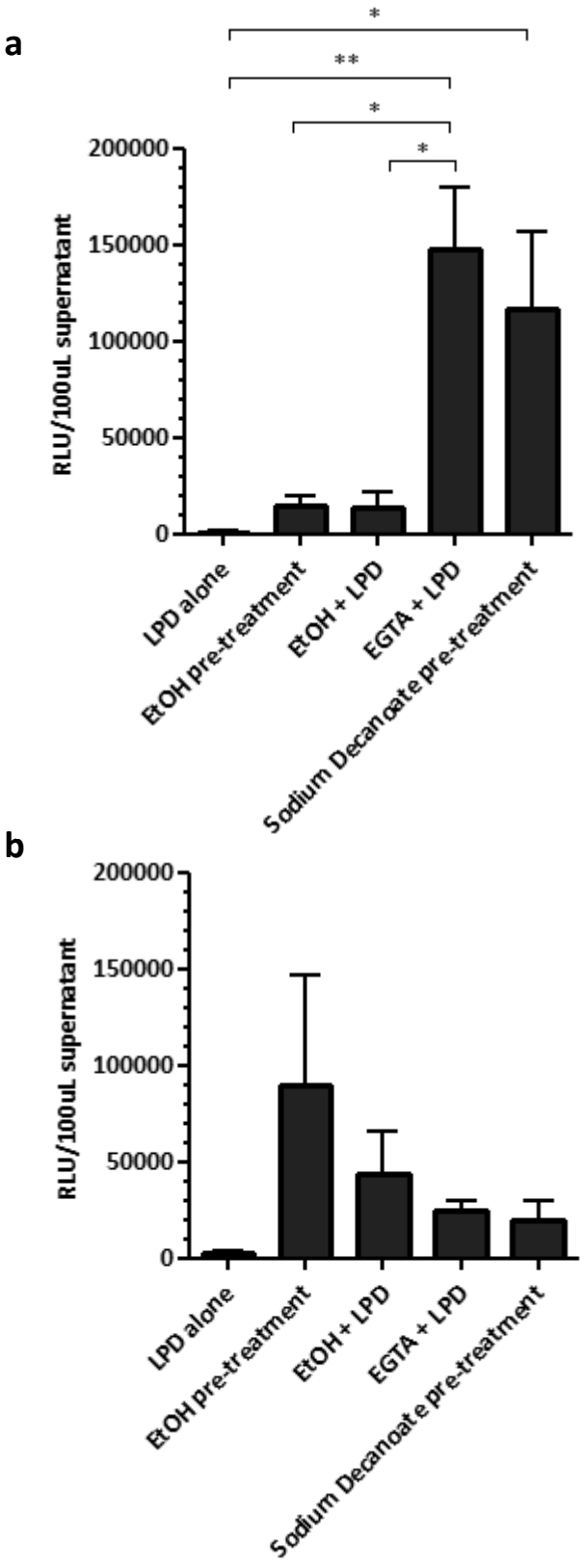
a
*
**
*
*
200000
150000
100000
50000
0
RLU/100uL supernatant
LPD alone
EtOH pre-treatment
EtOH + LPD
EGTA + LPD
Sodium Decanoate pre-treatment
b
200000
150000
100000
50000
0
RLU/100uL supernatant
LPD alone
EtOH pre-treatment
EtOH + LPD
EGTA + LPD
Sodium Decanoate pre-treatment

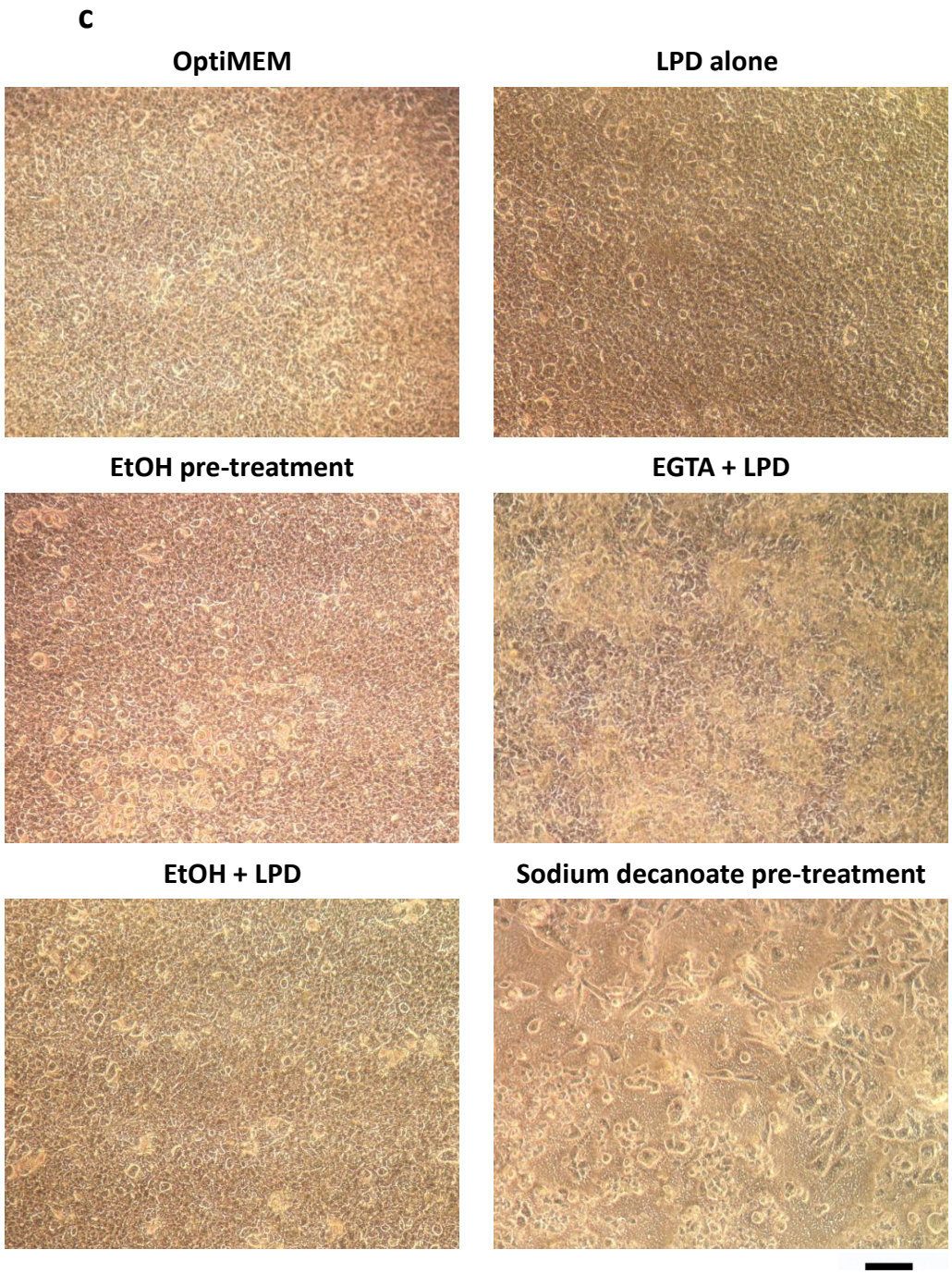

Figure 6.3. Tight junction disruption for enhanced gene delivery

Luciferase activity in (a) basolateral media and (b) apical wash was assessed 48 hours following transfections of ALI cultures with LPD and a variety of tight junction disruption treatment protocols. (c) Light microscopy of these transfected ALI cultures. *P<0.05; **P<0.01; one-way ANOVA with Bonferroni post-test analysis used to assess significance. Values are background subtracted and displayed as mean ±SEM.

As secreted luciferase was used to optimise transfections in differentiated ALI cultures, no data was available on the percentage of cells transfected, an important consideration for PCD gene therapy. To assess this MC.eGFP was transfected using 2.0µg of DNA on each the apical and basolateral surfaces (4µg total per well) and the different tight junction modulation strategies tested above were also used. It was evident that regardless of what treatment option was used far less than 1% of cells were transfected (fewer than 5 out of 500,000 cells seeded) highlighting the futility of using ALI culture transfections to provide proof-of-principle of PCD gene therapy. In attempting to quantify the percentage of cells transfected cells were fixed, the nucleus stained with DAPI and over 15 random fields of view per treatment were assessed for GFP positive cells but none were detected. Rather than proceeding with the approach of transfecting well differentiated ALI cultures a different strategy of transfecting cells prior to ALI culture was investigated.

6.3.3. REVERSE TRANSFECTION

Transfecting primary airway epithelial cells 24 hours following seeding onto tissue culture plates, the standard method for transfecting cells, resulted in significant toxicity as was described when transfecting primary nasal epithelial cells (Chapter 3.3.1.3; p121) and so was not utilised. Ramachandran et al., (441) have shown that transfecting primary human or porcine airway epithelial cells in suspension followed by seeding the cells on ALI culture did not affect cell viability and resulted in both enhanced transfection efficiency relative to differentiated cells and differentiation of the cells to a mucociliary phenotype. The authors were transfecting siRNA and gene silencing persisted for at least 2 weeks. This "reverse transfection" (441) method was utilised here in the context of DNA delivery.

Submerged NHBE BMI-1 cells were transfected for 30 minutes at room temperature with varying concentrations of MC.eGFP DNA packaged into LPD nanocomplexes. The percentage of cells transfected varied from 4.2 ±1.7% with a DNA concentration 2µg/mL/5x10^5 cells to 17.7 ±0.6% at 8µg /mL/5x10^5 cells (Figure 6.4a; $p<0.001$; one-way ANOVA with Bonferroni's post-test analysis). DNA concentrations above 8µg /mL/5x10^5 cells were found to be toxic resulting in significant cell death and so were considered unsuitable for further studies (Figure 6.4f and g). There was no significant difference in transfection efficiency at a dose of 4 and 6µg /mL/5x10^5 cells (Figure 6.4a). Given the desire to minimise potential toxicity that may impact on the ability of cells to undergo mucociliary differentiation 4µg /mL/5x10^5 cells was selected as the optimal dose that balanced efficient transfection with minimal toxicity and so was used in further studies.

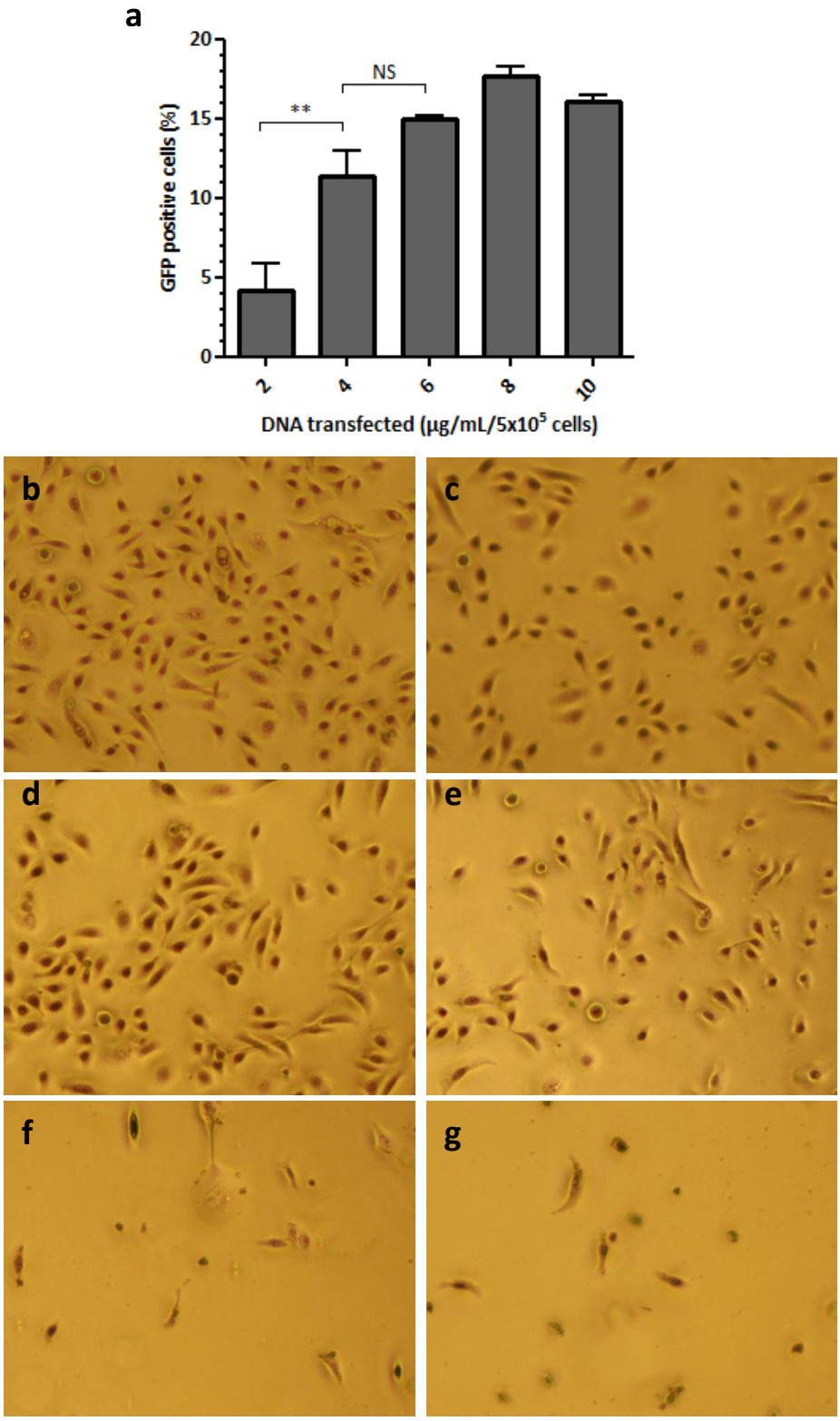

Figure 6.4. Reverse transfection protocol DNA dose optimisation

Following MC.eGFP transfection at a variety of doses (a) the percentage of cells transfected was assessed by flow cytometry. (b-g) Light microscopy images showing cell morphology following reverse transfection with (b) 0-, (c) 2-, (d) 4-, (e) 6-, (f) 8- and (g) 10µg/mL/5x10^5 cells. NS; not significant; **P<0.01; one-way ANOVA with Bonferroni post-test analysis used to assess significance. Values are background subtracted and displayed as mean ±SEM.

Having optimised the DNA concentration for transfection transgene persistence was assessed by transfecting cells pre-ALI with MC.eGFP, seeding the cells on ALI and obtaining whole well scans using a fluorescent microscope (Figure 6.5a) followed by quantification of the percentage of eGFP positive cells using ImageJ software. An aliquot of the same cells seeded on ALI were also seeded on standard tissue culture plates to allow more sensitive determination of initial levels of transgene expression by flow cytometry.

Transfection efficiency assessed by flow cytometry was 2.6 fold higher than that calculated using ImageJ (14.7±2.4% for flow cytometry and 5.6±0.8% for ImageJ; Figure 6.5b) thus highlighting the differences in sensitivity between the two approaches. Interestingly the percentage of GFP positive cells almost doubled 6 and 8 days post transfection from 5.6±0.8% at day 2 to 9.6±0.9% and 9.4±0.8% on day 6 and 8 respectively using the ImageJ calculation method (Figure 6.5b; $p<0.01$; one-way ANOVA with Bonferroni's post-test analysis). Transgene expression declined to day 2 levels at 15 days post-transfection and fell further at 29 days post-transfection. As cells on ALI typically produced cilia at around 14-21 days on ALI, that transgene expression was still present at these time point indicates that the reverse transfection method has the potential to allow proof-of-principle studies assessing PCD gene therapy *in vitro*.

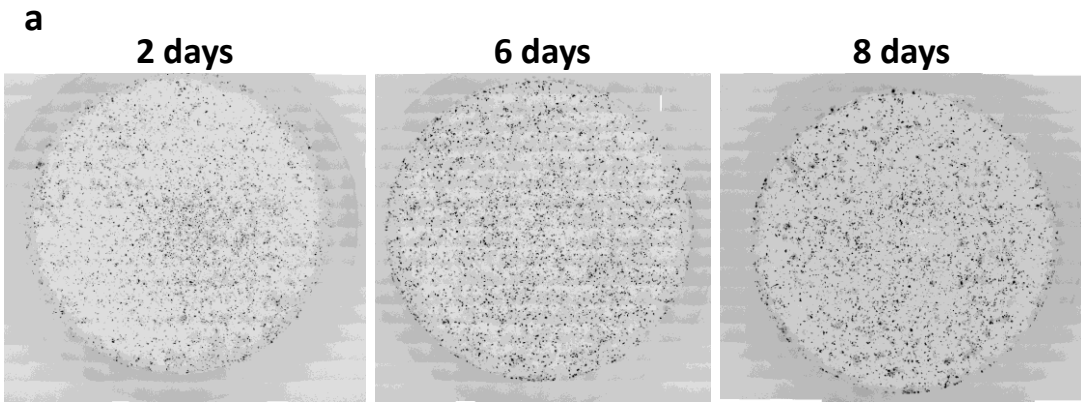

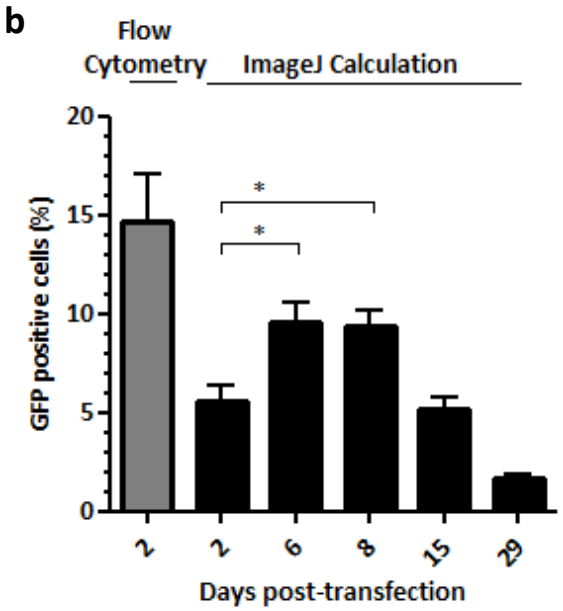

Figure 6.5. Persistence of transgene expression using reverse transfection

NHBE BMI-1 cells reverse transfected with MC.eGFP were placed on ALI and (a) whole well scan images taken and (b) GFP fluorescence quantified up to 29-days post transfection. *P<0.05; one-way ANOVA with Bonferroni post-test analysis used to assess significance. Values are background subtracted and displayed as mean ±SEM.

Having established that the reverse transfection protocol allowed efficient and persistent transgene expression, its effects on cilia formation and function were determined by assessing the levels of ciliogenesis and CBF 32 days following transfection. This time-point was chosen so as to minimise the potential effects of eGFP overexpression on cilia formation and function. Cells transfected using the reverse transfection method were found to undergo mucociliary differentiation as assessed by light microscopy (data not shown) and encouragingly no differences in the percentage active area (Figure 6.6a) and CBF (Figure 6.6b) were found when comparing transfected and untransfected cells so indicating that the reverse transfection method did not adversely affect cilia formation or function. This method was therefore considered suitable for assessing PCD gene therapy *in vitro*.

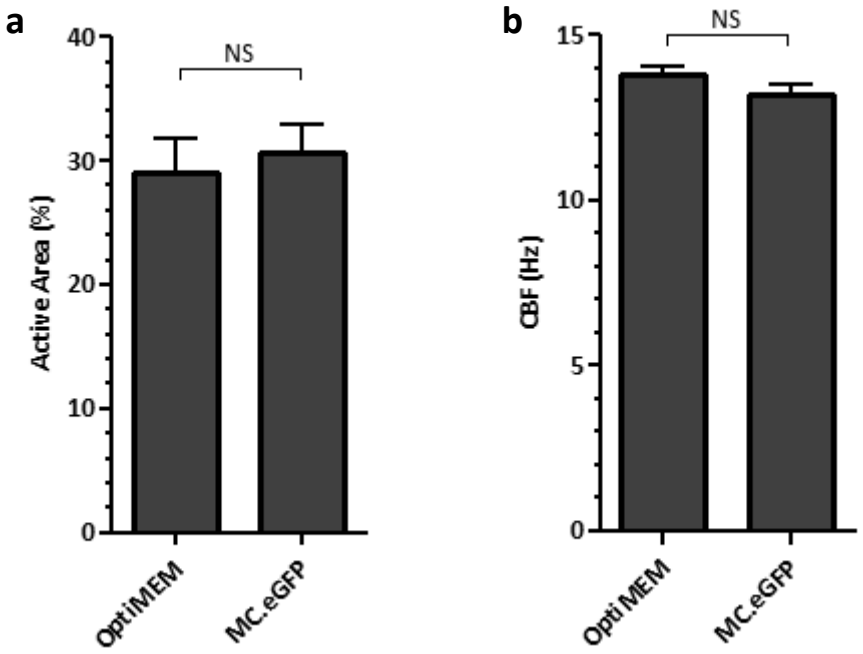

Figure 6.6. Cilia characterisation following reverse transfection

NHBE BMI-1 cells reverse transfected with MC.eGFP were placed on ALI and 32 days following transfection videos captured and the (a) percent active area and (b) CBF determined using CiliaFA ImageJ plugin. NS; not significant; Student's t-test used to assess significance. Values are mean ±SEM.

Having optimised the conditions for transfecting NHBE BMI-1 cells whilst retaining efficient transgene expression until at least the time point at which mucociliary differentiation takes place it was feasible to assess whether gene transfer of a functional DNAH5 cDNA would restore cilia beating in *in vitro* PCD disease models.

The cell model developed and described in this thesis - NHBE BMI-1 cells stably expressing *DNAH5*-targeted shRNA (Chapter 5; p183)- was transfected with MC.DNAH5 (shRNA) using the reverse transfection method and cells then seeded on to standard tissue culture plates. No significant difference in DNAH5 expression was found by qRT-PCR 48 hours following transfection when comparing transfected with untransfected cells (Figure 6.7a). As such, it was unsurprising that the PCD phenotypes observed from the NHBE BMI-1 *DNAH5* knockdown cells were not corrected with immunostaining of cells 30 days post-transfection (28 days post-ALI) failing to show any DNAH5 expression. Due to the lack of DNAH5 expression no further phenotyping studies of transfected cells were pursued.

To provide a guide as to the number of cells that could be expected to have been transfected in these correction studies NHBE BMI-1 cells were transfected with the eGFP-DNAH5 fusion plasmid pCI.eGFP.DNAH5. The fusion protein was expressed in around 0.35% of cells when accounting for auto-fluorescence detected in untransfected cells, this difference whilst small was significant (Figure 6.7b; $p<0.01$; Students t-test). This low transfection efficiency helps explain why no DNAH5 expression was seen in MC.DNAH5 (shRNA) transfected NHBE BMI-1 *DNAH5* knockdown cells. The biophysical properties of the LPD vector carrying MC.DNAH5 (shRNA) was compared to MC.eGFP containing LPD vectors to assess if any

differences here could explain the different transfection efficiencies observed when transfecting NHBE BMI-1 cells. With regards to zeta potential, a factor that impacts on vector binding to the cell surface, there was no significant difference between MC.DNAH5 (shRNA) and MC.eGFP containing LPD complexes which had a zeta potential of 35.4 ±0.5mV and 36.5 ±1.5mV respectively (Figure 6.7c). There was a small but significant difference of around 10nm to the hydrodynamic sizes of LPD complexes formulated with MC.DNAH5 (shRNA) and MC.eGFP DNA with the mean values being 110.5 ±1.1nm and 102.5 ±2.0nm respectively (Figure 6.7c; $p<0.01$; Student's t-test). However, it is unlikely that this small difference impacted significantly on transfection efficiency.

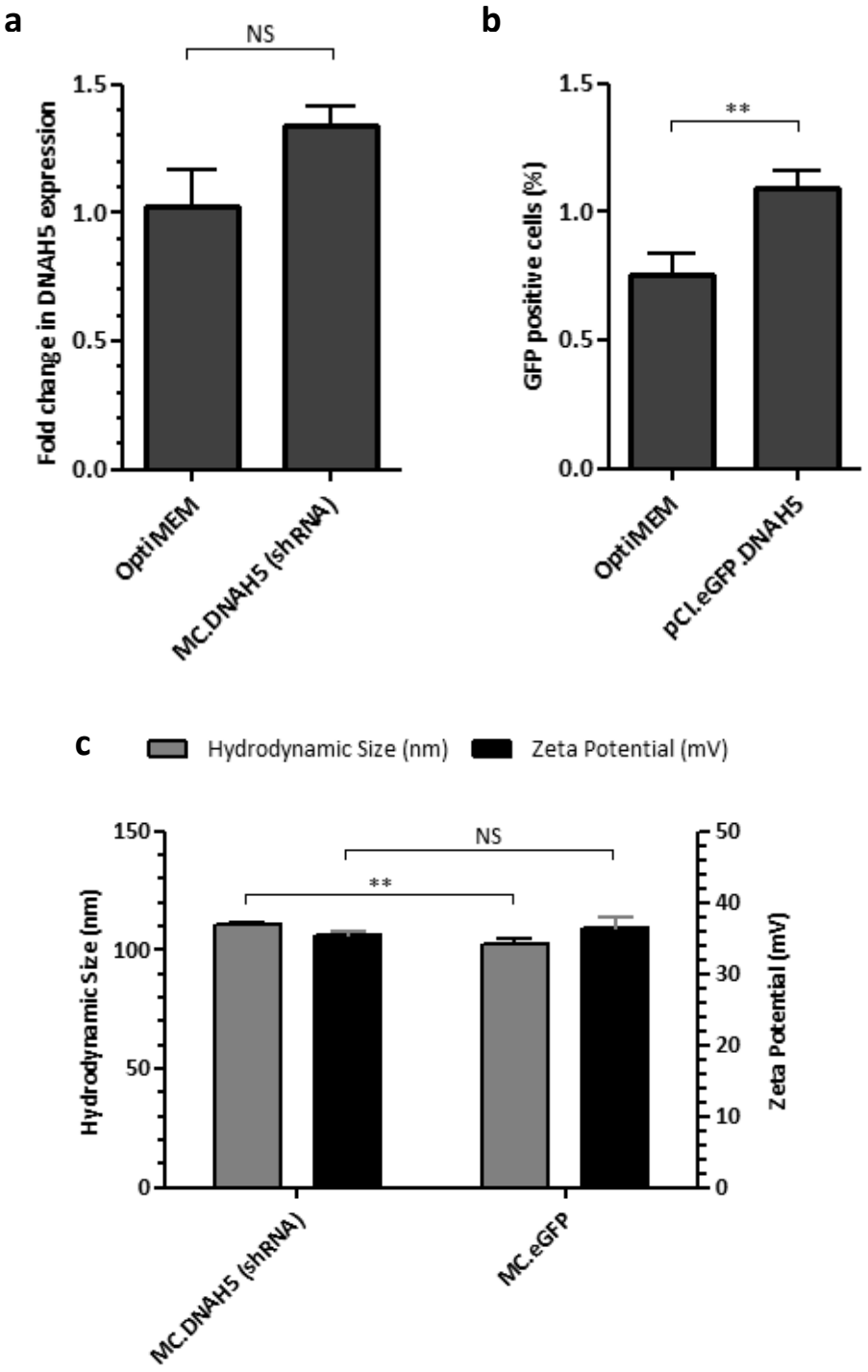

Figure 6.7. DNAH5 transfections

(a) DNAH5 expression was assessed by qRT-PCR following MC.DNAH5 (shRNA) transfection into DNAH5 knockdown NHBE BMI-1 cells. (b) GFP expression was assessed by flow cytometry following transfection of NHBE BMI-1 cells with pCI.eGFP.DNAH5 and (c) hydrodynamic size and zeta potential of LPD complexes containing MC.DNAH5 (shRNA) and MC.eGFP DNA was also assessed. NS, not significant; **P<0.01; Student's t-test used to assess significance. Values are mean ±SEM.

6.4. DISCUSSION

To assess whether gene therapy can correct PCD caused by *DNAH5* mutations it is imperative that the functional gene can be delivered and expressed in ciliated cells. In this chapter studies aimed at optimising gene delivery to ciliated cells are described. *In vitro* two culture methods have been used to differentiate primary airway epithelial cells to a ciliated phenotype, namely ALI cultures and the Jorissen culture method (315). The Jorissen culture method allows differentiation of airway epithelial cells to a ciliated phenotype under submerged conditions with cells grown in suspension. Airway cells in suspension, once in contact with neighbouring cells, form spheroids thus inducing differentiation with cilia protruding into the lumen of the spheroid structure. In contrast, ALI cultures present a more native system in that the basolateral surface of cells are exposed to culture media whilst the apical surface is exposed to air. Growing airway epithelia cells at this ALI induces mucociliary differentiation so this system has the added potential of allowing assessment of mucociliary clearance, a vital outcome measure in assessing potential clinical efficacy of a gene therapy treatment. However, transfections of differentiated ALI cultures are notoriously difficult presenting a number of challenges to vector uptake including polarisation of the cell epithelium, formation of tight junctions, production of mucus and cilia beating. In PCD, cilia are immotile but their presence may still hinder transfection given the presence of a periciliary bush preventing particles above 40nm from reaching the cell surface (442). In light of this it is unsurprising that the gene transfer was inefficient.

EGTA and sodium decanoate enhances gene transfer by LPD vectors to differentiated ALI cultures, as observed in other studies with different viral and non-viral vectors (244, 435-438). However, these treatments still resulted in less than 1% of cells showing transgene expression. Transfection of differentiated ALI cultures by the optimised LPD vector is thus too inefficient to allow correction to be observed *in vitro* given that the LPD vectors do not exclusively transfect ciliated cells and that the proportion of ciliated cells in ALI cultures are typically under a third of the cells present.

Transfection of ALI cultures with siRNA is also inefficient and a reverse transfection protocol was devised to overcome this (441). In this chapter, for the first time, the reverse transfection method was shown to also allow more efficient DNA transfection relative to transfection of fully differentiated ALI cultures. Using this protocol transgene expression persisted long enough for ciliogenesis to take place, a crucial requirement for the method to be utilised in gene therapy proof-of-principle studies *in vitro*. The percentage of cells expressing eGFP following the reverse transfection protocol peaked at around 6-8 days post-transfection whereas peak expression is typically 48-72 hours in dividing cells (443, 444). Native GFP has a relatively long half-life of ~26hours (445) (compared with native firefly luciferase with a half-life of ~2 hours (446)) and this stability combined with a lack of cell division would have contributed to the delayed peak in eGFP expression seen. The lack of cell division would have also contributed to the persistence of transgene expression where eGFP expression was still present 28-days post-transfection.

Whether the cells transfected by the reverse transfection protocol had a bias towards differentiation to a specific lineage, for example ciliated cells, was not assessed and this will be an important consideration in PCD gene therapy proof-of-principle studies, particularly if any potential bias was against differentiation to a ciliated cell phenotype. However, in these studies, of greater concern was the low transfection efficiency of the DNAH5 transgene. Correction studies of the *DNAH5* knockdown NHBE BMI-1 cells were unsuccessful most likely due to the size of the transgene being delivered, a phenomenon observed in previous studies (395, 447). As the 4µg/mL/5x10^5 cells dose was used in this correction study far fewer MC.DNA5 (shRNA) DNA molecules and so transgene constructs, would have been delivered compared to MC.eGFP DNA which was used to optimise the reverse transfection protocol for DNA transfections. Equimolar amounts of the larger MC.DNAH5 (shRNA) DNA (31.2µg/mL/5x10^5 cells) was not delivered in these studies due to toxicity concerns given the need to then induce mucociliary differentiation. Nevertheless when equimolar amounts of DNA were used in earlier studies in cell lines (Chapter 3.3.3; p144) transfection efficiency was not significantly enhanced as assessed by using the pCI.eGFP.DNAH5 construct.

The principle aim of this chapter was to assess the hypothesis that gene therapy could restore cilia beating in PCD caused by *DNAH5* mutations. Experiments described in this chapter highlight the need to improve expression of large transgenes as delivery of the smaller eGFP transgene was found to be more efficient than the larger DNAH5 coding cDNA. There are several barriers to the process of transfection and it will be important to assess where the bottleneck lies

when transfecting DNAH5 cDNA. One of the first steps in transfection is binding of the gene delivery vector and its uptake into cells. Low uptake of gene delivery vectors will invariably result in inefficient transfection. Cell uptake is determined by the biophysical properties of a gene delivery vector. That zeta potential did not differ when comparing MC.DNAH5 (shRNA) and MC.eGFP containing LPD nanocomplexes suggests that vector binding to the cell surface would have remained constant between the two complexes. Whilst a small but significant difference in particle size was seen when comparing complexes containing the small MC.eGFP DNA with the larger MC.DNAH5 transgene, as both complexes were around 100nm it is likely that both would have utilised the same uptake mechanism- namely clathrin-mediated endocytosis (396). As such poor cell uptake is unlikely to have been the cause of the poor expression of DNAH5 but this hypothesis should be assessed directly by fluorescence labelling of the MC.DNAH5 (shRNA) and MC.eGFP DNA delivered.

Following cell binding gene delivery vectors are taken up into endosomes which then go on to form lysosomes that degrade the contents within. It is vital that gene delivery vectors, or at least the DNA cargo, escapes the endosome prior to this occurring if transgene expression is to be successful. Given that the DOPE liposome within the LPD vector has been shown to aid in endosomal escape (401) and was present in the same quantity when transfecting with MC.eGFP and MC.DNAH5 (shRNA), poor endosomal escape when transfecting MC.DNAH5 (shRNA) is unlikely to be the explanation for poor transgene expression.

Downstream of endosomal escape nuclear entry is vital to allow transgene transcription and subsequent translation in the cytoplasm. The precise mechanisms by which nuclear entry is achieved is unclear but given that cells transfected by the reverse transfection method would have been dividing, even if only briefly, nuclear entry is unlikely to have been a significant barrier. Nevertheless, quantification of transfected DNA in cytoplasmic and nuclear fractions of cells would provide a method for addressing whether poor nuclear entry was involved in the differences in transfection efficiency when comparing MC.eGFP and MC.DNAH5 (shRNA) transfections.

Once inside the nucleus transfected DNA is transcribed and, as discussed, given that vector uptake, endosomal escape and nuclear entry are unlikely to sufficiently explain the poor transgene expression when transfecting MC.DNAH5 (shRNA) DNA, poor transcription of the large transgene may as long transcripts are invariably more prone to early termination. Hyper-phosphorylation of RNA polymerase is known to be important in preventing early transcription termination although the identity of the phosphatases involved remains elusive and the regulation of this mechanism is poorly understood (448). RNA viruses such as HIV-1 (around 9kb RNA genome) utilise cellular transcription factors, including RNA polymerase II, for replication of its RNA genome and employs the trans-activator of transcription (Tat) protein to prevent early termination by hyper-phosphorylation of RNA polymerase II (449, 450). Given the need for HIV-1 to employ the transactivator of transcription (Tat) protein for efficient replication of its 9kb genome by RNA polymerase II it is not inconceivable that early termination of DNAH5 transcription from MC.DNAH5

(shRNA) could be occurring given that no mechanism has been introduced to help prevent this. It will be important to assess if the limiting step in DNAH5 expression following MC.DNAH5 (shRNA) transfection is indeed at the transcription level. If so, studies aimed at elucidating the mechanisms involved in the transcription of *DNAH5* and other large genes, from chromosomal DNA would provide clues on how DNAH5 expression from cDNA could be enhanced.

In conclusion, in this chapter a reverse transfection protocol was optimised for DNA delivery and found to be a more efficient way of obtaining transgene expression in differentiated airway epithelial cells when compared to transfection of well-differentiated ALI cultures. In attempting to correct a PCD disease model generated by shRNA knockdown of *DNAH5* it was found that transfection of the DNAH5 transgene was too inefficient to allow assessment of the hypothesis that gene therapy could be used to restore cilia beating in PCD. In the interests of testing this hypothesis and providing proof-of-principle it is worth pursuing the use of viral vectors capable of delivering large transgenes. Adenovirus could be used in proof-of-principle studies given its large packaging capacity of ~30kb and the fact that it is an established airway gene delivery vector with protocols described for ALI culture transduction (451, 452).

Given the difficulty of transfecting and transducing ciliated cells, the target for PCD gene therapy studies, human RSV should also be considered a potential candidate vector for proof-of-principle studies given its preference towards transducing ciliated cells (453). With a genome of around 15kb the virus could package DNAH5 cDNA. A replication competent RSV vector should also be used in proof-of-principle

studies as this would allow for a 100% transduction efficiency removing poor gene delivery efficiency as a limiting step to determining whether recovery of cilia beating is feasible following gene therapy for PCD caused by *DNAH5* mutations. Of course, a replicating virus vector would not gain approval for clinical use and so would be unsuitable for gene therapy in patients.

Whilst currently inefficient when used to transfect the DNAH5 cDNA *in vitro*, the LPD vector is more suitable for clinical use and shown to be efficient for airway gene transfer of smaller transgenes. As such, efforts should be made to enhance DNAH5 expression using the LPD vector described in this thesis by addressing the issues behind why expression of large transgenes is inefficient.

CHAPTER SEVEN

GENERAL DISCUSSION AND CONCLUSION

7. General Discussion and Conclusion

PCD is a multi-systemic genetic disease resulting from ciliary dyskinesia. Chronic respiratory infections are the major cause of morbidity leading to bronchiectasis and potentially the need for lung transplantation (1). Current treatments are aimed at slowing this deterioration but none addresses the underlying ciliary defects. Gene therapy offers the potential to treat the primary defects in PCD. To date two proof-of-principle studies have been published both focussing on the *DNAI1* gene and both utilising a lentivirus vector (283, 314). However, the most common cause of PCD involves mutations in *DNAH5* (117), a large gene that cannot be packaged into a lentivirus vector. In this thesis advances have been made towards the development of gene therapy for PCD caused by mutations in *DNAH5*.

A non-viral vector previously optimised for respiratory gene delivery (287) was utilised to transfect DNAH5 cDNA, cloned into a mammalian expression vector and both mRNA and protein expression were shown. However, transfection of this large construct was found to be inefficient as assessed by the transfection of a GFP-DNAH5 fusion construct. To maximise the probability of observing gene correction it was important that transgene expression was optimised. To this end, minicircle DNA previously shown to enhance transgene expression in a number of organ systems (309, 311, 312, 404) was shown, for the first time, to enhance transgene expression in the airways. Importantly, expression of the DNAH5 transgene was increased by 50% at the mRNA level in airway epithelial cells. Next, a model in which to assess whether gene therapy could recover cilia beating in PCD patients was developed.

Transduction of cells with the proto-oncogene BMI-1 produced a semi-immortalised cell line capable of extended passaging whilst maintaining its mucociliary differentiation capacity. shRNA knockdown of *DNAH5* in these cells was then used to provide an *in vitro* PCD model that recapitulated most of the phenotypes observed in PCD patients. Finally, correction of this model was attempted utilising a reverse transfection protocol (441) that minimised cell toxicity observed when utilising a standard transfection protocol and also overcame the barriers of transfecting differentiated cells. In attempting to correct this *in vitro* PCD model it was clear that the transfection efficiency of the large DNAH5 cDNA was too low. Transfection efficiency was quantified using the GFP-DNAH5 fusion construct and protein expression was detected in less than 1% of cells. Significant improvements to delivering the large DNAH5 transgene are therefore required to allow assessment of the hypothesis that gene therapy could recover cilia beating in PCD resulting from *DNAH5* mutations.

Whilst recovery of cilia beating following DNAH5 transfection was not shown a number of key advances were made towards the development of a gene therapy treatment for PCD. The finding that minicircle DNA enhances airway gene delivery is novel and has implications for PCD gene therapy and gene therapy of other airway disorders such as CF where plasmid DNA transfections have so far proven inefficient in clinical trials (454). Also, whilst minicircle DNA provided enhanced DNAH5 expression, the enhancement in expression of smaller transgenes, such as eGFP and luciferase, was far greater. The majority of PCD causing genes, including *DNAI1*, the

second most common cause of PCD (122), have short ORFs and so would likely benefit more from minicircle based gene delivery.

To further enhance transgene expression the use of novel mini-intronic plasmids (MIPs) for airway gene delivery should be assessed as these have been found to be superior to minicircle DNA, at least in the liver (455). Also, the use of stronger promoter and enhancer elements, such as the use of CMV and SV40 viral promoters could be used to boost transgene expression (296). A short EF1α promoter with a CMV enhancer was utilised in this thesis due to previous studies showing greater transgene persistence with an EF1α promoter than with the stronger CMV promoter (296, 297), a beneficial feature in a clinical setting and one required with the reverse transfection protocol utilised.

In the context of airway gene delivery non-DNA constituents have been optimised with GL67A lipid found to be one of the most efficient to date (292). The LPD vector system shows similar transfection efficiencies to GL67A (287) but yet was still inefficient when transfecting DNAH5 cDNA. To assess the hypothesis that PCD caused by *DNAH5* mutations could be corrected by gene therapy viral vector systems should be considered, particularly replication competent vectors that would remove transfection efficiency as a limiting factor to addressing the hypothesis. Translating any success to a clinical setting will however prove challenging given that replicating vectors are unlikely to meet the safety criteria required for clinical approval.

With regards to clinical efficacy Ostrowski et al., (283) have shown, using a *Dnaic1* mouse model of PCD, that at least 40% of normal *Dnaic1* mRNA expression is

required to provide normal mucociliary clearance. This represents a significant challenge as to date no vector optimised for airway gene delivery and capable of packaging the large DNAH5 cDNA achieves this level of efficiency with a single dose. Whether repeated administration would provide accumulation of transgene expression and increase the percentage of cells transfected needs to be tested with the LPD vector. This approach may prove fruitful given the low turnover of differentiated airway epithelial cells, at least 6 months in the mouse (456, 457). It would be important to optimise the timing between doses to obtain accumulation of transgene expression but avoid accumulation of toxicity.

A repeated dosing strategy similar to that described above was undertaken in mice (278) and sheep (279) using the GL67A vector to deliver the CFTR transgene and found no accumulation of toxicity when using a dosing regimen of once per week and once per month in mice and sheep respectively. Whilst in mice repeated dosing did produce an accumulation of CFTR expression when transfecting a low dose of DNA (~1.2mg/kg), this was not seen when a medium (~4.8mg/kg) or high dose (~14.4mg/kg) was used (278). In addition, accumulation of CFTR expression was not observed in the sheep (279). In both studies the percentage of cells transfected was not quantified. It is important to note that these studies were undertaken as part of safety assessment of a repeat dosing strategy being investigated in man for CF gene therapy and so the goal was not to optimise transgene expression with the dosing regimen used but rather to show that repeated dosing does not lead to accumulated toxicity and that transgene expression was not diminished following repeated administration.

The development of a semi-immortalised cell line capable of undergoing mucociliary differentiation represents another significant novel development with the potential to impact the broader airway research field. Whilst in this thesis a PCD model was produced by shRNA knockdown of BMI-1 transformed NHBE cells, BMI-1 transduction of HBE cells obtained from patients could potentially be used to produce patient specific cell lines capable of undergoing mucociliary differentiation. In addition to utilising these cell models for gene therapy research they would also allow detailed study of disease mechanisms which would be particularly useful when studying rare genetic defects where the supply of patient tissue is limited. Patient specific models would be superior to models produced by shRNA knockdown as they are mutation specific and so potentially more relevant for study. Such models would allow for mutation specific therapeutics to be assessed, for example the use of small molecule drug screens targeted at common disease causing mutations. The ability to extensively expand BMI-1 transduced cells makes high-throughput drug screening approaches feasible.

Along with HBE cells, nasal brushing samples can also be used in mucociliary differentiation protocols *in vitro* and are less invasive to obtain than bronchial biopsies. Assessment of BMI-1 transduction of nasal brushing samples should be undertaken to see if this less invasive source of patient material could be utilised to generate cell models that could undergo mucociliary differentiation. This will be of particular advantage in the case of PCD where bronchial biopsies are not routinely taken for clinical purposes and obtaining samples for the sole purpose of research is unethical given the invasiveness of the procedure.

Recently the use of Rho-kinase inhibitor along with co-culture of NHBE cells with irradiated fibroblasts has been described to allow indefinite passage of NHBE cells whilst retaining the cells differentiation capacity by removal of the Rho-kinase inhibitor and feeder cells and placing the cells at an ALI (458). Being able to culture these "conditionally reprogrammed cells (CRC)" (458) indefinitely provides an obvious advantage over NHBE BMI-1 cells which senesce at around 25 passages. However, the need for cells to be co-cultured with freshly irradiated feeder cells limits the utility of the CRC approach to facilities equipped with irradiators and researchers with appropriate training and monitoring. With the CRC approach freshly irradiated feeder cells and the Y-27632 Rho-kinase inhibitor also represent recurring costs that are in addition to the media required to maintain NHBE cells. Together these issues impact on the potential for sharing CRC cell lines with different research groups. In contrast, NHBE BMI-1 cells are treated no differently to untransduced NHBE cells with only standard tissue culture techniques employed for cell maintenance. As such, BMI-1 transformed NHBE cells produced by one group can be disseminated to other groups who have standard tissue culture facilities. Only the producer of the BMI-1 transformed cells would require access to facilities allowing the production of lentivirus vectors. The transduction of NHBE cells with BMI-1 therefore represents a simpler and cheaper option for producing cells with an extended growth capacity that retain a mucociliary differentiation potential.

In conclusion a number of advances towards PCD gene therapy have been described in this thesis including the cloning of the DNAH5 cDNA, enhancement of

transgene expression, the development of an *in vitro* PCD model and optimisation of a transfection protocol that provides efficient transfection of NHBE cells and where transgene expression persists until at least after mucociliary differentiation takes place. The technologies developed in this thesis project also have broader applications beyond PCD gene therapy.

8. REFERENCES

1. J. S. Lucas, A. Burgess, H. M. Mitchison, E. Moya, M. Williamson, C. Hogg, (2014). Diagnosis and management of primary ciliary dyskinesia. *Arch. Dis. Child.*, In press.

2. A. K. Siewert, (1904). Ueber einen Fall von Bronchiectasie bei einem Patienten mit Situs inversus viscerum. *Berl. Klin. Wochenschr.* **41**, 139-141.

3. M. Kartagener, (1933). Zur pathogenese der bronchiektasien. I. mitteilung: bronchiektasien bei situs viscerum inversus. *Beitr. Klin. Erforsch. Tuberk. Lungenkr.* **83**, 489-501.

4. B. A. Afzelius, R. Eliasson, O. Johnsen, C. Lindholmer, (1975). Lack of dynein arms in immotile human spermatozoa. *J. Cell Biol.* **66**, 225-232.

5. H. Pedersen, H. Rebbe, (1975). Absence of arms in the axoneme of immobile human spermatozoa. *Biol. Reprod.* **12**, 541-544.

6. P. Camner, B. Mossberg, B. A. Afzelius, (1975). Evidence of congenitally nonfunctioning cilia in the tracheobronchial tract in two subjects. *Am. Rev. Respir. Dis.* **112**, 807-809.

7. B. A. Afzelius, (1976). A human syndrome caused by immotile cilia. *Science* **193**, 317-319.

8. R. Eliasson, B. Mossberg, P. Camner, B. A. Afzelius, (1977). The immotile-cilia syndrome. A congenital ciliary abnormality as an etiologic factor in chronic airway infections and male sterility. *N. Engl. J. Med.* **297**, 1-6.

9. B. A. Afzelius, R. Eliasson, (1979). Flagellar mutants in man: on the heterogeneity of the immotile-cilia syndrome. *J. Ultrastruct. Res.* **69**, 43-52.

10. C. M. Rossman, J. B. Forrest, R. M. K. W. Lee, M. T. Newhouse, (1980). The dyskinetic cilia syndrome. Ciliary motility in immotile cilia syndrome. *Chest* **78**, 580-582.

11. M. Pedersen, N. Mygind, (1980). Ciliary motility in the 'immotile cilia syndrome'. First results of microphoto-oscillographic studies. *Br. J. Dis. Chest* **74**, 239-244.

12. M. A. Sleigh, (1981). Primary ciliary dyskinesia. *Lancet* **2**, 476-476.

13. A. v. Leewenhoeck, (1677). Concerning little animals by him observed in rain-, well-, sea-, and snow-water; as also in water wherein pepper had lain infused. *Philos. Trans. R. Soc. Lond.* **12**, 821-831.

14. K. W. Zimmermann, (1898). Beiträge zur kenntniss einiger drüsen und epithelien. *Archiv f. mikrosk. Anat.* **52**, 552-706.

15. H. A. Praetorius, K. R. Spring, (2001). Bending the MDCK cell primary cilium increases intracellular calcium. *J. Membr. Biol.* **184**, 71-79.

16. G. J. Pazour, J. T. San Agustin, J. A. Follit, J. L. Rosenbaum, G. B. Witman, (2002). Polycystin-2 localizes to kidney cilia and the ciliary level is elevated in orpk mice with polycystic kidney disease. *Curr. Biol.* **12**, R378-R380.

17. R. Rohatgi, L. Milenkovic, M. P. Scott, (2007). Patched1 regulates hedgehog signaling at the primary cilium. *Science* **317**, 372-376.

18. K. C. Corbit, P. Aanstad, V. Singla, A. R. Norman, D. Y. R. Stainier, J. F. Reiter, (2005). Vertebrate Smoothened functions at the primary cilium. *Nature* **437**, 1018-1021.

19. N. S. Murcia, W. G. Richards, B. K. Yoder, M. L. Mucenski, J. R. Dunlap, R. P. Woychik, (2000). The Oak Ridge Polycystic Kidney (orpk) disease gene is required for left-right axis determination. *Development* **127**, 2347-2355.

20. D. Watanabe, Y. Saijoh, S. Nonaka, G. Sasaki, Y. Ikawa, T. Yokoyama *et al.*, (2003). The left-right determinant Inversin is a component of node monocilia and other 9+0 cilia. *Development* **130**, 1725-1734.

21. G. J. Pazour, B. L. Dickert, Y. Vucica, E. S. Seeley, J. L. Rosenbaum, G. B. Witman *et al.*, (2000). Chlamydomonas IFT88 and its mouse homologue, polycystic kidney disease gene Tg737, are required for assembly of cilia and flagella. *J. Cell Biol.* **151**, 709-718.

22. T. Yokoyama, N. G. Copeland, N. A. Jenkins, C. A. Montgomery, F. F. B. Elder, P. A. Overbeek, (1993). Reversal of left-right asymmetry: a situs inversus mutation. *Science* **260**, 679-682.

23. J. H. Moyer, M. J. Leetischler, H. Y. Kwon, J. J. Schrick, E. D. Avner, W. E. Sweeney *et al.*, (1994). Candidate gene associated with a mutation causing recessive polycystic kidney disease in mice. *Science* **264**, 1329-1333.

24. J. C. McIntyre, E. E. Davis, A. Joiner, C. L. Williams, I. C. Tsai, P. M. Jenkins *et al.*, (2012). Gene therapy rescues cilia defects and restores olfactory function in a mammalian ciliopathy model. *Nat. Med.* **18**, 1423-1428.

25. E. A. Otto, B. Schermer, T. Obara, J. F. O'Toole, K. S. Hiller, A. M. Mueller *et al.*, (2003). Mutations in INVS encoding inversin cause nephronophthisis type 2, linking renal cystic disease to the function of primary cilia and left-right axis determination. *Nat. Genet.* **34**, 413-420.

26. F. Hildebrandt, T. Benzing, N. Katsanis, (2011). Ciliopathies. *N. Engl. J. Med.* **364**, 1533-1543.

27. J. L. Tobin, P. L. Beales, (2009). The nonmotile ciliopathies. *Genet. Med.* **11**, 386-402.

28. K. Storm van's Gravesande, H. Omran, (2005). Primary ciliary dyskinesia: clinical presentation, diagnosis and genetics. *Ann. Med.* **37**, 439-449.

29. T. Schertler, D. Lardinois, T. Boehm, W. Weder, S. Wildermuth, H. Alkadhi, (2007). Lung transplantation in Kartagener syndrome and situs inversus: Potential of multidetector row computed tomography and three-dimensional postprocessing. *J. Thorac. Cardiovasc. Surg.* **134**, 814-815.

30. H. Date, M. Yamashita, I. Nagahiro, M. Aoe, A. Andou, N. Shimizu, (2001). Living-donor lobar lung transplantation for primary ciliary dyskinesia. *Ann. Thorac. Surg.* **71**, 2008-2009.

31. B. A. Afzelius, R. Eliasson, (1983). Male and female infertility problems in the immotile-cilia syndrome. *Eur. J. Respir. Dis.* **64**, 144-147.

32. N. C. Munro, D. C. Currie, K. S. Lindsay, T. A. Ryder, A. Rutman, A. Dewar *et al.*, (1994). Fertility in men with primary ciliary dyskinesia presenting with respiratory infection. *Thorax* **49**, 684-687.

33. S. A. Halbert, D. L. Patton, P. W. Zarutskie, M. R. Soules, (1997). Function and structure of cilia in the Fallopian tube of an infertile woman with Kartagener's syndrome. *Hum. Reprod.* **12**, 55-58.

34. A. Fernandez-Gonzalez, S. Kourembanas, T. A. Wyatt, S. A. Mitsialis, (2009). Mutation of murine adenylate kinase 7 underlies a primary ciliary dyskinesia phenotype. *Am. J. Respir. Cell Mol. Biol.* **40**, 305-313.

35. I. Ibanez-Tallon, S. Gorokhova, N. Heintz, (2002). Loss of function of axonemal dynein Mdnah5 causes primary ciliary dyskinesia and hydrocephalus. *Hum. Mol. Genet.* **11**, 715-721.

36. M. M. De Santi, A. Magni, E. A. Valletta, C. Gardi, G. Lungarella, (1990). Hydrocephalus, bronchiectasis, and ciliary aplasia. *Arch. Dis. Child.* **65**, 543-544.

37. M. A. Greenstone, R. W. A. Jones, A. Dewar, B. G. R. Neville, P. J. Cole, (1984). Hydrocephalus and primary ciliary dyskinesia. *Arch. Dis. Child.* **59**, 481-482.

38. I. Ibanez-Tallon, N. Heintz, H. Omran, (2003). To beat or not to beat: roles of cilia in development and disease. *Hum. Mol. Genet.* **12**, 27-35.

39. P. G. Noone, M. W. Leigh, A. Sannuti, S. L. Minnix, J. L. Carson, M. Hazucha *et al.*, (2004). Primary ciliary dyskinesia - diagnostic and phenotypic features. *Am. J. Respir. Crit. Care Med.* **169**, 459-467.

40. M. P. Kennedy, H. Omran, M. W. Leigh, S. Dell, L. Morgan, P. L. Molina *et al.*, (2007). Congenital heart disease and other heterotaxic defects in a large cohort of patients with primary ciliary dyskinesia. *Circulation* **115**, 2814-2821.

41. N. Nakhleh, R. Francis, R. A. Giese, X. Tian, Y. Li, M. A. Zariwala *et al.*, (2012). High prevalence of respiratory ciliary dysfunction in congenital heart disease patients with heterotaxy. *Circulation* **125**, 2232-2242.

42. S. Nonaka, Y. Tanaka, Y. Okada, S. Takeda, A. Harada, Y. Kanai *et al.*, (1998). Randomization of left-right asymmetry due to loss of nodal cilia generating leftward flow of extraembryonic fluid in mice lacking KIF3B motor protein. *Cell* **95**, 829-837.

43. S. Nonaka, H. Shiratori, Y. Saijoh, H. Hamada, (2002). Determination of left-right patterning of the mouse embryo by artificial nodal flow. *Nature* **418**, 96-99.

44. J. H. E. Cartwright, O. Piro, I. Tuval, (2004). Fluid-dynamical basis of the embryonic development of left-right asymmetry in vertebrates. *Proc. Natl. Acad. Sci. U. S. A.* **101**, 7234-7239.

45. C. J. Brokaw, (2005). Computer simulation of flagellar movement IX. Oscillation and symmetry breaking in a model for short flagella and nodal cilia. *Cell Motil. Cytoskelet.* **60**, 35-47.

46. Y. Okada, S. Takeda, Y. Tanaka, J. C. I. Belmonte, N. Hirokawa, (2005). Mechanism of nodal flow: A conserved symmetry breaking event in left-right axis determination. *Cell* **121**, 633-644.

47. S. Nonaka, S. Yoshiba, D. Watanabe, S. Ikeuchi, T. Goto, W. F. Marshall *et al.*, (2005). Hydrodynamic basis of nodal flow: De novo formation of leftright asymmetry in mouse development. *Dev. Biol.* **283**, 624-624.

48. J. L. Rosenbaum, F. M. Child, (1967). Flagellar regeneration in protozoan flagellates. *J. Cell Biol.* **34**, 345-364.

49. M. Fliegauf, T. Benzing, H. Omran, (2007). When cilia go bad: cilia defects and ciliopathies. *Nat. Rev. Mol. Cell Biol.* **8**, 880-893.

50. T. Kobayashi, B. D. Dynlacht, (2011). Regulating the transition from centriole to basal body. *J. Cell Biol.* **193**, 435-444.

51. J. M. Pan, W. Snell, (2007). The primary cilium: keeper of the key to cell division. *Cell* **129**, 1255-1257.

52. L. F. Henneguy, (1898). Sur les rapports des cils vibratiles avec les centrosomes. *Arch. Anat. Microsc.* **1**, 481-496.

53. M. v. Lenhossek, (1898). Ueber flimmerzellen. *Verh. Anat. Ges.* **12**, 106-128.

54. I. R. Gibbons, A. V. Grimstone, (1960). On flagellar structure in certain flagellates. *J. Biophys. Biochem. Cytol.* **7**, 697-716.

55. N. J. Wilsman, C. E. Farnum, (1983). Arrangement of C-tubule protofilaments in mammalian basal bodies. *J. Ultrastruct. Res.* **84**, 205-212.

56. L. B. Pedersen, J. L. Rosenbaum, (2008). Intraflagellar transport (IFT) role in ciliary assembly, resorption and signalling. *Curr. Top. Dev. Biol.* **85**, 23-61.

57. R. G. Anderson, (1972). The three-dimensional structure of the basal body from the rhesus monkey oviduct. *J. Cell Biol.* **54**, 246-265.

58. J. A. Deane, D. G. Cole, E. S. Seeley, D. R. Diener, J. L. Rosenbaum, (2001). Localization of intraflagellar transport protein IFT52 identifies basal body transitional fibers as the docking site for IFT particles. *Curr. Biol.* **11**, 1586-1590.

59. B. Craige, C. C. Tsao, D. R. Diener, Y. Q. Hou, K. F. Lechtreck, J. L. Rosenbaum *et al.*, (2010). CEP290 tethers flagellar transition zone microtubules to the membrane and regulates flagellar protein content. *J. Cell Biol.* **190**, 927-940.

60. F. D. Warner, P. Satir, (1973). The substructure of ciliary microtubules. *J. Cell Sci.* **12**, 313-326.

61. S. Li, J. J. Fernandez, W. F. Marshall, D. A. Agard, (2012). Three-dimensional structure of basal body triplet revealed by electron cryo-tomography. *EMBO J.* **31**, 552-562.

62. R. W. Linck, G. E. Olson, G. L. Langevin, (1981). Arrangement of tubulin subunits and microtubule-associated proteins in the central-pair microtubule apparatus of squid (Loligo pealei) sperm flagella. *J. Cell Biol.* **89**, 309-322.

63. K. Sulik, D. B. Dehart, T. Inagaki, J. L. Carson, T. Vrablic, K. Gesteland *et al.*, (1994). Morphogenesis of the murine node and notochordal plate. *Dev. Dyn.* **201**, 260-278.

64. T. Kikuchi, T. Takasaka, A. Tonosaki, H. Watanabe, (1989). Fine structure of guinea pig vestibular kinocilium. *Acta Otolaryngol. (Stockh.)* **108**, 26-30.

65. R. A. Bloodgood, (2010). Sensory reception is an attribute of both primary cilia and motile cilia. *J. Cell Sci.* **123**, 505-509.

66. I. M. Lorenzo, W. Liedtke, M. J. Sanderson, M. A. Valverde, (2008). TRPV4 channel participates in receptor-operated calcium entry and ciliary beat frequency regulation in mouse airway epithelial cells. *Proc. Natl. Acad. Sci. U. S. A.* **105**, 12611-12616.

67. A. S. Shah, Y. Ben-Shahar, T. O. Moninger, J. N. Kline, M. J. Welsh, (2009). Motile cilia of human airway epithelia are chemosensory. *Science* **325**, 1131-1134.

68. I. R. Gibbons, A. J. Rowe, (1965). Dynein: a protein with adenosine triphosphatase activity from cilia. *Science* **149**, 424-426.

69. K. K. Pfister, G. B. Witman, (1984). Subfractionation of Chlamydomonas 18 S dynein into two unique subunits containing ATPase activity. *J. Biol. Chem.* **259**, 2072-2080.

70. K. E. Summers, I. R. Gibbons, (1971). Adenosine triphosphate-induced sliding of tubules in trypsin-treated flagella of sea-urchin sperm. *Proc. Natl. Acad. Sci. U. S. A.* **68**, 3092-3096.

71. G. B. Witman, J. Plummer, G. Sander, (1978). Chlamydomonas flagellar mutants lacking radial spokes and central tubules. Structure, composition, and function of specific axonemal components. *J. Cell Biol.* **76**, 729-747.

72. M. A. Chilvers, A. Rutman, C. O'Callaghan, (2003). Ciliary beat pattern is associated with specific ultrastructural defects in primary ciliary dyskinesia. *J. Allergy Clin. Immunol.* **112**, 518-524.

73. M. E. Fowkes, D. R. Mitchell, (1998). The role of preassembled cytoplasmic complexes in assembly of flagellar dynein subunits. *Mol. Biol. Cell* **9**, 2337-2347.

74. H. M. Qin, D. R. Diener, S. Geimer, D. G. Cole, J. L. Rosenbaum, (2004). Intraflagellar transport (IFT) cargo: IFT transports flagellar precursors to the tip and turnover products to the cell body. *J. Cell Biol.* **164**, 255-266.

75. M. W. Brightman, S. L. Palay, (1963). The fine structure of ependyma in the brain of the rat. *J. Cell Biol.* **19**, 415-439.

76. T. S. Reese, (1965). Olfactory cilia in the frog. *J. Cell Biol.* **25**, 209-230.

77. L. E. Roth, Y. Shigenaka, (1964). The structure and formation of cilia and filaments in rumen protozoa. *J. Cell Biol.* **20**, 249-270.

78. E. Gluenz, J. L. Hoog, A. E. Smith, H. R. Dawe, M. K. Shaw, K. Gull, (2010). Beyond 9+0: noncanonical axoneme structures characterize sensory cilia from protists to humans. *FASEB J.* **24**, 3117-3121.

79. C. Fisch, P. Dupuis-Williams, (2011). Ultrastructure of cilia and flagella - back to the future! *Biol. Cell* **103**, 249-270.

80. E. R. Dirksen, P. Satir, (1972). Ciliary activity in the mouse oviduct as studied by transmission and scanning electron microscopy. *Tissue Cell* **4**, 389-403.

81. C. Kuhn III, W. Engleman, (1978). The structure of the tips of mammalian respiratory cilia. *Cell Tissue Res.* **186**, 491-498.

82. R. G. Anderson, C. E. Hein, (1977). Distribution of anionic sites on the oviduct ciliary membrane. *J. Cell Biol.* **72**, 482-492.

83. J. H. Luft, (1971). Ruthenium red and violet. II. Fine structural localization in animal tissues. *Anat. Rec.* **171**, 369-415.

84. H. Dalen, (1983). An ultrastructural study of the tracheal epithelium of the guinea-pig with special reference to the ciliary structure. *J. Anat.* **136**, 47-67.

85. X. Lam, C. Gieseke, M. Knoll, P. Talbot, (2000). Assay and importance of adhesive interaction between hamster (Mesocricetus auratus) oocyte-cumulus complexes and the oviductal epithelium. *Biol. Reprod.* **62**, 579-588.

86. J. T. Norwood, C. E. Hein, S. A. Halbert, R. G. Anderson, (1978). Polycationic macromolecules inhibit cilia-mediated ovum transport in the rabbit oviduct. *Proc. Natl. Acad. Sci. U. S. A.* **75**, 4413-4416.

87. B. Foliguet, E. Puchelle, (1986). Apical structure of human respiratory cilia. *Bull. Eur. Physiopathol. Respir.* **22**, 43-47.

88. M. W. Leigh, J. E. Pittman, J. L. Carson, T. W. Ferkol, S. D. Dell, S. D. Davis *et al.*, (2009). Clinical and genetic aspects of primary ciliary dyskinesia/Kartagener syndrome. *Genet. Med.* **11**, 473-487.

89. E. Escudier, P. Duquesnoy, J. F. Papon, S. Amselem, (2009). Ciliary defects and genetics of primary ciliary dyskinesia. *Paediatr. Respir. Rev.* **10**, 51-54.

90. M. R. Knowles, M. W. Leigh, J. L. Carson, S. D. Davis, S. D. Dell, T. W. Ferkol *et al.*, (2012). Mutations of DNAH11 in patients with primary ciliary dyskinesia with normal ciliary ultrastructure. *Thorax* **67**, 433-441.

91. G. C. Schwabe, K. Hoffmann, N. T. Loges, D. Birker, C. Rossier, M. M. De Santi *et al.*, (2008). Primary ciliary dyskinesia associated with normal axoneme ultrastructure is caused by DNAH11 mutations. *Hum. Mutat.* **29**, 289-298.

92. M. Pifferi, A. Michelucci, M. E. Conidi, A. M. Cangiotti, P. Simi, P. Macchia *et al.*, (2010). New DNAH11 mutations in primary ciliary dyskinesia with normal axonemal ultrastructure. *Eur. Respir. J.* **35**, 1413-1416.

93. J. S. Lucas, E. C. Adam, P. M. Goggin, C. L. Jackson, N. Powles-Glover, S. H. Patel *et al.*, (2012). Static respiratory cilia associated with mutations in Dnahc11/DNAH11: A mouse model of PCD. *Hum. Mutat.* **33**, 495-503.

94. M. Zariwala, M. Leigh, M. Hazucha, S. Minnix, M. Armstrong, A. Lori *et al.*, (2009). DNAH11 mutations are a common cause of primary ciliary dyskinesia

(PCD) in patients with normal ciliary dynein arms. *Am. J. Respir. Crit. Care Med.* **179**, 433-441.

95. A. Iannaccone, D. K. Breuer, X. F. Wang, S. F. Kuo, E. M. Normando, E. Filippova *et al.*, (2003). Clinical and immunohistochemical evidence for an X linked retinitis pigmentosa syndrome with recurrent infections and hearing loss in association with an RPGR mutation. *J. Med. Genet.* **40**, e118.

96. A. Moore, E. Escudier, G. Roger, A. Tamalet, B. Pelosse, S. Marlin *et al.*, (2006). RPGR is mutated in patients with a complex X linked phenotype combining primary ciliary dyskinesia and retinitis pigmentosa. *J. Med. Genet.* **43**, 326-333.

97. I. Zito, S. M. Downes, R. J. Patel, M. E. Cheetham, N. D. Ebenezer, S. A. Jenkins *et al.*, (2003). RPGR mutation associated with retinitis pigmentosa, impaired hearing, and sinorespiratory infections. *J. Med. Genet.* **40**, 609-615.

98. J. Milara, M. Armengot, M. Mata, E. J. Morcillo, J. Cortijo, (2010). Role of adenylate kinase type 7 expression on cilia motility: possible link in primary ciliary dyskinesia. *Am. J. Rhinol. Allergy* **24**, 181-185.

99. M. Mata, J. Lluch-Estelles, M. Armengot, I. Sarrion, C. Carda, J. Cortijo, (2012). New adenylate kinase 7 (AK7) mutation in primary ciliary dyskinesia. *Am. J. Rhinol. Allergy* **26**, 260-264.

100. R. Hjeij, A. Lindstrand, R. Francis, M. A. Zariwala, X. Liu, Y. Li *et al.*, (2013). ARMC4 mutations cause primary ciliary dyskinesia with randomization of left/right body asymmetry. *Am. J. Hum. Genet.* **93**, 357-367.

101. A. Onoufriadis, A. Shoemark, M. M. Munye, C. T. James, M. Schmidts, M. Patel *et al.*, (2014). Combined exome and whole-genome sequencing identifies mutations in ARMC4 as a cause of primary ciliary dyskinesia with defects in the outer dynein arm. *J. Med. Genet.* **51**, 61-67.

102. C. Austin-Tse, J. Halbritter, M. A. Zariwala, R. M. Gilberti, H. Y. Gee, N. Hellman *et al.*, (2013). Zebrafish ciliopathy screen plus human mutational analysis identifies C21orf59 and CCDC65 defects as causing primary ciliary dyskinesia. *Am. J. Hum. Genet.* **93**, 672-686.

103. J. R. Panizzi, A. Becker-Heck, V. H. Castleman, D. A. Al-Mutairi, Y. Liu, N. T. Loges *et al.*, (2012). CCDC103 mutations cause primary ciliary dyskinesia by disrupting assembly of ciliary dynein arms. *Nat. Genet.* **44**, 714-719.

104. M. R. Knowles, M. W. Leigh, L. E. Ostrowski, L. Huang, J. L. Carson, M. J. Hazucha *et al.*, (2013). Exome sequencing identifies mutations in CCDC114 as a cause of primary ciliary dyskinesia. *Am. J. Hum. Genet.* **92**, 99-106.

105. A. Onoufriadis, T. Paff, D. Antony, A. Shoemark, D. Micha, B. Kuyt *et al.*, (2013). Splice-site mutations in the axonemal outer dynein arm docking

complex gene CCDC114 cause primary ciliary dyskinesia. *Am. J. Hum. Genet.* **92**, 88-98.

106. D. H. Wu, R. R. Singaraja, (2013). Loss-of-function mutations in CCDC114 cause primary ciliary dyskinesia. *Clin. Genet.* **83**, 526-527.

107. M. Wirschell, H. Olbrich, C. Werner, D. Tritschler, R. Bower, W. S. Sale *et al.*, (2013). The nexin-dynein regulatory complex subunit DRC1 is essential for motile cilia function in algae and humans. *Nat. Genet.* **45**, 262-268.

108. A. C. Merveille, E. E. Davis, A. Becker-Heck, M. Legendre, I. Amirav, G. Bataille *et al.*, (2011). CCDC39 is required for assembly of inner dynein arms and the dynein regulatory complex and for normal ciliary motility in humans and dogs. *Nat. Genet.* **43**, 72-78.

109. S. Blanchon, M. Legendre, B. Copin, P. Duquesnoy, G. Montantin, E. Kott *et al.*, (2012). Delineation of CCDC39/CCDC40 mutation spectrum and associated phenotypes in primary ciliary dyskinesia. *J. Med. Genet.* **49**, 410-416.

110. A. Becker-Heck, I. E. Zohn, N. Okabe, A. Pollock, K. B. Lenhart, J. Sullivan-Brown *et al.*, (2011). The coiled-coil domain containing protein CCDC40 is essential for motile cilia function and left-right axis formation. *Nat. Genet.* **43**, 79-84.

111. P. Duquesnoy, E. Escudier, L. Vincensini, J. Freshour, A. M. Bridoux, A. Coste *et al.*, (2009). Loss-of-function mutations in the human ortholog of Chlamydomonas reinhardtii ODA7 disrupt dynein arm assembly and cause primary ciliary dyskinesia. *Am. J. Hum. Genet.* **85**, 890-896.

112. H. Omran, D. Kobayashi, H. Olbrich, T. Tsukahara, N. T. Loges, H. Hagiwara *et al.*, (2008). Ktu/PF13 is required for cytoplasmic pre-assembly of axonemal dyneins. *Nature* **456**, 611-616.

113. H. M. Mitchison, M. Schmidts, N. T. Loges, J. Freshour, A. Dritsoula, R. A. Hirst *et al.*, (2012). Mutations in axonemal dynein assembly factor DNAAF3 cause primary ciliary dyskinesia. *Nat. Genet.* **44**, 381-386.

114. L. Bartoloni, J. L. Blouin, Y. Z. Pan, C. Gehrig, A. K. Maiti, N. Scamuffa *et al.*, (2002). Mutations in the DNAH11 (axonemal heavy chain dynein type 11) gene cause one form of situs inversus totalis and most likely primary ciliary dyskinesia. *Proc. Natl. Acad. Sci. U. S. A.* **99**, 10282-10286.

115. H. Omran, K. Haffner, A. Volkel, J. Kuehr, U. P. Ketelsen, U. H. Ross *et al.*, (2000). Homozygosity mapping of a gene locus for primary ciliary dyskinesia on chromosome 5p and identification of the heavy dynein chain DNAH5 as a candidate gene. *Am. J. Respir. Cell Mol. Biol.* **23**, 696-702.

116. H. Olbrich, K. Haffner, A. Kispert, A. Volkel, A. Volz, G. Sasmaz *et al.*, (2002). Mutations in DNAH5 cause primary ciliary dyskinesia and randomization of left-right and asymmetry. *Nat. Genet.* **30**, 143-144.

117. M. Failly, L. Bartoloni, A. Letourneau, A. Munoz, E. Falconnet, C. Rossier *et al.*, (2009). Mutations in DNAH5 account for only 15% of a non-preselected cohort of patients with primary ciliary dyskinesia. *J. Med. Genet.* **46**, 281-286.

118. N. Hornef, H. Olbrich, J. Horvath, M. A. Zariwala, M. Fliegauf, N. T. Loges *et al.*, (2006). DNAH5 mutations are a common cause of primary ciliary dyskinesia with outer dynein arm defects. *Am. J. Respir. Crit. Care Med.* **174**, 120-126.

119. M. A. Zariwala, M. W. Leigh, F. Ceppa, M. P. Kennedy, P. G. Noone, J. L. Carson *et al.*, (2006). Mutations of DNAI1 in primary ciliary dyskinesia: evidence of founder effect in a common mutation. *Am. J. Respir. Crit. Care Med.* **174**, 858-866.

120. G. Pennarun, E. Escudier, C. Chapelin, A. M. Bridoux, V. Cacheux, G. Roger *et al.*, (1999). Loss-of-function mutations in a human gene related to Chlamydomonas reinhardtii dynein IC78 result in primary ciliary dyskinesia. *Am. J. Hum. Genet.* **65**, 1508-1519.

121. C. Guichard, M. C. Harricane, J. J. Lafitte, P. Godard, M. Zaegel, V. Tack *et al.*, (2001). Axonemal dynein intermediate-chain gene (DNAI1) mutations result in situs inversus and primary ciliary dyskinesia (Kartagener syndrome). *Am. J. Hum. Genet.* **68**, 1030-1035.

122. M. Failly, A. Saitta, A. Munoz, E. Falconnet, C. Rossier, F. Santamaria *et al.*, (2008). DNAI1 mutations explain only 2% of primary ciliary dykinesia. *Respiration* **76**, 198-204.

123. N. T. Loges, H. Olbrich, L. Fenske, H. Mussaffi, J. Horvath, M. Fliegauf *et al.*, (2008). DNAI2 mutations cause primary ciliary dyskinesia with defects in the outer dynein arm. *Am. J. Hum. Genet.* **83**, 547-558.

124. M. Mazor, S. Alkrinawi, V. Chalifa-Caspi, E. Manor, V. C. Sheffield, M. Aviram *et al.*, (2011). Primary ciliary dyskinesia caused by homozygous mutation in DNAL1, encoding dynein light chain 1. *Am. J. Hum. Genet.* **88**, 599-607.

125. A. Horani, T. E. Druley, M. A. Zariwala, A. C. Pate, B. T. Levinson, L. G. Van Arendonk *et al.*, (2012). Whole-exome capture and sequencing identifies HEATR2 mutation as a cause of primary ciliary dyskinesia. *Am. J. Hum. Genet.* **91**, 685-693.

126. K. F. Lechtreck, G. B. Witman, (2007). Chlamydomonas reinhardtii hydin is a central pair protein required for flagellar motility. *J. Cell Biol.* **176**, 473-482.

127. H. Olbrich, M. Schmidts, C. Werner, A. Onoufriadis, N. T. Loges, J. Raidt *et al.*, (2012). Recessive HYDIN mutations cause primary ciliary dyskinesia without randomization of left-right body asymmetry. *Am. J. Hum. Genet.* **91**, 672-684.

128. E. Kott, P. Duquesnoy, B. Copin, M. Legendre, F. Dastot-Le Moal, G. Montantin *et al.*, (2012). Loss-of-function mutations in LRRC6, a gene essential for proper axonemal assembly of inner and outer dynein arms, cause primary ciliary dyskinesia. *Am. J. Hum. Genet.* **91**, 958-964.

129. A. Horani, T. W. Ferkol, D. Shoseyov, M. G. Wasserman, Y. S. Oren, B. Kerem *et al.*, (2013). LRRC6 mutation causes primary ciliary dyskinesia with dynein arm defects. *PLoS ONE* **8**, e59436.

130. B. Budny, W. Chen, H. Omran, M. Fliegauf, A. Tzschach, M. Wisniewska *et al.*, (2006). A novel X-linked recessive mental retardation syndrome comprising macrocephaly and ciliary dysfunction is allelic to oral-facial-digital type I syndrome. *Hum. Genet.* **120**, 171-178.

131. M. R. Knowles, L. E. Ostrowski, M. W. Leigh, P. R. Sears, S. D. Davis, W. E. Wolf *et al.*, (2014). Mutations in RSPH1 cause primary ciliary dyskinesia with a unique clinical and ciliary phenotype. *Am. J. Respir. Crit. Care Med.* **189**, 707-717.

132. E. Kott, M. Legendre, B. Copin, J. F. Papon, F. D. L. Moal, G. Montantin *et al.*, (2013). Loss-of-function mutations in RSPH1 cause primary ciliary dyskinesia with central-complex and radial-spoke defects. *Am. J. Hum. Genet.* **93**, 561-570.

133. A. Onoufriadis, A. Shoemark, M. Schmidts, M. Patel, G. Jimenez, H. Liu *et al.*, (2014). Targeted NGS gene panel identifies mutations in RSPH1 causing primary ciliary dyskinesia and a common mechanism for ciliary central pair agenesis due to radial spoke defects. *Hum. Mol. Genet.*, In press.

134. V. H. Castleman, L. Romio, R. Chodhari, R. A. Hirst, S. C. P. de Castro, K. A. Parker *et al.*, (2009). Mutations in radial spoke head protein genes RSPH9 and RSPH4A cause primary ciliary dyskinesia with central-microtubular-pair abnormalities. *Am. J. Hum. Genet.* **84**, 197-209.

135. E. Zietkiewicz, Z. Bukowy-Bieryllo, K. Voelkel, B. Klimek, H. Dmenska, A. Pogorzelski *et al.*, (2012). Mutations in radial spoke head genes and ultrastructural cilia defects in east-european cohort of primary ciliary dyskinesia patients. *PLoS ONE* **7**, e33667.

136. M. L. Daniels, M. W. Leigh, S. D. Davis, M. C. Armstrong, J. L. Carson, M. Hazucha *et al.*, (2013). Founder mutation in RSPH4A identified in patients of Hispanic descent with primary ciliary dyskinesia. *Hum. Mutat.* **34**, 1352-1356.

137. O. Reish, M. Slatkin, D. Chapman-Shimshoni, A. Elizur, B. Chioza, V. Castleman *et al.*, (2010). Founder mutation(s) in the RSPH9 gene leading to primary ciliary dyskinesia in two inbred bedouin families. *Ann. Hum. Genet.* **74**, 117-125.

138. B. Duriez, P. Duquesnoy, E. Escudier, A. M. Bridoux, D. Escalier, I. Rayet *et al.*, (2007). A common variant in combination with a nonsense mutation in a member of the thioredoxin family causes primary ciliary dyskinesia. *Proc. Natl. Acad. Sci. U. S. A.* **104**, 3336-3341.

139. D. J. Moore, A. Onoufriadis, A. Shoemark, M. A. Simpson, P. I. zur Lage, S. C. de Castro *et al.*, (2013). Mutations in ZMYND10, a gene essential for proper axonemal assembly of inner and outer dynein arms in humans and flies, cause primary ciliary dyskinesia. *Am. J. Hum. Genet.* **93**, 346-356.

140. M. A. Zariwala, H. Y. Gee, M. Kurkowiak, D. A. Al-Mutairi, M. W. Leigh, T. W. Hurd *et al.*, (2013). ZMYND10 is mutated in primary ciliary dyskinesia and interacts with LRRC6. *Am. J. Hum. Genet.* **93**, 336-345.

141. A. Kispert, M. Petry, H. Olbrich, A. Volz, U. P. Ketelsen, J. Horvath *et al.*, (2003). Genotype-phenotype correlations in PCD patients carrying DNAH5 mutations. *Thorax* **58**, 552-554.

142. A. Ellerman, H. Bisgaard, (1997). Longitudinal study of lung function in a cohort of primary ciliary dyskinesia. *Eur. Respir. J.* **10**, 2376-2379.

143. J. S. Lucas, P. Chetcuti, F. Copeland, C. Hogg, T. Kenny, E. Moya *et al.*, (2013). Overcoming challenges in the management of primary ciliary dyskinesia: The UK model. *Paediatr. Respir. Rev.*, In press.

144. C. E. Kuehni, T. Frischer, M. P. Strippoli, E. Maurer, A. Bush, K. G. Nielsen *et al.*, (2010). Factors influencing age at diagnosis of primary ciliary dyskinesia in European children. *Eur. Respir. J.* **36**, 1248-1258.

145. F. Griffith, (1928). The significance of pneumococcal types. *J. Hyg. (Lond.)* **27**, 113-159.

146. J. L. Alloway, (1932). The transformation in vitro of R pneumococci into S forms of different specific types by the use of filtered pneumococcus extracts. *J. Exp. Med.* **55**, 91-99.

147. O. T. Avery, C. M. MacLeod, M. McCarty, (1944). Studies on the chemical nature of the substance inducing transformation of pneumococcal types. Induction of transformation by a desoxyribonucleic acid fraction isolated from Pneumococcus type III. *J. Exp. Med.* **79**, 137-158.

148. A. D. Hershey, M. Chase, (1952). Independent functions of viral protein and nucleic acid in growth of bacteriophage. *J. Gen. Physiol.* **36**, 39-56.

149. E. R. Kay, (1961). Incorporation of deoxyribonucleic acid by mammalian cells in vitro. *Nature* **191**, 387-388.

150. E. H. Szybalska, W. Szybalski, (1962). Genetics of human cess line. IV. DNA-mediated heritable transformation of a biochemical trait. *Proc. Natl. Acad. Sci. U. S. A.* **48**, 2026-2034.

151. S. Rogers, Lowentha.A, Terhegge.Hg, J. P. Columbo, (1973). Induction of arginase activity with the Shope papilloma virus in tissue culture cells from an argininemic patient. *J. Exp. Med.* **137**, 1091-1096.

152. H. G. Terheggen, A. Lowenthal, F. Lavinha, J. P. Colombo, S. Rogers, (1975). Unsuccessful trial of gene replacement in arginase deficiency. *Z. Kinderheilkd.* **119**, 1-3.

153. M. Gellert, (1967). Formation of covalent circles of lambda DNA by E. coli extracts. *Proc. Natl. Acad. Sci. U. S. A.* **57**, 148-155.

154. S. B. Zimmerman, J. W. Little, C. K. Oshinsky, M. Gellert, (1967). Enzymatic joining of DNA strands: a novel reaction of diphosphopyridine nucleotide. *Proc. Natl. Acad. Sci. U. S. A.* **57**, 1841-1848.

155. S. E. Luria, M. L. Human, (1952). A nonhereditary, host-induced variation of bacterial viruses. *J. Bacteriol.* **64**, 557-569.

156. G. Bertani, J. J. Weigle, (1953). Host controlled variation in bacterial viruses. *J. Bacteriol.* **65**, 113-121.

157. W. Arber, D. Dussoix, (1962). Host specificity of DNA produced by Escherichia coli. I. Host controlled modification of bacteriophage lambda. *J. Mol. Biol.* **5**, 18-36.

158. D. Dussoix, W. Arber, (1962). Host specificity of DNA produced by Escherichia coli. II. Control over acceptance of DNA from infecting phage lambda. *J. Mol. Biol.* **5**, 37-49.

159. S. Linn, W. Arber, (1968). Host specificity of DNA produced by Escherichia coli, X. In vitro restriction of phage fd replicative form. *Proc. Natl. Acad. Sci. U. S. A.* **59**, 1300-1306.

160. S. N. Cohen, A. C. Y. Chang, (1973). Recircularization and autonomous replication of a sheared R-factor DNA segment in Escherichia coli transformants. *Proc. Natl. Acad. Sci. U. S. A.* **70**, 1293-1297.

161. T. Maniatis, R. C. Hardison, E. Lacy, J. Lauer, C. Oconnell, D. Quon *et al.*, (1978). The isolation of structural genes from libraries of eucaryotic DNA. *Cell* **15**, 687-701.

162. J. T. Wilson, B. G. Forget, L. B. Wilson, S. M. Weissman, (1977). Human globin messenger RNA: importance of cloning for structural analysis. *Science* **196**, 200-202.

163. J. T. Wilson, L. B. Wilson, J. K. Deriel, L. Villakomaroff, A. Efstratiadis, B. G. Forget *et al.*, (1978). Insertion of synthetic copies of human globin genes into bacterial plasmids. *Nucleic Acids Res.* **5**, 563-581.

164. M. R. Green, R. Treisman, T. Maniatis, (1983). Transcriptional activation of cloned human beta-globin genes by viral immediate-early gene products. *Cell* **35**, 137-148.

165. M. J. Cline, H. Stang, K. Mercola, L. Morse, R. Ruprecht, J. Browne *et al.*, (1980). Gene transfer in intact animals. *Nature* **284**, 422-425.

166. E. Beatler, (2001). The cline affair. *Mol. Ther.* **4**, 396-397.

167. A. C. Nathwani, A. M. Davidoff, D. C. Linch, (2005). A review of gene therapy for haematological disorders. *Br. J. Haematol.* **128**, 3-17.

168. S. P. Goff, P. Berg, (1976). Construction of hybrid viruses containing SV40 and lambda phage DNA segments and their propagation in cultured monkey cells. *Cell* **9**, 695-705.

169. R. C. Mulligan, B. H. Howard, P. Berg, (1979). Synthesis of rabbit beta-globin in cultured monkey kidney cells following infection with a SV40 beta-globin recombinant genome. *Nature* **277**, 108-114.

170. K. Shimotohno, H. M. Temin, (1981). Formation of infectious progeny virus after insertion of herpes simplex thymidine kinase gene into DNA of an avian retrovirus. *Cell* **26**, 67-77.

171. K. Vandoren, D. Hanahan, Y. Gluzman, (1984). Infection of eucaryotic cells by helper-independent recombinant adenoviruses: early region 1 is not obligatory for integration of viral DNA. *J. Virol.* **50**, 606-614.

172. P. L. Hermonat, N. Muzyczka, (1984). Use of adeno-associated virus as a mammalian DNA cloning vector: transduction of neomycin resistance into mammalian tissue culture cells. *Proc. Natl. Acad. Sci. U. S. A.* **81**, 6466-6470.

173. R. Mann, R. C. Mulligan, D. Baltimore, (1983). Construction of a retrovirus packaging mutant and its use to produce helper-free defective retrovirus. *Cell* **33**, 153-159.

174. L. Naldini, U. Blomer, P. Gallay, D. Ory, R. Mulligan, F. H. Gage *et al.*, (1996). In vivo gene delivery and stable transduction of nondividing cells by a lentiviral vector. *Science* **272**, 263-267.

175. K. A. Page, N. R. Landau, D. R. Littman, (1990). Construction and use of a human immunodeficiency virus vector for analysis of virus infectivity. *J. Virol.* **64**, 5270-5276.

176. S. M. Cashman, D. J. Morris, R. Kumar-Singh, (2004). Adenovirus type 5 pseudotyped with adenovirus type 37 fiber uses sialic acid as a cellular receptor. *Virology* **324**, 129-139.

177. M. Fechheimer, J. F. Boylan, S. Parker, J. E. Sisken, G. L. Patel, S. G. Zimmer, (1987). Transfection of mammalian cells with plasmid DNA by scrape loading and sonication loading. *Proc. Natl. Acad. Sci. U. S. A.* **84**, 8463-8467.

178. E. Neumann, M. Schaeferridder, Y. Wang, P. H. Hofschneider, (1982). Gene transfer into mouse lyoma cells by electroporation in high electric fields. *EMBO J.* **1**, 841-845.

179. M. R. Capecchi, (1980). High efficiency transformation by direct microinjection of DNA into cultured mammalian cells. *Cell* **22**, 479-488.

180. T. M. Klein, E. D. Wolf, R. Wu, J. C. Sanford, (1987). High-velocity microprojectiles for delivering nucleic acids into living cells. *Nature* **327**, 70-73.

181. V. Budker, G. Zhang, I. Danko, P. Williams, J. Wolff, (1998). The efficient expression of intravascularly delivered DNA in rat muscle. *Gene Ther.* **5**, 272-276.

182. G. F. Zhang, V. Budker, J. A. Wolff, (1999). High levels of foreign gene expression in hepatocytes after tail vein injections of naked plasmid DNA. *Hum. Gene Ther.* **10**, 1735-1737.

183. F. Liu, Y. K. Song, D. Liu, (1999). Hydrodynamics-based transfection in animals by systemic administration of plasmid DNA. *Gene Ther.* **6**, 1258-1266.

184. F. L. Graham, A. J. Vandereb, (1973). A new technique for the assay of infectivity of human adenovirus 5 DNA. *Virology* **52**, 456-467.

185. Mccutcha.Jh, J. S. Pagano, (1968). Enchancement of the infectivity of simian virus 40 deoxyribonucleic acid with diethylaminoethyl-dextran. *J. Natl. Cancer Inst.* **41**, 351-357.

186. O. Boussif, F. Lezoualch, M. A. Zanta, M. D. Mergny, D. Scherman, B. Demeneix *et al.*, (1995). A versatile vector for gene and oligonucleotide transfer into cells in culture and in vivo: polyethylenimine. *Proc. Natl. Acad. Sci. U. S. A.* **92**, 7297-7301.

187. J. P. Behr, (1997). The proton sponge: a trick to enter cells the viruses did not exploit. *Chimia* **51**, 34-36.

188. R. Fraley, S. Subramani, P. Berg, D. Papahadjopoulos, (1980). Introduction of liposome-encapsulated SV40 DNA into cells. *J. Biol. Chem.* **255**, 431-435.

189. T. K. Wong, C. Nicolau, P. H. Hofschneider, (1980). Appearance of beta-lactamase activity in animal cells upon liposome-mediated gene transfer. *Gene* **10**, 87-94.

190. M. Schaeferridder, Y. Wang, P. H. Hofschneider, (1982). Liposomes as gene carriers: efficient transformation of mouse L cells by thymidine kinase gene. *Science* **215**, 166-168.

191. P. L. Felgner, T. R. Gadek, M. Holm, R. Roman, H. W. Chan, M. Wenz *et al.*, (1987). Lipofection: a highly efficient, lipid-mediated DNA-transfection procedure. *Proc. Natl. Acad. Sci. U. S. A.* **84**, 7413-7417.

192. X. Gao, L. Huang, (1996). Potentiation of cationic liposome-mediated gene delivery by polycations. *Biochemistry* **35**, 1027-1036.

193. A. L. Klibanov, K. Maruyama, V. P. Torchilin, L. Huang, (1990). Amphipathic polyethyleneglycols effectively prolong the circulation time of liposomes. *FEBS Lett.* **268**, 235-237.

194. S. L. Hart, L. Collins, K. Gustafsson, J. W. Fabre, (1997). Integrin-mediated transfection with peptides containing arginine-glycine-aspartic acid domains. *Gene Ther.* **4**, 1225-1230.

195. A. S. Manjappa, K. R. Chaudhari, M. P. Venkataraju, P. Dantuluri, B. Nanda, C. Sidda *et al.*, (2011). Antibody derivatization and conjugation strategies: Application in preparation of stealth immunoliposome to target chemotherapeutics to tumor. *J. Control. Release* **150**, 2-22.

196. I. Wrobel, D. Collins, (1995). Fusion of cationic liposomes with mammalian cells occurs after endocytosis. *Biochim. Biophys. Acta* **1235**, 296-304.

197. S. W. Hui, M. Langner, Y. L. Zhao, P. Ross, E. Hurley, K. Chan, (1996). The role of helper lipids in cationic liposome-mediated gene transfer. *Biophys. J.* **71**, 590-599.

198. D. A. Dean, B. S. Dean, S. Muller, L. C. Smith, (1999). Sequence requirements for plasmid nuclear import. *Exp. Cell Res.* **253**, 713-722.

199. D. A. Dean, (1997). Import of plasmid DNA into the nucleus is sequence specific. *Exp. Cell Res.* **230**, 293-302.

200. P. Collas, P. Alestrom, (1997). Rapid targeting of plasmid DNA to zebrafish embryo nuclei by the nuclear localization signal of SV40 T antigen. *Mol. Mar. Biol. Biotechnol.* **6**, 48-58.

201. A. I. Aronsohn, J. A. Hughes, (1998). Nuclear localization signal peptides enhance cationic liposome-mediated gene therapy. *J. Drug Target.* **5**, 163-169.

202. A. Subramanian, P. Ranganathan, S. L. Diamond, (1999). Nuclear targeting peptide scaffolds for lipofection of nondividing mammalian cells. *Nat. Biotechnol.* **17**, 873-877.

203. R. M. Blaese, K. W. Culver, A. D. Miller, C. S. Carter, T. Fleisher, M. Clerici *et al.*, (1995). T Lymphocyte Directed Gene Therapy for ADA$^-$ SCID: Initial Trial Results after 4 Years. *Science* **270**, 475-480.

204. D. T. Zallen, (2000). US gene therapy in crisis. *Trends Genet.* **16**, 272-275.

205. S. Hacein-Bey-Abina, J. Hauer, A. Lim, C. Picard, G. P. Wang, C. C. Berry *et al.*, (2010). Efficacy of gene therapy for X-linked severe combined immunodeficiency. *N. Engl. J. Med.* **363**, 355-364.

206. H. B. Gaspar, S. Cooray, K. C. Gilmour, K. L. Parsley, S. Adams, S. J. Howe *et al.*, (2011). Long-term persistence of a polyclonal T cell repertoire after gene therapy for X-linked severe combined immunodeficiency. *Sci. Transl. Med.* **3**, 97ra79.

207. A. Aiuti, F. Cattaneo, S. Galimberti, U. Benninghoff, B. Cassani, L. Callegaro *et al.*, (2009). Gene therapy for immunodeficiency due to adenosine deaminase deficiency. *N. Engl. J. Med.* **360**, 447-458.

208. H. B. Gaspar, S. Cooray, K. C. Gilmour, K. L. Parsley, F. Zhang, S. Adams *et al.*, (2011). Hematopoietic stem cell gene therapy for adenosine deaminase-deficient severe combined immunodeficiency leads to long-term immunological recovery and metabolic correction. *Sci. Transl. Med.* **3**, 97ra80.

209. A. C. Nathwani, E. G. Tuddenham, S. Rangarajan, C. Rosales, J. McIntosh, D. C. Linch *et al.*, (2011). Adenovirus-associated virus vector-mediated gene transfer in hemophilia B. *N. Engl. J. Med.* **365**, 2357-2365.

210. J. Bennett, M. Ashtari, J. Wellman, K. A. Marshall, L. L. Cyckowski, D. C. Chung *et al.*, (2012). AAV2 gene therapy readministration in three adults with congenital blindness. *Sci. Transl. Med.* **4**, 120ra115.

211. A. Biffi, E. Montini, L. Lorioli, M. Cesani, F. Fumagalli, T. Plati *et al.*, (2013). Lentiviral hematopoietic stem cell gene therapy benefits metachromatic leukodystrophy. *Science* **341**, 1233158.

212. A. Aiuti, L. Biasco, S. Scaramuzza, F. Ferrua, M. P. Cicalese, C. Baricordi *et al.*, (2013). Lentiviral hematopoietic stem cell gene therapy in patients with Wiskott-Aldrich syndrome. *Science* **341**, 1233151.

213. R. E. MacLaren, M. Groppe, A. R. Barnard, C. L. Cottriall, T. Tolmachova, L. Seymour *et al.*, (2014). Retinal gene therapy in patients with choroideremia: initial findings from a phase 1/2 clinical trial. *Lancet* **383**, 1129-1137.

214. D. Gaudet, J. Methot, S. Dery, D. Brisson, C. Essiembre, G. Tremblay *et al.*, (2013). Efficacy and long-term safety of alipogene tiparvovec (AAV1-LPLS447X) gene therapy for lipoprotein lipase deficiency: an open-label trial. *Gene Ther.* **20**, 361-369.

215. S. Yla-Herttuala, (2012). Endgame: glybera finally recommended for approval as the first gene therapy drug in the European union. *Mol. Ther.* **20**, 1831-1832.

216. J. R. Riordan, J. M. Rommens, B. S. Kerem, N. Alon, R. Rozmahel, Z. Grzelczak *et al.*, (1989). Identification of the cystic fibrosis gene: cloning and characterization of complementary DNA. *Science* **245**, 1066-1072.

217. E. W. F. W. Alton, P. G. Middleton, N. J. Caplen, S. N. Smith, D. M. Steel, F. M. Munkonge *et al.*, (1993). Non-invasive liposome-mediated gene delivery can correct the ion transport defect in cystic fibrosis mutant mice. *Nat. Genet.* **5**, 135-142.

218. M. L. Drumm, H. A. Pope, W. H. Cliff, J. M. Rommens, S. A. Marvin, L. C. Tsui *et al.*, (1990). Correction of the cystic fibrosis defect in vitro by retrovirus-mediated gene transfer. *Cell* **62**, 1227-1233.

219. D. P. Rich, M. P. Anderson, R. J. Gregory, S. H. Cheng, S. Paul, D. M. Jefferson *et al.*, (1990). Expression of cystic fibrosis transmembrane conductance regulator corrects defective chloride channel regulation in cystic fibrosis airway epithelial cells. *Nature* **347**, 358-363.

220. S. C. Hyde, D. R. Gill, C. F. Higgins, A. E. O. Trezise, L. J. Macvinish, A. W. Cuthbert *et al.*, (1993). Correction of the ion transport defect in cystic fibrosis transgenic mice by gene therapy. *Nature* **362**, 250-255.

221. U. Griesenbach, E. W. F. W. Alton, (2009). Gene transfer to the lung: lessons learned from more than 2 decades of CF gene therapy. *Adv. Drug Deliv. Rev.* **61**, 128-139.

222. E. W. F. W. Alton, M. Stern, R. Farley, A. Jaffe, S. L. Chadwick, J. Phillips *et al.*, (1999). Cationic lipid-mediated CFTR gene transfer to the lungs and nose of patients with cystic fibrosis: a double-blind placebo-controlled trial. *Lancet* **353**, 947-954.

223. D. J. Porteous, J. R. Dorin, G. McLachlan, H. DavidsonSmith, H. Davidson, B. J. Stevenson *et al.*, (1997). Evidence for safety and efficacy of DOTAP cationic liposome mediated CFTR gene transfer to the nasal epithelium of patients with cystic fibrosis. *Gene Ther.* **4**, 210-218.

224. T. R. Flotte, P. L. Zeitlin, T. C. Reynolds, A. E. Heald, P. Pedersen, S. Beck *et al.*, (2003). Phase I trial of intranasal and endobronchial administration of a recombinant adeno-associated virus serotype 2 (rAAV2)-CFTR vector in adult cystic fibrosis patients: A two-part clinical study. *Hum. Gene Ther.* **14**, 1079-1088.

225. J. A. Wagner, I. B. Nepomuceno, A. H. Messner, M. L. Moran, E. P. Batson, S. Dimiceli *et al.*, (2002). A phase II, double-blind, randomized, placebo-controlled clinical trial of tgAAVCF using maxillary sinus delivery in patients with cystic fibrosis with antrostomies. *Hum. Gene Ther.* **13**, 1349-1359.

226. R. B. Moss, C. Milla, J. Colombo, F. Accurso, P. L. Zeitlin, J. P. Clancy *et al.*, (2007). Repeated aerosolized AAV-CFTR for treatment of cystic fibrosis: a randomized placebo-controlled phase 2B trial. *Hum. Gene Ther.* **18**, 726-732.

227. R. B. Moss, D. Rochman, L. T. Spencer, M. L. Aitken, P. L. Zeitlhi, D. Waltz *et al.*, (2004). Repeated adeno-associated virus serotype 2 aerosol-mediated cystic fibrosis transmembrane regulator gene transfer to the lungs of patients with cystic fibrosis - A multicenter, double-blind, placebo-controlled trial. *Chest* **125**, 509-521.

228. M. Vareille, E. Kieninger, M. R. Edwards, N. Regamey, (2011). The airway epithelium: soldier in the fight against respiratory viruses. *Clin. Microbiol. Rev.* **24**, 210-229.

229. Z. Zsengeller, K. Otake, S. A. Hossain, P. Y. Berclaz, B. C. Trapnell, (2000). Internalization of adenovirus by alveolar macrophages initiates early proinflammatory signaling during acute respiratory tract infection. *J. Virol.* **74**, 9655-9667.

230. G. Diamond, D. Legarda, L. K. Ryan, (2000). The innate immune response of the respiratory epithelium. *Immunol. Rev.* **173**, 27-38.

231. P. M. Joseph, B. P. O'Sullivan, A. Lapey, H. Dorkin, J. Oren, R. Balfour *et al.*, (2001). Aerosol and lobar administration of a recombinant adenovirus to individuals with cystic fibrosis. I. Methods, safety, and clinical implications. *Hum. Gene Ther.* **12**, 1369-1382.

232. M. A. Perricone, J. E. Morris, K. Pavelka, M. S. Plog, B. P. O'Sullivan, P. M. Joseph *et al.*, (2001). Aerosol and lobar administration of a recombinant adenovirus to individuals with cystic fibrosis. II. Transfection efficiency in airway epithelium. *Hum. Gene Ther.* **12**, 1383-1394.

233. J. B. Zuckerman, C. B. Robinson, K. S. McCoy, R. Shell, T. J. Sferra, N. Chirmule *et al.*, (1999). A phase I study of adenovirus-mediated transfer of the human cystic fibrosis transmembrane conductance regulator gene to a lung segment of individuals with cystic fibrosis. *Hum. Gene Ther.* **10**, 2973-2985.

234. B. G. Harvey, P. L. Leopold, N. R. Hackett, T. M. Grasso, P. M. Williams, A. L. Tucker *et al.*, (1999). Airway epithelial CFTR mRNA expression in cystic fibrosis patients after repetitive administration of a recombinant adenovirus. *J. Clin. Invest.* **104**, 1245-1255.

235. J. Zabner, B. W. Ramsey, D. P. Meeker, M. L. Aitken, R. P. Balfour, R. L. Gibson *et al.*, (1996). Repeat administration of an adenovirus vector encoding cystic fibrosis transmembrane conductance regulator to the nasal epithelium of patients with cystic fibrosis. *J. Clin. Invest.* **97**, 1504-1511.

236. R. G. Crystal, N. G. Mcelvaney, M. A. Rosenfeld, C. S. Chu, A. Mastrangeli, J. G. Hay *et al.*, (1994). Administration of an adenovirus containing the human CFTR cDNA to the respiratory tract of individuals with cystic fibrosis. *Nat. Genet.* **8**, 42-51.

237. J. Zabner, L. A. Couture, R. J. Gregory, S. M. Graham, A. E. Smith, M. J. Welsh, (1993). Adenovirus-mediated gene transfer transiently corrects the chloride transport defect in nasal epithelia of patients with cystic fibrosis. *Cell* **75**, 207-216.

238. M. R. Knowles, K. W. Hohneker, Z. Zhou, J. C. Olsen, T. L. Noah, P. C. Hu *et al.*, (1995). A controlled study of adenoviral-vector-mediated gene transfer in the nasal epithelium of patients with cystic fibrosis. *N. Engl. J. Med.* **333**, 823-831.

239. B. G. Harvey, N. R. Hackett, T. El-Sawy, T. K. Rosengart, E. A. Hirschowitz, M. D. Lieberman *et al.*, (1999). Variability of human systemic humoral immune responses to adenovirus gene transfer vectors administered to different organs. *J. Virol.* **73**, 6729-6742.

240. S. J. Howe, M. R. Mansour, K. Schwarzwaelder, C. Bartholomae, M. Hubank, H. Kempski *et al.*, (2008). Insertional mutagenesis combined with acquired somatic mutations causes leukemogenesis following gene therapy of SCID-X1 patients. *J. Clin. Invest.* **118**, 3143-3150.

241. J. M. Bergelson, J. A. Cunningham, G. Droguett, E. A. Kurt-Jones, A. Krithivas, J. S. Hong *et al.*, (1997). Isolation of a common receptor for Coxsackie B viruses and adenoviruses 2 and 5. *Science* **275**, 1320-1323.

242. G. A. Mayr, P. Freimuth, (1997). A single locus on human chromosome 21 directs the expression of a receptor for adenovirus type 2 in mouse A9 cells. *J. Virol.* **71**, 412-418.

243. R. W. Walters, T. Grunst, J. M. Bergelson, R. W. Finberg, M. J. Welsh, J. Zabner, (1999). Basolateral localization of fiber receptors limits adenovirus infection from the apical surface of airway epithelia. *J. Biol. Chem.* **274**, 10219-10226.

244. L. G. Gregory, R. P. Harbottle, L. Lawrence, H. J. Knapton, M. Themis, C. Coutelle, (2003). Enhancement of adenovirus-mediated gene transfer to the airways by DEAE dextran and sodium caprate in vivo. *Mol. Ther.* **7**, 19-26.

245. T. Beckett, L. Bonneau, A. Howard, J. Blanchard, J. Borda, D. J. Weiner *et al.*, (2012). Inhalation of nebulized perfluorochemical enhances recombinant adenovirus and adeno-associated virus-mediated gene expression in lung epithelium. *Hum. Gene Ther. Methods* **23**, 98-110.

246. D. R. Koehler, H. Frndova, K. Leung, E. Louca, D. Palmer, P. Ng *et al.*, (2005). Aerosol delivery of an enhanced helper-dependent adenovirus formulation to rabbit lung using an intratracheal catheter. *J. Gene Med.* **7**, 1409-1420.

247. D. M. McCarty, S. M. Young, Jr., R. J. Samulski, (2004). Integration of adeno-associated virus (AAV) and recombinant AAV vectors. *Annu. Rev. Genet.* **38**, 819-845.

248. T. R. Flotte, A. C. Fischer, J. Goetzmann, C. Mueller, L. Cebotaru, Z. Y. Yan *et al.*, (2010). Dual reporter comparative indexing of rAAV pseudotyped vectors in chimpanzee airway. *Mol. Ther.* **18**, 594-600.

249. M. P. Limberis, L. H. Vandenberghe, L. Q. Zhang, R. J. Pickles, J. M. Wilson, (2009). Transduction efficiencies of novel AAV vectors in mouse airway epithelium in vivo and human ciliated airway epithelium in vitro. *Mol. Ther.* **17**, 294-301.

250. X. Liu, M. Luo, C. Guo, Z. Yan, Y. Wang, J. F. Engelhardt, (2007). Comparative biology of rAAV transduction in ferret, pig and human airway epithelia. *Gene Ther.* **14**, 1543-1548.

251. N. Maheshri, J. T. Koerber, B. K. Kaspar, D. V. Schaffer, (2006). Directed evolution of adeno-associated virus yields enhanced gene delivery vectors. *Nat. Biotechnol.* **24**, 198-204.

252. K. J. D. A. Excoffon, J. T. Koerber, D. D. Dickey, M. Murtha, S. Keshavjee, B. K. Kaspar *et al.*, (2009). Directed evolution of adeno-associated virus to an infectious respiratory virus. *Proc. Natl. Acad. Sci. U. S. A.* **106**, 3865-3870.

253. C. I. Thompson, W. S. Barclay, M. C. Zambon, R. J. Pickles, (2006). Infection of human airway epithelium by human and avian strains of influenza a virus. *J. Virol.* **80**, 8060-8068.

254. L. Q. Zhang, A. Bukreyev, C. I. Thompson, B. Watson, M. E. Peeples, P. L. Collins *et al.*, (2005). Infection of ciliated cells by human parainfluenza virus type 3 in an in vitro model of human airway epithelium. *J. Virol.* **79**, 1113-1124.

255. A. R. Kwilas, M. A. Yednak, L. Q. Zhang, R. Liesman, P. L. Collins, R. J. Pickles *et al.*, (2010). Respiratory syncytial virus engineered to express the cystic

fibrosis transmembrane conductance regulator corrects the bioelectric phenotype of human cystic fibrosis airway epithelium in vitro. *J. Virol.* **84**, 7770-7781.

256. O. Malykhina, M. A. Yednak, P. L. Collins, P. D. Olivo, M. E. Peeples, (2011). A respiratory syncytial virus replicon that is noncytotoxic and capable of long-term foreign gene expression. *J. Virol.* **85**, 4792-4801.

257. P. Faisca, D. Desmecht, (2007). Sendai virus, the mouse parainfluenza type 1: A longstanding pathogen that remains up-to-date. *Res. Vet. Sci.* **82**, 115-125.

258. H. O. Li, Y. F. Zhu, M. Asakawa, H. Kuma, T. Hirata, Y. Ueda *et al.*, (2000). A cytoplasmic RNA vector derived from nontransmissible Sendai virus with efficient gene transfer and expression. *J. Virol.* **74**, 6564-6569.

259. S. Ferrari, U. Griesenbach, T. Shirai-Iida, T. Shu, T. Hironaka, X. Hou *et al.*, (2004). A defective nontransmissible recombinant Sendai virus mediates efficient gene transfer to airway epithelium in vivo. *Gene Ther.* **11**, 1659-1664.

260. U. Griesenbach, G. McLachlan, T. Owaki, L. Somerton, T. Shu, A. Baker *et al.*, (2011). Validation of recombinant Sendai virus in a non-natural host model. *Gene Ther.* **18**, 182-188.

261. P. Cmielewski, D. S. Anson, D. W. Parsons, (2010). Lysophosphatidylcholine as an adjuvant for lentiviral vector mediated gene transfer to airway epithelium: effect of acyl chain length. *Respir. Res.* **11**, 84.

262. G. S. Wang, V. Slepushkin, J. Zabner, S. Keshavjee, J. C. Johnston, S. L. Sauter *et al.*, (1999). Feline immunodeficiency virus vectors persistently transduce nondividing airway epithelia and correct the cystic fibrosis defect. *J. Clin. Invest.* **104**, R55-R62.

263. S. Fuller, C. H. Vonbonsdorff, K. Simons, (1984). Vesicular stomatitis virus infects and matures only through the basolateral surface of the polarized epithelial cell line, MDCK. *Cell* **38**, 65-77.

264. A. G. Stocker, K. L. Kremer, R. Koldej, D. S. Miller, D. S. Anson, D. W. Parsons, (2009). Single-dose lentiviral gene transfer for lifetime airway gene expression. *J. Gene Med.* **11**, 861-867.

265. N. Farrow, D. Miller, P. Cmielewski, M. Donnelley, R. Bright, D. W. Parsons, (2013). Airway gene transfer in a non-human primate: lentiviral gene expression in marmoset lungs. *Sci. Rep.* **3**, 1287.

266. P. L. Sinn, E. R. Burnight, M. A. Hickey, G. W. Blissard, P. B. McCray, (2005). Persistent gene expression in mouse nasal epithelia following feline

immunodeficiency virus-based vector gene transfer. *J. Virol.* **79**, 12818-12827.

267. P. L. Sinn, A. C. Arias, K. A. Brogden, P. B. McCray, (2008). Lentivirus Vector Can Be Readministered to Nasal Epithelia without Blocking Immune Responses. *J. Virol.* **82**, 10684-10692.

268. S. M. K. Buckley, S. J. Howe, V. Sheard, N. J. Ward, C. Coutelle, A. J. Thrasher *et al.*, (2008). Lentiviral transduction of the murine lung provides efficient pseudotype and developmental stage-dependent cell-specific transgene expression. *Gene Ther.* **15**, 1167-1175.

269. M. F. Medina, G. P. Kobinger, J. Rux, M. Gasmi, D. J. Looney, P. Bates *et al.*, (2003). Lentiviral vectors pseudotyped with minimal filovirus envelopes increased gene transfer in murine lung. *Mol. Ther.* **8**, 777-789.

270. M. Kobayashi, A. Iida, Y. Ueda, M. Hasegawa, (2003). Pseudotyped lentivirus vectors derived from simian immunodeficiency virus SIVagm with envelope glycoproteins from paramyxovirus. *J. Virol.* **77**, 2607-2614.

271. U. Griesenbach, M. Inoue, C. X. Meng, R. Farley, M. Chan, N. K. Newman *et al.*, (2012). Assessment of F/HN-pseudotyped lentivirus as a clinically relevant vector for lung gene therapy. *Am. J. Respir. Crit. Care Med.* **186**, 846-856.

272. K. Mitomo, U. Griesenbach, M. Inoue, L. Somerton, C. X. Meng, E. Akiba *et al.*, (2010). Toward gene therapy for cystic fibrosis using a lentivirus pseudotyped with Sendai virus envelopes. *Mol. Ther.* **18**, 1173-1182.

273. T. McKay, M. Patel, R. J. Pickles, L. G. Johnson, J. C. Olsen, (2006). Influenza M2 envelope protein augments avian influenza hemagglutinin pseudotyping of lentiviral vectors. *Gene Ther.* **13**, 715-724.

274. M. Patel, A. M. Giddings, J. Sechelski, J. C. Olsen, (2013). High efficiency gene transfer to airways of mice using influenza hemagglutinin pseudotyped lentiviral vectors. *J. Gene Med.* **15**, 51-62.

275. J. Zabner, S. H. Cheng, D. Meeker, J. Launspach, R. Balfour, M. A. Perricone *et al.*, (1997). Comparison of DNA-lipid complexes and DNA alone for gene transfer to cystic fibrosis airway epithelia in vivo. *J. Clin. Invest.* **100**, 1529-1537.

276. N. J. Caplen, E. W. F. W. Alton, P. G. Middleton, J. R. Dorin, B. J. Stevenson, X. Gao *et al.*, (1995). Liposome-mediated CFTR gene transfer to the nasal epithelium of patients with cystic fibrosis. *Nat. Med.* **1**, 39-46.

277. D. R. Gill, K. W. Southern, K. A. Mofford, T. Seddon, L. Huang, F. Sorgi *et al.*, (1997). A placebo-controlled study of liposome-mediated gene transfer to the nasal epithelium of patients with cystic fibrosis. *Gene Ther.* **4**, 199-209.

278. E. W. Alton, A. C. Boyd, S. H. Cheng, J. C. Davies, L. A. Davies, A. Dayan *et al.*, (2014). Toxicology study assessing efficacy and safety of repeated administration of lipid/DNA complexes to mouse lung. *Gene Ther.* **21**, 89-95.

279. E. W. F. W. Alton, A. Baker, E. Baker, A. C. Boyd, S. H. Cheng, R. L. Coles *et al.*, (2013). The safety profile of a cationic lipid-mediated cystic fibrosis gene transfer agent following repeated monthly aerosol administration to sheep. *Biomaterials* **34**, 10267-10277.

280. S. C. Hyde, K. W. Southern, U. Gileadi, E. M. Fitzjohn, K. A. Mofford, B. E. Waddell *et al.*, (2000). Repeat administration of DNA/liposomes to the nasal epithelium of patients with cystic fibrosis. *Gene Ther.* **7**, 1156-1165.

281. E. W. F. W. Alton, A. C. Boyd, S. H. Cheng, S. Cunningham, J. C. Davies, D. R. Gill *et al.*, (2013). A randomised, double-blind, placebo-controlled phase IIB clinical trial of repeated application of gene therapy in patients with cystic fibrosis. *Thorax* **68**, 1075-1077.

282. L. Q. Zhang, B. Button, S. E. Gabriel, S. Burkett, Y. Yan, M. H. Skiadopoulos *et al.*, (2009). CFTR delivery to 25% of surface epithelial cells restores normal rates of mucus transport to human cystic fibrosis airway epithelium. *PLoS Biol.* **7**, e1000155.

283. L. E. Ostrowski, W. Yin, M. Patel, J. Sechelski, T. Rogers, K. Burns *et al.*, (2014). Restoring ciliary function to differentiated primary ciliary dyskinesia cells with a lentiviral vector. *Gene Ther.* **21**, 253-261.

284. S. Xenariou, U. Griesenbach, S. Ferrari, P. Dean, R. K. Scheule, S. H. Cheng *et al.*, (2006). Using magnetic forces to enhance non-viral gene transfer to airway epithelium in vivo. *Gene Ther.* **13**, 1545-1552.

285. S. Xenariou, U. Griesenbach, H. D. Liang, J. Zhu, R. Farley, L. Somerton *et al.*, (2007). Use of ultrasound to enhance nonviral lung gene transfer in vivo. *Gene Ther.* **14**, 768-774.

286. A. G. Ziady, T. J. Kelley, E. Milliken, T. Ferkol, P. B. Davis, (2002). Functional evidence of CFTR gene transfer in nasal epithelium of cystic fibrosis mice in vivo following luminal application of DNA complexes targeted to the serpin-enzyme complex receptor. *Mol. Ther.* **5**, 413-419.

287. A. D. Tagalakis, R. J. McAnulty, J. Devaney, S. E. Bottoms, J. B. Wong, M. Elbs *et al.*, (2008). A receptor-targeted nanocomplex vector system optimized for respiratory gene transfer. *Mol. Ther.* **16**, 907-915.

288. M. J. Writer, B. Marshall, M. A. Pilkington-Miksa, S. E. Barker, M. Jacobsen, A. Kritz *et al.*, (2004). Targeted gene delivery to human airway epithelial cells with synthetic vectors incorporating novel targeting peptides selected by phage display. *J. Drug Target.* **12**, 185-193.

289. M. D. I. Manunta, R. J. McAnulty, A. D. Tagalakis, S. E. Bottoms, F. Campbell, H. C. Hailes *et al.*, (2011). Nebulisation of receptor-targeted nanocomplexes for gene delivery to the airway epithelium. *PLoS ONE* **6**, e26768.

290. M. D. I. Manunta, R. J. McAnulty, A. McDowell, J. Jin, D. Ridout, J. Fleming *et al.*, (2013). Airway deposition of nebulized gene delivery nanocomplexes monitored by radioimaging agents. *Am. J. Respir. Cell Mol. Biol.* **49**, 471-480.

291. I. Koltover, T. Salditt, J. O. Radler, C. R. Safinya, (1998). An inverted hexagonal phase of cationic liposome-DNA complexes related to DNA release and delivery. *Science* **281**, 78-81.

292. G. McLachlan, H. Davidson, E. Holder, L. A. Davies, I. A. Pringle, S. G. Sumner-Jones *et al.*, (2011). Pre-clinical evaluation of three non-viral gene transfer agents for cystic fibrosis after aerosol delivery to the ovine lung. *Gene Ther.* **18**, 996-1005.

293. C. M. Chen, J. Krohn, S. Bhattacharya, B. Davies, (2011). A comparison of exogenous promoter activity at the ROSA26 locus using a phiC31 integrase mediated cassette exchange approach in mouse ES cells. *PLoS ONE* **6**, e23376.

294. J. Y. Qin, L. Zhang, K. L. Clift, I. Hulur, A. P. Xiang, B. Z. Ren *et al.*, (2010). Systematic comparison of constitutive promoters and the doxycycline-inducible promoter. *PLoS ONE* **5**, e10611.

295. K. Norrman, Y. Fischer, B. Bonnamy, F. W. Sand, P. Ravassard, H. Semb, (2010). Quantitative comparison of constitutive promoters in human ES cells. *PLoS ONE* **5**, e12413.

296. D. R. Gill, S. E. Smyth, C. A. Goddard, I. A. Pringle, C. F. Higgins, W. H. Colledge *et al.*, (2001). Increased persistence of lung gene expression using plasmids containing the ubiquitin C or elongation factor 1 alpha promoter. *Gene Ther.* **8**, 1539-1546.

297. S. C. Hyde, I. A. Pringle, S. Abdullah, A. E. Lawton, L. A. Davies, A. Varathalingam *et al.*, (2008). CpG-free plasmids confer reduced inflammation and sustained pulmonary gene expression. *Nat. Biotechnol.* **26**, 549-551.

298. A. M. Krieg, (1996). Lymphocyte activation by CpG dinucleotide motifs in prokaryotic DNA. *Trends Microbiol.* **4**, 73-77.

299. S. Yamamoto, T. Yamamoto, T. Kataoka, E. Kuramoto, O. Yano, T. Tokunaga, (1992). Unique palindromic sequences in synthetic oligonucleotides are required to induce IFN and augment IFN-mediated natural killer activity. *J. Immunol.* **148**, 4072-4076.

300. N. S. Yew, K. X. Wang, M. Przybylska, R. G. Bagley, M. Stedman, J. Marshall *et al.*, (1999). Contribution of plasmid DNA to inflammation in the lung after administration of cationic lipid : pDNA complexes. *Hum. Gene Ther.* **10**, 223-234.

301. J. M. McMahon, K. E. Wells, J. E. Bamfo, M. A. Cartwright, D. J. Wells, (1998). Inflammatory responses following direct injection of plasmid DNA into skeletal muscle. *Gene Ther.* **5**, 1283-1290.

302. H. Hemmi, O. Takeuchi, T. Kawai, T. Kaisho, S. Sato, H. Sanjo *et al.*, (2000). A Toll-like receptor recognizes bacterial DNA. *Nature* **408**, 740-745.

303. E. Lesina, P. Dames, A. Flemmer, K. Hajek, T. Kirchner, I. Bittmann *et al.*, (2010). CpG-free plasmid DNA prevents deterioration of pulmonary function in mice. *Eur. J. Pharm. Biopharm.* **74**, 427-434.

304. I. A. Pringle, S. C. Hyde, M. M. Connolly, A. E. Lawton, B. H. Xu, G. Nunez-Alonso *et al.*, (2012). CpG-free plasmid expression cassettes for cystic fibrosis gene therapy. *Biomaterials* **33**, 6833-6842.

305. L. A. Davies, S. C. Hyde, G. Nunez-Alonso, R. P. Bazzani, R. Harding-Smith, I. A. Pringle *et al.*, (2012). The use of CpG-free plasmids to mediate persistent gene expression following repeated aerosol delivery of pDNA/PEI complexes. *Biomaterials* **33**, 5618-5627.

306. E. Lesina, P. Dames, C. Rudolph, (2010). The effect of CpG motifs on gene expression and clearance kinetics of aerosol administered polyethylenimine (PEI)-plasmid DNA complexes in the lung. *J. Control. Release* **143**, 243-250.

307. Z. Y. Chen, E. Riu, C. Y. He, H. Xu, M. A. Kay, (2008). Silencing of episomal transgene expression in liver by plasmid bacterial backbone DNA is independent of CpG methylation. *Mol. Ther.* **16**, 548-556.

308. J. M. Lu, F. F. Zhang, S. Q. Xu, A. Z. Fire, M. A. Kay, (2012). The extragenic spacer length between the 5' and 3' ends of the transgene expression cassette affects transgene silencing from plasmid-based vectors. *Mol. Ther.* **20**, 2111-2119.

309. Z. Y. Chen, C. Y. He, A. Ehrhardt, M. A. Kay, (2003). Minicircle DNA vectors devoid of bacterial DNA result in persistent and high-level transgene expression in vivo. *Mol. Ther.* **8**, 495-500.

310. M. J. Osborn, R. T. McElmurry, C. J. Lees, A. P. DeFeo, Z. Y. Chen, M. A. Kay *et al.*, (2011). Minicircle DNA-based gene therapy coupled with immune modulation permits long-term expression of alpha-L-iduronidase in mice with mucopolysaccharidosis type I. *Mol. Ther.* **19**, 450-460.

311. M. Huang, Z. Y. Chen, S. J. Hu, F. J. Jia, Z. J. Li, G. Hoyt *et al.*, (2009). Novel minicircle vector for gene therapy in murine myocardial infarction. *Circulation* **120**, S230-S237.

312. S. Stenler, A. Andersson, O. E. Simonson, K. E. Lundin, Z. Y. Chen, M. A. Kay *et al.*, (2009). Gene transfer to mouse heart and skeletal muscles using a minicircle expressing human vascular endothelial growth factor. *J. Cardiovasc. Pharmacol.* **53**, 18-23.

313. L. E. Ostrowski, W. Yin, P. S. Diggs, T. D. Rogers, W. K. O'Neal, B. R. Grubb, (2007). Expression of CFTR from a ciliated cell-specific promoter is ineffective at correcting nasal potential difference in CF mice. *Gene Ther.* **14**, 1492-1501.

314. B. Chhin, D. Negre, O. Merrot, J. Pham, Y. Tourneur, D. Ressnikoff *et al.*, (2009). Ciliary beating recovery in deficient human airway epithelial cells after lentivirus ex vivo gene therapy. *PLoS Genet.* **5**, e1000422.

315. M. Jorissen, T. Willems, B. Van der Schueren, E. Verbeken, K. De Boeck, (2000). Ultrastructural expression of primary ciliary dyskinesia after ciliogenesis in culture. *Acta Otorhinolaryngol. Belg.* **54**, 343-356.

316. L. E. Ostrowski, W. N. Yin, T. D. Rogers, K. B. Busalacchi, M. Chua, W. K. O'Neal *et al.*, (2010). Conditional deletion of Dnaic1 in a murine model of primary ciliary dyskinesia causes chronic rhinosinusitis. *Am. J. Respir. Cell Mol. Biol.* **43**, 55-63.

317. I. M. Reichler, A. Hoerauf, F. Guscetti, O. Gardelle, M. H. Stoffel, B. Jentsch *et al.*, (2001). Primary ciliary dyskinesia with situs inversus totalis, hydrocephalus internus and cardiac malformations in a dog. *J. Small Anim. Pract.* **42**, 345-348.

318. R. Cavrenne, V. De Busscher, G. Bolen, F. Billen, C. Clercx, F. Snaps, (2008). Primary ciliary dyskinesia and situs inversus in a young dog. *Vet. Rec.* **163**, 54-55.

319. M. De Scally, R. G. Lobetti, E. Van Wilpe, (2004). Primary ciliary dyskinesia in a Staffordshire bull terrier. *J. S. Afr. Vet. Assoc.* **75**, 150-152.

320. J. F. Randolph, W. L. Castleman, (1984). Immotile cilia syndrome in two Old English Sheepdog litter-mates. *J. Small Anim. Pract.* **25**, 679-686.

321. P. C. Zamecnik, M. L. Stephenson, (1978). Inhibition of Rous sarcoma virus replication and cell transformation by a specific oligodeoxynucleotide. *Proc. Natl. Acad. Sci. U. S. A.* **75**, 280-284.

322. M. L. Stephenson, P. C. Zamecnik, (1978). Inhibition of Rous sarcoma viral RNA translation by a specific oligodeoxyribonucleotide. *Proc. Natl. Acad. Sci. U. S. A.* **75**, 285-288.

323. N. Dias, C. A. Stein, (2002). Antisense oligonucleotides: basic concepts and mechanisms. *Mol. Cancer Ther.* **1**, 347-355.

324. C. Napoli, C. Lemieux, R. Jorgensen, (1990). Introduction of a Chimeric Chalcone Synthase Gene into Petunia Results in Reversible Co-Suppression of Homologous Genes in trans. *Plant Cell* **2**, 279-289.

325. A. R. Vanderkrol, L. A. Mur, M. Beld, J. N. M. Mol, A. R. Stuitje, (1990). Flavonoid genes in petunia: addition of a limited number of gene copies may lead to a suppression of gene expression. *Plant Cell* **2**, 291-299.

326. C. J. S. Smith, C. F. Watson, C. R. Bird, J. Ray, W. Schuch, D. Grierson, (1990). Expression of a truncated tomato polygalacturonase gene inhibits expression of the endogenous gene in transgenic plants. *Mol. Gen. Genet.* **224**, 477-481.

327. R. Vanblokland, N. Vandergeest, J. N. M. Mol, J. M. Kooter, (1994). Transgene-mediated suppression of chalcone synthase expression in Petunia hybrida results from an increase in RNA turnover. *Plant J.* **6**, 861-877.

328. N. Romano, G. Macino, (1992). Quelling: transient inactivation of gene expression in Neurospora crassa by transformation with homologous sequences. *Mol. Microbiol.* **6**, 3343-3353.

329. M. PalBhadra, U. Bhadra, J. A. Birchler, (1997). Cosuppression in Drosophila: gene silencing of Alcohol dehydrogenase by white-Adh transgenes is Polycomb dependent. *Cell* **90**, 479-490.

330. S. Guo, K. J. Kemphues, (1995). par-1, a gene required for establishing polarity in C. elegans embryos, encodes a putative Ser/Thr kinase that is asymmetrically distributed. *Cell* **81**, 611-620.

331. C. E. Rocheleau, W. D. Downs, R. L. Lin, C. Wittmann, Y. X. Bei, Y. H. Cha *et al.*, (1997). Wnt signaling and an APC-related gene specify endoderm in early C-elegans embryos. *Cell* **90**, 707-716.

332. A. Fire, S. Q. Xu, M. K. Montgomery, S. A. Kostas, S. E. Driver, C. C. Mello, (1998). Potent and specific genetic interference by double-stranded RNA in Caenorhabditis elegans. *Nature* **391**, 806-811.

333. J. A. Lindbo, L. Silvarosales, W. M. Proebsting, W. G. Dougherty, (1993). Induction of a highly specific antiviral state in transgenic plants: implications for regulation of gene expression and virus resistance. *Plant Cell* **5**, 1749-1759.

334. F. Ratcliff, B. D. Harrison, D. C. Baulcombe, (1997). A similarity between viral defense and gene silencing in plants. *Science* **276**, 1558-1560.

335. S. N. Covey, N. S. AlKaff, A. Langara, D. S. Turner, (1997). Plants combat infection by gene silencing. *Nature* **385**, 781-782.

336. R. Lu, M. Maduro, F. Li, H. W. Li, G. Broitman-Maduro, W. X. Li *et al.*, (2005). Animal virus replication and RNAi-mediated antiviral silencing in Caenorhabditis elegans. *Nature* **436**, 1040-1043.

337. C. Wilkins, R. Dishongh, S. C. Moore, M. A. Whitt, M. Chow, K. Machaca, (2005). RNA interference is an antiviral defence mechanism in Caenorhabditis elegans. *Nature* **436**, 1044-1047.

338. G. C. Segers, X. M. Zhang, F. Y. Deng, Q. H. Sun, D. L. Nuss, (2007). Evidence that RNA silencing functions as an antiviral defense mechanism in fungi. *Proc. Natl. Acad. Sci. U. S. A.* **104**, 12902-12906.

339. Y. H. Han, Y. J. Luo, Q. F. Wu, J. Jovel, X. H. Wang, R. Aliyari *et al.*, (2011). RNA-based immunity terminates viral infection in adult drosophila in the absence of viral suppression of RNA interference: characterization of viral small interfering RNA populations in wild-type and mutant Flies. *J. Virol.* **85**, 13153-13163.

340. Y. Li, J. F. Lu, Y. H. Han, X. X. Fan, S. W. Ding, (2013). RNA interference functions as an antiviral immunity mechanism in mammals. *Science* **342**, 231-234.

341. P. V. Maillard, C. Ciaudo, A. Marchais, Y. Li, F. Jay, S. W. Ding *et al.*, (2013). Antiviral RNA interference in mammalian cells. *Science* **342**, 235-238.

342. E. Bernstein, A. A. Caudy, S. M. Hammond, G. J. Hannon, (2001). Role for a bidentate ribonuclease in the initiation step of RNA interference. *Nature* **409**, 363-366.

343. S. M. Hammond, E. Bernstein, D. Beach, G. J. Hannon, (2000). An RNA-directed nuclease mediates post-transcriptional gene silencing in Drosophila cells. *Nature* **404**, 293-296.

344. S. M. Elbashir, J. Harborth, W. Lendeckel, A. Yalcin, K. Weber, T. Tuschl, (2001). Duplexes of 21-nucleotide RNAs mediate RNA interference in cultured mammalian cells. *Nature* **411**, 494-498.

345. P. J. Paddison, A. A. Caudy, E. Bernstein, G. J. Hannon, D. S. Conklin, (2002). Short hairpin RNAs (shRNAs) induce sequence-specific silencing in mammalian cells. *Genes Dev.* **16**, 948-958.

346. L. K. Lee, E. Siapati, R. G. Jenkins, R. J. McAnulty, S. L. Hart, P. A. Shamlou, (2003). Biophysical characterization of an integrin-targeted non-viral vector. *Med. Sci. Monit.* **9**, 54-61.

347. R. S. Pillai, S. N. Bhattacharyya, W. Filipowicz, (2007). Repression of protein synthesis by miRNAs: how many mechanisms? *Trends Cell Biol.* **17**, 118-126.

348. J. Seibler, A. Kleinridders, B. Kuter-Luks, S. Niehaves, J. C. Bruning, F. Schwenk, (2007). Reversible gene knockdown in mice using a tight, inducible shRNA expression system. *Nucleic Acids Res.* **35**, e54.

349. T. Abbas-Terki, W. Blanco-Bose, N. Deglon, W. Pralong, P. Aebischer, (2002). Lentiviral-mediated RNA interference. *Hum. Gene Ther.* **13**, 2197-2201.

350. X. F. Qin, D. S. An, I. S. Y. Chen, D. Baltimore, (2003). Inhibiting HIV-1 infection in human T cells by lentiviral-mediated delivery of small interfering RNA against CCR5. *Proc. Natl. Acad. Sci. U. S. A.* **100**, 183-188.

351. G. Iliakis, H. Wang, A. R. Perrault, W. Boecker, B. Rosidi, F. Windhofer *et al.*, (2004). Mechanisms of DNA double strand break repair and chromosome aberration formation. *Cytogenet. Genome Res.* **104**, 14-20.

352. Y. G. Kim, J. Cha, S. Chandrasegaran, (1996). Hybrid restriction enzymes: zinc finger fusions to Fok I cleavage domain. *Proc. Natl. Acad. Sci. U. S. A.* **93**, 1156-1160.

353. J. Bitinaite, D. A. Wah, A. K. Aggarwal, I. Schildkraut, (1998). FokI dimerization is required for DNA cleavage. *Proc. Natl. Acad. Sci. U. S. A.* **95**, 10570-10575.

354. M. Christian, T. Cermak, E. L. Doyle, C. Schmidt, F. Zhang, A. Hummel *et al.*, (2010). Targeting DNA double-strand breaks with TAL effector nucleases. *Genetics* **186**, 757-761.

355. T. Li, S. Huang, W. Z. Jiang, D. Wright, M. H. Spalding, D. P. Weeks *et al.*, (2011). TAL nucleases (TALNs): hybrid proteins composed of TAL effectors and FokI DNA-cleavage domain. *Nucleic Acids Res.* **39**, 359-372.

356. M. M. Mahfouz, L. X. Li, M. Shamimuzzaman, A. Wibowo, X. Y. Fang, J. K. Zhu, (2011). De novo-engineered transcription activator-like effector (TALE) hybrid nuclease with novel DNA binding specificity creates double-strand breaks. *Proc. Natl. Acad. Sci. U. S. A.* **108**, 2623-2628.

357. J. E. DiCarlo, J. E. Norville, P. Mali, X. Rios, J. Aach, G. M. Church, (2013). Genome engineering in Saccharomyces cerevisiae using CRISPR-Cas systems. *Nucleic Acids Res.* **41**, 4336-4343.

358. W. Y. Hwang, Y. F. Fu, D. Reyon, M. L. Maeder, S. Q. Tsai, J. D. Sander *et al.*, (2013). Efficient genome editing in zebrafish using a CRISPR-Cas system. *Nat. Biotechnol.* **31**, 227-229.

359. H. Y. Wang, H. Yang, C. S. Shivalila, M. M. Dawlaty, A. W. Cheng, F. Zhang *et al.*, (2013). One-step generation of mice carrying mutations in multiple genes by CRISPR/Cas-mediated genome engineering. *Cell* **153**, 910-918.

360. P. Mali, L. H. Yang, K. M. Esvelt, J. Aach, M. Guell, J. E. DiCarlo *et al.*, (2013). RNA-guided human genome engineering via Cas9. *Science* **339**, 823-826.

361. M. Weibel, B. Pettmann, J. C. Artault, M. Sensenbrenner, G. Labourdette, (1986). Primary culture of rat ependymal cells in serum-free defined medium. *Dev. Brain Res.* **25**, 199-209.

362. T. E. Gray, K. Guzman, C. W. Davis, L. H. Abdullah, P. Nettesheim, (1996). Mucociliary differentiation of serially passaged normal human tracheobronchial epithelial cells. *Am. J. Respir. Cell Mol. Biol.* **14**, 104-112.

363. M. Jorissen, B. Vanderschueren, H. Vandenberghe, J. J. Cassiman, (1989). The preservation and regeneration of cilia on human nasal epithelial cells cultured in vitro. *Arch. Otorhinolaryngol.* **246**, 308-314.

364. R. A. Lewin, (1954). Mutants of Chlamydomonas moewusii with impaired motility. *J. Gen. Microbiol.* **11**, 358-363.

365. S. S. Merchant, S. E. Prochnik, O. Vallon, E. H. Harris, S. J. Karpowicz, G. B. Witman *et al.*, (2007). The Chlamydomonas genome reveals the evolution of key animal and plant functions. *Science* **318**, 245-251.

366. G. J. Pazour, N. Agrin, J. Leszyk, G. B. Witman, (2005). Proteomic analysis of a eukaryotic cilium. *J. Cell Biol.* **170**, 103-113.

367. C. G. Wilkerson, S. M. King, A. Koutoulis, G. J. Pazour, G. B. Witman, (1995). The 78,000 M(r) intermediate chain of Chlamydomonas outer arm dynein isa WD-repeat protein required for arm assembly. *J. Cell Biol.* **129**, 169-178.

368. M. Schroda, (2006). RNA silencing in Chlamydomonas: mechanisms and tools. *Curr. Genet.* **49**, 69-84.

369. E. J. Kim, H. Cerutti, (2009). Targeted gene silencing by RNA interference in Chlamydomonas. *Methods Cell Biol.* **93**, 99-110.

370. A. Tarkar, N. T. Loges, C. E. Slagle, R. Francis, G. W. Dougherty, J. V. Tamayo *et al.*, (2013). DYX1C1 is required for axonemal dynein assembly and ciliary motility. *Nat. Genet.* **45**, 995-1003.

371. E. van Rooijen, R. H. Giles, E. E. Voest, C. van Rooijen, S. Schulte-Merker, F. J. van Eeden, (2008). LRRC50, a conserved ciliary protein implicated in polycystic kidney disease. *J. Am. Soc. Nephrol.* **19**, 1128-1138.

372. K. P. Hummel, D. B. Chapman, (1959). Visceral inversion and associated anomalies in the mouse. *J. Hered.* **50**, 9-13.

373. D. M. Supp, D. P. Witte, S. S. Potter, M. Brueckner, (1997). Mutation of an axonemal dynein affects left right asymmetry in inversus viscerum mice. *Nature* **389**, 963-966.

374. D. M. Supp, M. Brueckner, M. R. Kuehn, D. P. Witte, L. A. Lowe, J. McGrath *et al.*, (1999). Targeted deletion of the ATP binding domain of left-right dynein confirms its role in specifying development of left-right asymmetries. *Development* **126**, 5495-5504.

375. S. Y. Tan, J. Rosenthal, X. Q. Zhao, R. J. Francis, B. Chatterjee, S. L. Sabol *et al.*, (2007). Heterotaxy and complex structural heart defects in a mutant mouse model of primary ciliary dyskinesia. *J. Clin. Invest.* **117**, 3742-3752.

376. A. L. Cozens, M. J. Yezzi, K. Kunzelmann, T. Ohrui, L. Chin, K. Eng *et al.*, (1994). CFTR expression and chloride secretion in polarized immortal human bronchial epithelial cells. *Am. J. Respir. Cell Mol. Biol.* **10**, 38-47.

377. R. G. Jenkins, Q. H. H. Meng, R. J. Hodges, L. K. Lee, S. E. W. Bottoms, G. J. Laurent *et al.*, (2003). Formation of LID vector complexes in water alters physicochemical properties and enhances pulmonary gene expression in vivo. *Gene Ther.* **10**, 1026-1034.

378. K. Rousseau, C. Wickstrom, D. B. Whitehouse, I. Carlstedt, D. M. Swallow, (2003). New monoclonal antibodies to non-glycosylated domains of the secreted mucins MUC5B and MUC7. *Hybrid. Hybridomics* **22**, 293-299.

379. H. Inoue, H. Nojima, H. Okayama, (1990). High efficiency transformation of Escherichia coli with plasmids. *Gene* **96**, 23-28.

380. K. J. Livak, T. D. Schmittgen, (2001). Analysis of relative gene expression data using real-time quantitative PCR and the 2(T)(-Delta Delta C) method. *Methods* **25**, 402-408.

381. M. Z. Li, S. J. Elledge, (2007). Harnessing homologous recombination in vitro to generate recombinant DNA via SLIC. *Nat. Meth.* **4**, 251-256.

382. I. Barde, P. Salmon, D. Trono, (2010). Production and titration of lentiviral vectors. *Curr. Protoc. Neurosci.* **53**, 4.21.21–24.21.23.

383. C. M. Smith, J. Djakow, R. C. Free, P. Djakow, R. Lonnen, G. Williams *et al.*, (2012). ciliaFA: a research tool for automated, high-throughput measurement of ciliary beat frequency using freely available software. *Cilia* **1**, 14.

384. B. Wang, S. B. Zhang, S. H. Cui, B. L. Yang, Y. A. Zhao, H. Y. Chen *et al.*, (2012). Chitosan enhanced gene delivery of cationic liposome via non-covalent conjugation. *Biotechnol. Lett.* **34**, 19-28.

385. T. Kurosaki, R. Kishikawa, M. Matsumoto, Y. Kodama, T. Hamamoto, H. To *et al.*, (2009). Pulmonary gene delivery of hybrid vector, lipopolyplex containing N-lauroylsarcosine, via the systemic route. *J. Control. Release* **136**, 213-219.

386. L. Garcia, M. Bunuales, N. Duzgunes, C. T. de Ilarduya, (2007). Serum-resistant lipopolyplexes for gene delivery to liver tumour cells. *Eur. J. Pharm. Biopharm.* **67**, 58-66.

387. M. Whitmore, S. Li, L. Huang, (1999). LPD lipopolyplex initiates a potent cytokine response and inhibits tumor growth. *Gene Ther.* **6**, 1867-1875.

388. H. M. Song, G. Wang, B. He, L. Li, C. X. Li, Y. S. Lai *et al.*, (2012). Cationic lipid-coated PEI/DNA polyplexes with improved efficiency and reduced cytotoxicity for gene delivery into mesenchymal stem cells. *Int. J. Nanomedicine* **7**, 4637-4648.

389. J. DeRouchey, B. Hoover, D. C. Rau, (2013). A comparison of DNA compaction by arginine and lysine peptides: a physical basis for arginine rich protamines. *Biochemistry* **52**, 3000-3009.

390. A. Mann, G. Thakur, V. Shukla, A. K. Singh, R. Khanduri, R. Naik *et al.*, (2011). Differences in DNA condensation and release by lysine and arginine homopeptides govern their DNA delivery efficiencies. *Mol. Pharm.* **8**, 1729-1741.

391. D. V. Schaffer, N. A. Fidelman, N. Dan, D. A. Lauffenburger, (2000). Vector unpacking as a potential barrier for receptor-mediated polyplex gene delivery. *Biotechnol. Bioeng.* **67**, 598-606.

392. R. Maurisse, D. De Semir, H. Emamekhoo, B. Bedayat, A. Abdolmohammadi, H. Parsi *et al.*, (2010). Comparative transfection of DNA into primary and transformed mammalian cells from different lineages. *BMC Biotechnol.* **10**, 9.

393. G. K. Min, M. A. Bevan, D. C. Prieve, G. D. Patterson, (2002). Light scattering characterization of polystyrene latex with and without adsorbed polymer. *Colloids Surf., A* **202**, 9-21.

394. K. Schätzel, J. Merz, (1984). Measurement of small electrophoretic mobilities by light scattering and analysis of the amplitude weighted phase structure function. *J. Chem. Phys.* **81**, 2482-2488.

395. P. Kreiss, B. Cameron, R. Rangara, P. Mailhe, O. Aguerre-Charriol, M. Airiau *et al.*, (1999). Plasmid DNA size does not affect the physicochemical properties of lipoplexes but modulates gene transfer efficiency. *Nucleic Acids Res.* **27**, 3792-3798.

396. J. Rejman, V. Oberle, I. S. Zuhorn, D. Hoekstra, (2004). Size-dependent internalization of particles via the pathways of clathrin-and caveolae-mediated endocytosis. *Biochem. J.* **377**, 159-169.

397. S. L. Hart, C. V. Arancibia-Carcamo, M. A. Wolfert, C. Mailhos, N. J. O'Reilly, R. R. Ali *et al.*, (1998). Lipid-mediated enhancement of transfection by a nonviral integrin-targeting vector. *Hum. Gene Ther.* **9**, 575-585.

398. A. Elouahabi, J. M. Ruysschaert, (2005). Formation and intracellular trafficking of lipoplexes and polyplexes. *Mol. Ther.* **11**, 336-347.

399. J. H. Felgner, R. Kumar, C. N. Sridhar, C. J. Wheeler, Y. J. Tsai, R. Border *et al.*, (1994). Enhanced gene delivery and mechanism studies with a novel series of cationic lipid formulations. *J. Biol. Chem.* **269**, 2550-2561.

400. E. Wagner, C. Plank, K. Zatloukal, M. Cotten, M. L. Birnstiel, (1992). Influenza virus hemagglutinin HA-2 N-terminal fusogenic peptides augment gene transfer by transferrin-polylysine-DNA complexes: toward a synthetic virus-like gene-transfer vehicle. *Proc. Natl. Acad. Sci. U. S. A.* **89**, 7934-7938.

401. M. C. Pedroso de Lima , S. Simoes, P. Pires, H. Faneca, N. Duzgunes, (2001). Cationic lipid-DNA complexes in gene delivery: from biophysics to biological applications. *Adv. Drug Deliv. Rev.* **47**, 277-294.

402. A. M. Darquet, B. Cameron, P. Wils, D. Scherman, J. Crouzet, (1997). A new DNA vehicle for nonviral gene delivery: supercoiled minicircle. *Gene Ther.* **4**, 1341-1349.

403. A. M. Darquet, R. Rangara, P. Kreiss, B. Schwartz, S. Naimi, P. Delaere *et al.*, (1999). Minicircle: an improved DNA molecule for in vitro and in vivo gene transfer. *Gene Ther.* **6**, 209-218.

404. D. Kobelt, M. Schleef, M. Schmeer, J. Aumann, P. M. Schlag, W. Walther, (2013). Performance of high quality minicircle DNA for in vitro and in vivo gene transfer. *Mol. Biotechnol.* **53**, 80-89.

405. M. A. Kay, C. Y. He, Z. Y. Chen, (2010). A robust system for production of minicircle DNA vectors. *Nat. Biotechnol.* **28**, 1287-1289.

406. V. F. Simmon, Lederber.S, (1972). Degradation of bacteriophage lambda deoxyribonucleic acid after restriction by Escherichia coli K-12. *J. Bacteriol.* **112**, 161-169.

407. L. E. G. Maniar, J. M. Maniar, Z. Y. Chen, J. M. Lu, A. Z. Fire, M. A. Kay, (2013). Minicircle DNA vectors achieve sustained expression reflected by active chromatin and transcriptional level. *Mol. Ther.* **21**, 131-138.

408. R. K. Scheule, J. A. StGeorge, R. G. Bagley, J. Marshall, J. M. Kaplan, G. Y. Akita *et al.*, (1997). Basis of pulmonary toxicity associated with cationic lipid-

mediated Gene transfer to the mammalian lung. *Hum. Gene Ther.* **8**, 689-707.

409. B. H. C. Jenke, C. P. Fetzer, I. M. Stehle, F. Jonsson, F. O. Fackelmayer, H. Conradt *et al.*, (2002). An episomally replicating vector binds to the nuclear matrix protein SAF-A in vivo. *EMBO Rep.* **3**, 349-354.

410. C. Piechaczek, C. Fetzer, A. Baiker, J. Bode, H. J. Lipps, (1999). A vector based on the SV40 origin of replication and chromosomal S/MARs replicates episomally in CHO cells. *Nucleic Acids Res.* **27**, 426-428.

411. O. Argyros, S. P. Wong, M. Niceta, S. N. Waddington, S. J. Howe, C. Coutelle *et al.*, (2008). Persistent episomal transgene expression in liver following delivery of a scaffold/matrix attachment region containing non-viral vector. *Gene Ther.* **15**, 1593-1605.

412. D. J. Giard, S. A. Aaronson, G. J. Todaro, P. Arnstein, J. H. Kersey, H. Dosik *et al.*, (1973). In vitro cultivation of human tumors: establishment of cell lines derived from a series of solid tumors. *J. Natl. Cancer Inst.* **51**, 1417-1423.

413. A. S. Lundberg, S. H. Randell, S. A. Stewart, B. Elenbaas, K. A. Hartwell, M. W. Brooks *et al.*, (2002). Immortalization and transformation of primary human airway epithelial cells by gene transfer. *Oncogene* **21**, 4577-4586.

414. J. Zabner, P. Karp, M. Seiler, S. L. Phillips, C. J. Mitchell, M. Saavedra *et al.*, (2003). Development of cystic fibrosis and noncystic fibrosis airway cell lines. *Am. J. Physiol. Lung Cell. Mol. Physiol.* **284**, L844-L854.

415. D. C. Gruenert, C. B. Basbaum, M. J. Welsh, M. Li, W. E. Finkbeiner, J. A. Nadel, (1988). Characterization of human tracheal epithelial cells transformed by an origin-defective simian virus 40. *Proc. Natl. Acad. Sci. U. S. A.* **85**, 5951-5955.

416. T. Masui, J. F. Lechner, G. H. Yoakum, J. C. Willey, C. C. Harris, (1986). Growth and differentiation of normal and transformed human bronchial epithelial cells. *J. Cell. Physiol. Suppl.* **4**, 73-81.

417. S. P. Sorokin, (1968). Reconstructions of centriole formation and ciliogenesis in mammalian lungs. *J. Cell Sci.* **3**, 207-230.

418. D. N. Wheatley, A. M. Wang, G. E. Strugnell, (1996). Expression of primary cilia in mammalian cells. *Cell Biol. Int.* **20**, 73-81.

419. A. Spektor, W. Y. Tsang, D. Khoo, B. D. Dynlacht, (2007). Cep97 and CP110 suppress a cilia assembly program. *Cell* **130**, 678-690.

420. R. U. Lukacs, S. Memarzadeh, H. Wu, O. N. Witte, (2010). Bmi-1 is a crucial regulator of prostate stem cell self-renewal and malignant transformation. *Cell Stem Cell* **7**, 682-693.

421. I. K. Park, D. L. Qian, M. Kiel, M. W. Becker, M. Pihalja, I. L. Weissman *et al.*, (2003). Bmi-1 is required for maintenance of adult self-renewing haematopoietic stem cells. *Nature* **423**, 302-305.

422. C. A. Fasano, T. N. Phoenix, E. Kokovay, N. Lowry, Y. Elkabetz, J. T. Dimos *et al.*, (2009). Bmi-1 cooperates with Foxg1 to maintain neural stem cell self-renewal in the forebrain. *Genes Dev.* **23**, 561-574.

423. M. L. Fulcher, S. E. Gabriel, J. C. Olsen, J. R. Tatreau, M. Gentzsch, E. Livanos *et al.*, (2009). Novel human bronchial epithelial cell lines for cystic fibrosis research. *Am. J. Physiol. Lung Cell. Mol. Physiol.* **296**, L82-L91.

424. M. Milyavsky, I. Shats, N. Erez, X. H. Tang, S. Senderovich, A. Meerson *et al.*, (2003). Prolonged culture of telomerase-immortalized human fibroblasts leads to a premalignant phenotype. *Cancer Res.* **63**, 7147-7157.

425. T. R. McKay, M. V. Camarasa, B. Iskender, J. P. Ye, N. Bates, D. Miller *et al.*, (2011). Human feeder cell line for derivation and culture of hESc/hiPSc. *Stem Cell Res.* **7**, 154-162.

426. J. C. Ho, K. N. Chan, W. H. Hu, W. K. Lam, L. Zheng, G. L. Tipoe *et al.*, (2001). The effect of aging on nasal mucociliary clearance, beat frequency, and ultrastructure of respiratory cilia. *Am. J. Respir. Crit. Care Med.* **163**, 983-988.

427. M. Kumar, B. Keller, N. Makalou, R. E. Sutton, (2001). Systematic determination of the packaging limit of lentiviral vectors. *Hum. Gene Ther.* **12**, 1893-1905.

428. F. Herbst, C. R. Ball, F. Tuorto, A. Nowrouzi, W. Wang, O. Zavidij *et al.*, (2012). Extensive methylation of promoter sequences silences lentiviral transgene expression during stem cell differentiation in vivo. *Mol. Ther.* **20**, 1014-1021.

429. G. Wu, N. Liu, I. Rittelmeyer, A. D. Sharma, M. Sgodda, H. Zaehres *et al.*, (2011). Generation of healthy mice from gene-corrected disease-specific induced pluripotent stem cells. *PLoS Biol.* **9**, e1001099.

430. S. Mukherjee, G. Santilli, M. P. Blundell, S. Navarro, J. A. Bueren, A. J. Thrasher, (2011). Generation of functional neutrophils from a mouse model of X-linked chronic granulomatous disorder using induced pluripotent stem cells. *PLoS ONE* **6**, e17565.

431. F. Zhang, A. R. Frost, M. P. Blundell, O. Bales, M. N. Antoniou, A. J. Thrasher, (2010). A ubiquitous chromatin opening element (UCOE) confers resistance to DNA methylation-mediated silencing of lentiviral vectors. *Mol. Ther.* **18**, 1640-1649.

432. N. Pfaff, N. Lachmann, M. Ackermann, S. Kohlscheen, C. Brendel, T. Maetzig *et al.*, (2013). A ubiquitous chromatin opening element prevents transgene silencing in pluripotent stem cells and their differentiated progeny. *Stem Cells* **31**, 488-499.

433. L. E. Ostrowski, J. R. Hutchins, K. Zakel, W. K. O'Neal, (2003). Targeting expression of a transgene to the airway surface epithelium using a ciliated cell-specific promoter. *Mol. Ther.* **8**, 637-645.

434. M. Limberis, D. S. Anson, M. Fuller, D. W. Parsons, (2002). Recovery of airway cystic fibrosis transmembrane conductance regulator function in mice with cystic fibrosis after single-dose lentivirus-mediated gene transfer. *Hum. Gene Ther.* **13**, 1961-1970.

435. Q. H. Meng, D. Robinson, R. G. Jenkins, R. J. McAnulty, S. L. Hart, (2004). Efficient transfection of non-proliferating human airway epithelial cells with a synthetic vector system. *J. Gene Med.* **6**, 210-221.

436. Q. Chu, J. D. Tousignant, S. Fang, C. Jiang, L. H. Chen, S. H. Cheng *et al.*, (1999). Binding and uptake of cationic lipid : pDNA complexes by polarized airway epithelial cells. *Hum. Gene Ther.* **10**, 25-36.

437. Q. Chu, J. A. St George, M. Lukason, S. H. Cheng, R. K. Scheule, S. J. Eastman, (2001). EGTA enhancement of adenovirus-mediated gene transfer to mouse tracheal epithelium in vivo. *Hum. Gene Ther.* **12**, 455-467.

438. C. B. Coyne, M. M. Kelly, R. C. Boucher, L. G. Johnson, (2000). Enhanced epithelial gene transfer by modulation of tight junctions with sodium caprate. *Am. J. Respir. Cell Mol. Biol.* **23**, 602-609.

439. D. S. Duan, Y. P. Yue, Z. Y. Yan, P. B. McCray, J. F. Engelhardt, (1998). Polarity influences the efficiency of recombinant adenoassociated virus infection in differentiated airway epithelia. *Hum. Gene Ther.* **9**, 2761-2776.

440. S. M. Simet, T. A. Wyatt, J. DeVasure, D. Yanov, D. Allen-Gipson, J. H. Sisson, (2012). Alcohol increases the permeability of airway epithelial tight junctions in Beas-2B and NHBE Cells. *Alcohol. Clin. Exp. Res.* **36**, 432-442.

441. S. Ramachandran, S. Krishnamurthy, A. M. Jacobi, C. Wohlford-Lenane, M. A. Behlke, B. L. Davidson *et al.*, (2013). Efficient delivery of RNA interference oligonucleotides to polarized airway epithelia in vitro. *Am. J. Physiol. Lung Cell. Mol. Physiol.* **305**, L23-L32.

442. B. Button, L. H. Cai, C. Ehre, M. Kesimer, D. B. Hill, J. K. Sheehan *et al.*, (2012). A periciliary brush promotes the lung health by separating the mucus layer from airway epithelia. *Science* **337**, 937-941.

443. P. Kirsch, M. Hafner, H. Zentgraf, L. Schilling, (2003). Time course of fluorescence intensity and protein expression in HeLa cells stably transfected with hrGFP. *Mol. Cells* **15**, 341-348.

444. K. L. Grinnell, B. L. Yang, R. L. Eckert, J. R. Bickenbach, (2007). De-differentiation of mouse interfollicular keratinocytes by the embryonic transcription factor Oct-4. *J. Invest. Dermatol.* **127**, 372-380.

445. P. Corish, C. Tyler-Smith, (1999). Attenuation of green fluorescent protein half-life in mammalian cells. *Protein Eng.* **12**, 1035-1040.

446. J. M. Ignowski, D. V. Schaffer, (2004). Kinetic analysis and modeling of firefly luciferase as a quantitative reporter gene in live mammalian cells. *Biotechnol. Bioeng.* **86**, 827-834.

447. R. E. White, R. Wade-Martins, S. L. Hart, J. Frampton, B. Huey, A. Desai-Mehta *et al.*, (2003). Functional delivery of large genomic DNA to human cells with a peptide-lipid vector. *J. Gene Med.* **5**, 883-892.

448. R. J. Sim, R. Belotserkovskaya, D. Reinberg, (2004). Elongation by RNA polymerase II: the short and long of it. *Genes Dev.* **18**, 2437-2468.

449. C. A. Parada, R. G. Roeder, (1996). Enhanced processivity of RNA polymerase II triggered by Tat-induced phosphorylation of its carboxy-terminal domain. *Nature* **384**, 375-378.

450. S. Y. Kao, A. F. Calman, P. A. Luciw, B. M. Peterlin, (1987). Anti-termination of transcription within the long terminal repeat of HIV-1 by tat gene product. *Nature* **330**, 489-493.

451. J. Zabner, B. G. Zeiher, E. Friedman, M. J. Welsh, (1996). Adenovirus-mediated gene transfer to ciliated airway epithelia requires prolonged incubation time. *J. Virol.* **70**, 6994-7003.

452. J. Zabner, S. C. Wadsworth, A. E. Smith, M. J. Welsh, (1996). Adenovirus-mediated generation of cAMP-stimulated Cl- transport in cystic fibrosis airway epithelia in vitro: effect of promoter and administration method. *Gene Ther.* **3**, 458-465.

453. L. Q. Zhang, M. E. Peeples, R. C. Boucher, P. L. Collins, R. J. Pickles, (2002). Respiratory syncytial virus infection of human airway epithelial cells is polarized, specific to ciliated cells, and without obvious cytopathology. *J. Virol.* **76**, 5654-5666.

454. U. Griesenbach, E. W. F. W. Alton, (2013). Moving forward: cystic fibrosis gene therapy. *Hum. Mol. Genet.* **22**, R52-R58.

455. J. M. Lu, F. J. Zhang, M. A. Kay, (2013). A mini-intronic plasmid (MIP): a novel robust transgene expression vector in vivo and in vitro. *Mol. Ther.* **21**, 954-963.

456. E. L. Rawlins, B. L. M. Hogan, (2008). Ciliated epithelial cell lifespan in the mouse trachea and lung. *Am. J. Physiol. Lung Cell. Mol. Physiol.* **295**, L231-L234.

457. J. C. Snyder, R. M. Teisanu, B. R. Stripp, (2009). Endogenous lung stem cells and contribution to disease. *J. Pathol.* **217**, 254-264.

458. F. A. Suprynowicz, G. Upadhyay, E. Krawczyk, S. C. Kramer, J. D. Hebert, X. F. Liu *et al.*, (2012). Conditionally reprogrammed cells represent a stem-like state of adult epithelial cells. *Proc. Natl. Acad. Sci. U. S. A.* **109**, 20035-20040.

9. APPENDICES

9.1. APPENDIX A – NANOCOMPLEX FORMULATION

In Vitro Transfection with LPD complexes

Day 1

- Seed cells at $2x10^4$ cells/well in complete medium in a 96-well plate

Day 2

- Make up LPD complexes in Optimem

Example for 0.75:4:1 L:P:D weight ratio for 8 wells of 96 well plate.

1) 0.75 µL of **L** at 2mg/ml + 49.25 µL Optimem mixed well in eppendorf 1 (e.g. DHDTMA:DOPE)
2) 40 µL of **P** at 0.2 mg/ml + 60 µL Optimem mixed well in eppendorf 2 (e.g. $K_{16}E$)
3) 2 µL of **D** at 1mg/ml + 48 µL Optimem mixed well in eppendorf 3 (e.g. pCI.Luc)

Then, using pipette, add content of eppendorf 2 into 1 and mix 5 times, then add contents of eppendorf 3 into 1 and mix 5 times and incubate at room temperature for 30 minutes. **(ORDER OF MIXING IS IMPORTANT)**

- Add 25 µL of formed complexes to each well
- Centrifuge cells at 1500rpm for 5min **(VITAL, IF SKIPPED THEN TRANSFECTION EFFICIENCY DRAMATICALLY FALLS)**
- Put plate in Incubator for 24h

Day 3 (Luciferase and Protein Assays)

- Prepare enough 1x Reporter Lysis Buffer (dilute 5x in MilliQ water) to give 20µL per well

e.g. for one 96 well plate will need to prepare 20µL x 100 wells = 2mL of 1x RLB

- After 24h incubation, remove media from wells
- Wash with 100µL 1x PBS and add 20µL 1x RLB
- Wrap plate in cling film and place at 4^{o}C for 20minutes
- Transfer plate to -80^{o}C and leave for at least 30mins (can leave overnight if you wish to perform luciferase assay following day).

Day 3 or 4 (Luciferase and Protein Assays)

- Thaw Luciferase Buffer and Substrate at RT approx 1h (1 pair of bottles per 96-well plate)
- Thaw plate from -80^{o}C, approx 0.5-1h
- Mix Luciferase Buffer and Substrate to make reagent
- Perform luciferase and protein assay using Optima (100µL of reagent added by Optima)

In Vivo Transfection with LPD complexes

- Make up complexes in sterile ddH_2O

Example for 0.75:4:1 L:P:D weight ratio for 3 mice each receiving 16.7µg of DNA.

1) 18.75 µL of **L** at 2mg/ml + 31.25 µL ddH_2O mixed well in eppendorf 1 (e.g. DHDTMA:DOPE)
2) 20 µL of **P** at 10 mg/ml + 30 µL ddH_2O mixed well in eppendorf 2 (e.g. $K_{16}E$)
3) 10 µL of **D** at 5mg/ml + 40 µL ddH_2O mixed well in eppendorf 3 (e.g. pCI.Luc)

Then, using pipette, add content of eppendorf 2 into 1 and mix 5 times, then add contents of eppendorf 3 into 1 and mix 5 times and incubate at room temperature for 30 minutes. **(ORDER OF MIXING IS IMPORTANT)**

- Deliver 50µL of formed complexes per mouse via oropharyngeal instillation.

9.2. APPENDIX B – PLASMID MAPS

Plasmid maps are displayed in alphabetical order and were obtained directly from the supplier's websites or produced in Vector NTI (v.11.5)

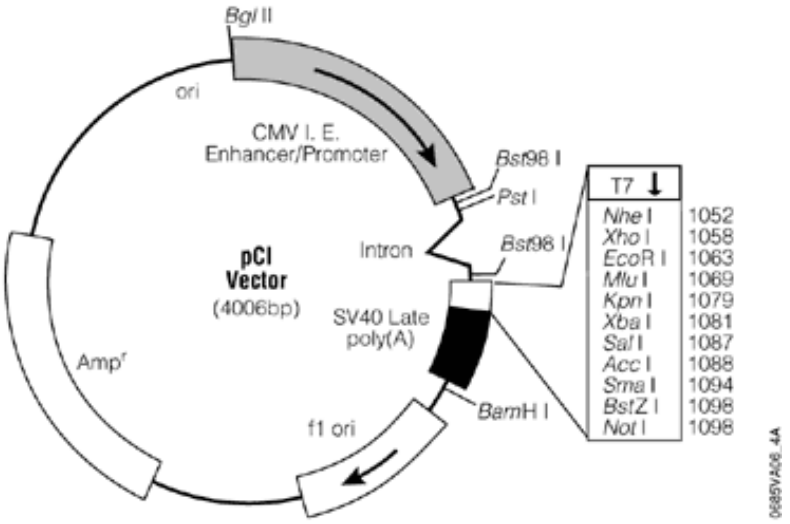

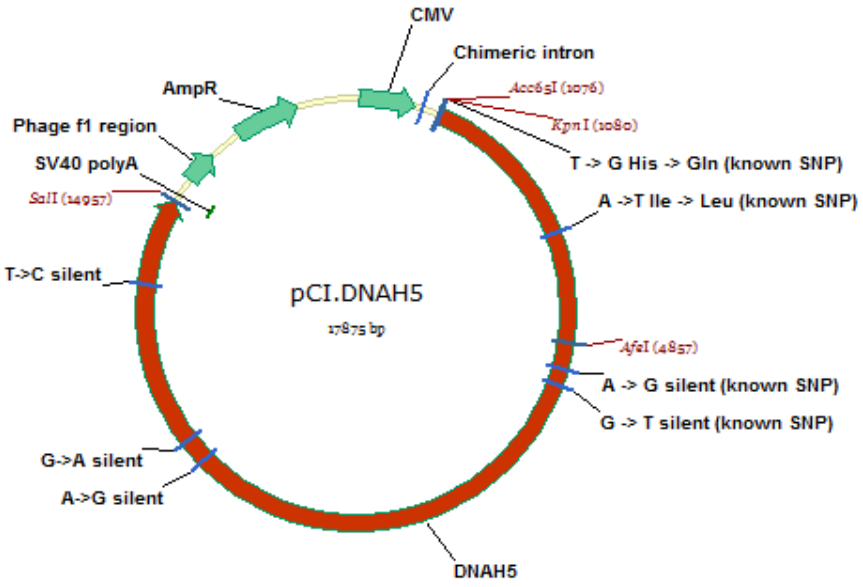

Nucleotides that differ from the NCBI reference sequence NM_001369.2 are highlighted and their effect on translation, if any, is also shown.

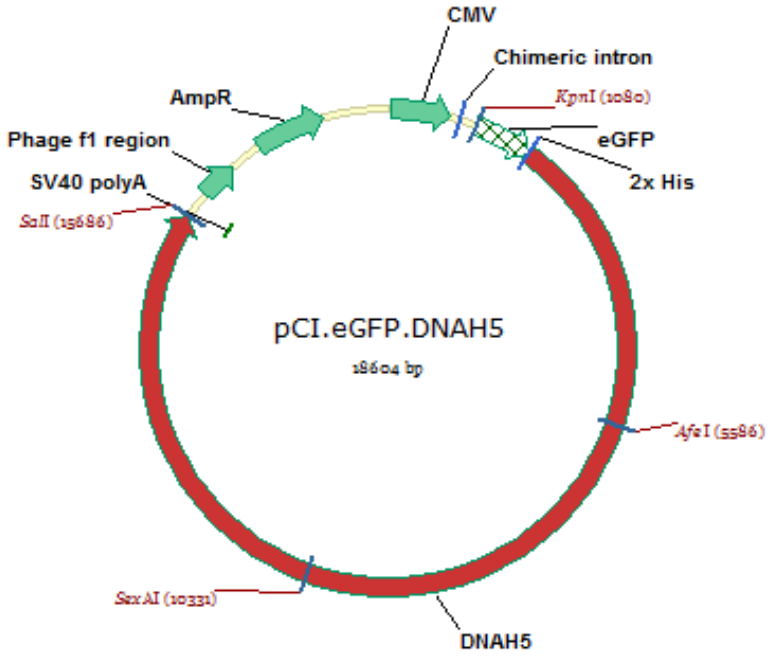

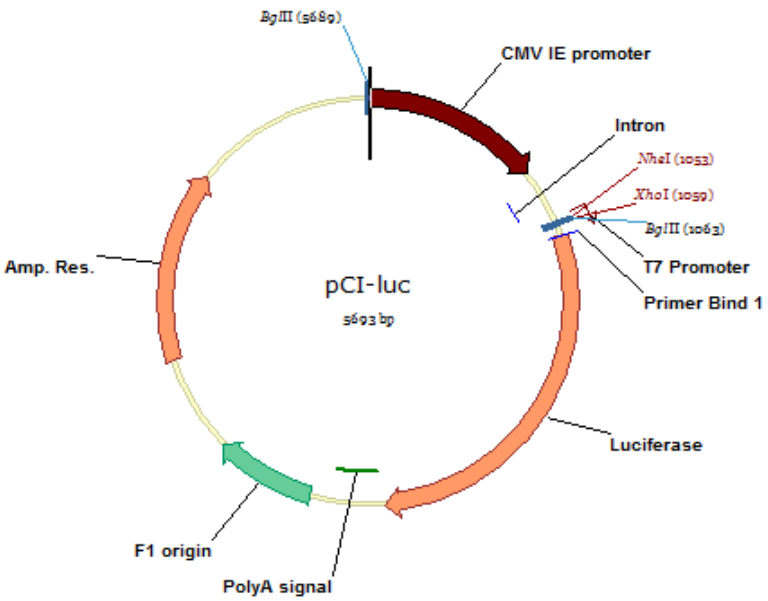
BglII (5689)
CMV IE promoter
Intron
NheI (1053)
XhoI (1059)
BglII (1063)
T7 Promoter
Primer Bind 1
Amp. Res.
pCI-luc
5693 bp
Luciferase
F1 origin
PolyA signal

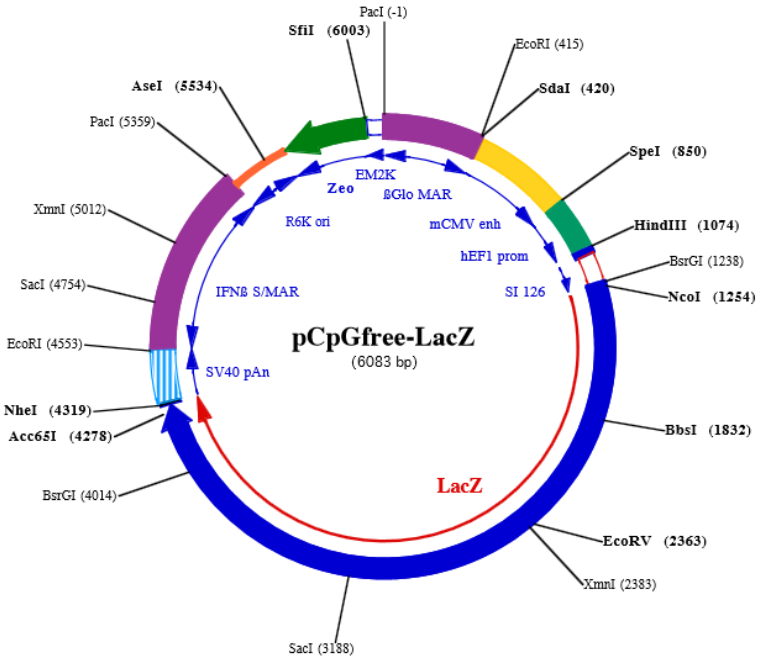
PacI (-1)
SfiI (6003)
EcoRI (415)
AseI (5534)
SdaI (420)
PacI (5359)
SpeI (850)
EM2K
Zeo
ßGlo MAR
XmnI (5012)
R6K ori
mCMV enh
HindIII (1074)
hEF1 prom
BstGI (1238)
SacI (4754)
IFNß S/MAR
SI 126
NcoI (1254)
pCpGfree-LacZ
(6083 bp)
EcoRI (4553)
SV40 pAn
NheI (4319)
BbsI (1832)
Acc65I (4278)
LacZ
BstGI (4014)
EcoRV (2363)
XmnI (2383)
SacI (3188)

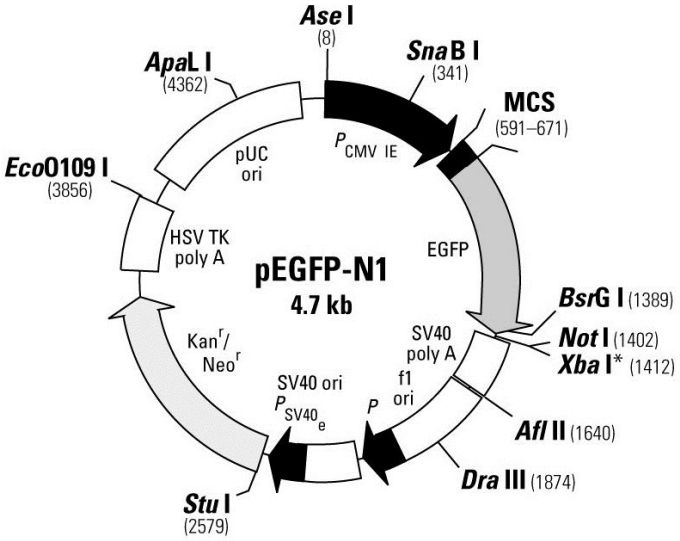
Ase I
(8)
Sna B I
(341)
MCS
(591–671)
ApaL I
(4362)
pUC
ori
P CMV IE
Eco0109 I
(3856)
HSV TK
poly A
EGFP
pEGFP-N1
4.7 kb
BsrG I (1389)
Not I (1402)
Xba I* (1412)
SV40
poly A
Kanr/
Neor
SV40 ori
P SV40e
f1
ori
P
Afl II (1640)
Dra III (1874)
Stu I
(2579)

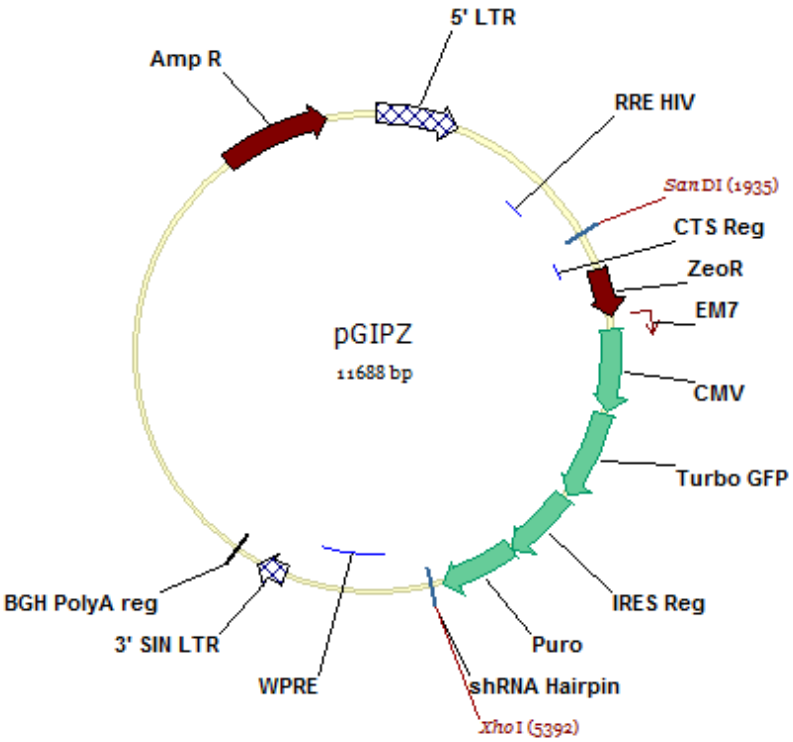
5' LTR
Amp R
RRE HIV
SanDI (1935)
CTS Reg
ZeoR
EM7
pGIPZ
11688 bp
CMV
Turbo GFP
IRES Reg
BGH PolyA reg
3' SIN LTR
WPRE
Puro
shRNA Hairpin
XhoI (5392)

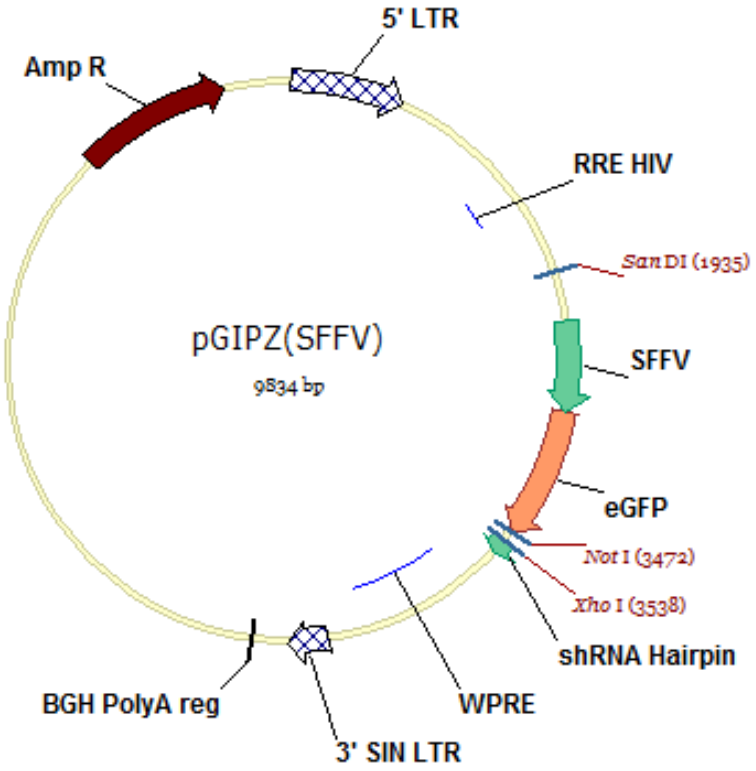
5' LTR
Amp R
RRE HIV
SanDI (1935)
pGIPZ(SFFV)
9834 bp
SFFV
eGFP
NotI (3472)
XhoI (3538)
shRNA Hairpin
BGH PolyA reg
WPRE
3' SIN LTR

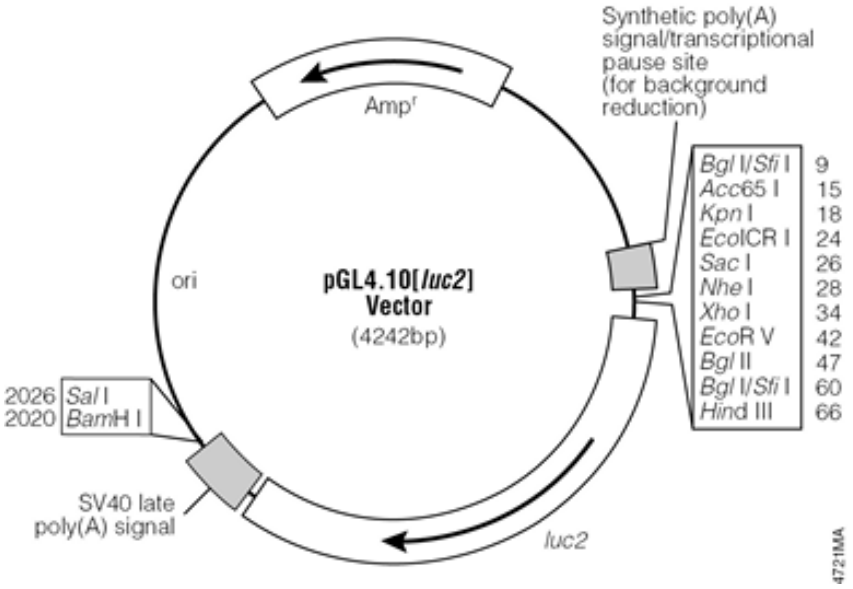
Synthetic poly(A) signal/transcriptional pause site (for background reduction)
Amp'
ori
pGL4.10[luc2] Vector
(4242bp)
BglII/SfiI 9
Acc65I 15
KpnI 18
EcoICRI 24
SacI 26
NheI 28
XhoI 34
EcoRV 42
BglII 47
BglII/SfiI 60
HindIII 66
2026 SalI
2020 BamHI
SV40 late poly(A) signal
luc2
4721MA

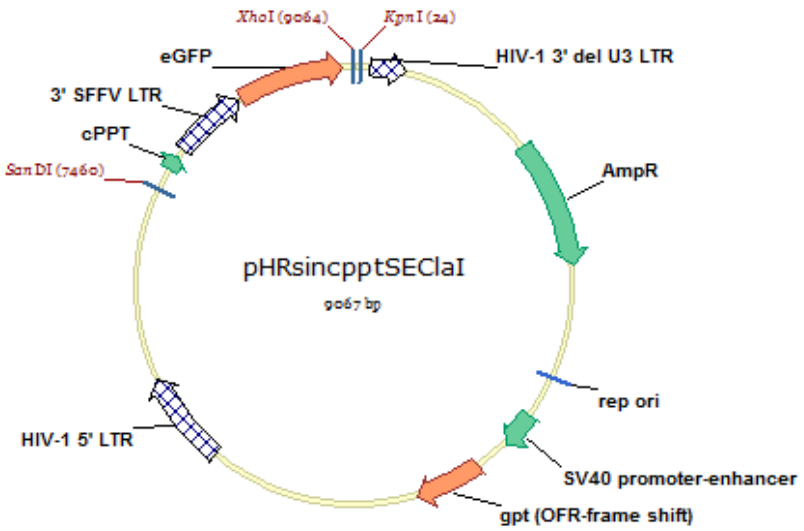
XhoI (9064)
KpnI (24)
eGFP
HIV-1 3' del U3 LTR
3' SFFV LTR
cPPT
SanDI (7460)
AmpR
pHRsincpptSEClaI
9067 bp
rep ori
HIV-1 5' LTR
SV40 promoter-enhancer
gpt (OFR-frame shift)

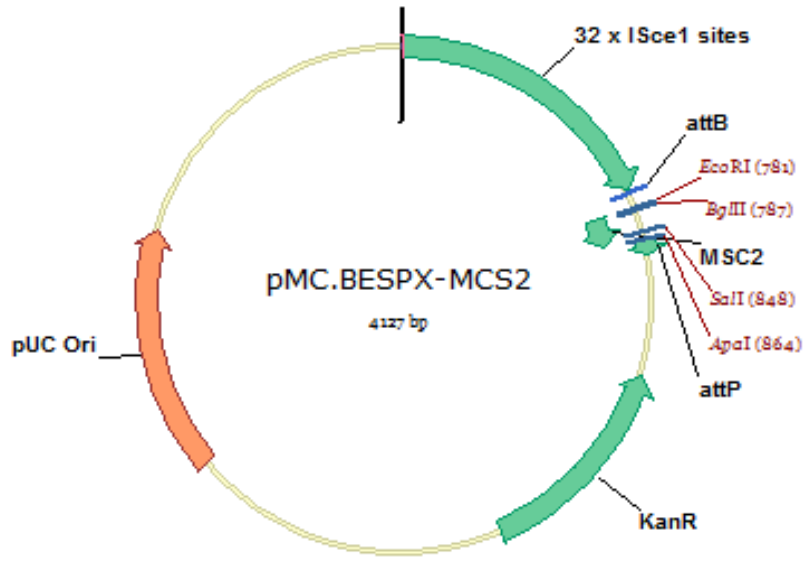
32 x ISce1 sites
attB
EcoRI (781)
BglII (787)
MSC2
pMC.BESPX-MCS2
4127 bp
SalI (848)
ApaI (864)
pUC Ori
attP
KanR

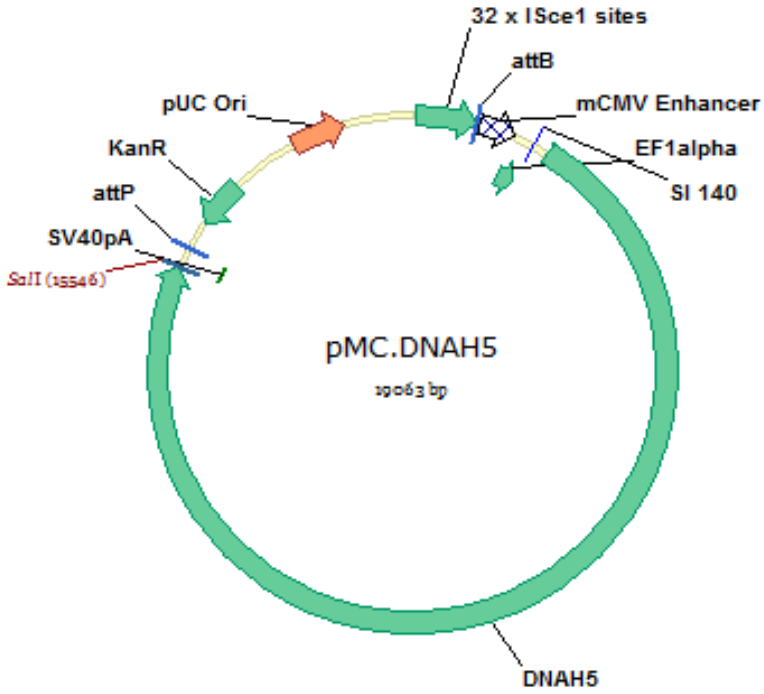
32 x ISce1 sites
attB
pUC Ori
mCMV Enhancer
KanR
EF1alpha
attP
SI 140
SV40pA
SalI (15546)
pMC.DNAH5
19063 bp
DNAH5

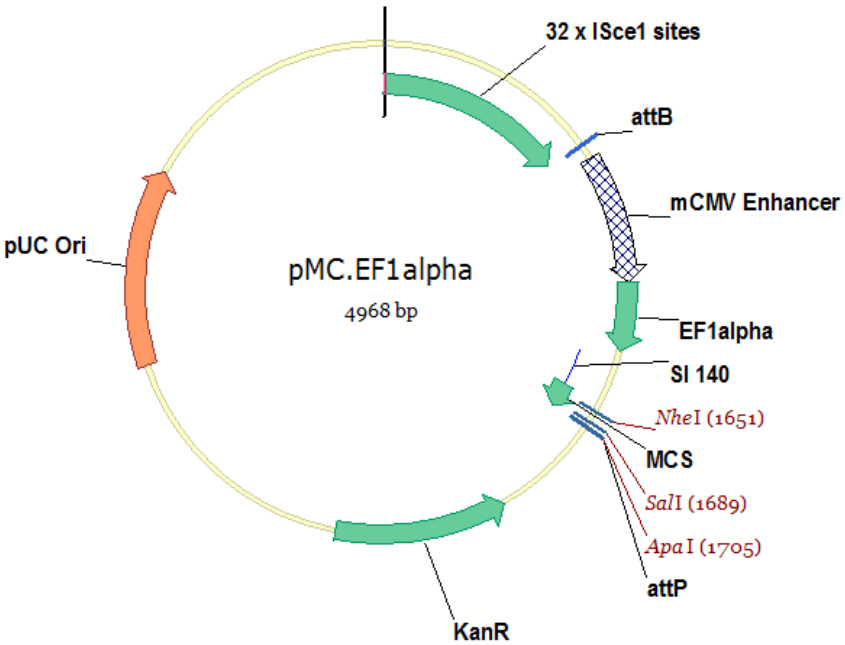
32 x ISce1 sites
attB
mCMV Enhancer
pUC Ori
pMC.EF1alpha
4968 bp
EF1alpha
SI 140
NheI (1651)
MCS
SalI (1689)
ApaI (1705)
attP
KanR

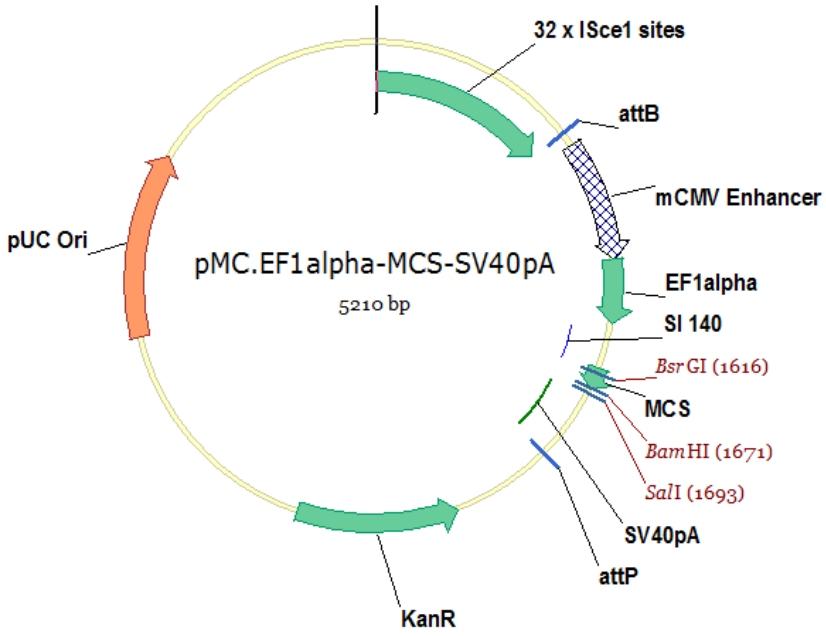
32 x ISce1 sites
attB
mCMV Enhancer
EF1alpha
SI 140
BsrGI (1616)
MCS
BamHI (1671)
SalI (1693)
SV40pA
attP
KanR
pUC Ori
pMC.EF1alpha-MCS-SV40pA
5210 bp

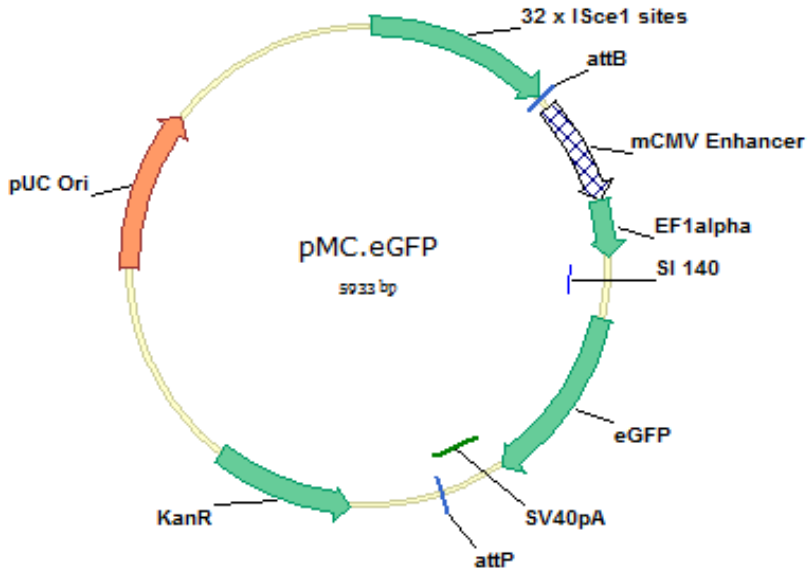
32 x ISce1 sites
attB
mCMV Enhancer
EF1alpha
SI 140
eGFP
SV40pA
attP
KanR
pUC Ori
pMC.eGFP
5933 bp

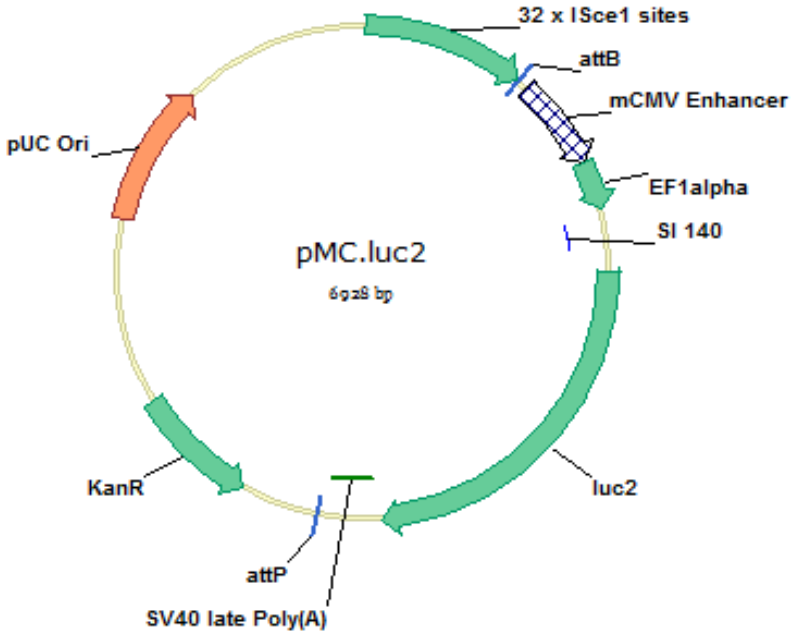
32 x ISce1 sites
attB
mCMV Enhancer
EF1alpha
SI 140
pUC Ori
pMC.luc2
6928 bp
KanR
luc2
attP
SV40 late Poly(A)

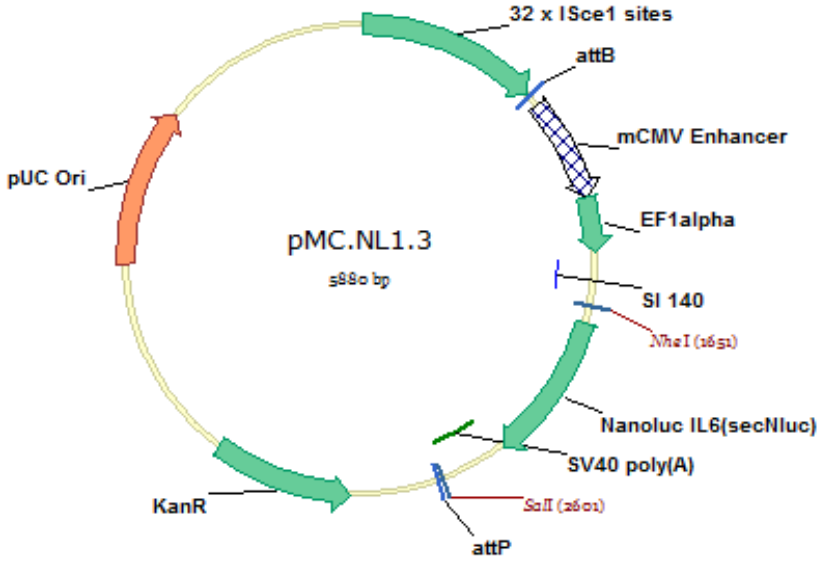
32 x ISce1 sites
attB
mCMV Enhancer
EF1alpha
pUC Ori
pMC.NL1.3
5980 bp
SI 140
NheI (1651)
Nanoluc IL6(secNluc)
SV40 poly(A)
KanR
SalI (2601)
attP

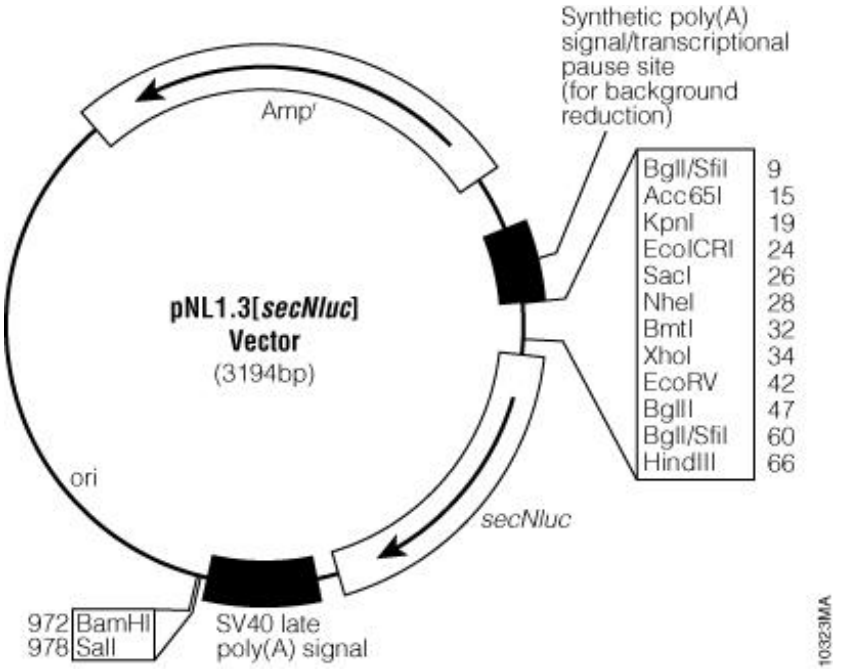
Synthetic poly(A)
signal/transcriptional
pause site
(for background
reduction)
Amp'
pNL1.3[secNluc]
Vector
(3194bp)
ori
secNluc
SV40 late
poly(A) signal
BglI/SfiI 9
Acc65I 15
KpnI 19
EcoICRI 24
SacI 26
NheI 28
BmtI 32
XhoI 34
EcoRV 42
BglI 47
BglI/SfiI 60
HindIII 66
972 BamHI
978 SalI
10323MA